

CORNERSTONE

 MINNESOTA STATE UNIVERSITY MANKATO

Minnesota State University, Mankato
**Cornerstone: A Collection of
Scholarly and Creative Works for
Minnesota State University,
Mankato**

All Theses, Dissertations, and Other Capstone
Projects

Theses, Dissertations, and Other Capstone Projects

2018

Assessing Historical Planform Channel Change in an Altered Watershed with Quantification of Error and Uncertainty Present in a GIS/Aerial Photography-based Analysis; Case Study: Minnesota River, Minnesota, USA.

Devon Libby

Minnesota State University, Mankato

Follow this and additional works at: <https://cornerstone.lib.mnsu.edu/etds>

 Part of the [Geographic Information Sciences Commons](#), [Physical and Environmental Geography Commons](#), and the [Water Resource Management Commons](#)

Recommended Citation

Libby, Devon, "Assessing Historical Planform Channel Change in an Altered Watershed with Quantification of Error and Uncertainty Present in a GIS/Aerial Photography-based Analysis; Case Study: Minnesota River, Minnesota, USA." (2018). *All Theses, Dissertations, and Other Capstone Projects*. 789.

<https://cornerstone.lib.mnsu.edu/etds/789>

This Thesis is brought to you for free and open access by the Theses, Dissertations, and Other Capstone Projects at Cornerstone: A Collection of Scholarly and Creative Works for Minnesota State University, Mankato. It has been accepted for inclusion in All Theses, Dissertations, and Other Capstone Projects by an authorized administrator of Cornerstone: A Collection of Scholarly and Creative Works for Minnesota State University, Mankato.

**Assessing Historical Planform Channel Change in an Altered
Watershed with Quantification of Error and Uncertainty Present in a
GIS/Aerial Photography-based Analysis; Case Study: Minnesota River,
Minnesota, USA.**

By

Devon J. Libby

A Thesis Submitted in Partial Fulfillment of the
Requirements for the Degree of
Master of Science
in
Geography

Minnesota State University, Mankato

Mankato, Minnesota

May 2017

December 7, 2017

Assessing Historical Planform Channel Change in an Altered Watershed with
Quantification of Error and Uncertainty Present in a GIS/Aerial Photography-based
Analysis; Case Study: Minnesota River, Minnesota, USA.

Devon J. Libby

This thesis has been examined and approved by the following members of the student's
committee.

Dr. Phillip Larson

Dr. Patrick Belmont

Dr. Woo Jang

Dr. Cynthia Miller

Abstract

Little is known about the historic planform channel change of the Minnesota River of south-central Minnesota, USA. This is despite research that demonstrates anthropogenic activities have altered the Minnesota River Basin's hydrology, land use, and climate. In addition, the threat of invasive carp infestation requires an understanding of Minnesota River planform change to assess mitigation strategies. This thesis focuses on the lower Minnesota River (LMR) by measuring planform channel change (lateral channel migration, width, and sinuosity) from 1937 to 2013. Analysis is conducted by utilizing remote/GIS analysis of historic aerial photographs. A secondary focus addresses and quantifies the inherent/introduced error/uncertainty within remote analysis in channel planform studies. Error in image referencing and channel digitization were quantified and applied to planform measurements throughout the LMR, as opposed to spatially uniform or borrowed values utilized in past literature. The results reveal the LMR exhibits an average increase in channel migration from ~ 0.77 meters per year (m/y) during the 1937-1951 interval to ~ 0.99 m/y during the 1980-1991 interval. Despite a decrease in lateral migration observed between the 1980-1991 and 1991-2013 intervals (~ 0.17 m/y decrease), the highest observed maximum migration rates are in these two recent intervals, with the most significant lateral migration (~ 16 m/y) in the 1980-1991 interval. Average channel width increased from ~ 70 m to ~ 113 m from 1937 to 2013. Sinuosity has decreased associated with a decrease in stream length from 180 km to 167 km from 1937 to 2013. These Planform changes are interpreted as a result of anthropogenic induced alteration in the MRB's hydrology, impacting processes that control channel behavior. Beyond spatially averaged temporal trends, spatial variability

of measured planform characteristics within the LMR correlate with locations where: 1) anthropogenic structures control river behavior (low rates of planform change), 2) distinct valley segments identified as sediment sinks in low gradient reaches (high rates of planform change), and 3) major tributary systems enter the LMR (increase in lateral migration downstream from the confluence). Given ongoing historic change observed here and the underfit nature of the LMR, we believe this work demonstrates a substantial challenge to any invasive carp mitigation strategy.

Acknowledgements

I would first like to thank God for the opportunities provided through my educational experience and sustaining me through this chapter of my life. I feel incredibly grateful and blessed.

I want to dedicate this thesis to my parents. Their continued support and belief in me was an integral component in completing this process. I also cannot begin to repay them for watching my dog Bear when I would periodically leave town for conferences, internships, etc. I love you both and cannot begin to express how much I appreciate everything you have done for me.

I want to thank my advisor Dr. Phillip Larson for encouraging me to pursue graduate school. Without you physically handing me the various applications in my senior year as an undergraduate, I likely would not be where I am today. I also owe a huge thank you to Dr. Larson and the rest of my committee (Dr. Patrick Belmont, Dr. Woo Jang, and Dr. Cindy Miller), for the immense amount of time and effort that went into guiding and refining the research presented in this thesis.

I would like to thank rest of the Geography Department faculty, staff, and fellow students for creating an excellent and enjoyable educational community. Finally, I would like to thank the department, college, university and private contributors for providing various forms of financial assistance. Specifically, the James F. Goff Research Endowment and Dr. Mary T. Dooley's various generous contributions have allowed me to carry out my research and present my findings at several national conferences. I cannot express enough how grateful I am for those opportunities.

Contents

Abstract.....	i
Acknowledgements.....	iii
Tables.....	vii
Figures.....	viii
Equations.....	xii
Appendix.....	xiii
Chapter 1 : Literature Review.....	1
1.1 Overview and Importance of Planform Analysis.....	3
1.1.1 Infrastructure and Development	5
1.1.2 Pollutant Impacts on Humans and the Ecosystems.....	6
1.2 Understanding Fluvial System and Channel Change.....	8
1.3 Process of Channel Change	15
1.3.1 Channel Classification in Fluvial Studies	15
1.3.1.1 Channel Classification Based on Substrate.....	15
1.3.1.2 Alluvial Channel Classification Based on Channel Planform and Sinuosity	15
1.3.2 Planform Channel Change in Alluvial Sinuous-Meandering Channels	17
1.3.2.1 Channel Migration and Meandering	18
1.3.2.2 Channel Width	24
1.4 Methodological Considerations for Understanding Planform Change.....	28
1.4.1 Range of Techniques.....	28
1.4.2 Geographic Information Systems and Planform Analysis.....	31
1.4.2.1 Brief Summary of the Four Major Processes.....	32
1.4.2.2 Data Classification: Primary vs Secondary.....	33
1.4.2.3 Error, Uncertainty, and Inconsistencies	35
1.5 Study Area: Minnesota River.....	39
1.5.1 Overview	39
1.5.2 Geomorphic Evolution of the Minnesota River Valley	42
1.5.3 Contemporary Concerns in the Minnesota River Basin	45

1.5.3.1 Land Use Change and Altered Hydrology	46
1.5.3.2 Altered Hydrology and Sediment	50
1.5.3.3 Phosphorus, Nitrogen, and Bacteria.....	51
1.5.3.4 Invasive Carp	52
1.6 Significance of Understanding Planform Change on the Minnesota River	57
1.7 Conclusion and Research Questions	60
Chapter 2 Assessing and Quantifying the Error and Uncertainty Associated with Aerial Photograph-based Channel Planform Change Studies	63
2.1 Introduction.....	63
2.1.1 Data Acquisition and Classification.....	64
2.1.2 Review of Image Registration Processes in Planform Channel Change Studies	65
2.1.2.1 Historic Aerial Photographs.....	65
2.1.2.2 Digital Ortho-imagery.....	72
2.1.3 Review of Assessing Digitizing Error in Planform Channel Change Studies .	74
2.2 Methods for Assessing Channel Planform Change on the Minnesota River (year to year)	75
2.2.1 Aerial Photograph Acquisition for the Minnesota River Valley	75
2.2.2 Minnesota River Image Registration	78
2.2.3 Minnesota River Image Registration Error Assessment	80
2.2.4 Bank and Centerline Digitization of the Minnesota River.....	89
2.2.5 Bank and Centerline Digitizing Error Assessment	91
2.3 Results.....	94
2.3.1 Image Collection, Registration, and Error Assessment	94
2.3.2 Bank and Centerline Digitization and Error Assessment	101
2.4 Discussion	110
2.4.1 Imagery	110
2.4.2 Digitization	115
2.5 Conclusion	118
Chapter 3 : Planform Channel Change of the Lower Minnesota River (1937-2013).....	120
3.1 Introduction.....	120

3.1.1 Study Area	122
3.1.2 Significance of the Study Area	126
3.1.2.1 Fluvial Geomorphology and River Management	126
3.1.2.2 Ecological/Biological Management.....	129
3.2 Methods.....	130
3.2.1 Channel Migration	131
3.2.1.1 National Center for Earth Surface Dynamics Planform Statistics Toolbox	132
3.2.1.2 Pre MATLAB Processing.....	138
3.2.1.3 MATLAB “ChannelChangeSignif”.....	142
3.2.1.4 Post MATLAB Processing	145
3.2.1.5 Cutoff vs Non-Cutoff Datasets	152
3.2.2 Width Change and Sinuosity/Stream Length.....	153
3.2.3 River Reach and Pinch Point Analysis	154
3.3 Results.....	158
3.3.1 Channel Migration	158
3.3.1.1 Large Scale Data Analysis	158
3.3.1.2 Color Migration Maps (Preserving Spatial Attributes of the Data).....	162
3.3.1.3 Geomorphic Break Reach Analysis	166
3.3.1.3.1 Average Annual Channel Migration (AACM)	167
3.3.1.3.2 Maximum Annual Channel Migration (MACM)	172
3.3.1.3.2 Cutoff location relation to AACM and MACM	175
3.3.2 Channel Width Change	176
3.3.2.1 Average Channel Width (ACW).....	179
3.3.2.2 Maximum Channel Width (MaxCW).....	182
3.3.2.2 Minimum Channel Width (MinCW)	184
3.3.3 Sinuosity and Channel Length.....	186
3.3.4 Pinch Points and the Consideration of Invasive Carp Barriers.....	190
3.4.2.1 Mankato	190
3.4.2.2 Highway 14 Bridge (Mankato).....	192
3.4.2.3 Highway 22 Bridge (St. Peter).....	193

3.4.2.4 Highway 169 Bridge (Le Sueur).....	195
3.4.2.5 Dan Patch Line Bridge (Savage).....	196
3.4 Discussion.....	198
3.4.1 Methodological Considerations	198
3.4.1.1 Trajectory Method vs Polygon Method	198
3.4.1.2 Error Metrics	203
3.4.1.3 Problems Overcome.....	206
3.4.1.3.1 MATLAB “ChannelChangeSignif”	206
3.4.1.3.2 Errored Trajectory File Lines.....	206
3.4.2 Planform Channel Change	210
3.4.2.1 Channel Migration	213
3.4.2.2 Channel Width	217
3.4.2.3 Channel Sinuosity/Stream Length	218
3.5 Conclusion	220
References.....	222
Appendix.....	256

Tables

Table 1.1 Channel Migration Literature	4
Table 1.2 Meandering River Mechanisms/Concepts	24
Table 1.3 Channel Widening Processes.....	25
Table 1.4 Seven Major Channel Migration Quantification Techniques	30
Table 2.1 DOQ Accuracies	73
Table 2.2 Collected Aerial Imagery	77
Table 2.3 Individual Student GCP Error Assessment.....	95
Table 2.4 Combined GCP Error Assessment.....	97
Table 2.5 Digitization Error Assesment.....	108

Table 3.1 Average Annual Channel Migration (AACM)	169
Table 3.2 Maximum Annual Channel Migration (MACM)	173
Table 3.3 Average Channel Width (ACW).....	180
Table 3.4 Maximum Channel Width (MaxCW).....	183
Table 3.5 Minimum Channel Width (MinCW)	185
Table 3.6 Sinuosity	189
Table 3.7 Highway 14 Bridge Upstream/Downstream Migration and Width	193
Table 3.8 Highway 22 Bridge Upstream/Downstream Migration and Width	194
Table 3.9 Highway 169 Bridge Upstream/Downstream Migration and Width	196
Table 3.10 Dan Patch Line Bridge Upstream/Downstream Migration and Width.....	197

Figures

Figure 1.1 Lane's Balance	9
Figure 1.2 Fluvial Interrelationships.....	14
Figure 1.3 Sinuosity Ratio	16
Figure 1.4 Meander Dynamics.....	20
Figure 1.5 Meander Pattern Developments	21
Figure 1.6 Polygon vs National Center for Earth Surface Dynamics (NCED) Channel Migration Calculations.....	37
Figure 1.7 Minnesota River Gradient/Slope	39
Figure 1.8 Minnesota River Basin (MRB).....	41
Figure 1.9 Minnesota River Valley (MRV) Cross Section.....	44
Figure 1.10 Longitudinal Profiles of Minnesota River Tributaries (Knick Zones)	45
Figure 1.11 Minnesota River Peak Flow Events by Year.....	49

Figure 1.12 Lake Pepin Sedimentation Rates	51
Figure 1.13 Bighead vs Silver Carp.....	53
Figure 1.14 Study Area: Lower Minnesota River (LMR)	62
Figure 2.1 Aerial Photograph Relief Displacement.....	67
Figure 2.2 Imagery Processing Flow Chart	80
Figure 2.3 Ground Control Point (GCP) Displacement.....	82
Figure 2.4 MRV LiDAR and GCP Placement Guidelines	84
Figure 2.5 All GCPs Placed for Error Analysis.....	86
Figure 2.6 Image Registration Error Assessment Workflow.....	88
Figure 2.7 Centerline Algorithm for Centerline Creation.....	90
Figure 2.8 NCED Channel Planform Statistics “Interpolate Centerline” tool.....	91
Figure 2.9 Repeat Bankline Digitization (Digitizing Error)	92
Figure 2.10 Georeferenced Aerial Photography and Digitized Centerlines	94
Figure 2.11 Image Registration Error 1937-1951.....	98
Figure 2.12 Image Registration Error 1951-1964.....	99
Figure 2.13 Image Registration Error 1964-1980.....	99
Figure 2.14 Image Registration Error 1980-1991.....	100
Figure 2.15 Image Registration Error 1991-2013.....	100
Figure 2.16 Image Registration Error 1937-2013.....	101
Figure 2.17 1937 Banklines and Centerlines	102
Figure 2.18 1951 Banklines and Centerlines	103
Figure 2.19 1964 Banklines and Centerlines	104

Figure 2.20 1980 Banklines and Centerlines	105
Figure 2.21 1991 Banklines and Centerlines	106
Figure 2.22 2013 Banklines and Centerlines	107
Figure 2.23 Box Plot of Digitizing Error	109
Figure 2.24 Errors Associated with ArcMap’s “Collapse Dual Lines To Centerline” Tool	117
Figure 3.1 Study Area: Lower Minnesota River (Duplicate)	122
Figure 3.2 NCED “Lateral Migration” Tool Errors.....	134
Figure 3.3 NCED “Lateral Migration” Tool Errors at Cutoffs.....	136
Figure 3.4 NCED Channel Planform Statistics “Lateral Measurement” Tool Workflow	137
Figure 3.5 “Pre MATLAB Processing” Tool GUI	140
Figure 3.6 “Pre MATLAB Processing” Model.....	141
Figure 3.7 “Post MATLAB Processing” Tool GUI.....	147
Figure 3.8 “Post MATLAB Processing” Model	148
Figure 3.9 Post MATLAB Processing Inputs/Outputs	150
Figure 3.10 Trajectory Line Gap Error	152
Figure 3.11 Cutoff vs Non-Cutoff	153
Figure 3.12 Geomorphic Reach Break Down.....	156
Figure 3.13 “Color Migration” Reach Break Down	157
Figure 3.14 Annual Channel Migration for All Intervals (1937-2013)	160
Figure 3.15 Annual Channel Migration for All Intervals (1937-2013) without Cutoffs	161

Figure 3.16 Reach 3 Color Migration Map (Mankato to Henderson)	163
Figure 3.17 Reach 2 Color Migration Map (Henderson to Chaska).....	164
Figure 3.18 Reach 1 Color Migration Map (Chaska to Mendota).....	165
Figure 3.19 Average Annual Channel Migration by Reach (1937-2013)	170
Figure 3.20 Overall Averaged Annual Channel Migration for Each Reach (1937-2013)	171
Figure 3.21 Maximum Annual Channel Migration (Reach 2 in 1980).....	174
Figure 3.22 Cutoff Locations by Interval and Reach.....	175
Figure 3.23 Channel Width from 1937-2013.....	177
Figure 3.24 Average Channel Width from 1937-2013	178
Figure 3.25 Average Channel Width by Reach from 1937-2013	181
Figure 3.26 Sinuosity Change by Reach from 1937-2013.....	187
Figure 3.27 Stream Length Change from 1937-2013	188
Figure 3.28 Mankato Planform	190
Figure 3.29 Mankato Annual Channel Migration from 1937-2013.....	191
Figure 3.30 Mankato Channel Width Change from 1937-2013	191
Figure 3.31 Highway 14 Bridge Planform.....	192
Figure 3.32 Highway 22 Bridge Planform.....	194
Figure 3.33 Highway 169 Bridge Planform.....	195
Figure 3.34 Dan Patch Line Bridge Planform	197
Figure 3.35 Polygon Method Inputs	199
Figure 3.36 Polygon Method Model.....	200

Figure 3.37 Polygon Method Output	201
Figure 3.38 NCED Planform Statistics Output.....	201
Figure 3.39 Polygon vs National Center for Earth Surface Dynamics (NCED) Channel Migration Calculations (Duplicate)	202
Figure 3.40 Spatial Comparison of Spatial Variable Error (SVE), Root Mean Square Error (RMSE), and 90 th Percentile Error	204
Figure 3.41 Graphical Comparison of SVE, RMSE, and 90 th Percentile Error.....	205
Figure 3.42 Errored Downstream Measurements	209
Figure 3.43 Average Annual Channel Migration and Average Channel Width by Reach (1937-2013).....	211
Figure 3.44 Stream Length and Sinuosity by Reach (1937-2013).....	212
Figure 3.45 Minnesota River Stream Gradient/Slope with Breaks.....	214
Figure 3.46 Reach 12 Planform	216
Figure 3.47 Planform of Two 1991-2013 Cutoffs	219

Equations

Equation 1.1 Channel Response to Increased Discharge.....	11
Equation 1.2 Channel Response to Decreased Discharge	11
Equation 1.3 Channel Response to Increased Bedload Supply	12
Equation 1.4 Channel Response to Decreased Bedload Supply	12
Equation 1.5 Channel Response to Increased Discharge and Increased Bedload Supply	12
Equation 1.6 Channel Response to Decreased Discharge and Decreased Bedload Supply	12

Equation 1.7 Channel Response to Increased Discharge and Decreased Bedload Supply	12
Equation 1.8 Channel Response to Decreased Discharge and Increased Bedload Supply	12
Equation 1.9 Annual Channel Migration (Polygon Method).....	36
Equation 2.1 Single Point Root Mean Square Error (RMSE)	68
Equation 2.2 Total Image RMSE.....	69
Equation 2.3 Image Registration Error Vector	71
Equation 2.4 Image Registration X Directional Error	71
Equation 2.5 Image Registration Y Directional Error	71
Equation 3.1 Channel Response to Increased Discharge (Duplicate).....	126
Equation 3.2 Total Spatial Error (DOQs)	130
Equation 3.3 Total Spatial Error (Georeferenced Aerial Photographs)	131
Equation 3.4 Annual Channel Migration (Polygon Method) (Duplicate)	198

Appendix

Appendix A. Aerial Photograph Registry.....	256
Appendix B. “QuantifyingRegistrationError” MATLAB Script.....	262
Appendix C. Digitizing Error Quantification R Script	271
Appendix D. “ChannelChangeSignif” MATLAB Script.....	273
Appendix E. “Pre MATLAB Processing” Python Script	285
Appendix F. “csv_with_headers” MATLAB function	288
Appendix G. “Post MATLAB Processing” Python Script	290
Appendix H. Reach Break Down Justification	296
Appendix I. Annual Channel Migration by Year with and without Cutoffs	300

Appendix J. Channel Width Change by Year 305

Appendix K. Individual Reach Break Down of Platform Characteristics 308

“It is true that much recent geomorphic work is not concerned with the historical perspective; rather it is the working of and relation among the components of the system that have been of major concern (Hack, 1960, 1976). Thus it is possible to view the fluvial system either as a physical system or as a historical system. In actuality the fluvial system is a physical system with a history. Hence the objective of the geomorphologist is to understand not only the physics and chemistry of the landscape, but its alternation and evolution through time.”

-Stanely A Schumm, 1977

Chapter 1 : Literature Review

The research presented in this thesis quantifies and interprets historic geomorphic change within the Minnesota River floodplain of south-central Minnesota, USA. The primary focus is centered on quantifying planform channel change and the dynamics of historic channel migration using aerial photography and geospatial methods. This work is conducted in the context of significant riverine/aquatic environmental issues both within the Minnesota River watershed and in the Upper Mississippi River Basin to which it drains. Importantly, the Minnesota River watershed is an active, dynamic geomorphic landscape still adjusting to base-level lowering from outburst floods from proglacial Lake Agassiz between 13 and 14ka (Clayton and Moran 1982; Matsch 1983; Wright Jr, Lease, and Johnson 1998; Gran et al. 2013). Thus, natural rates of erosion and sediment transport are inherently high in this watershed (Gran et al. 2009; Belmont et al. 2011; Groten, Ellison, and Hendrickson 2016). More recently the Minnesota River watershed has experienced significant change in land cover, hydrology and nutrient/sediment loading possibly resulting from historic anthropogenic activities (Brezonik et al. 1999; Novotny and Stefan 2007; Musser, Kudelka, and Moore 2009; Schottler et al. 2014; Yuan and Mitchell 2014). Several researchers (Schottler et al. 2010; Belmont et al. 2011; Gran, Belmont, Day, Jennings, et al. 2011; Jennings, et al. 2011; Schottler et al. 2014.) have attempted to quantify, identify, and understand how anthropogenic influences are impacting the environmental issues of concern. However, despite the abundance of research investigating this watershed, a paucity of data exists regarding how the behavior and geomorphology of the Minnesota River has changed through time. Given this, the

Minnesota River serves as a poorly understood, ideal case study to examine how anthropogenic activity throughout a watershed impacts stream processes and floodplain geomorphology.

To investigate the planform channel change dynamics of the Minnesota River, a secondary focus of this thesis is to determine the most efficient and effective methodologies to accurately measure planform channel change. A thorough and comprehensive examination of error and uncertainty associated with geospatial techniques used in planform analysis is presented within this thesis. Unfortunately, it appears that compound error and uncertainty is often underestimated, not well-documented, and/or not consistent based on our examination of prior published research.

The remainder of Chapter 1 introduces the background literature pertinent to this thesis research. The chapter begins by examining the prior scholarly literature on planform analysis by defining what “planform analysis” is and discussing what others have done to understand the planform characteristics of fluvial systems. The chapter then transitions to a review of the controls on planform channel change and the dynamics of the fluvial channel itself necessary for interpretation of planform change. This is followed by a brief overview of prior methods utilized in planform change studies in the literature and the error and uncertainties inherent these methods. Finally, the chapter concludes with a synthesis of the geography, geomorphology and environmental context of this research in our study area, the Minnesota River Valley.

1.1 Overview and Importance of Planform Analysis

The umbrella term “channel planform” is used extensively in the literature of fluvial studies and simply refers to the pattern and form of a river when viewed from above (Rhoads 2003). Research on planform characteristics have been studied for well over a century and attempt to quantify geometric variables like sinuosity, stream length, channel width, and channel/meander migration (Davis 1889; Mackin 1948; Schumm 1979; Downward, Gurnell, and Brookes 1994; Gilvear, Winterbottom, and Sickingabula 2000; Rhoads 2003; Richardson and Fuller 2010; Block 2014). Most commonly associated with “planform” studies are investigations of lateral migration rates of rivers (Hickin and Nanson 1984; Shields, Simon, and Steffen 2000; Micheli, Kirchner, and Larsen 2004; Giardino and Lee 2011). Giardino and Lee (2011) make a vocabulary distinction between studies on meander migration and channel migration (or channel change) that will be used in the remainder of this thesis. They state that studies focused on meander migration are concerned with the measurements of discrete meanders (Motta et al. 2012), whereas the focus of channel migration accounts for lateral variations along a continuous channel (Urban and Rhoads 2003).

The reasons for studying planform channel change can vary significantly from trying to better understand the theoretical behavior of river morphology (Schumm 1985; Hooke 2003; Wickert et al. 2013) to more applied studies aimed at assessing how specific river reach behavior is influenced by variables within that study. Prevalent examples of stream/variable specific planform research include: reservoir impoundments/dams, riparian vegetation and land use, and hydrologic and climatic factors. Although it is

recognized that complete isolation of individual factors is improbable in a real world setting (Micheli, Kirchner, and Larsen 2004), these studies help move the science forward which can guide best management practices and aid the collective understanding of fluvial system variables when applied to geographically unique settings (Table 1.1; Shields et al. 2000).

Table 1.1: This table displays the literature covering variables that influence migration rates. It should be noted that often multiple driving and boundary variables are considered in any given study.

Variables Influencing Migration Rates	Summary	Citation
Reservoir/Dams	Reservoirs often reduce the rate of lateral channel migration by a factor of 3 to 6 as a result of reduced high flow frequency and duration.	(Bradley and Smith 1984; Shields, Simon, and Steffen 2000; Richard, Julien, and Baird 2005; Wellmeyer, Slattery, and Phillips 2005)
Riparian Vegetation / Land use	Riparian forest and vegetation has been shown to decrease the rates of channel migration, while land use activities that remove vegetation (e.g. agriculture) see an increase in lateral migrations.	(Garofalo 1980; Johannesson and Parker 1985; Odgaard 1987; Osterkamp, Scott, and Auble 1998; Micheli and Kirchner 2002; Micheli, Kirchner, and Larsen 2004)
Hydrologic and Climatic	As discussed earlier, the hydrologic regime of a river is a driving variable so it is commented on in nearly every planform study. However, certain studies focus specific attention on climatic variables (precipitation, discharge, temperature, etc.) more than others.	(Nanson and Hickin 1986; Giardino and Lee 2011; Yao et al. 2013; Block 2014)

The factors discussed above are of interest because they can change the morphology, behavior, and rates of change within a fluvial system. Meandering rivers have the capacity to degrade infrastructure (Haque and Zaman 1989; Larsen, Girvetz, and Fremier 2007), contribute to various types of pollution through sediment and nutrient loading (Dodds 2006; Petrolia and Gowda 2006), and create conditions leading to biological/ecological relationships among aquatic, riparian, and terrestrial zones within the river valley (Bunn and Arthington 2002; Grabowski, Surian, and Gurnell 2014). Each of these will be highlighted to provide examples of the importance of planform channel change analysis.

1.1.1 Infrastructure and Development

Entire cities and their inhabitants can be threatened by the erosional processes of channel migration down to rather mundane issues of protecting water pumps or parks (Haque and Zaman 1989; Micheli, Kirchner, and Larsen 2004; Larsen, Girvetz, and Fremier 2007). For instance, houses, buildings, bridges, and roads built in floodplains near actively migrating channels are at risk of being undermined and destroyed from channel migration. This often requires further preventative infrastructure to be placed to stabilize the channel which can be expensive and hinder natural processes leading to other adverse effects (e.g. ecological impacts). The societal impact of understanding and quantifying the planform characteristics and rates of change on a river is necessary to better plan future infrastructure and prioritize at risk infrastructure. In the 1970's, it was estimated that losses due to stream erosion were costing around \$270 million dollars in the United States alone (Lawler 1993), a number likely much higher today.

1.1.2 Pollutant Impacts on Humans and the Ecosystems

Pollutants entering the fluvial system are another concern. They can bind to sediment and be transported with flow and stored via deposition. As a channel migrates throughout a valley, it erodes sediment from cut-banks, bars, alluvial fans, and the surrounding floodplain; all of which are forms of alluvial sediment storage. Channel inundation, incision, and lateral movement serve as mechanisms to entrain these sediment sources via the stream's erosive processes (Macklin and Lewin 1989). Various pollutant problems like this are faced around the world from Waynesboro, Virginia, where a DuPont textile factory released thousands of pounds of mercury into the South River during the early to mid-twentieth century (Rhoades, O'Neal, and Pizzuto 2009) to the River South Tyne in northern England dealing with the legacy of heavy metals from mining operations which bind with sediment (Macklin and Lewin 1989; Miller 1997). The South River and South Tyne both have pollutants stored in their fluvial systems that are periodically re-activated as the channels erode depositional features entraining contaminated sediment. Pollutants like these are a concern for the biota but also can travel directly up the food chain to human consumption of fish (Sin et al. 2001). In the case of the South River in Virginia, mercury levels in fish still exceed state regulations fifty years after the contamination inputs were terminated (Rhoades, O'Neal, and Pizzuto 2009).

Another major contributor to river pollution comes from nonpoint-sources (NPS) associated with agricultural activities through application of herbicides and pesticides, tilling practices, and waste management. Although NPS are a nationwide concern, the Midwest agricultural industry applies millions of kilograms of active herbicide

ingredients to protect plants and increase yields which are then carried into lakes and rivers through precipitation events (Pereira and Hostettler 1993). These nutrients can then lead to excessive algae blooms creating anoxic conditions which kill native organisms both locally near the pollution source and extend far downstream (e.g. Gulf of Mexico Deadzone; Rabalais, Turner, and Scavia 2002; Dodds 2006)

Although bank erosion is a natural behavior of a river, it is often the human modification of the riparian corridor or watershed that alters flow regime, sediment regime, and longitudinal and lateral river connectivity (Grabowski, Surian, and Gurnell 2014). These engineered changes often come at the expense of the biota. A reduction in lateral movement caused by dams, bank stabilization mechanisms (i.e. rip-rap), and other river control structures change the mesohabitats of ecologic communities associated with the river (Shields, Simon, and Steffen 2000; Florsheim, Mount, and Chin 2008). Both bank stabilization and reduced high flows can cause reduced channel avulsions which will reduce key low-velocity habitats such as abandoned channels, backwaters, and oxbow lakes (Shields, Simon, and Steffen 2000). The activation of floodplains through bank erosion is a natural geomorphic process needed to promote healthy riparian ecosystems through vegetation succession and creating specific habitats that are crucial for both flora and fauna despite the human/political desire to stabilize the landscape (Florsheim, Mount, and Chin 2008).

It is being recognized that a middle ground approach is desirable when considering how to manage river channel dynamics (Grabowski, Surian, and Gurnell 2014). From a regulatory standpoint, many countries acknowledge the need to strike a

balance between human use and maintaining and preserving ecological diversity in riparian environments (Larsen, Girvetz, and Fremier 2007; Grabowski, Surian, and Gurnell 2014). This sociopolitical realm of balancing natural fluvial and ecological dynamics while maintaining economic and human stability is yet another reason why it is important to understand current and historical rates of planform channel change.

1.2 Understanding Fluvial System and Channel Change

In most simplistic terms, flow and sediment regimes are the two driving variables that dictate channel form and behavior. Within these two regimes countless other variables and relationships exist (e.g. geology, climate, anthropogenic impacts, etc.) and will be discussed later on this chapter. The purpose of the beginning of this section is to build a simplified conceptual framework. Both flow and sediment are constantly fluctuating through time causing sediment to be reworked by processes of erosion and deposition. Flow regime is governed by the precipitation within a drainage basin and is characterized by the frequency and magnitude of flood and drought events along with seasonal variations of precipitation. Sediment regime considers both the amount and the size distribution of the sediment present in a system (Schumm 1969; Charlton 2007).

When considering the relationship of changing flow and sediment on river morphology, a good starting place is with Lane's (1955) balance equation (Figure 1.1). Lane himself acknowledged that this equation is useful for qualitative analysis to better understand stream morphology problems. This concept balances sediment size and sediment load to stream slope and stream discharge. If a stream is in a state of equilibrium the scale will be balanced and the stream power will pass the sediment load

with no net erosion or deposition (Schumm 1969). However, if the sediment load or sediment size is increased the scale will begin to tip creating a condition for an aggrading stream with positive net deposition. Conversely, if discharge or stream slope is increased, conditions will set up for a degrading stream with positive net erosion (Charlton 2007).

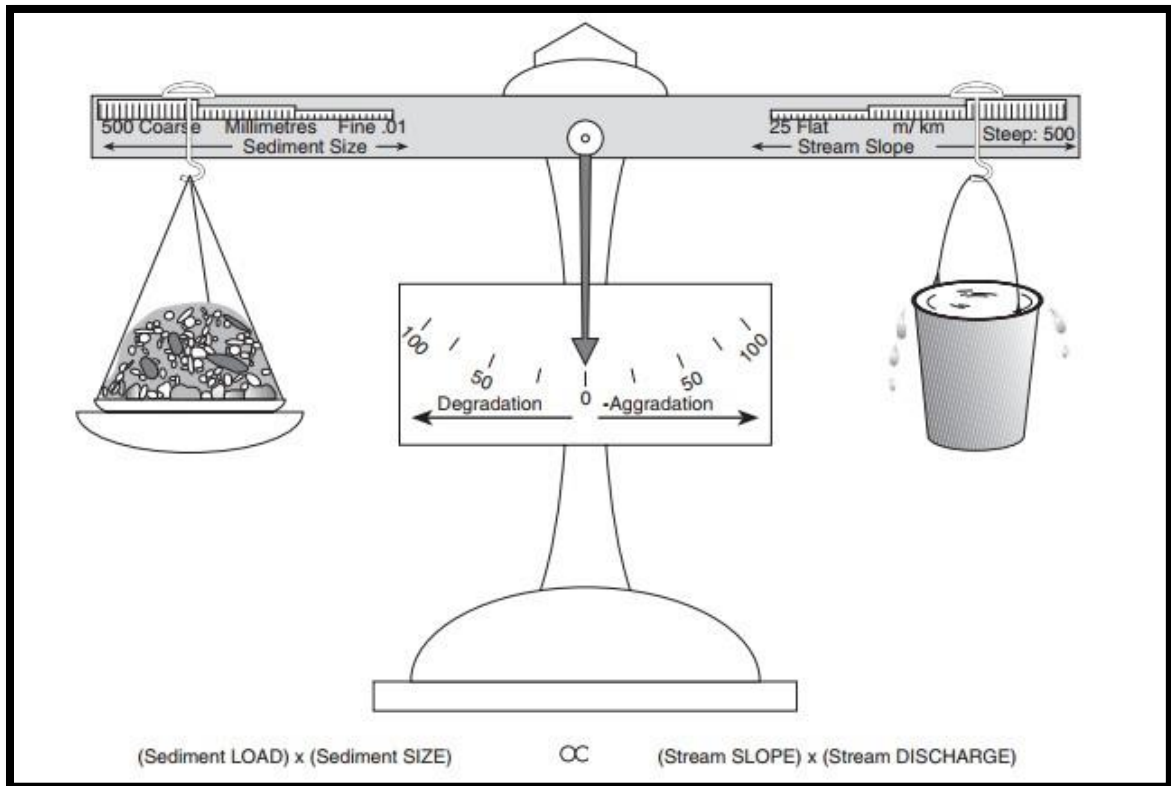


Figure 1.1: This figure from Charlton (2007) is an illustration to help visually interpret Lane's balance. Sediment load and size are represented on the left side while stream discharge and slope are represented on the right side.

These vertical adjustments (aggradation and degradation) of a channel are a system's response to flow and sediment changes in an effort to reach a state of equilibrium through a graded longitudinal profile. The concept of a graded stream extends back to Gilbert (1877) and Davis (1902) with a refined definition presented by Mackin (1948, p. 471) as follows:

“A graded stream is one in which, over a period of years, slope is delicately adjusted to provide, with available discharge and with prevailing channel characteristics, just the velocity required for the transportation of the load supplied from the drainage basin. The graded stream is a system in equilibrium; its diagnostic characteristic is that any change in any of the controlling factors will cause a displacement of the equilibrium in a direction that will tend to absorb the effect of the change.”

A system is never or rarely in equilibrium as there are constant fluctuations in discharge and sediment inputs (Knighton 2014) along with interruptions in the longitudinal profile that can arise from features like highly resistant substrate or anthropogenic modifications (e.g. dams). Therefore, the graded stream is best utilized as a conceptual framework for understanding what a river is attempting to accomplish.

Although Lane’s equation and the graded stream concept primarily focus on vertical movement of the channel (aggrading or degrading streambed), rivers are three-dimensional phenomena and planform characteristics of the channel are directly affected by the same forces that result in vertical fluctuations of the river. For example, a degrading stream will cut down into the stream bed that can lead to entrenchment and reduce or completely cut off the stream-floodplain connectivity. This creates steep unstable banks which can lead to bank failures and channel widening (Thorne et al. 1998). In the case of an aggrading stream, depositional features (e.g. mid-channel bars, point bars, etc.) will appear creating a channel that is wider and shallower. This can lead to an increased channel migration and greater likelihood of floodplain inundation

(Charlton 2007). These relationships will be discussed in further detail in section 1.3.2.2 (Thorne et al. 1998).

Schumm (1969) expanded concepts presented by Lane (1955) and others researching discharge, sediment, and gradient relationships on channel form including: cross-sectional response to gradient change (Mackin 1948; Rubey 1952), influence of mean discharge on channel width and depth (Leopold and Maddock Jr 1953), effect of discharge on meander dimension (Leopold and Wolman 1957; Dury 1964), and the relation of bed and bank material on width, depth, and width-depth ratios (Simons and Albertson 1960; Carlston 1965). The findings of Schumm (1969), later expressed by Charlton (2007), used the equations below for predicting potential basic channel response to changes in discharge (Q) and bedload supply (Q_b). The variables are as follows: discharge (Q), bedload supply (Q_b), channel width (w), depth (d), width-depth ratio (w/d), meander wave length (λ), channel slope (s), and sinuosity (S). Plus signs (+) indicate an increase while negative signs (-) indicate a decrease.

Discharge:

Equation 1.1

$$Q^+ \cong \frac{w^+ d^+ (w/d)^+ \lambda^+}{s^-}$$

Equation 1.2

$$Q^- \cong \frac{w^- d^- (w/d)^- \lambda^-}{s^+}$$

Bedload Supply:

Equation 1.3

$$Qb^+ \cong \frac{w^+ (w/d)^+ \lambda^+ s^+}{d^- S^-}$$

Equation 1.4

$$Qb^- \cong \frac{w^- (w/d)^- \lambda^- s^-}{d^+ S^+}$$

Both Discharge and Bedload Supply:**Equation 1.5**

$$Q^+ Qb^+ \cong \frac{w^+ (w/d)^+ \lambda^+}{S^-} d^\pm s^\pm$$

Equation 1.6

$$Q^- Qb^- \cong \frac{w^- (w/d)^- \lambda^-}{S^+} d^\pm s^\pm$$

Equation 1.7

$$Q^+ Qb^- \cong \frac{d^+ S^+}{s^-} w^\pm (w/d)^\pm \lambda^\pm$$

Equation 1.8

$$Q^- Qb^+ \cong \frac{d^- S^-}{s^+} w^\pm (w/d)^\pm \lambda^\pm$$

These theoretical relationships serve to build the conceptual framework for understanding how a fluvial system responds to change, particularly to variability in discharge and sediment supply.

Anthropogenic impacts (e.g. deforestation, river impoundment, etc.) often lead to these discharge and sediment supply changes and have the ability expedite and increase

the magnitude of channel adjustments compared to that of natural rivers notwithstanding a natural phenomenon (e.g. volcanic eruption, natural climatic variation, etc.; Surian and Cisotto 2007). For example, deforestation and agriculture lead to major increases in both sediment loading and increased peak discharges within fluvial systems (Naden 2010; Schottler et al. 2014). Conversely, sediment starved rivers exist due to the some 45,000 registered global reservoirs that store approximately 25-30% of global fine sediment (Vörösmarty et al. 2003; Naden 2010).

In reality, there are many complicated interrelated factors that dictate how a channel morphology develops (Figure 1.2; Schumm 1977; Knighton 2014). Often, both allogenic (external – e.g. anthropogenic activity, climatic change, base-level change) and autogenic (internal -- e.g. cut-offs, avulsions, bar deposition and erosion) changes are acting on streams (Charlton 2007). These internal and external factors are constantly changing in presence and magnitude and operate at process specific rates (Davis 1889; Schumm 1977) with furthering complexity from feedbacks. Feedbacks occur when a variable changes within a system thereby directly effecting one or more other variables within the same system. Positive feedbacks will enhance the original change often moving a system further from a state of equilibrium while negative feedbacks counteract the original change often dampening the effect (Charlton 2007). These complexities of a fluvial system create a vast number of outcomes for channel form dimension, rate, and magnitude, driving the need for stream specific research.

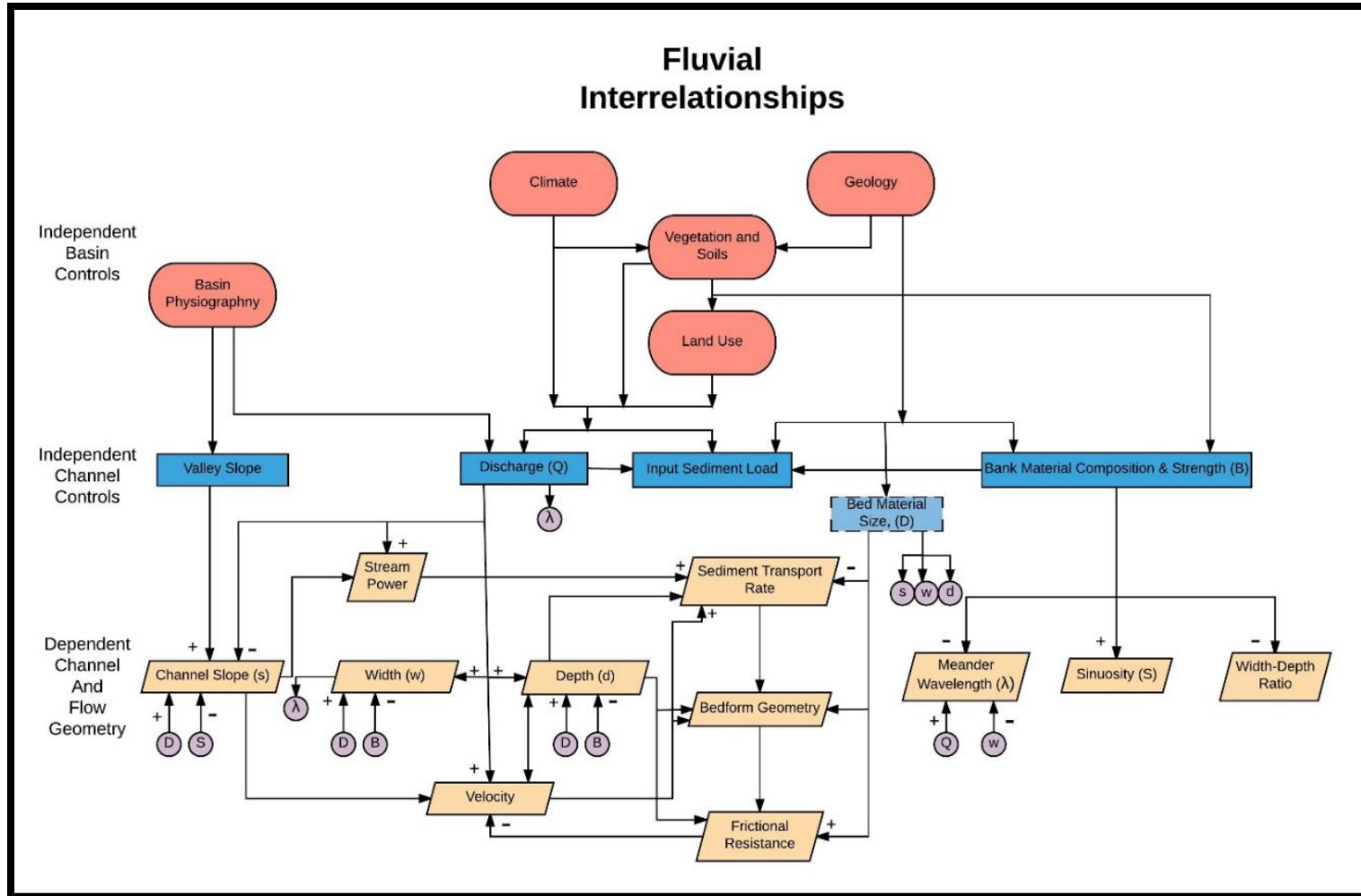


Figure 1.2: This figure was adapted from Knighton (2014) and shows the complexity of interrelationships with a fluvial system. (+) indicate positive relationships while (-) indicate inverse relationships.

1.3 Process of Channel Change

1.3.1 Channel Classification in Fluvial Studies

1.3.1.1 Channel Classification Based on Substrate

Montgomery and Buffington (1997) classified channel type based on substrate into three main categories: 1) bedrock, 2) colluvium, and 3) alluvium. Intuitively, bedrock channels are carved directly into the underlying bedrock and are characterized by lacking an alluvial bed, often found in confined, steep valleys, and can effectively transport the local sediment supply. Colluvial channels are most often associated with headwater streams eroding the surrounding hillslope and debris flows (primary erosion). Sediment transport in these reaches may be ephemeral and is less effective than bedrock channels at transporting sediment. Alluvial channels have a wider range of morphological characteristics causing Montgomery and Buffington (1997) to create five sub-categories, which, more broadly, all have characteristic beds consisting of alluvium (fluvially transported sediment) with sediment input from bank failures, hillslopes, and debris flows as well. The focus of this research is on those defined by Montgomery and Buffington (1997) as alluvial channels.

1.3.1.2 Alluvial Channel Classification Based on Channel Planform and Sinuosity

Leopold and Wolman (1957) classify alluvial rivers into three categories based on planform characteristics: 1) straight, 2) meandering, and 3) braided (including anastomosing).

Straight channels rarely occur naturally except in short reaches (Leopold and Langbein 1966; Dey 2014) and are defined by a sinuosity ratio of less than 1.1. Sinuosity

refers to how much a river bends back and forth, laterally, along its downstream course and is a function of valley slope and stream power (Figure 1.3; Dey 2014). The sinuosity ratio is calculated by taking the channel length and dividing it by valley length under normal bankfull conditions (Charlton 2007). “Under normal bankfull conditions” is an important distinction since the thalweg of a straight channel often shifts back and forth (evident in low flow conditions). The behavior of a streams shifting thalweg will be discussed later on in reference to meander formation (Section 1.3.2.1). Channels with a sinuosity ratio between 1.1 (straight channel) and 1.5 (meandering channel) are termed “sinuous” and are recognized as a transitional phase (Figure 1.3; Dey 2014).

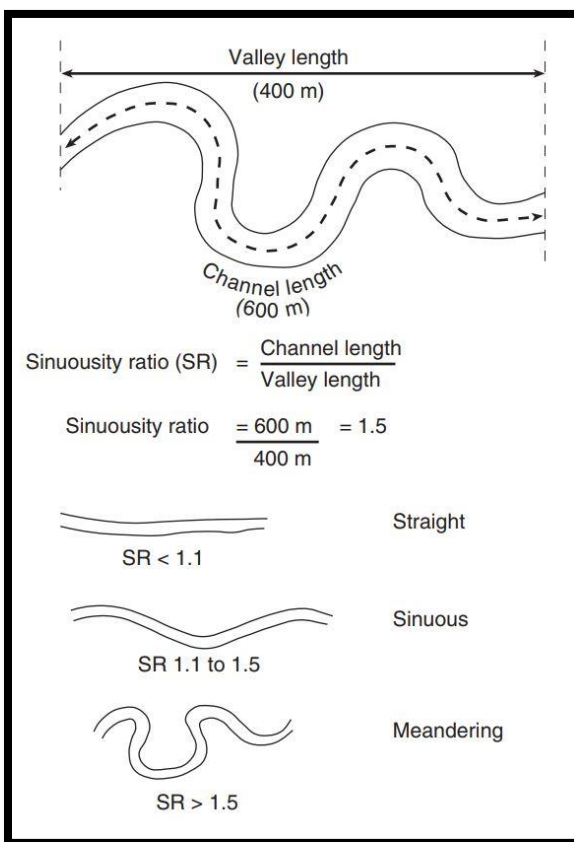


Figure 1.3: Sinuosity ratio definition and examples of straight, sinuous, and meandering channels from (Charlton 2007).

A channel is considered meandering when the sinuosity ratio is greater than 1.5 (Figure 1.3). Meandering channels are characteristic of low gradient systems where the river channel consists of a series of alternating bends/curves that are connected by points of inflection or the straight line “crossover” of the channel curvature (Leopold and Langbein 1966; Dey 2014).

Finally, braided rivers are characterized by the existence of multiple mid-channel islands or bars that divert flow into multiple branches. In high flows these bars may be completely submerged but become emergent in low flows. It is also common for braided channels to have one established main channel with multiple highly unstable subsidiary channels branching from it (Dey 2014). The focus of this research is predominately on sinuous to meandering channels.

1.3.2 Planform Channel Change in Alluvial Sinuous-Meandering Channels

In alluvial channels, the mechanism responsible for changing a river’s course is the ability of the flow to erode, transport, and deposit sediment from the channel bed and bank (Leopold and Langbein 1966). For erosion to occur, the flow’s stream power (function of discharge and slope) needs to exert a force on the channel bed/boundary which exceeds the resistance of the bed and bank material to erosion (Thorne and Tovey 1981). The erodibility of a channel can vary greatly from highly resistant bedrock channels to unconsolidated alluvial channels. Other than channel composition, many other factors influence a flow’s ability to erode sediment. For instance, much of the energy of flow is lost overcoming inherent frictional flow resistant forces of the channel boundary and the flow itself. Various vegetation types can influence a bank’s resistance to erosion depending on depth and type of root networks (Micheli and Kirchner 2002;

Simon and Collison 2002). Land use changes (e.g. forest to agriculture) can remove this stability all together making banks especially susceptible to erosion (Simon and Collison 2002; Micheli, Kirchner, and Larsen 2004; Charlton 2007;).

1.3.2.1 Channel Migration and Meandering

Giardino and Lee (2011) differentiate between channel migration and meander migration by stating that channel migration considers a continuous channel while meander migration is concerned with discrete meanders. The primary focus of this research is on channel migration, however; working knowledge of the driving forces behind meander migration is necessary to understand what may be driving temporal, spatial and study reach variability in channel migration.

Understanding and predicting why rivers meander has been of great interest to mankind for centuries. In fact, the word “meander” traces its origin back to the ancient Greek city of Miletus that overlooked the river known as Maeander (Baker 2013). Even the great minds of Albert Einstein and Leonardo Da Vinci pondered the nature of meandering rivers (Einstein 1926; Baker 2013). Despite this lengthy curiosity in meandering rivers, with many hypotheses and general concepts surrounding meander formation and prediction, a comprehensive, holistic theory is not yet fully developed, and no singular consensus is agreed upon (Charlton 2007; Kleinhans 2010). In what follows, we will explore the research and hypotheses surrounding meander development.

Keller (1972) developed a five-stage conceptual model of meander formation that begins with 1) alternating bar formation leading to 2) pool and riffle formation which 3) promotes further erosion on the outside banks leading to 4) bend formation which is then 5) further extended creating additional riffles and pools to the lengthened channel.

Keller's stage 1 and 2 development is supported by Leopold and Wolman's (1957) research showing "the wandering thalweg" that exists in a straight channel causing, at least in part, the development of pool, riffle, and alternating bars. This helped advance Schaffernak's (1950) observation of alternating mud deposits adjacent to the banks in straight channels, which resembling meanders.

In river channels, lateral erosion is driven by centrifugal acceleration into, and secondary helical motion eroding, the concave outer bank (cut bank) -with subsequent point bar deposition on the convex inner bank downstream where velocity slows (Figure 1.4A; Dey 2014). This process both destroys and creates the floodplain simultaneously (Kleinhans 2010). Cut bank erosion often occurs in a two-step process. First, the river itself erodes the lower portion of the bank through direct contact with the flow (Thorne and Tovey 1981; Darby, Rinaldi, and Dapporto 2007). Second, bank failure occurs by mass wasting from the undermined cut-bank. This directly contributes sediment to the channel, as well as deposits at the toe of the bank which can be easily be entrained by the flow (Thorne and Tovey 1981; Osman and Thorne 1988; Kleinhans 2010). Hickin and Nanson (1984) specifically identify variables likely influencing channel migration as: stream power (rate at which work can be carried out) per unit channel/bed area, the opposing/resistive force per unit boundary area resisting migration, bank height, bend radius, and channel width. This is yet another example of the complexity of factors effecting varying rates of channel migration.

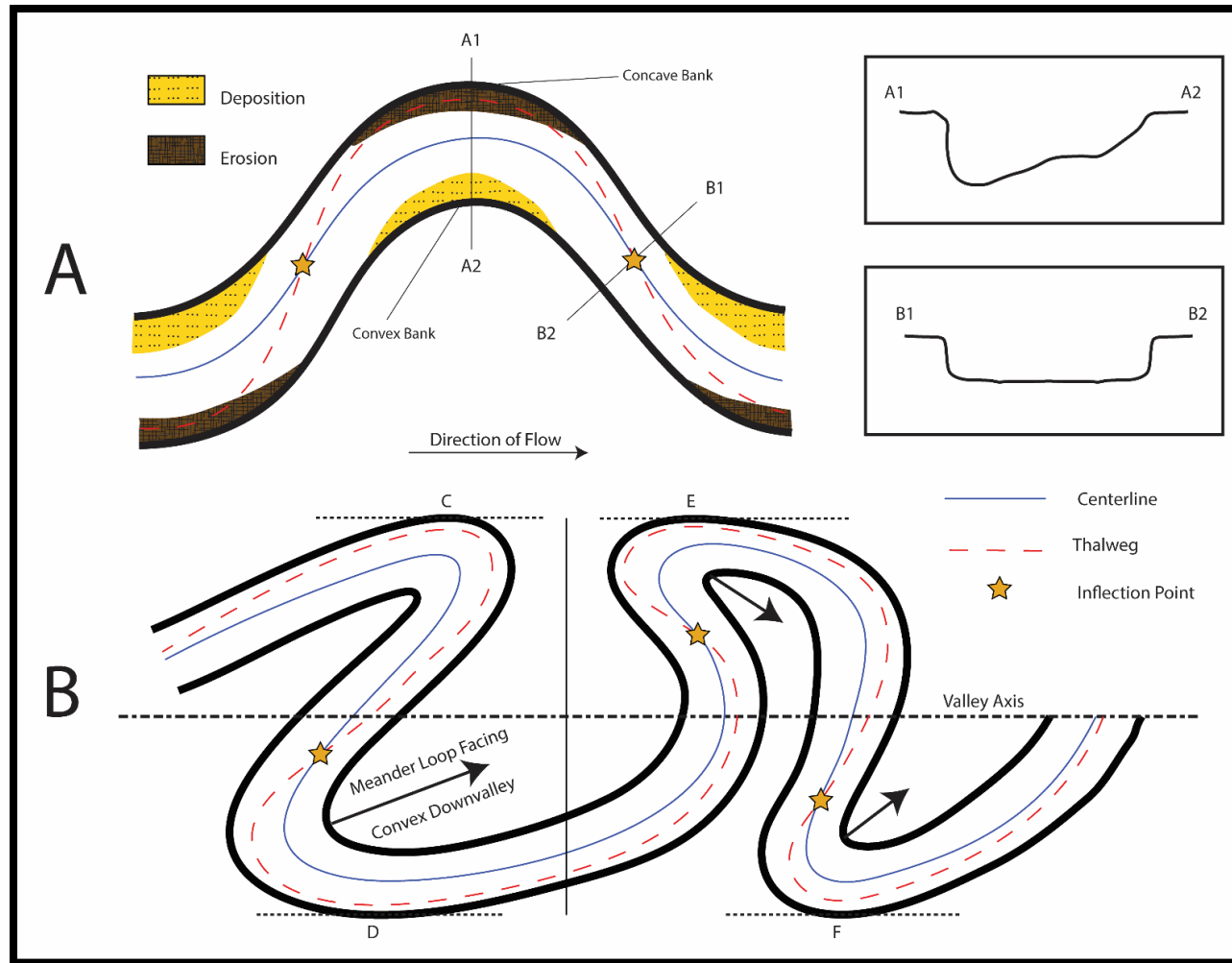


Figure 1.4: **A.** Depicts a simplistic example of a meander with erosion concentrated on the outer (concave) bank and deposition occurring on the inside (convex) bank. On the right, cross sections of pool (A1 to A2) and riffle (B1 to B2). **B.** This represent a tortuous meander with delayed inflection points and resulting meander loops facing convex down valley.

Because of these various factors, rivers rarely have uniform sine-generated curves as conceptualized by Leopold and Langbein (1966), but rather are riddled with asymmetries and can even appear completely chaotic at times (Carson and Lapointe 1983). Local bank erodibility characteristics strongly influence meander irregularities from areas of higher or lower resistance to erosional forces (Dey 2014). This is also evident in the various planform patterns that are seen in meandering streams (Figure 1.5).

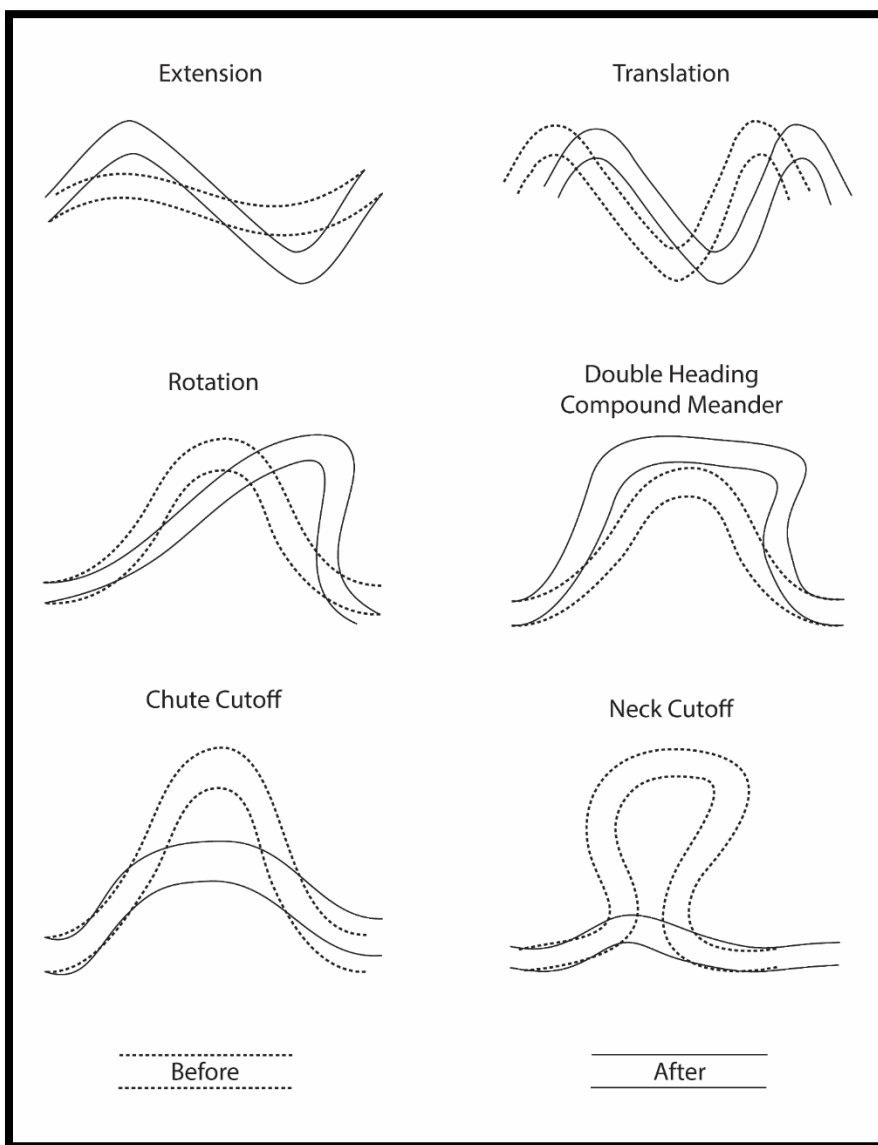


Figure 1.5: Variable patterns of meander development and change.

In sand bed channels, irregularities in meander dimensions can also be strongly influenced by delayed inflection points (Carson and Lapointe 1983; Dey 2014). Delayed inflection points occur when the inflection point alternates between sides of the valley axis, hence “delaying” it (Figure 1.4B). Another way of thinking about this is that the inflection point is further downstream than the midpoint between meander loops (Robert 2014). This is attributed to the delay of the thalweg crossover which is directly related to the inertia of the flow (Carson and Lapointe 1983). This irregularity results in meander loops oriented convex down-valley (inner bank facing in the down valley direction opposed to the valley walls; Figure 1.4B). This process is noted as being especially prevalent in rivers carrying a large amount of suspended load (Carson and Griffiths 1987).

Since river channels migrate both transversely and downstream at variable rates, it is no surprise that cut-offs are a natural process of meandering river evolution (Dey 2014). Cut-offs are simply the abandonment of meander loops and come in two main types: 1) Neck (more prevalent) and 2) Chute (Figure 1.5; Charlton 2007; Knighton 2014). In a neck cut-off, as the meander loop shifts and grows, the upstream and downstream channel will come closer together creating a “bulb” formation. The “neck” will then breach thereby abandoning the meander loop. A chute cut-off is formed in flood conditions where flow inundates and incises into the floodplain creating a “chute” which becomes the new primary channel (Hooke 1995; Gay et al. 1998; Dey 2014;). In both cases, the abandoned meander loop will become an oxbow lake slowly in-filling

over time. The new channel will experience a decrease in stream length resulting in a greater localized slope (Charlton 2007).

Dey (2014) highlights a handful of concepts regarding the cause and overall understanding of meanders contributed by various literature. Table 1.2 summarizes these concepts, but special attention will be given to the “Instability Concept” due to its specific insight and use it provides to the research presented in this thesis. This concept reveals that irregularities or perturbations in the upstream relate to modified structure in the downstream regime leading to meandering. This could result from sediment deposition on the bed (Griggs 1906), velocity changes due to turbulence (Hjulström 1957), or oblique entry of flow in a channel (Friedkin 1945).

Table 1.2: This summarizes a handful of important concepts and insights that have contributed to the literature regarding cause of meandering in rivers and understanding of the mechanism of meander development.

Concept	Summary	Contributing Literature
Earth's Revolution	The Coriolis effect influences erosional tendencies in the north and south hemisphere and induces rotational motion into the flow (helicoidal flow).	(Gilbert 1884; Eakin 1910; Lacey 1923; Einstein 1926; Chatley 1938; Quraishy 1943; Neu 1967)
Instability	<i>See paragraph above</i>	<i>See paragraph above</i>
Helicoidal Flow	Secondary flows initiate meandering followed by secondary currents of Prandtl's first kind (helicoidal flows) being the governing mechanism thereafter.	(Prus-Chacinski 1954; Leliavsky 1966; Onishi, Jain, and Kennedy 1976)
Excess Flow Energy	Flow meanders to reduce energy excess energy which reduces slope and increases stream length. Arguments of meanders being the mechanism for minimization of energy are countered by a near-equilibrium river finds a meandering course allowing for the minimum time rate of energy expenditure.	(Schoklitsch 1937; Inglis 1947; Leopold and Wolman 1960; Yang 1971)
Large Scale Eddy	Large scale eddies or large scale turbulent structures initiate alternating bars and meanders.	(Yalin and Da Silva 2001)

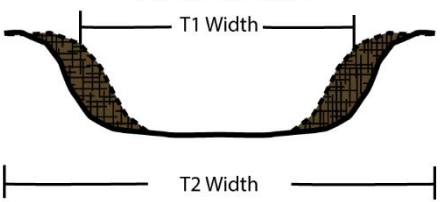
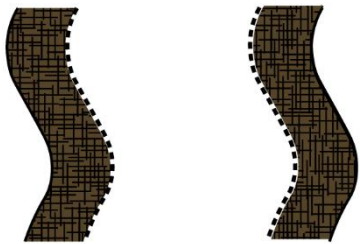
1.3.2.2 Channel Width

Although channel and meander migration receive most of the attention in planform channel change studies, channel width is another important planform characteristic to consider. Width change impacts those living in floodplains, riparian ecosystems, bridge crossings, and any other developed structures (e.g. rip-rap, pump houses, etc.). Channel width change is also an indicator that fundamental inputs (e.g. discharge, sediment supply) are changing within a fluvial system as well (refer to section

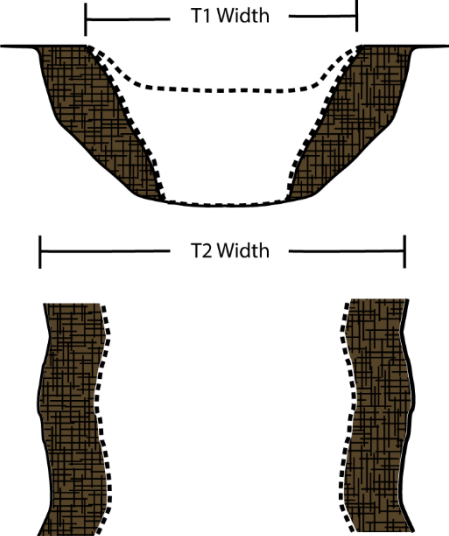
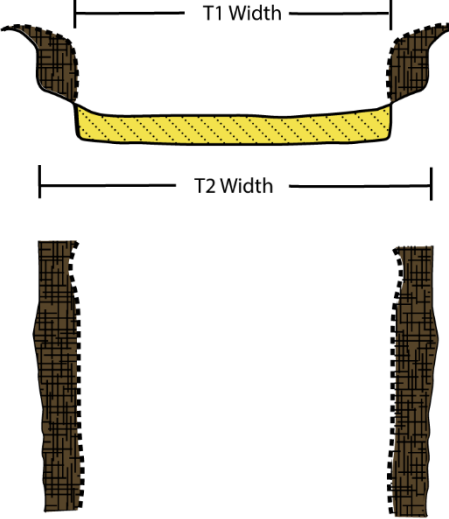
1.2). Width change can result from bank erosion, bank accretion, or channel bank abandonment when a river channel changes course (Thorne et al. 1998). Channel width changes can come through either narrowing or widening of the channel, but the primary consideration moving forward will be on channel widening.

Thorne et al. (1998) formed a Task Committee (TC) of the American Society of Civil Engineers (ASCE) to study the hydraulics, bank mechanics, and modeling of width adjustments in alluvial channels as well as providing review of width adjustment processes and mechanisms. They identified five major processes under which a channel widens which is summarized in Table 1.3.

Table 1.3: This table is adapted from the information and figures found in Thorne et al. (1998). This table serves to summarize major channel widening processes with graphical representations and supporting documentation.

<p style="text-align: center;">Process</p>	<p style="text-align: center;">Graphic</p> <p style="text-align: center;">Erosion Deposition</p> <div style="display: flex; justify-content: center; gap: 10px;"> <div style="border: 1px solid black; width: 20px; height: 20px; background-color: #444;"></div> <div style="border: 1px solid black; width: 20px; height: 20px; background-color: #fff; border-style: dashed;"></div> </div> <p style="text-align: center;"><i>(Next 3 Pages)</i></p>	<p style="text-align: center;">Supporting References as cited by Thorne et al. (1998)</p>
<p>A) Channel enlargement from erosion of both banks without channel incision</p>	<p style="text-align: center;">Cross-Section</p>  <p style="text-align: center;">Plan View</p> 	<p>(Everitt 1968; Burkham 1972; Hereford 1984; Pizzuto 1994)</p>

<p>B) Accelerated meander growth from erosion on the outer bend occurring more rapidly than deposition on the inner point bar</p>		<p>(Nanson and Hickin 1983; Pizzuto 1994)</p>
<p>C) Mid-channel accretion deflecting flow towards outer banks (typical in braided systems)</p>		<p>(Leopold and Wolman 1957; Bristow and Best 1993; Thorne, Russell, and Alam 1993)</p>

<p>D) Channel incision followed by unstable bank failures and retreat</p>		<p>(Thorne, Murphey, and Little 1981; Little, Thorne, and Murphey 1982; Harvey and Watson 1986; Simon 1989)</p>
<p>E) Bank erosion following channel aggradation in coarse bed streams causing flow acceleration from reduced cross-sectional area</p>		<p>(Simon and Thorne 1996)</p>

There is a great deal of crossover between channel migration and width adjustment processes. The variables and erosional mechanisms considered in both processes are largely the same extending the complexity and insufficient understanding seen in channel migration to channel width adjustment as well (Smith and Smith 1984; Charlton 2007; Dey 2014). However, when considering a meandering alluvial river in

equilibrium, there is a major difference between channel migration and channel width. The difference being that the channel will continue to migrate across its floodplain while maintaining the balance between sediment and flow (Figure 1.1), whereas, a meandering alluvial channel in equilibrium should remain stable in terms of width adjustment. Large floods or extreme events may temporarily impact channel width, but, with sufficient time, the width will recover (Thorne et al. 1998).

Therefore, a system undergoing width adjustment change is an indicator the system is reacting to a disturbance in sediment regime or flow regime (Schumm 1969; Smith and Smith 1984; Charlton 2007; Lauer et al. 2017). These disturbances could be a natural process of the river on its course to finding an equilibrium or could be due to anthropogenic influences changing the natural condition of the system or both. Some examples of these include: changing valley slope (Patton and Schumm 1975; Daniels 2003), change in riparian vegetation through succession or human modification (Huang and Nanson 1997; Hession et al. 2003; Tal et al. 2004; Tal and Paola 2007), climate change (Hereford 1984; Arora and Boer 2001; Goudie 2006;), and land-use changes with watersheds (Dunne and Leopold 1978; Booth and Jackson 1997).

1.4 Methodological Considerations for Understanding Planform Change

1.4.1 Range of Techniques

When considering how to quantify channel change, it is important to consider not only the spatial scale of the study reach necessary to address your research question(s), but also temporal scale of concern when determining the appropriate methodology

(Grabowski, Surian, and Gurnell 2014). Lawler (1993) provides a thorough review of the various techniques applied in bank erosion and lateral channel change studies to bring standardization to a subject that is broached by numerous researchers with distinctive discipline-specific goals. That review links various techniques to the appropriate temporal scale (expressed as “long, intermediate, and short”), as well as assessing the “accuracy and repeatability” of the given methods. He identifies seven main techniques including: sedimentological evidence from valley-fills, botanical evidence from floodplains, serial historical sources, repeated planimetric surveys, repeated cross-profiling, erosion pins, and repeated terrestrial photogrammetric surveys. Table 1.4 serves as an overview of the delineations made by Lawler (1993).

Table 1.4: This table summarizes the seven major techniques identified by Lawler (1993) along with associated problems and the temporal scales appropriate for the study and the resolution at which the data can be collected.

Temporal Scale	Techniques	Associated Problems	Time Scale of Interest	Resolution of Data
Long	Sedimentological Evidence- Assessing the stratigraphy fluvial deposits through various dating techniques.	Difficult to interpret do to stratigraphic complexities, Need a persevered deposit, Interpretations are not guaranteed to be correct	50 – 15,000 years	10-100 years
	Botanical Evidence –Various methods but primarily dendrochronological dating of floodplain surfaces.	Unsteady rates at which trees recolonize point bars, Climatic variabilities further convoluting colonization rates, Absent or double tree rings caused by stressors, limited to areas with arboreal vegetation	50 – 1000 years	~ 8 – 80 years with several studies around 25 -30 years
	Historical Sources – using various sources including older maps, surveyor notes, journal information but most commonly aerial photography. From these sources the channel of the stream is plotted and often overlaid with other years channel course for analysis	A specific region is highly dependent on the availability to these types of sources for this technique to be a viable option. The resolution of data is often rather coarse and simplifies the complexity between years of record. Other problems include error in the data sources along with inherent errors associated with surveyor biases and miscommunications on early maps.	10- 150 years	~ 1 – 30 years
Intermediate	Planimetric Resurvey – A variety of different planform survey techniques employed in the field followed by resurveys which are then used for comparison and measurement.	Certain techniques like chain-and-offset mapping suffer from replicability issues, while all are vulnerable to the interpretation of the field surveyor to channel boundary delineation.	~ 1 – 30 years	~ 0.1 – 3 years
	Repeated Cross Profiling – Tracking bank movement/erosion by mounting permanent place marker for repeatability of cross-sections.	This section has in depth discussion on proper decision making, procedures, and precautions related to choosing cross-sections, level positions, role of the staff person and positioning, and calculation of technique precision	~ 1 – 30 years	~ 0.05 – 3 years
Short	Erosion Pins – By inserting a rod into a stream bank, rates of erosion can be measured as more of the rod becomes exposed. This can be done at specific flows to also help understand the driving variables of erosion. This process is simple, cheap, sensitive, and can be used in various environments.	It is difficult to get a good spatial distribution because a pin measures a site specific erosional rate that does not necessarily correspond to the entire bank. Readings can also be in error if the bank swells or contracts or if the pin is moved or even lost. Another concern is the various impact the pin itself has on erosional rates	0.5 -10 years	1 day to < 1 year
	Terrestrial Photogrammetry – A technique that employs repeated photography of a river bank that is then turned into a three dimensional model that can then be quantified to measure erosion rates. This method shows erosion for the entire site without interfering with the natural processes. It also has the advantage of collecting other site features like vegetation as well.	The disadvantages include a sights lighting characteristics can hinder the ability to get quality photographs, the scale of the river including both rivers that erode at too slow of a rate and ones that are so wide that the camera to bank distance is too far and causes high errors. Another drawback to studies like this include a fairly significant start-up cost to get all of the equipment.	0.5 -10 years	1 hour – 1day

Another rapidly developing technique to determine soil erosion is the use of radionuclide tracers including unsupported or excess lead-210 (^{210}Pb) and artificial radioactive fallout from nuclear weapon testing like Cesium-137 (^{137}Cs) (He and Walling 1996; Zapata 2003; Belmont et al. 2011; Matisoff and Whiting 2012). The concept is relatively basic. Over a given area, a uniform distribution of radionuclide fallout occurs, primarily by rainfall, which is strongly absorbed by surface soil particles. Therefore, redistribution of the tracers indicates the redistribution of the sediment. Depending on the tracer, the origin, fallout record, and half-life used for dating there are various options depending on the temporal scale and spatial location (He and Walling 1996). This makes the tracers valuable indicators for tracking the soil's physical movements including: initial erosion, delivery process, and ending deposition (Ritchie and McHenry 1990; He and Walling 1996). For example, Black et al. (2010) used ^{210}Pb to specifically look at the migration rates of three different rivers in the eastern United States. These results were compared to and agreed well with independent migration rates for the same study area obtained through a commonly used technique of registering and superimposing historical aerial photographs using Geographic Information Systems (GIS). This common technique of using GIS is the primary method utilized in the research presented in this thesis and will be the focus moving forward.

1.4.2 Geographic Information Systems and Planform Analysis

Using GIS for tracking historic channel change has drastically transformed the ability for researchers to understand channel change dynamics. A major advantage of a GIS environment is the versatility of the software to run multiple functions and computations using automated processes — a method that is effortless when compared to

Hickin and Nanson (1984) superimposing various years of river channels using transparencies and a projector to detect channel change. GIS also enables data and results to be stored and accessed with ease in future land use planning and channel change monitoring beyond the life of the initial study (Micheli, Kirchner, and Larsen 2004).

For the capabilities of GIS analysis to be of any use in channel migration studies, four steps need to be conducted: 1) Data Acquisition, 2) Image Registration, 3) Bankline Digitization, and 4) Planimetric Channel Change Calculation. Since these are methods-based processes, these steps, as well as the error and uncertainty associated with them, are covered in detail in Chapter 2 (process 1-3) and Chapter 3 (process 4), but a brief overview of the literature regarding these steps will be provided in this section.

1.4.2.1 Brief Summary of the Four Major Processes

The first step to use GIS to quantify historical channel change is acquiring historical planimetric data. Historical planimetric data includes: topographic maps, historical surveys, satellite imagery, and aerial photography (Lawler 1993; Gurnell 1997; Giardino and Lee 2011). Aerial photography and satellite imagery offer historical context which is an indispensable tool for geomorphologists and all geographers to help isolate variables of complex environmental issues that are further complicated by natural and anthropogenic influences (Trimble and Cooke 1991; Winterbottom 2000). Remotely sensed imagery offers viewers a planform (or in some cases oblique) visual of the landscape at a given moment in time. These snap shots of the past become even more useful to understanding continuous processes when imagery can be collected over numerous years for the same area of interest (see 2.1.1 and 2.2.1).

Once planimetric data is obtained it needs to be incorporated into GIS so channel change measurements can be calculated (Hughes, McDowell, and Marcus 2006). First, this requires having all the planimetric data in digital format, if it is not already. If the digital imagery is lacking a coordinate system (unreferenced), it needs to be referenced using discrete points throughout the image to match it to a referenced base image. This process is known as image registration (see section 2.1.2, 2.2.4) and will be referred to as such throughout the thesis but is also known as georeferencing. Image registration is often necessary since historical aerial photographs are frequently obtained as image files (e.g. .jpeg or .tiff) without any accompanying spatial reference (Chang 2014).

When all the imagery is registered, the banklines of the river for each year can be digitized (see 2.1.3, 2.2.4). These banklines serve as the input data for calculating planform channel change. In this thesis, width and channel migration were calculated using the National Center for Earth Surface Dynamics's (NCED) Planform Statistics toolbox (Lauer 2006).

The tools within the NCED toolbox create river centerlines from the bankline data along with tabular width measurement data (see 3.2.2). The centerlines are then able to be superimposed to calculate channel migration measurements (see 3.2.1). The centerline data was further used to calculate sinuosity data using standard ArcMap tools and editing functions (see 3.2.2).

1.4.2.2 Data Classification: Primary vs Secondary

Steinberg and Steinberg (2015) distinguish GIS data as either primary or secondary. Primary data is “data collected directly by the research staff for the specific project” and secondary data is “data collected by someone else, for a different purpose”

(p.121-122). Since a study like this is historic in nature, the existence and availability of secondary data (aerial imagery) becomes the most crucial part of the project. If the imagery is not available, a different approach will have to be used. If the imagery is available, then primary data (digitized banklines) can be created and measurements can be made. The distinct advantage primary data offers is the control given to the researcher to create study-specific inputs that remain valid and reliable throughout all data sets if integrity measures are maintained. The major disadvantage of primary data is that it can require copious amounts of time and often large amounts of money to create. Secondary data on the other hand can often be acquired for free (sometimes with a simple download), but compromises are made in the form of study specific control in which things like poorly documented metadata can create further uncertainty in the research (Steinberg and Steinberg 2015).

Although the raw aerial photographs themselves are secondary data, the unique collection of photographs acquires some characteristics of primary data since it is pulled from multiple sources and further processed through image registration; a method in which user-defined parameters are set. This new set of data could be viewed as a hybrid data type that shares qualities of both primary and secondary data. The theoretical understanding of the data is important to consider because error is not always properly documented when secondary data sources are made available compounding the uncertainty of the error within the study. The next section will highlight this process of taking raw aerial imagery and processing it in a GIS environment.

1.4.2.3 Error, Uncertainty, and Inconsistencies

Lawler (1993) identifies “methodological incompatibility” as a major issue when comparing the results of multiple studies that use a wide-range of techniques (Table 1.4) to measure erosion and lateral channel change. This concern is equally applicable when considering the quantification of error and uncertainty and methodological incongruities that can transpire during remote analysis with superimposed data created from aerial and satellite imagery (Chrisman 1982; Unwin 1995; Leung and Yan 1998; Mount et al. 2003; Mount and Louis 2005; Hughes, McDowell, and Marcus 2006;).

The first major source of error introduced is during the image registration process. The error is present from both inherent geometric distortion in the photograph and potential introduced error from user selected ground control points (GCPs), which are used to tie-together and warp an image to a coordinate system (see 2.1.2, 2.2.2-3). The second major source of error is introduced during bankline digitization through misidentification or uncertainty in the location of the channel bank. Digitization error can result from visual obstructions (tree canopy, bridges, shadows, etc.), imagery resolution/scale, or simply by careless digitization (see 2.1.3 2.2.4-5). These two major sources of error have been recognized (Mount and Louis 2005; Hughes, McDowell, and Marcus 2006; Lea and Legleiter 2016), yet there has been no uniform approach to quantifying this error, which leads to inconsistencies hindering comparative analysis among different studies and researchers.

Beyond inconsistencies in error quantification, there have also been different approaches used to calculate channel migration. One approach uses the intersection of centerlines from two time periods to create polygons (Figure 1.6A; Giardino and Lee

2011; Urban and Rhoads 2003). Then the following equation is used to calculate a migration rate:

Equation 1.9

$$R_m = \frac{A}{L} / y$$

Where R_m = migration rate, A = the area of the polygon, L = the length of the centerline of the earlier time period, and y = is the number of years between the centerlines. This approach is less prevalent but is still seen in past literature (Urban and Rhoads 2003; Giardino and Lee 2011) and requires evaluation since it creates a methodological inconsistency in channel migration calculation. This “Polygon Method” will be further examined in Chapter 3 (see 3.4.1.1).

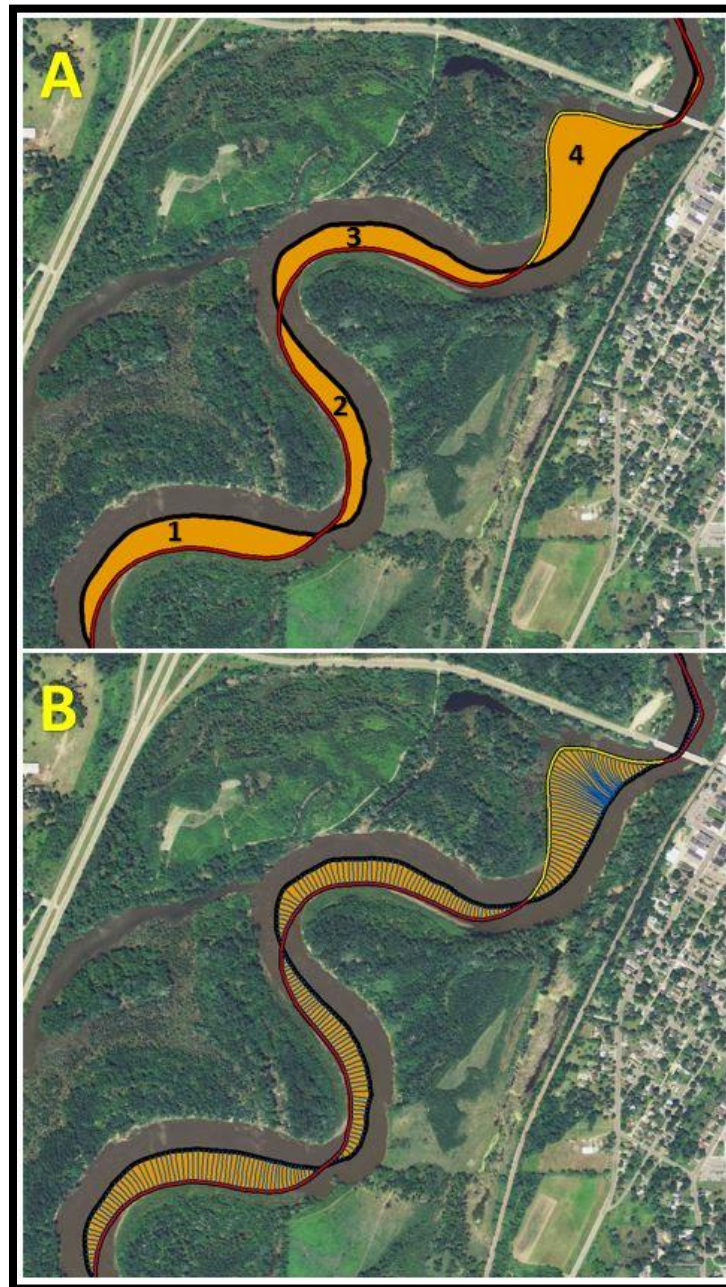


Figure 1.6: A) This figure displays the inputs needed in order to calculate channel migration using the polygon method. For each orange polygon (1-4), the red centerline (T1) length is used to divide the area of the polygon. Polygon has this measurement highlighted in yellow. This number is then divided by the number of years between the centerlines. In the example above, twenty-two would be used since the two input centerlines are 1991 (Red) and 2013 (Black). B) This shows an example of the trajectory lines (Blue lines) created using the planform statistics toolbox. The user defined intervals selected was ten meters therefore a new trajectory line or measurement is generated laterally between the centerlines for every 10 meters in the downstream distance.

The more commonly used method for measuring channel migration is conducted by creating trajectory lines at user defined intervals to measure the linear distance between centerlines from different years (Figure 1.6B). This process can be automated using recently developed ArcGIS toolboxes. Block (2014) used a toolbox from ET Geo Wizards (available at <http://www.ian-ko.com/>). Another set of ArcGIS tools is available in the Planform Statistics toolbox from the National Center for Earth-Surface Dynamics (NCED) Data Repository (available at <http://www.nced.umn.edu/>) and has been highly utilized (Aalto, Lauer, and Dietrich 2008; Gran et al. 2009; Belmont et al. 2011; Wohl 2012; Legleiter 2014). Lea and Legleiter's (2016) error assessment for image registration error (discussed above) integrates the Planform Statistics toolbox within their methodology.

The quantification of error and uncertainty has traditionally been ignored in geomorphological studies, but in more recent years has gained recognition as an independent research subject (Mount and Louis 2005; Hughes, McDowell, and Marcus 2006). Properly identifying the amount of geospatial error in a repeatable, standardized manner is essential to produce accurate, comparable results between researchers and their studies. In addition, a consideration that is surprisingly missed in some studies is that river channel change can only be considered valid if the amount of change exceeds the potential error that is present (Gurnell, Downward, and Jones 1994; Mount and Louis 2005). Standardizing the methods for quantifying channel change characteristics is also important so future studies can be used in comparative analysis to further the understanding of planform channel change at a particular site. Therefore, understanding

error in each of the four steps is extremely important in any planform channel change study.

1.5 Study Area: Minnesota River

1.5.1 Overview

The Minnesota River originates at Big Stone Lake on the South Dakota/Minnesota border in the upper Midwest USA. The Minnesota flows in a southeasterly direction until taking a sharp N-NE bend in Mankato and until it reaches the Minnesota-Mississippi confluence near St. Paul, Minnesota. The river's course totals ~540 kilometers (335 miles) and has a low, average gradient (approximately 0.15 meters per kilometer or 0.8 feet per mile), dropping a total of 274 feet from the headwaters to its confluence (Figure 1.7, Minnesota River Basin Data Center [MRBDC], 2003). The Minnesota River is also the state's largest tributary to the Mississippi River and doubles the Mississippi's flow upon convergence (MRBDC 2011).

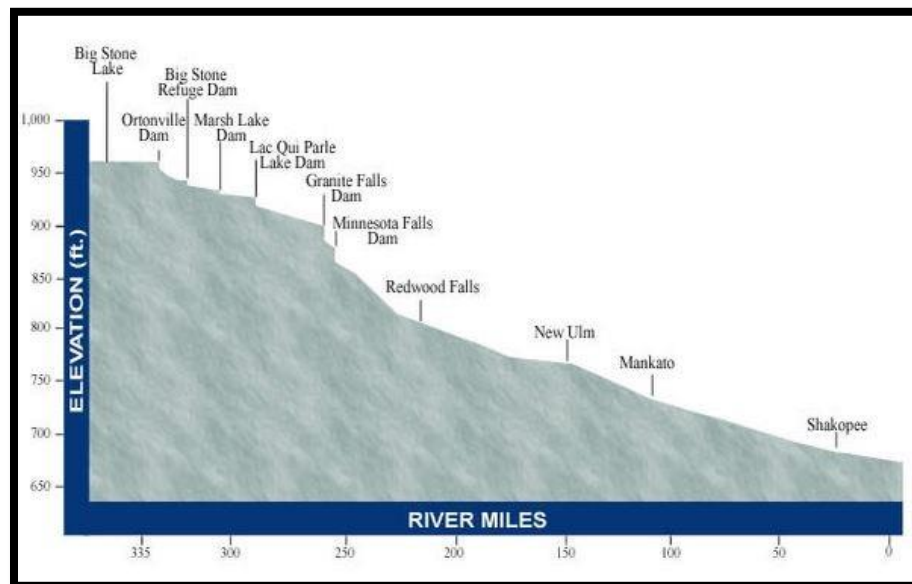


Figure 1.7: This figure graphically represents the low gradient on the Minnesota River with major dams and cities marked (MRBDC 2003).

The Minnesota River Basin (MRB) covers ~44,000 square kilometers (17,000 square miles) and drains approximately 20 percent of the state of Minnesota (all or part of 38 counties), as well as parts of North Dakota, South Dakota, and Iowa (Figure 1.8). The MRB consists of 12 hydrologic major watersheds and 13 management watersheds as well (Johannesson and Parker 1985; Novotny and Stefan 2007; MRBDC 2011). Originally, the MRB was predominately prairie pothole wetlands, yet few remain in the landscape today because of drastic alterations through conversion to agricultural land use (Musser, Kudelka, and Moore 2009; Lenhart et al. 2011). The impact of land conversion among a host of other anthropogenic influences on the Minnesota River and its tributaries creates a highly relevant purpose for this research (see 1.5.3). However, to understand the contemporary setting of the study area, it is essential to first understand the geomorphic evolution of the Minnesota River Valley to address the natural, background processes impacting this fluvial system.

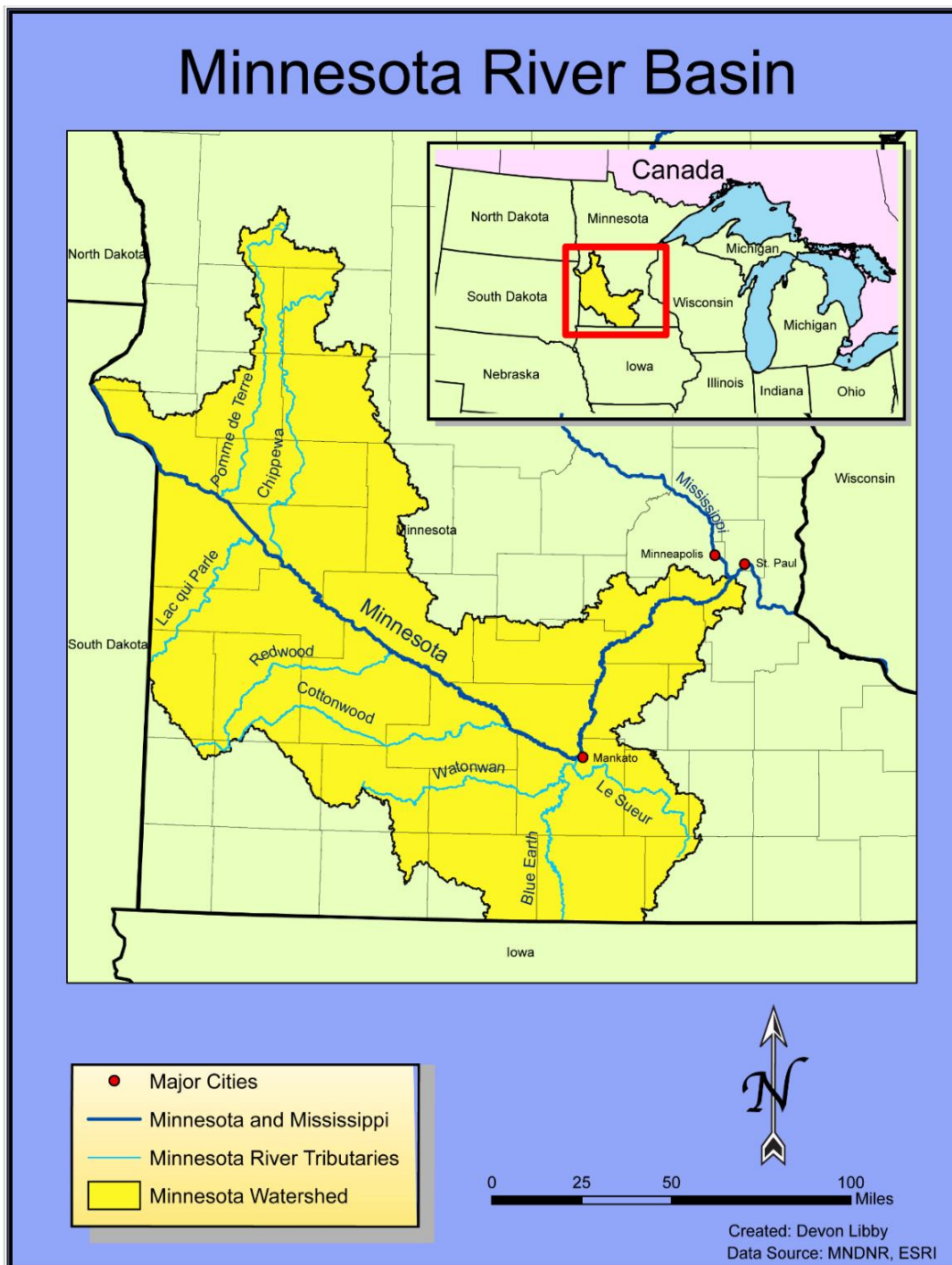


Figure 1.8: This map shows the Minnesota River Basin in relation to its location in the United States, the Minnesota Watershed, and major cities on the river. It also shows several of the major tributaries that contribute flow and sediment to the Minnesota River before it drains into the Mississippi River.

1.5.2 Geomorphic Evolution of the Minnesota River Valley

Minnesota's present-day geomorphology and surficial geology are almost entirely the direct or indirect result of the last major glacial advance known as the Wisconsin Glaciation (Patterson and Wright 1998; Groten, Ellison, and Hendrickson 2016). The Wisconsin ice sheet covered much of Minnesota with various lobes extending through state (MRBDC 2004). The Des Moines Lobe extended into the MRB carrying with it, large amounts of poorly sorted sediment from the north and west, leaving much of the MRB covered in thick layer of unconsolidated glacial sediment (Groten, Ellison, and Hendrickson 2016).

Following recession of the Des Moines Lobe north, the Red River Lobe of the Laurentide Ice Sheet advanced into the present day Red River Valley and then, subsequently retreated. Its terminus is reflected by the Big Stone Moraine in west-central Minnesota and this moraine served to dam meltwater from the retreating glacier forming proglacial Lake Agassiz (Thorleifson 1996; Fisher 2003; MRBDC 2004). Glacial activity ceased at the Big Stone Moraine 12,000 ^{14}C BP (Lepper et al. 2007). Further evidence suggests full glacial recession north of the continental divide occurred 11,810 ^{14}C BP with Lake Agassiz forming at this same time or slightly earlier (Clayton and Moran 1982; Thorleifson 1996; Lepper et al. 2007). Lake Agassiz covered approximately 123,500 square miles with a maximum depth of 400 feet receiving glacial meltwater and nonglacial runoff from an area in exceedance of two million km^2 (Thorleifson 1996; MRBDC 2004).

As the Laurentide Ice Sheet retreated, Lake Agassiz experienced episodic releases of discharge into the Gulf of Mexico, Arctic Ocean, North Atlantic Ocean, and Hudson

Bay through various outlets (Teller, Leverington, and Mann 2002). The southern outlet was controlled by low glacial moraine on the north sloping land in the Red River Valley (Thorleifson 1996). This southern spillway was likely active at the time of Lake Agassiz's formation ~11,770-11,810 ¹⁴C BP (Fenton et al. 1983; Fisher 2004; Lepper et al. 2007), and experienced episodic releases of discharge as lake levels fluctuated with other outlets being activated (Thorleifson 1996). Radiocarbon dated wood in the lacustrine sediment of Big Stone Lake indicates that the southern outlet of Agassiz formed by 10,800 ¹⁴C BP and was finally abandoned by 9,400 ¹⁴C BP (Fisher 2003).

The discharge through the southern outlet of Lake Agassiz, known as Glacial River Warren, was responsible for carving out the Minnesota River Valley (Fisher 2004). Fisher (2004) estimates the discharge of Glacial River Warren between 0.364 and 0.102 Sverdrup (SV) based on boulders he interpreted as fluvially aligned and transported. A sverdrup equals one million cubic meters per second (264 million gallons per second). The Minnesota River now occupies this deeply incised, broad channel (up to 8 km wide) as a underfit stream (Figure 1.9; MRBDC 2004; Kelley et al. 2006; Groten, Ellison, and Hendrickson 2016).

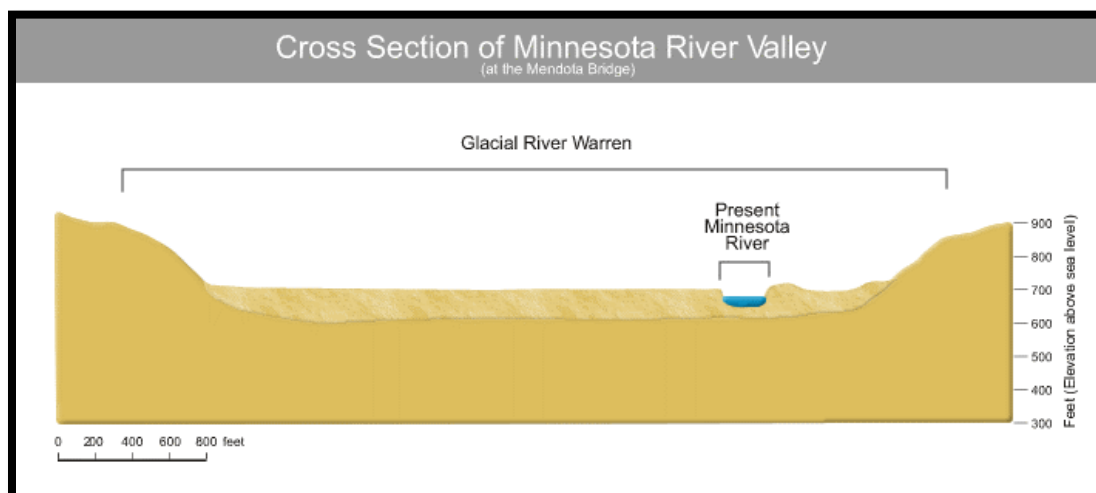


Figure 1.9: This cross section shows the immense reach and volume of Glacial River Warren in the context of the present-day Minnesota River (MRBDC 2004).

The incision from Glacial River Warren created a substantial drop in base level which is presently reflected in the Minnesota River tributaries and their retreating knick zones and knickpoints (Belmont et al. 2011; Gran et al. 2013; Groten, Ellison, and Hendrickson 2016). These knick zones/knickpoints mark the upstream extent of progressing incision as they rapidly excavate the tributaries' valleys of consolidated glacial till (Figure 1.10; Gran et al. 2013; Lauer et al. 2017). The large amount of glacial till and glaciofluvial sands present in the MRB and the entire upper Mississippi River Basin (UMR) naturally primes the area to produce large volumes of sediment from the erosional processes in these fluvial systems (Blumentritt, Engstrom, and Balogh 2013; Faulkner et al. 2016; Yuan et al. 2017).

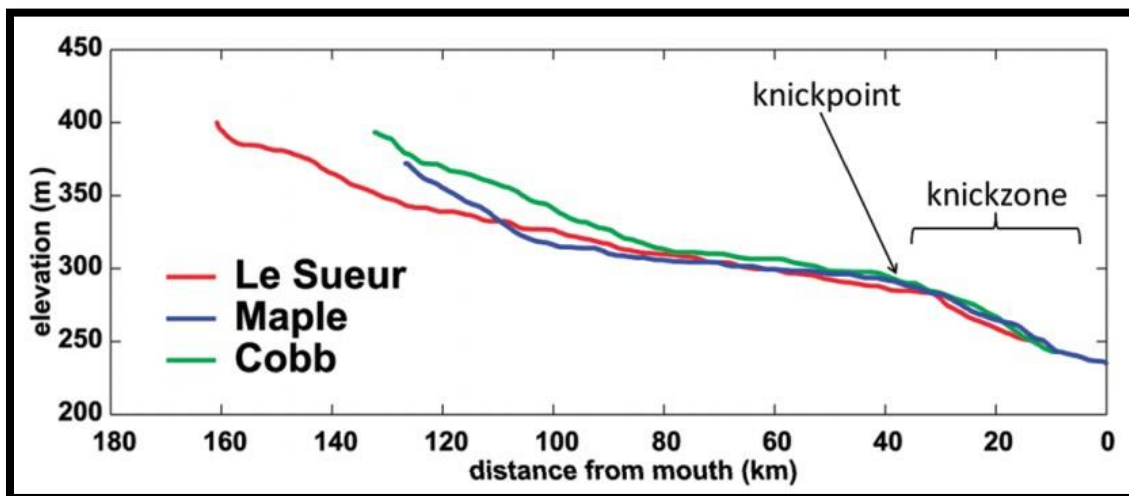


Figure 1.10: This figure from Belmont et al. (2011) displays the longitudinal profile Le Sueur River and its two main tributaries, the Cobb River and Maple River, and their knick zones where active incision is occurring.

1.5.3 Contemporary Concerns in the Minnesota River Basin

The Minnesota River began attracting attention in the late 1980's due to its impaired condition. Algae blooms and unhealthy fish populations resulted from various forms of pollutants, including excess nutrients (phosphorus and nitrogen), dissolved oxygen levels, sediment, and bacteria. Conditions were so bad that in 1992 Governor Arne Carlson called for “making the Minnesota River fishable and swimmable in ten years.” Although this proclamation was a step in the right direction, the following ten years were used to identify the issues plaguing the river rather than solving the cause of this complex problem (Minnesota Pollution Control Agency [MPCA], 2002).

The collective issues facing the Minnesota River Basin are a result of natural processes, in part, but are drastically exacerbated by human-induced impacts (Schottler et al. 2014). The Minnesota River and many of its tributaries (e.g. Blue Earth River, Le Sueur River) exceed state standards (25 Nephelometric Turbidity Units [NTU] for Minnesota Class 2B waters [cool/warm water fisheries]) and federal standards (outlined

in section 303(d) Clean Water Act) for turbidity due to excess suspended sediment loading (Belmont et al. 2011; Lenhart et al. 2011; Yuan et al. 2017). Although these negative effects are felt locally, the broader implications and detrimental effects extend far beyond the basin or even the state. The various pollutants have degraded the Mississippi River and Lake Pepin with sediment, phosphorus, and nitrogen resulting in the need for constant dredging to stabilize the environmental and economic impacts on the region (Kelley and Nater 2000; Engstrom, Almendinger, and Wolin 2009; Mulla and Sekely 2009; Groten, Ellison, and Hendrickson 2016).

Even further-reaching, broader impacts of these environmental problems are felt as far away as the Gulf of Mexico from upstream nutrients that fuel the increasing hypoxic zone, also called “Dead Zone” (MPCA 1998; MPCA 2002; Petrolia and Gowda 2006; NOAA 2015). This impact is in large part due to intensive agricultural activities which jeopardize coastal fisheries in the Gulf (Rabalais, Turner, and Scavia 2002; Dodds 2006; Moore et al. 2010). The Mississippi River drainage basin receives 90% of its nitrate inputs from NPS, of this, 74% is from agriculture and 56% of the total nitrate enters north of the confluence of the Ohio River (Rabalais, Turner, and Scavia 2002). It is estimated that ~5-7% of the nutrient load to the Gulf is from the MRB alone (Magdalene 2004; Steil 2007).

1.5.3.1 Land Use Change and Altered Hydrology

Prior to agriculture dominating the MRB, the landscape was predominately poorly drained prairie pothole wetlands (Musser, Kudelka, and Moore 2009; Lenhart et al. 2011; Groten, Ellison, and Hendrickson 2016). Wetlands serve a vital function by regulating sediment, chemicals, and water capacity by retaining, filtering, and slowly releasing these

elements over time (Mitsch and Gosselink 2000; Lenhart et al. 2011). However, beginning in the early 1900s, many of the prairie-pothole wetlands found in the MRB were drained for agricultural use through surface drainage and ditching (Lenhart et al. 2011). Currently, 78% of the MRB is row crop agriculture (Musser, Kudelka, and Moore 2009; Belmont et al. 2011). In total, Minnesota has lost a total of 80% of its prairie-pothole wetlands with concentrations as high as 95% in certain areas, and it was not until 1991 that Minnesota passed its first comprehensive act to protect wetlands within the state through the Minnesota Wetland Conservation Act (Forsberg 1992).

Schottler (2012) defines artificial drainage as “any physical alteration to the landscape that changes the natural flow pattern and rate of removal of water” (p. 4). Traditional, artificial surface water drainage techniques (e.g. ditching) are now accompanied by the popular technique of subsurface drainage where a network of pipes (commonly called tiling) capture and remove water infiltrating through the soil profile in order to increase agricultural productivity. The water collected by tiling is then routed to surface water drainage networks which is often constructed ditches, but also terminate directly into nearby rivers if proximal (; Kovacic et al. 2000; Schottler 2012; Schottler et al. 2014).

The hydrology in the MRB is further altered by increased precipitation from climate change (Novotny and Stefan 2007; Yuan and Mitchell 2014; Kelly et al. 2017). Given both the land use and climate change it is no surprise that the MRB, and much of the Midwest in general, has seen a marked increase in mean annual stream flows, peak flows, and high flow days (Figure 1.11; Novotny and Stefan 2007; Wang and Hejazi

2011; Kelly et al. 2017). However, teasing out the increase in river discharge in the MRB is a much more difficult and controversial task, but the science is beginning to show artificial drainage is playing a significant role (Schottler et al. 2014; Belmont and Foufoula-Georgiou 2017; Kelly et al. 2017). Regardless, both are impacting rivers in MRB with increased flows creating more erosive rivers and drastically increasing sediment loading (Schottler et al. 2014).

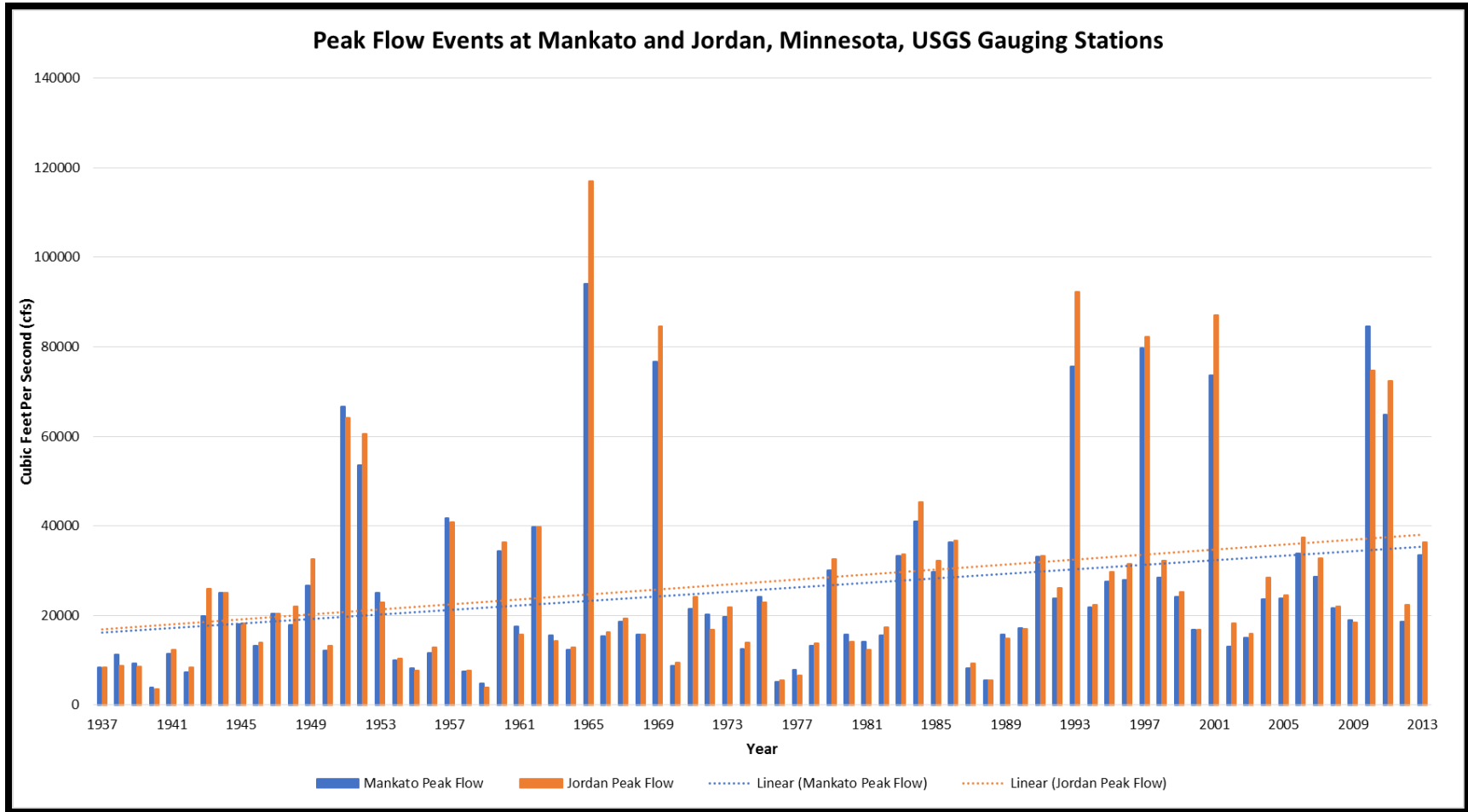


Figure 1.11: This graphical representation of United States Geological Survey (USGS) gauging statistics of peak high flows in Mankato and Jordan, Minnesota, shows the increased trend in yearly peak flow events.

1.5.3.2 Altered Hydrology and Sediment

As discussed in section 1.5.2, the geomorphic context of the MRB makes it a primed system to produce high volumes of sediment – a natural pre-existing condition (Gran et al. 2009; Gran et al. 2013; Faulkner et al. 2016; Yuan et al. 2017). However, the altered hydrology has in turn had major influences on modern erosion and sediment loading (Belmont et al. 2011; Schottler et al. 2014). Lake Pepin, a naturally dammed lake on the Mississippi, has received a ten-fold increase in sedimentation rates over the past 150 years. Of that order of magnitude increase, the MRB contributes 80-90% of the sediment while only adding 38% of the water to the lake (Kelley et al. 2006; Engstrom, Almendinger, and Wolin 2009; Belmont and Foufoula-Georgiou 2017). Within the MRB, the Le Sueur River watershed has the highest sediment yield of any tributary contributing up to 30% of the sediment load to the Minnesota River while only occupying 7% of the MRB (Belmont et al. 2011).

Belmont et al. (2011) used various techniques including geochemical finger printing to identify where the predominant sources of erosion were by creating a sediment budget of fine grained sediment for the Le Sueur River. Their findings show a fascinating swing from pre-settlement near channel sources to agricultural soil erosion in the middle of the twentieth century accompanying the rapid increase in overall sedimentation, but while sedimentation remains high the primary contribution is once again near channel sources (Figure 1.12; Belmont and Foufoula-Georgiou 2017).

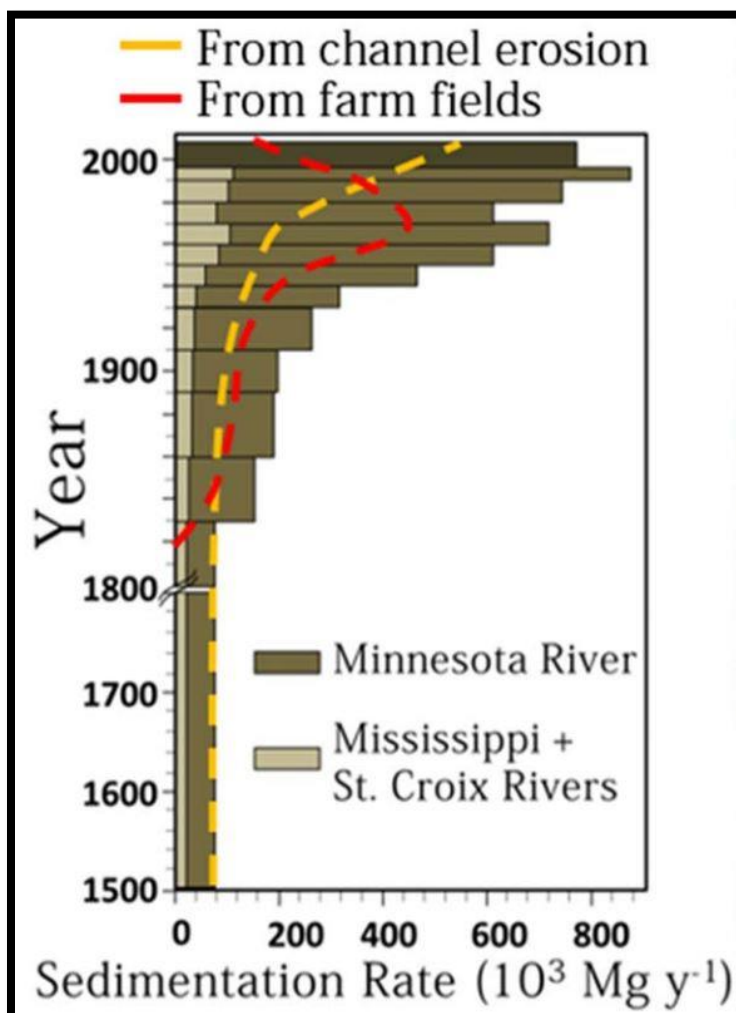


Figure 1.12: This figure from Belmont and Foufoula-Georgiou 2017 shows the 10-fold increase in Lake Pepin sedimentation post-European settlement along with the swing in sediment source from near channel to agricultural fields back to near channel. It is also seen the Minnesota River is the primary contributor to the sedimentation rates experienced in Lake Pepin.

1.5.3.3 Phosphorus, Nitrogen, and Bacteria

Common agricultural practice involves the application of fertilizers rich in phosphorus and nitrogen to promote plant growth. When these nutrients reach lakes and rivers in overabundance, they can cause excessive algae growths that will die off and decompose. This process reduces dissolved oxygen in the water which can then suffocate fish and other plant life. Certain forms of algae (e.g. blue green) can produce toxins

which if ingested can harm humans and animals (Carpenter et al. 1998; MPCA 2008). Lake Pepin has had a 15-fold increase (60-900 metric tons annually) in phosphorus since pre-settlement (Engstrom, Almendinger, and Wolin 2009). The MRB contributes 45% of this phosphorus load along with 56% of the nitrogen in lake (MPCA 2008; Engstrom, Almendinger, and Wolin 2009; Mulla and Sekely 2009). Aside from farming, other major contributors of phosphorus and nitrogen come from urban activities, including industrial waste waters, sanitary landfills, and garbage dumps. These nutrients are also capable of enabling growth of bacteria which is also a concern for human and animal safety (Carpenter et al. 1998; MPCA 2008).

The presence of bacteria, specifically fecal coliform, has been one of the most dangerous pollutants found in the Minnesota River Basin. Bacteria can originate from multiple sources including agricultural runoff from feedlot manure, improperly treated sewage mishandled by municipalities and septic tank leakage, and wildlife waste. Although it is difficult to distinguish exact sources, fecal coliform can be tested and determined if it originated in the intestinal tract of a mammal. Not all forms of this bacterium can cause disease in humans, but if it is found in levels that exceed the water-quality standards, it is an indicator that other pathogens may also be present that can cause a major risk to human health (MPCA 1998).

1.5.3.4 Invasive Carp

As unprecedented amounts of sediment, nitrogen, phosphorus, and bacteria travel downstream, a new threat to the MRB health is traveling upstream – the bighead carp (*Hypthalmichthys nobilis*, Figure 1.13) and silver carp (*H. molitrix*, Figure 1.13) which will be collectively referred to as invasive carp from this point forward. In recent

decades, the invasive carp have been introduced to North America from eastern Asia. (Kolar et al. 2007). They were first introduced to Arkansas in 1973 to improve the habitat of aquaculture ponds (Koel, Irons, and Ratcliff 2000). They were also used in research projects and wastewater treatment lagoons as planktonic biological control organisms (Kolar et al. 2007). Shortly after arriving in the United States, invasive carp entered the unconfined waters of the Mississippi River Basin (MSRB) via deliberate introduction and unintentional pond escapement (Koel, Irons, and Ratcliff 2000). The invasion quickly spread from the Mississippi River to the Missouri, Ohio, and Illinois rivers – all of which presently have established reproductive populations (Chick and Pegg 2001).

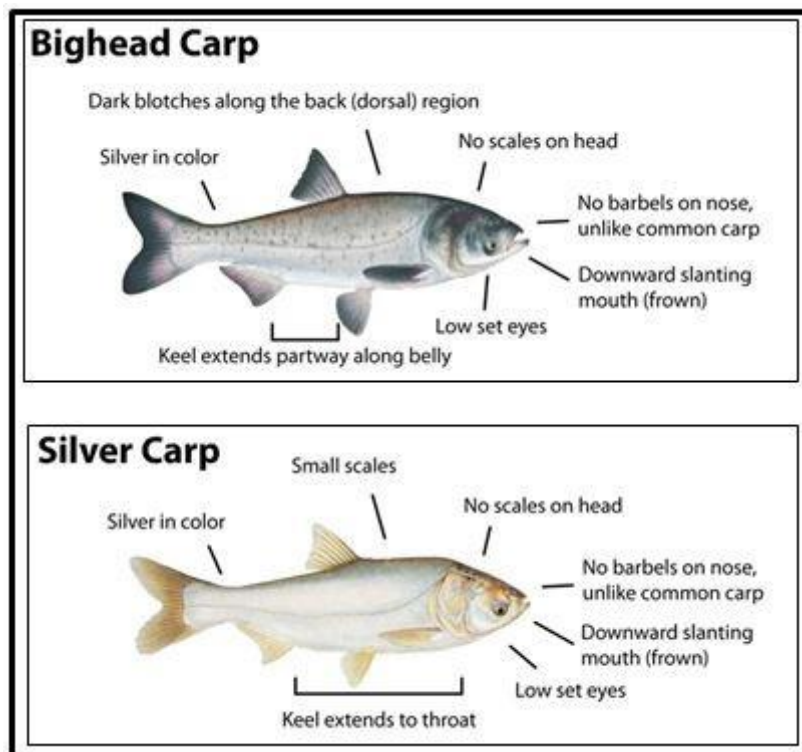


Figure 1.13: The bighead carp and silver carp are shown above with special attention given to identifiable characteristics. Aside from their many similarities, they differ in coloration hue, length of ventral keel, and mature adult size with bigheads reaching 5 feet in length and silvers around 3.3 feet (Tip of the Mitt Watershed Council 2014).

Given the geographic variables of the invasive carp's native range, it is believed that they can inhabit waters throughout the United States as well as parts of Mexico and Canada (Kolar et al. 2007). Exponential population growth has already been seen in parts of the MSRB, and without proper management, the spread will continue throughout North America (Chick and Pegg 2001). Natural migration is exacerbated by transportation of live invasive carp for bait, food, and prayer animal release practices which is a religious belief that releasing captive animals into the wild is virtuous (Severinghaus and Chi 1999; Kolar et al. 2007). These various avenues for introduction certainly make the Minnesota River a susceptible system to invasive carp occupation with several bighead carp being caught in the Minnesota River this past year. However, no confirmed reproducing population have been found yet (Smith 2017).

Invasive carp pose significant ecological threats to non-native waters (Chick and Pegg 2001). They are planktivores that voraciously consume 5 to 20 percent of their body weight every day from filtering planktonic organisms (phytoplankton and zooplankton) out of the water. This is substantial considering bighead carp and silver carp can reach 110 pounds and 60 pounds, respectively. This consumption rate can place an acute stress on low levels of the food chain by depleting planktonic organisms which all fish depend on at some point in their life cycle, often in the larval stage (Sampson, Chick, and Pegg 2009; MNDNR 2014). A magnified stress can be put on native planktivorous fish like gizzard shad (*Dorosoma cepedianum*), bigmouth buffalo (*Ictiobus cyprinellus*), and paddlefish (*Polyodon spathula*) which are currently listed as a species of special

concern by the U.S. Fish and Wildlife Service (Chick and Pegg 2001; Pegg and Chick 2004; Kolar et al. 2007; Sampson, Chick, and Pegg 2009).

Alongside ecological degradation, invasive species have placed major financial burden on state and federal natural resource agencies (Rasmussen 2011; Carlson and Vondracek 2014; Spangler 2014). It is estimated that non-indigenous species cost the United States approximately \$137 billion in damage and losses every year (Pimentel et al. 2000). The economic impact is further magnified by proposed and executed prevention measures. For instance, the United States Army Corps of Engineers (USACE 2014) determined that the most effective option for keeping invasive carp out of the Great Lakes would cost between \$15 and \$18 billion over 25 years. This option is likely politically, financially, and temporally unrealistic (Spangler 2014). Given the monetary burden that accompanies invasive species prevention, mitigation methods need to be carefully considered in order to avoid mistakes that can reach into the billions of dollars.

In the face of this threat, the MNDNR has begun to explore options to contain the present reproducing population in Mississippi River through a non-physical barrier on the Minnesota River. Many methods of containment have been applied to deter fish passage including non-physical practices such as: electrical, visual, acoustic, chemical, and hydrological deterrence techniques (Dawson, Reinhardt, and Savino 2006; Rasmussen 2011; Ruebush 2011; Noatch and Suski 2012).

However, for barriers to be effective, geomorphic conditions need to be assessed as well so impediments are not easily circumvented by invasive carp (Carlson and Vondracek 2014). Specifically, attention needs to be focused on periods of high flow

(usually in the spring) that would inundate floodplains and increase the likelihood that invasive carp could find passages around barriers (DeGrandchamp, Garvey, and Colombo 2008; Rasmussen 2011; USACE 2014). Predicting flood magnitude and recurrence intervals, which already has inherent uncertainties, is further complicated by natural and anthropogenically induced non-stationary factors such as urbanization and climate change (Strupczewski, Singh, and Feluch 2001; Vogel, Yaindl, and Walter 2011; Gilroy and McCuen 2012).

Another imperative geomorphic consideration for barrier placement is the lateral migration/stability of meandering rivers. Unconfined rivers that flow through broad floodplains of easily reworked sediment, like the Minnesota River, can adjust channel form relatively freely. This characteristic can lead to the undermining of barriers by erosional events or cause cut-offs to abandon meander bends that create a new river channel (Urban and Rhoads 2003; Charlton 2007; Hooke 2007). If a barrier were placed on a meander bend that became cut-off, it would be instantly rendered useless. Rivers with high sediment loads (i.e. the Minnesota River) characteristically have higher lateral migration rates and higher cut-off potential (Constantine et al. 2014). Understanding historical channel change is imperative to aid decision makers in this task so a multi-million-dollar project isn't buried in sediment or washed downstream in the next high flow event.

1.6 Significance of Understanding Planform Change on the Minnesota River

Despite the vast research that has been focused on the MRB and the upper Mississippi River (Schottler et al. 2010; Belmont et al. 2011; Gran, Belmont, Day, Jennings, et al. 2011, Schottler et al. 2014), relatively little is known about the Minnesota River (Johannesson and Parker 1985). The watershed has undergone drastic change in land use/land cover, hydrology, and nutrient/sediment loading (see 1.5.3) from recent (past ~150 years) anthropogenic activities (Brezonik et al. 1999; Novotny and Stefan 2007; Engstrom, Almendinger, and Wolin 2009; Musser, Kudelka, and Moore 2009; Schottler et al. 2014; Yuan and Mitchell 2014; Belmont and Fofoula-Georgiou 2017). Given these changes, the Minnesota River offers a unique and ideal study area to better understand channel behavior response to anthropogenic influences as well as filling the current gap in the literature about the contemporary behavior and geomorphology of the river. A few studies have begun to identify width changes on the Minnesota River (Lenhart et al. 2013; Lauer et al. 2017), but no current research has sought to fully understand planform channel change of the Lower Minnesota River.

By nature, rivers are dynamic features on the landscape and can quickly undergo morphological changes from anthropogenic and climatic changes (VanLooy and Martin 2005). Knox (1977) notes that channel morphology and stability is a result from the prevailing hydrological conditions of which surface runoff and sediment yield are the most influential to channel characteristics. His research on the Platte River in Wisconsin showed post-settlement, agricultural land use conversion led rapid morphological

changes. Sediment from anthropogenically accelerated surface flow was only transported short distances before being deposited on alluvial fans and the surface of floodplains. These changes caused areas to experience increases in flood magnitude and frequency.

Within the MRB, increased discharge and peak flows leading to more erosive rivers have been identified (Novotny and Stefan 2007; Schottler et al. 2014; Kelly et al. 2017), yet it has not been quantified how the Minnesota River has adjusted temporally or spatially to accommodate for these changes. Groten, Ellison, and Hendrickson (2016) recently identified the stretch of Minnesota River from Mankato to Jordan as being a major sediment contributor. Jordan currently has a sediment yield that is two and half times greater than that of Mankato, yet beyond Jordan to Fort Snelling the sediment yield significantly reduces revealing this latter portion of the River as a sediment sink.

Knowing that these anthropogenically influenced changes in morphological driving variables exist demands a working knowledge of the Minnesota River's temporal and spatial planform change. This will not only be of scientific benefit to better understand river process and geomorphic response to changes in hydrological conditions but will be of great societal importance. It is common for humans to expect a river system to act in a manner that is stable or consistent with the past behavior. However, this can come with great consequence. In Bangladesh, human encroachment on Brahmaputra-Jamuna floodplain has been met with rapid channel migration destroying village settlements, towns, and markets while displacing thousands of people in the process (Haque and Zaman 1989).

The Minnesota River Valley is heavily occupied by humans and infrastructure (homes, cities, roads, bridges, hospitals, etc.), all of which can be impacted by the erosional forces of lateral channel migration and channel widening (Johannesson and Parker 1985). For instance, undermining of bridges and homes from these planform changes can not only come at monetary costs but at the cost of human life. Since it is known that present hydrologic variables within the watershed are different than that of the past (Schottler et al. 2014), it is not viable to consider areas or infrastructure as safe or stable based on historical river behavior. Rather historical rates need to be examined in order to detect trends and changes which can then aid in better assessing current infrastructure and guide decisions for placement or non-placement of future infrastructure.

Another current issue facing the Minnesota River is the rapidity in sedimentation rates leading to reduced health in the ecosystem and becoming a socioeconomic burden since dredging is needed to keep barge traffic navigable (USACE 2007; Jennings 2016). Dredging is an expensive treatment to a “symptom” which will have to be done indefinitely unless the “cause” of the problem is identified and addressed. An understanding of planform change on the Minnesota River will help to identify areas of acute sediment contributions enabling decision makers to make informed decisions and guide best management practices. Specifically, planform analysis in combination with the recent findings of Groten, Ellison, and Hendrickson (2016) will bring to light areas between Mankato and Jordan that are major sediment contributors from the erosional

processes of lateral migration and channel widening while offering a new view on areas serving as sediment sinks.

This research stemmed from state funding that identified not enough was known about the Minnesota River to make an informed decision on placing instream infrastructure to block the advancement of invasive carp. The findings from this research will not only address that gap of knowledge but will create the building blocks for future researchers to ask more informed questions to advance the collective effort of identifying and reducing modern detrimental impacts both at a local and national scale; benefitting the residents of Minnesota as well as our southern neighbors all the way to the Gulf of Mexico.

1.7 Conclusion and Research Questions

The Minnesota River has been identified as the major source of sediment and nutrients leading to growing environmental problems in Lake Pepin, as well as being a surprisingly significant contributor to the issues being faced in the hypoxic zone Gulf of Mexico (Kelley and Nater 2000; Rabalais, Turner, and Scavia 2002; Steil 2007).

Furthermore, the Minnesota River is threatened by the aggressive spread of invasive carp. Yet with all of these recognized issues stemming from MRB and its tributaries, very little is understood about the morphology of the transport corridor, the Minnesota River, moving the excessive suspended sediment and nutrient loads out of the basin. A working knowledge of the historical planform change of the Minnesota River is essential to better equip decision makers with the information necessary to foster best management practices.

The purpose of the research in this thesis is to first evaluate past methods of quantifying historical planform channel change and suggest the best methods for accounting for all the inherent and introduced errors and uncertainties within a GIS-based remote analysis. Second, the methodology will be applied to the Minnesota River to start filling the immense gap that currently exists on the main stem Minnesota River. Since discharge and sediment have significantly increased from various anthropogenic activities, primarily linked to land use change, several initial research questions are:

- 1) Have the channel migration rates remained stable over the past 76 years of aerial photographic record (1937-2013), or are increases or decreases seen? If the latter, do these increases and decreases show any spatial or temporal patterns?
- 2) Does channel width fluctuate over this similar time frame? If so, are there spatial or temporal patterns related to this change?
- 3) How have human modifications on the river (e.g. bridges, flood control structures, etc.) effected planform channel change in the upstream and downstream directions?
- 4) In relation to the invasive carp problem, are there controlled reaches of the Minnesota River that exhibit very little change and could potentially be suitable for invasive carp barriers?

Specifically, these research questions will be applied on the last 160 km (100 mi) of the Minnesota River, extending from the Blue Earth/Minnesota River confluence down the Minnesota/Mississippi River confluence (Figure 1.14).

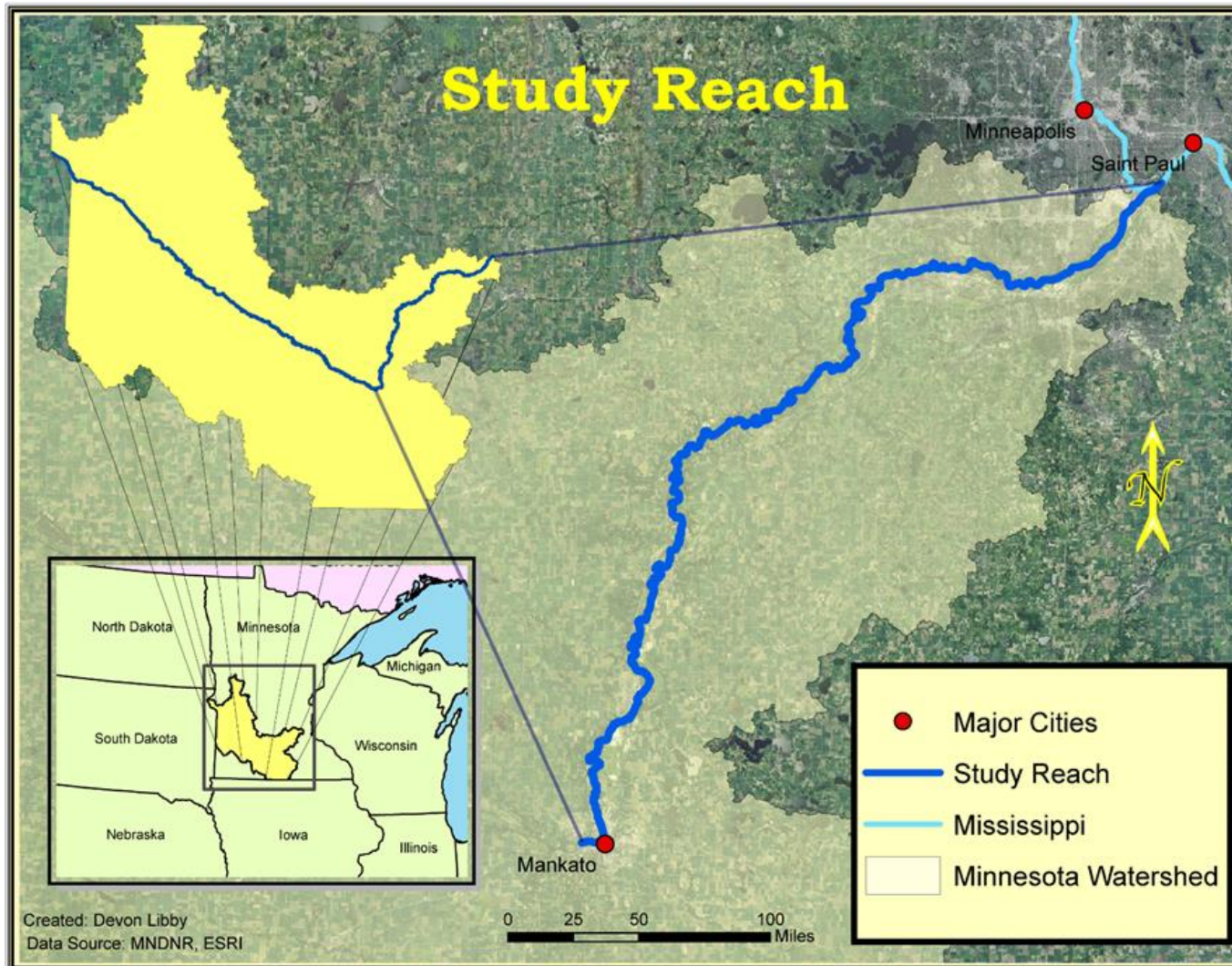


Figure 1.14: The study reach for this research is the 160 km (100 mi) of the Minnesota River beginning in Mankato and ending with the confluence with the Mississippi River

Chapter 2 Assessing and Quantifying the Error and Uncertainty Associated with Aerial Photograph-based Channel Planform Change Studies

2.1 Introduction

The ability of geomorphologists to answer questions about fluvial systems has been transformed by technological advancements in GIS alongside the increased accessibility of historic imagery and the affordability of new imagery from satellites, airplanes, and unmanned aerial vehicles (UAV's). Although these advancements in technology garner much attention in GIS-based fluvial studies, it is of the utmost importance to consider potential errors and uncertainty that can bias measurements and interpretations and sometime lead to erroneous conclusions. Attention to error and uncertainty is growing (Unwin 1995; Mount et al. 2003; Mount and Louis 2005; Hughes, McDowell, and Marcus 2006; Lea and Legleiter 2016), however common pitfalls and incongruities can be seen throughout the past literature (Lawler, 1993).

Although there are many different approaches (dependent on spatial and temporal scale) that can be taken to quantify channel change (section 1.4.1; Table 1.4; Lawler 1993), the focus of this chapter will be on the methodologies that utilize remotely sensed (e.g, aerial, satellite or UAV) imagery in a GIS environment to measure planform channel change (Brewer and Lewin 1998; Graf 2000; O'Connor, Jones, and Haluska 2003; Buckingham and Whitney 2007; Zanoni et al. 2008; Giardino and Lee 2011; Legleiter 2014; Lea and Legleiter 2016;). Methodological inconsistencies and study specific approaches to error assessment have resulted in a need to identify and standardize an

approach for accurately measuring and reporting planform channel change for future studies (Unwin 1995; Mount and Louis 2005; Hughes, McDowell, and Marcus 2006). Both the GIS environment and the use of remote imagery, focusing on aerial photographs, will be explored in this chapter by focusing on best practice in the three important steps in 1) Data Acquisition 2) Image Registration 3) Bankline Digitization. The final step of calculating planform change will be covered in Chapter 3. This chapter aims to standardize the process of analyzing and reporting error in remote planform change studies of fluvial systems through inspection of past literature and combining approaches to account for total spatial error in the measurements. This will also provide an error assessment for the measurements calculated in Chapter 3.

2.1.1 Data Acquisition and Classification

While it may seem intuitive, the first step to any study of this nature is to check the availability of aerial imagery for the study area over the temporal range desired. Often, this will include combining modern satellite imagery with historical aerial photographs (digital and physical). This data is the foundation of assessing historical planform change in a GIS and requires accessibility to imagery that covers the extent of the study area from different time periods for comparative analysis.

The United States Department of Agriculture (USDA) offers some of the earliest and most complete sets of aerial photography dating back to the 1930's (Trimble and Cooke 1991). Other agencies like the US Forest Service have collected photographs of non-agricultural land and commercial photography gained popularity following World War I (Trimble & Cooke 1991; Professional Aerial Photographers Association 2015). These historical photographs originated from various sources and are presently stored in

collections all over the country such as universities, county and state offices, state libraries and archives, and state geological surveys (Trimble and Cooke 1991). In many of these places, the aerial photographs only exist as hard copies and need to be scanned in order to be usable in a GIS. Recently, aerial photographs have become easier to obtain through online resources like the United States Geological Survey (USGS) Earth Explorer or from other organizations like the University of Minnesota's Historical Aerial Photographs Online (MHAPO available at <https://www.lib.umn.edu/apps/mhapo/>), which allow users to download previously scanned aerial photographs for free. This accessibility to historical imagery in combination with modern GIS technology has drastically changed the ability of geomorphologists to understand planform channel change and floodplain dynamics. A process much different when compared to Nanson and Hickin (1986) who superimposed imagery for planform measurement using overhead projectors and transparencies.

Once the imagery is in digital format the next step is registering it to a coordinate system and, then, digitizing banklines can be accomplished. Each of these processes will be discussed independently in following two sections (2.1.2 and 2.1.3).

2.1.2 Review of Image Registration Processes in Planform Channel Change Studies

2.1.2.1 Historic Aerial Photographs

Error in the image registration process is present from both inherent geometric distortion in the photograph and potential introduced error from ground control point (GCP) selection (Crowell, Leatherman, and Buckley 1991). The inherent geometric distortion exists from both scale distortion, which increases radially from the photographs

principal point (center point), and from terrain relief (Figure 2.1). Scale distortion can be corrected through image registration (photo rectification) but introduces new error with GCP placement and image warping – issues that will be addressed later in this section (Crowell, Leatherman, and Buckley 1991; Hughes, McDowell, and Marcus 2006). To completely remove the distortion from an aerial photograph, a more intensive process of orthorectification needs to be performed. This requires significant computational power, is mathematically demanding, and requires field collected survey points from which to make corrections (Crowell, Leatherman, and Buckley 1991; Kimmerling et al. 2011). The amount of terrain relief error needs to be considered on a study specific basis. In the case of the Minnesota River, it was not necessary orthorectify the imagery since all the measurements were made and GCPs placed in the wide river valley.

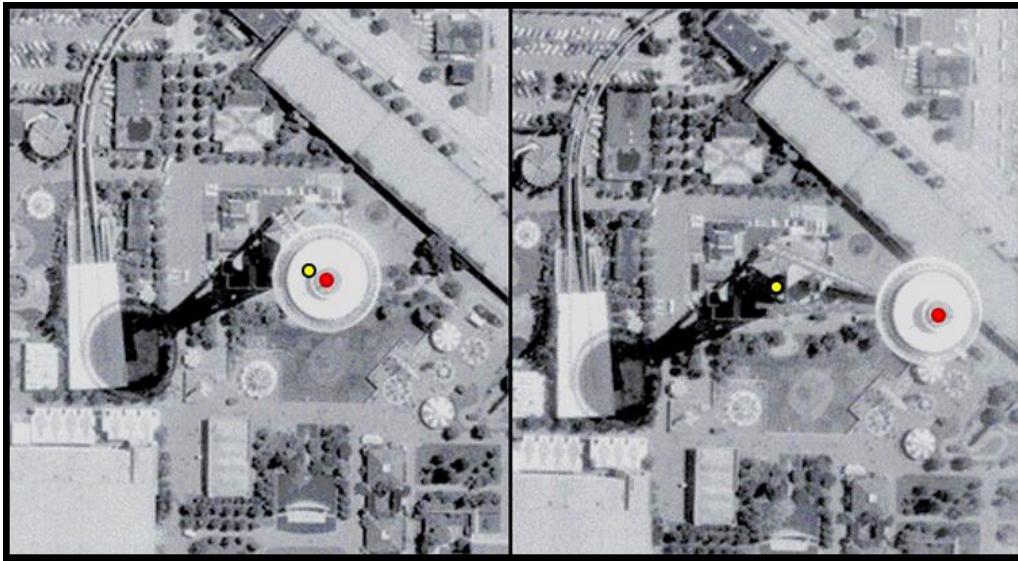


Figure 2.1: These two aerial photographs display the Space Needle in Seattle yet have different principal points. In the left photograph the Space Needle is very close to the principal point while the second photograph it is near the edge where scale and relief distortion is highest causing it to appear to lean to the left. Dots were added to represent the top center (red) and bottom center on the ground (yellow) of the Space Needle. We know these two areas are on top of each other in the real world. However, the relief displacement from scale distortion can be easily seen in tall structures. In the left photograph these points are very close since these reside near the center of the photograph while in the left they are displaced significantly. Imagery obtained from http://gsp.humboldt.edu/olm_2015/Courses/GSP_216_Online/lesson2-2/distortion.html.

When an image is registered, it receives a spatial reference which is essential for comparative analysis between time periods (Mount et al. 2003). This process will be referred to as image registration however in ArcGIS, this process, known as georectification. This process is accomplished with three tasks: 1) aligning the unregistered image with GCPs to a registered image (preferably orthorectified), 2) transforming the image, and 3) resampling the pixels in the dataset.

- 1) This process entails finding distinguishable features between the unregistered image and the registered image (one that has a spatial reference often called base image) to tie them together.

- 2) Once the images have been tied together, a transformation (shift or warp) is applied to best align the coordinate system between the two images.
- 3) The final step is to resample the pixels assigning the new values in the image that were shifted or warped because of the transformation (Hughes, McDowell, and Marcus 2006).

Hughes, McDowell, and Marcus (2006) examined these steps in detail specifically for measuring lateral channel movement in a GIS. They suggest optimal parameters for registering images with the least amount of error and suggest calculating image registration error using independent GCPs placed in areas of interest in addition to the built in ArcGIS error metric, Root Mean Square Error (RMSE).

Since RMSE is automatically calculated when registering aerial photographs in ArcGIS it has commonly been used in past channel planform studies to assess error (e.g. Urban and Rhoads 2003; Rhoades, O'Neal, and Pizzuto 2009; Surian et al. 2009; Day et al. 2013a, 2013b;). RMSE is a calculation of the difference (offset) between the x and y coordinates of the newly registered image to that of the base image to which it was registered. The equation for calculating the RMSE of a point is based on the Pythagorean Theorem and is as follows:

Equation 2.1

$$RMSE \text{ of a point} = \sqrt{(x_s - x_r)^2 + (y_s - y_r)^2}$$

where x_s and y_s are the coordinates of the point on the base image and x_r and y_r are the corresponding coordinates on the newly registered image. The total RMSE for the newly registered image is the square root of the averaged squared error vectors of all the points

(Slama, Theurer, and Henriksen 1980; Hughes, McDowell, and Marcus 2006; Lea and Legleiter 2016). The following equation shows this:

Equation 2.2

$$\text{RMSE total for the whole image} = \sqrt{\frac{\varepsilon_1^2 + \varepsilon_2^2 + \dots + \varepsilon_n^2}{n}}$$

where ε_1^2 through ε_n^2 is the error vector for each point and n is the total number of points.

Hughes, McDowell, and Marcus (2006) clearly demonstrates the need for a metric to quantify image registration error apart from RMSE. Their work has been fundamental to guiding the image registration process in numerous fluvial studies of planform channel change (Zanoni et al. 2008; Morgan, Gergel, and Coops 2010; Comiti et al. 2011).

The importance of using a metric to calculate error outside of RMSE is evident in Hughes, McDowell, and Marcus (2006) test of GPC selection (task 1 above) of the image registration process. Hughes, McDowell, and Marcus (2006) found that the RMSE values along with independent test points' (the points placed after image registration in the area of interest) mean and median error did not change significantly when more than eight GCPs were placed. However, the independent test point's 90th percentile cumulative distribution did show a significant decrease in error when increasing the number of GCPs beyond eight. This finding shows the importance of using a minimum of eight GCPs for image registration, with more being beneficial to overall accuracy by achieving a decreased number of highest ten percent error values. Thus, RMSE is ineffective and insufficient as a sole assessment of error and uncertainty in this kind of analysis. The inadequacy of RMSE was further demonstrated by Hughes, McDowell, and Marcus

(2006) when RMSE increased from <1.0 to ~ 4.0 m when the number of GCPs used in the study increased from six to eight, meanwhile all the same increase (six to eight) in independent test points showed a decrease in error.

In the transformation and pixel resampling steps (task 2 and 3 above), Hughes, McDowell, and Marcus (2006) suggest optimal results can be obtained by using a second-polynomial transformation with a cubic convolution pixel resampling. These are simply settings selected within the image registration process. Transformations are driven by algorithms that warp images based on the input GCPs to remove distortion in the photograph. Since this warping process changes, the geometry of the raster, pixel resampling is necessary to realign the data to match the new locations of the cell value (ArcGIS for Desktop 2016). Hughes, McDowell, and Marcus's (2006) final analysis concluded that floodplain landscapes similar to their study site in northwest Oregon can consistently be registered to an accuracy of ± 5 meters with a $\sim 10\%$ chance of greater error. Although, this number should only be used to demonstrate their conclusions as a means to best assess error. We suggest that error should be assessed for each individual study due to data and study site specific variability (see section 2.4.1). This is a common mistake that researchers make, by assuming their error is the same as error calculated in prior work. It is not the same from study site to study site or from data set to data set.

The findings of Hughes, McDowell, and Marcus (2006) were confirmed by Lea and Legleiter (2016), who use a leave-one-out cross-validation (LOOCV) strategy to evaluate the error of each individual GCP placement in a series of different image transformations. The LOOCV process withheld a single GCP at a time while each

transformation was iterated establishing the error for each GCP individually. In their final analysis, they agree that a second order polynomial transformation yields the most accurate results and assert that the best placement for GCP's is in the floodplain rather than adjacent hillslopes due to relief displacement (see 2.1.2).

Lea and Legleiter (2016) further recognize the limitation of assigning a uniform error across an entire photograph (Eq. 2.2), as opposed to accounting for the spatial variability of error within the photograph. They addressed this problem by creating a MATLAB script that uses the LOOCV to establish an error for each GCP used. The error is broken down into ϵ_x and ϵ_y , representing the x and y directional image registration error. This method withholds one GCP from the base image (x_h and y_h) and newly registered image. The location of the withheld point is then calculated for the newly registered image (x'_h and y'_h) by using the withheld coordinates of the base image (x_h and y_h). The equations are as follows where ϵ is the image registration error vector, ϵ_x is the x directional component of the vector, and ϵ_y is the y directional component of the vector.

Equation 2.3

$$\epsilon = \sqrt{(x_h - x'_h)^2 + (y_h - y'_h)^2}$$

Equation 2.4

$$\epsilon_x = (x_h - x'_h)^2$$

Equation 2.5

$$\epsilon_y = (y_h - y'_h)^2$$

ε , ε_x , and ε_y then serve as error point values at each GCP and an error surface can be interpolated between these individual points. Spatial Variable Error (SVE) across the image is then determined by interpolating a surface from each of the individual GCP's error. The output of this script is then used as the input for another MATLAB script to determine if migration distance is significant or insignificant based on the SVE. This will be covered in Chapter 3.

2.1.2.2 Digital Ortho-imagery

Along with aerial photographs, another imagery resource is computer generated digital orthophoto quadrangles (DOQs). DOQs have a several advantages to registered imagery. They have undergone the process of orthorectification (mentioned above) which corrects for spatial displacement including terrain relief (not corrected in registered imagery), camera optics, and camera tilt with the final orthophoto being uniform and planimetrically corrected. This means everything in the image will appear as though the viewer is looking directly down opposed to scanned images that will have an outward look from the principle point (Kimmerling et al. 2011; Chang 2014). However, creating DOQs is time intensive, mathematically demanding, and requires special software packages and computing capabilities (Amhar, Jansa, and Ries 1998; Kimmerling et al. 2011). For these reasons along with the photogrammetric expertise required to create DOQs, their usefulness to geomorphologists extends to what is currently available.

The quality of reported DOQ accuracy has been called into question especially when used in GIS applications (Rogers et al. 2006). The USGS began creating DOQs in 1991 as part of the National Aerial Photography Program (Chang 2014).

“Digital orthophoto quadrangles and quarter-quadrangles must meet horizontal National Map Accuracy Standards (NMAS) at 1:24,000 and 1:12,000 scale, respectively. The NMAS specify that 90 percent of the well-defined points tested must fall within 40 feet (1/50 inch) at 1:24,000 scale and 33.3 feet (1/30 inch) at 1:12,000 scale” (U.S. Department of the Interior 1996, 2-4).

Rogers et al. (2006) showed accuracy of Farm Service Agency (FSA) DOQs with respect to elevation when compared to 1991 USGS DOQs and GPS readings and found the FSA DOQs were highly accurate (Table 2.1) falling within 3 to 11 feet or ~ 1-3 meters (depending on elevation and relative comparison used) with a 95% confidence (National Standard for Spatial Data Accuracy criteria). This high accuracy is beneficial to those accessing the Minnesota Geospatial Information Office (MnGeo) web map service (WMS) which provides statewide FSA DOQs in color and select years in color infrared from 2013, 2010, 2009, 2008, 2006, and 2003, as well as a black and white USGS DOQ from 1991 (MnGeo 2014).

Table 2.1: Table A and B modified from Rogers et al. (2006) displays the accuracies relative to both the 1991 USGS DOQs and GPS readings. The discrepancy in terrain and accuracy seen in the GPS readings was attributed to the ability to obtain accurate readings in open terrain thereby increasing horizontal accuracy on the DOQs.

A. Accuracy Relative to 1991 USGS DOQs			B. Accuracy Relative to GPS Readings		
Terrain	Horizontal Accuracy (ft)	Confidence	Terrain	Horizontal Accuracy (ft)	Confidence
Flat	6	95%	Flat	5	95%
Moderate Hills	10	95%	Moderate Hills	8	95%
Hills	11	95%	Hills	3	95%

2.1.3 Review of Assessing Digitizing Error in Planform Channel Change Studies

Once the imagery is registered, the next step is to digitize channel boundaries, or banklines, from the imagery so measurements can be made in a GIS. A uniform distinction for addressing a river's boundary/edge is to use its bankfull level, but issues stem from the definition of the word "bankfull" since it has been assigned various meanings in the literature depending on the application, the field of study, and the investigator (Williams 1978). In the case of planform analysis, a suitable way to establish bankfull is by identifying boundary features which differentiate the wetted perimeter for flows at maximum channel capacity from the floodplain (Mount and Louis 2005). In low flows, these boundary features can be distinguished as areas lacking vegetation or sparsely vegetated (Winterbottom 2000; Wishart, Warburton, and Bracken 2008; Giardino and Lee 2011). Areas having no or sporadic vegetation indicate regular inundation and can be considered part of the active channel (Lauer and Parker 2008; Richardson and Fuller 2010; Yao et al. 2013). Even with these descriptive definitions, it is impossible to fully avoid the subjective nature of boundary feature identification or misidentification during the digitization process. This subjectivity by individual digitizers, in turn, introduces another form of error which must be accounted for when considering total geospatial error in planform analysis (Mount et al. 2003).

It should be noted that using vegetation as an indicator for banklines can only be used in regions where this is a viable option. Large trees can be problematic by inhibiting the view of the bankfull edge (Mount and Louis 2005) but digitizing through the crown of the trees has been suggested as a solution (Winterbottom 2000; Giardino

and Lee 2011) leaving some further uncertainty as to the digitizing accuracy of the channel boundary.

Once the banklines are delineated, they can be used for calculating planform characteristics like channel width (Winterbottom 2000) or can be collapsed using a GIS tool to create a centerline for measuring other characteristics like lateral migration (Giardino and Lee 2011). Micheli, Kirchner, and Larsen (2004) digitized a centerline from low flow water edges in the Sacramento River instead of digitizing bankfull edges. In this study, repeated digitization with two different analysts were used to quantify digitizing error at 5% for the approximately 15 meter wide channel. Legleiter (2014) handled the quantification of digitizing error by referencing another research paper's (Micheli and Kirchner 2002) error margin for digitizing. Variations in these different digitizing methods and error quantification techniques along with critiques and suggestions for how to best handle this process are covered in the discussion (section 2.4.2).

2.2 Methods for Assessing Channel Planform Change on the Minnesota River (year to year)

2.2.1 Aerial Photograph Acquisition for the Minnesota River Valley

The first step to this research was exploring as many physical and digital collections of aerial imagery as possible to obtain temporal and spatial coverage of the study area. Various sources were explored to obtain historical aerial imagery (e.g. USGS Earth Explorer, Minnesota State University, Mankato's Dooley Map Library, University of Minnesota's John R. Borchert Map Library), however all but four aerial photographs

were able to be obtained from the University of Minnesota's free online database, Minnesota Historical Aerial Photographs Online (MHAPO). The other four photographs were physically obtained at the University of Minnesota's John R. Borchert Map Library. The years collected were primarily dictated by the availability of imagery for the entire study reach. Those years selected were the most complete records available, although some years may contain several photographs that vary by a year to complete the dataset. The gap between the years collected had to allow enough time for measurable detectable change that was greater than error present (Gurnell, Downward, and Jones 1994). Lea and Legleiter (2016) reported very little statistically significant change when using years 1-3 year intervals, but in their analysis of 9 and 17 year intervals over half the measurements were statistically significant. For this reason, along with the time intensive nature of making historical imagery usable in a GIS approximately 10-20 year intervals were used in this study. The years of historical aerial photographs used in this study were 1937, 1951, 1964, and 1980 (Table 2.2).

Table 2.2: Summary of the aerial imagery collected for planform analysis.

Year	Photograph Date (# of Photos)	Originator	Obtained From	Pixel Resolution	Type
1937	11/26/37 (3) 11/29/37 (13) 11/9/37 (2) 11/3/37 (10) 10/30/37 (6) 10/11/37 (1) 9/23/37 (1) 7/1/37 (1) 9/21/38 (1) 9/20/38 (2) 10/25/38 (2) 7/10/38 (2)	U.S. Agricultural Adjustment Administration (AAA)	University of Minnesota MHAPO	<u>1938</u> Range .91-.95 Ave .927 <u>1937</u> Range .62-.95 Ave .73	Black and White
1951	8/20/50 (3) 9/5/50 (1) 7/12/51 (1) 7/14/51 (5) 7/31/51 (1) 7/20/51 (1) 7/21/51 (2) 7/23/51 (13) 7/25/51 (7) 7/24/51 (2)	U.S. Department of Agriculture, Production, and Marketing Administration Park Aerial Surveys Inc. (1950) Robinson Aerial Surveys, Inc. (1951)	University of Minnesota MHAPO	<u>1950</u> Range .9-.91 Ave .908 <u>1951</u> Range .65-.96 Ave .758	Black and White
1964	6/25/64 (2) 9/29/64 (3) 7/14/64 (1) 7/23/64 (2) 10/9/64 (3) 10/2/64 (2) 8/8/64 (1) 6/27/64 (1) 7/21/64 (2) 10/14/64(5) 7/4/64(4) 8/7/64 (4) 10/13/64 (8)	U.S. Agricultural Stabilization and Conservation Service Mark Hurd Aerial Surveys Inc.	University of Minnesota MHAPO	<u>1964</u> Range .63-.9 Ave .736	Black and White
1980	1979 (12) 1980 (49) 1981 (7)	Mark Hurd Aerial Surveys Inc.	University of Minnesota MHAPO and Borchert Map Library	1:9,600 <u>1980</u> Ave 1.186 Range .245 – 1.614	Natural Color and Black and White
1991	Spring	U.S. Geological Survey (USGS) DOQ	MN Geospatial Information Office (MnGeo)	1	Black and White
2013	Summer and Fall	FSA DOQ	MnGeo	1	Natural Color

Apart from these unreferenced aerial photographs, digital orthoimagery (DOQs) were used from the Minnesota Geospatial Information Office's (MnGEO) Web Map Service (WMS). This service provides state-wide orthoimagery coverage for various years between 2013 and 1991 (Table 2.2). For this study, measurements were taken using only 2013 and 1991 to match the temporal intervals of the complete aerial photograph sets.

2.2.2 Minnesota River Image Registration

Once the imagery (both aerial photographs and DOQs) were collected, the unreferenced aerial images were brought into ArcMap 10.2.2 and registered to a common coordinate system (NAD 83 UTM 15 N) using the georeferencing toolbar. To reference the images, the MnGeo hosted 1991 USGS DOQ was used as a base layer, and ground control points common to both images were used to tie the unreferenced photographs to the base layer. The 1991 DOQ was referenced because it offered the earliest orthoimagery available, increasing the likelihood of finding common GCPs with historical imagery. The process and specifications closely followed the suggestions made by Hughes, McDowell, and Marcus (2006) and Lea and Legleiter (2016) on the best practice for registering aerial imagery for measuring lateral channel change in a GIS.

Each image was assigned a minimum of eight ground control points with preferential placement near the river and surrounding floodplain to avoid distortion from local terrain relief (Hughes, McDowell, and Marcus 2006). A second order polynomial transformation was applied to all the photographs in order to correct for some of the radial error presented by the earth's curved surface, unavoidable geometric error

presented by local topography, and lens distortion (Hughes, McDowell, and Marcus 2006).

Finally, the images' pixels were resampled due to the stretching and compressing of the pixels during the transformation process (warping of the image). Hughes, McDowell, and Marcus (2006) suggest experimentation with pixel resampling for specific photosets and research applications. After applying a nearest neighbor, bilinear interpolation, and cubic convolution resampling to several photographs and viewing them at a scale of 1:2000 (the scale digitized at), it was difficult to distinguish among the three resampling types. Since a handful of photographs were already rectified using a bilinear interpolation and there seemed to be little-to-no visual effect at the scale digitized at (1:2000), we chose to remain consistent and rectify all imagery using a bilinear interpolation.

A final step that is optional, but recommended, is rectifying the photographs. This process creates a new raster dataset that has the coordinate information permanently associated with the file. Another option is to store the coordinate information in auxiliary (external) files and not create a new raster dataset. If the data is going to be used for analysis purposes or in other software packages, the data should be rectified, which was done in this analysis (Hughes, McDowell, and Marcus 2006).

The four photographs that had to be converted from paper to digital format were scanned at a resolution of 600 dpi which gave the photographs a resolution under 1 meter after image registration and pixel resampling. This was consistent with the range of the

rest of the aerial photographs (Table 2.2). The workflow for these processes is summarized in Figure 2.2.

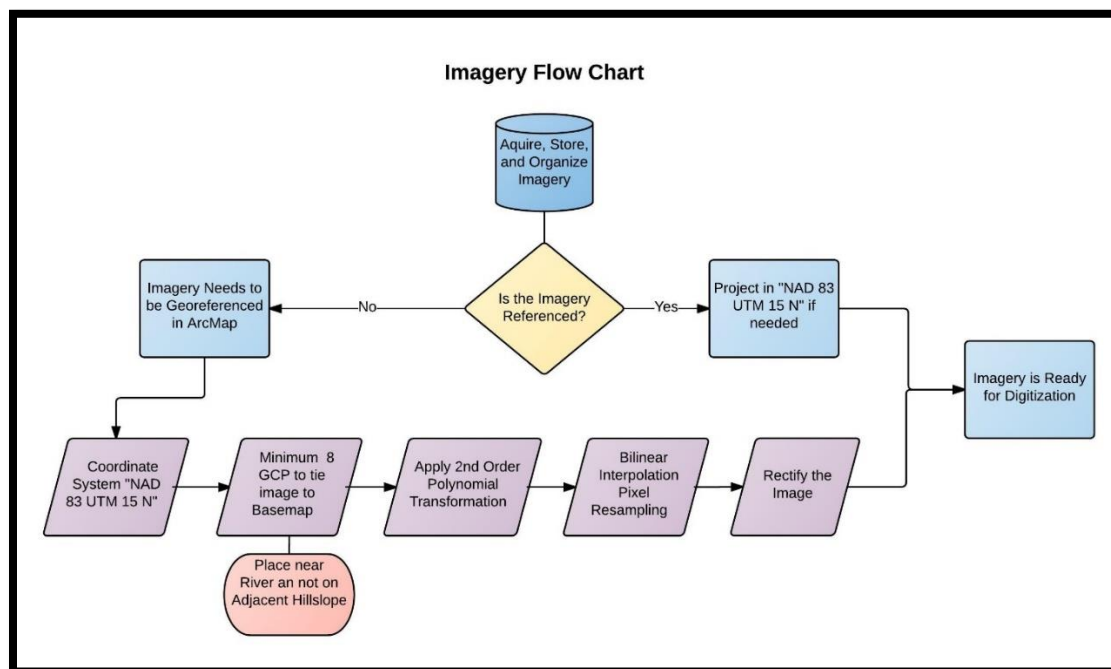


Figure 2.2: Flow chart outlining the step by step process of taking collected imagery and registering it to a coordinate system, so it can be digitized for analysis.

2.2.3 Minnesota River Image Registration Error Assessment

To assess the error associated with image registration, multiple metrics were examined and recorded. The first metric was simply recording the RMSE value that is automatically calculated during the image registration process in ArcMap (Appendix A). The RMSE value was commonly used in past studies (e.g. Urban and Rhoads 2003; Giardino and Lee 2011) as the sole source of the error assessment, but more recently the positional error of linear features has been reevaluated as an independent research topic (Mount and Louis 2005; Hughes, McDowell, and Marcus 2006; Lea and Legleiter 2016). These studies have discredited the former assessments of error quantification (RMSE) and offered new suggestions that will be detailed and implemented in this section.

A novel approach was being formulated based off the ideas of Hughes, McDowell, and Marcus (2006) to use scattered independent GCPs to test error independently of the RMSE value. However, as the methodology was being developed, Lea and Legleiter (2016) published an approach that mirrored what was trying to be accomplished using MATLAB scripts. These scripts not only incorporate robust statistical evaluations but also account for the spatial variability of the error. Therefore, their scripts were used along with newly created python scripts to further the automation of the overall process.

We quantified spatially variable uncertainty for each time interval (1937 to 1951, 1951 to 1964, 1964 to 1980, 1980 to 1991, 1991 to 2013), as well as for the entire record from 1937 to 2013. Next, GCPs identified in both sets of imagery for a given interval were collected in two separate shapefiles. This process is similar to registering aerial photographs (Figure 2.3). The major difference is that these points are stored in shapefiles and are collected independently from the image registration process giving a metric for error aside from the points used to calculate RMSE.

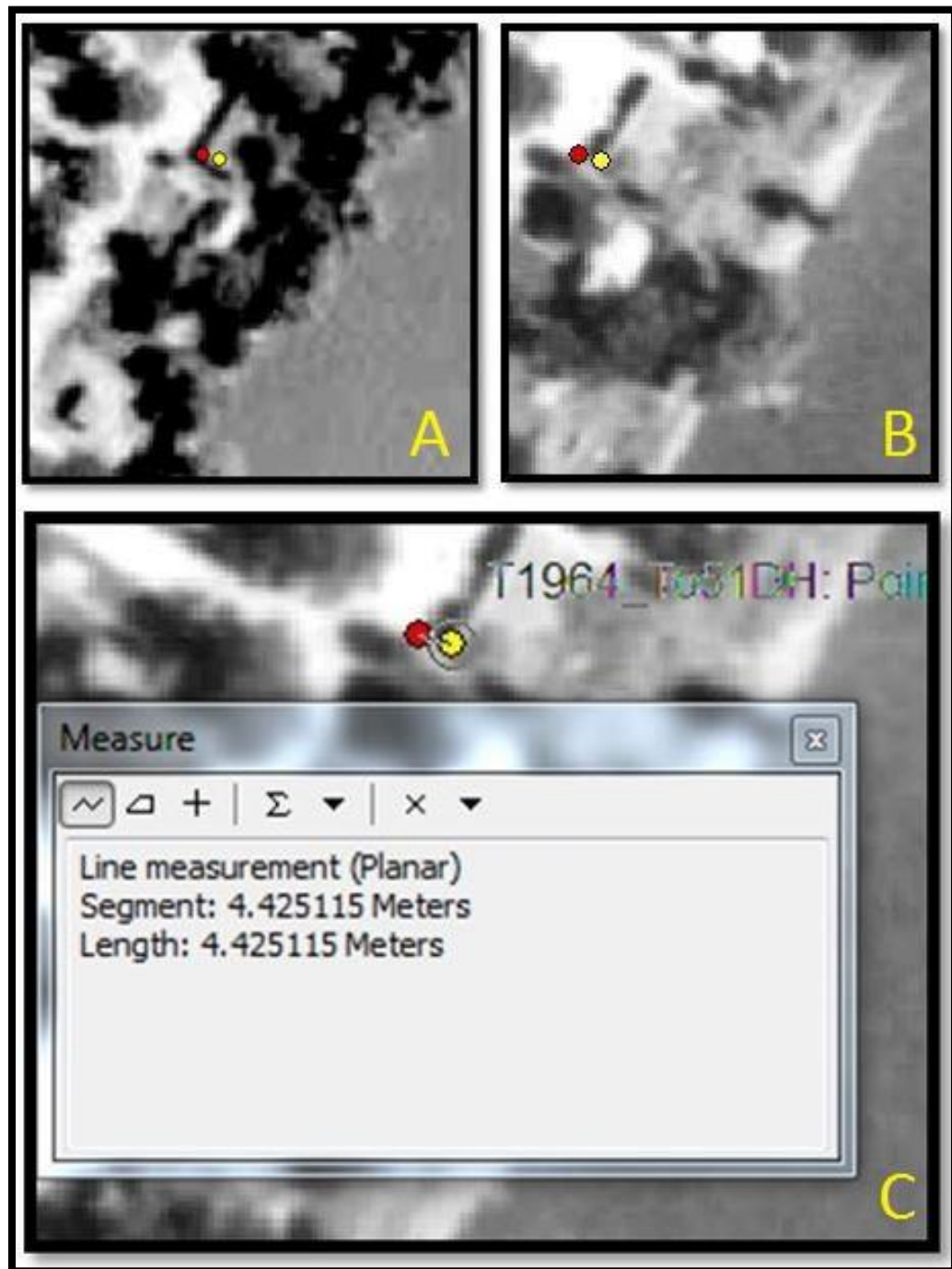


Figure 2.3: The displacement between a pair of GCPs on two sets of aerial images is shown. The red dot represents a GCP for 1951 and the yellow dot for 1964. A) This displays the referenced aerial photograph for 1951 and the corner of the building being marked. B) This displays the referenced aerial photograph for 1964 and the corner of the same building being marked. C) This displays the displacement between the two referenced photographs at ~4.4 meters.

Ground control points for this analysis were created by an upper division fluvial geomorphology class at Minnesota State University, Mankato (Geography 416/516: Fluvial Geomorphology & Hydrology). In total, there were five undergraduate and five graduate students separated into groups of two. Although each student created their own GCPs for the entire reach, they were assigned the same interval to assess so they could help each other if problems presented themselves. This allowed for a comparison between students to further validate the GCP error for each interval. It also allowed for a larger sample size by combining the GCPs placed by both students for each interval.

All students were provided with a polygon shapefile that outlined the Minnesota River Valley (Figure 2.4). This file was created to concentrate the student's GCP placement in the river valley where all the measurements of interest were made (Hughes, McDowell, and Marcus 2006). This reduces the incorporation of unnecessary error from terrain relief that cannot be corrected from image rectification process as discussed in section 2.1.2 and follows the recommendation of both Hughes, McDowell, and Marcus (2006) and Lea and Legleiter (2016). The file was digitized from the USGS 30 meter resolution DEM for the state of Minnesota hosted on the Minnesota Geospatial Commons.

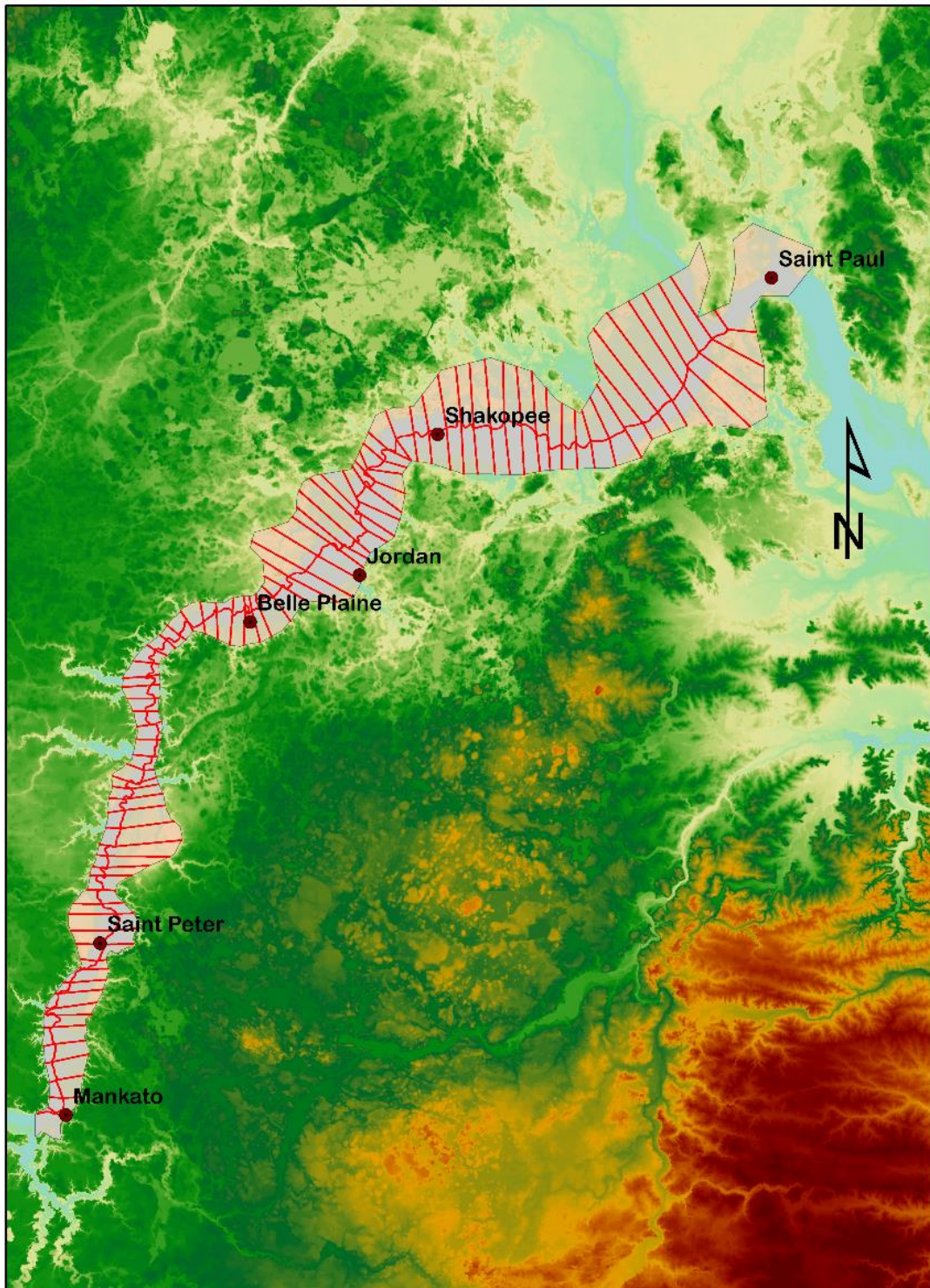


Figure 2.4: The shapefile in light pink was provided to show the river valley and the red lines intersect the Minnesota River approximately every two river kilometers. These two shapefiles served as guides for GCP placement.

Another shapefile was provided that included transects approximately every two river kilometers through the river valley (Figure 2.4). This file was provided to aid with the spatial density of point selection to get a more accurate overview of the entire study area. This file was created by taking the 2013 river centerline, which is 167831.8 meters long, and using the split tool in the ArcMap editor toolbar to divide the 2013 centerline into 84 equal parts (1998.0 meters each). Transects were then manually digitized across the river valley at each line break. The students were told that these were only presented as guidelines and if they could not find suitable GCPs within a two-kilometer section or within the river valley that it was acceptable to skip or look outside the given area in those instances.

Once all the sets of GCPs were collected for all six intervals of interest (Figure 2.5), the “Spatial Join” tool in ArcMap’s Analysis Toolbox was used to calculate a new field that had the distance between GCP pairs for every interval. For example, if the same building is found in each photograph, the northwest corner will be marked in a 1951 shapefile and in a 1964 shapefile. The distance was then measured between the two points to see how far the photo shifted (Figure 2.3). Since the building likely did not move between the two years, the measured GCP offset can be used as a proxy for the error vector present in this given area resulting from image registration. This was used to calculate basic statistics for overall error among all the time intervals considered.

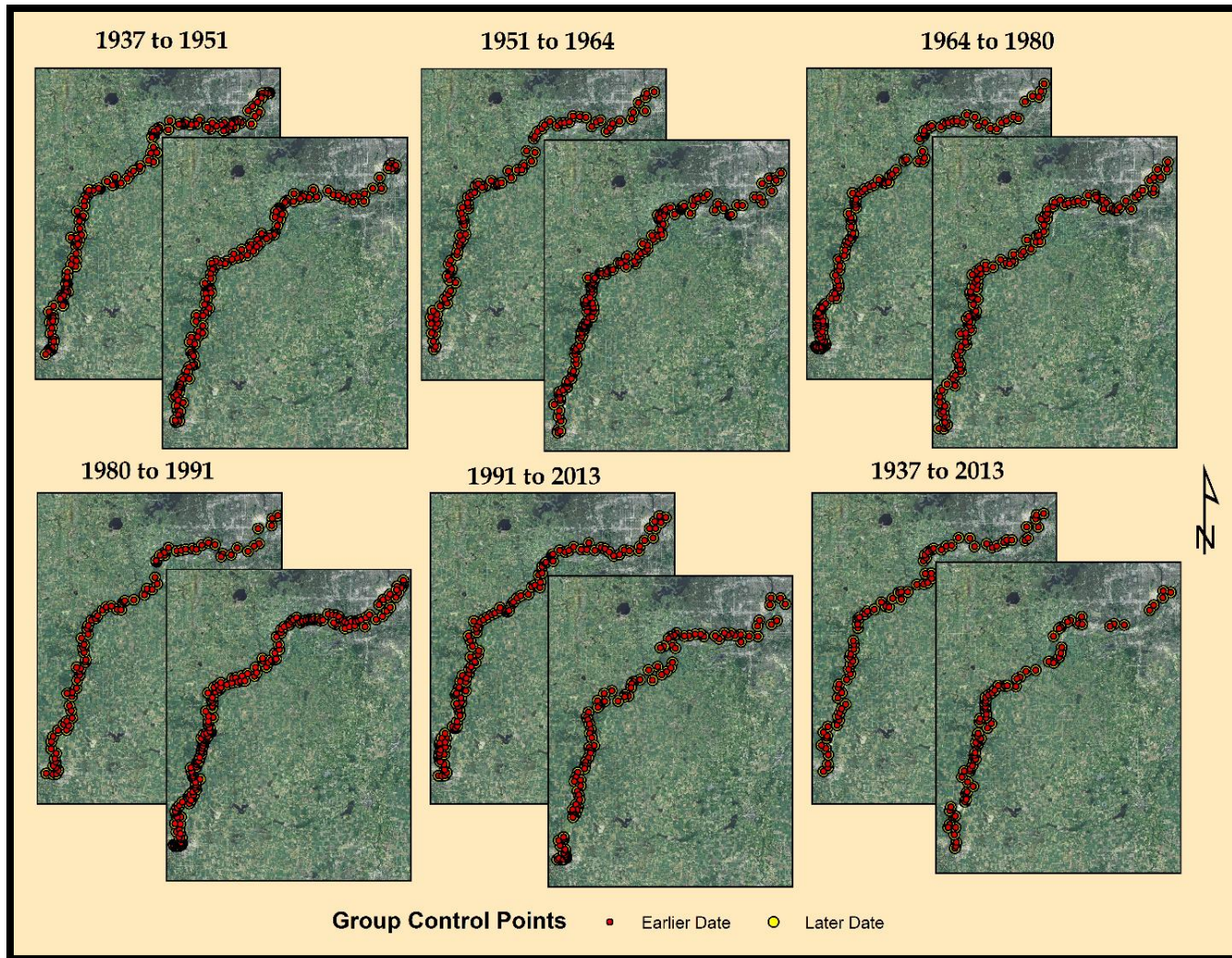


Figure 2.5: This figure displays each student's set of ground controls points for each time interval considered in this study. Two students analyzed every interval so both students GCPs are shown.

The GCPs were further processed so they could be used as inputs into Lea and Legleiter's (2016) MATLAB script "QuantifyRegistrationError" (Appendix B). The only user-required inputs for this script are two separate text files (one for each year) that contain the ID, X coordinate, and Y coordinate for the GCPs from the interval of interest. In order to give the GCP shapefiles x and y coordinates the "Add XY Coordinates" tool was run located in the "Data Management" > "Features" toolbox. The points were then examined manually to make sure all coordinate pairs had matching IDs between the two shapefiles. The IDs are what the MATLAB script uses to identify which coordinate pairs' displacement is being measured. These shapefile attribute tables were then exported as CSV and TXT files. The script uses the IDs to match coordinate pairs between the two files and the x and y coordinates to calculate the error vector in that given location. From here, the script can be run to create an output for the registration error based on spatial variability which serves as the input for the next MATLAB script covered in Chapter 3. For further detail on the script, see Appendix B which contains the full script with comments explaining the process step-by-step. The workflow for the final image registration error assessment is displayed in Figure 2.6.

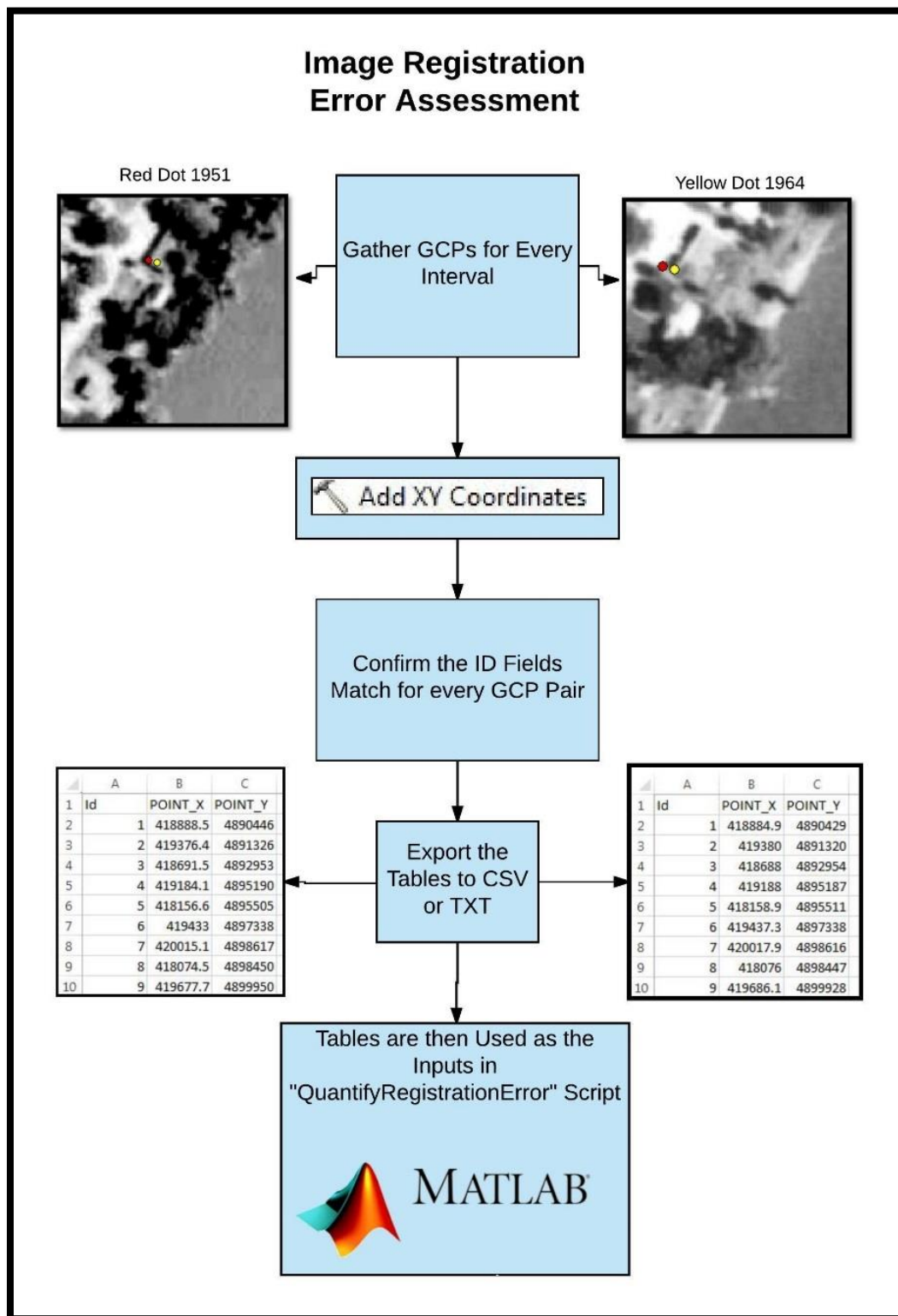


Figure 2.6: This workflow displays the process for the image registration error assessment.

2.2.4 Bank and Centerline Digitization of the Minnesota River

To make all the collected and assessed imagery useful for quantifying planform change, the banklines were digitized for every year of interest. This study followed the same definition that was commonly agreed upon by prior planform studies (Winterbottom 2000; Wishart, Warburton, and Bracken 2008; Giardino and Lee 2011).

For this study, banklines were primarily determined by vegetation rather than the water itself. Bankline feature identification was approached this way due to the variability of the river stage from one set of photographs to the next (Lauer and Parker 2008). Lines were digitized to separate active channel areas by differentiating no or sparse vegetation from areas of dense vegetation (Winterbottom 2000). This was chosen because areas that have no or sparse vegetation are areas commonly inundated causing a disruption in vegetation establishment due to being part of the active channel (Richardson and Fuller 2010). In areas where tree cover marked this division, the bankline was digitized through the crown of the tree (Winterbottom 2000). This is justifiable considering a tree that is large enough to eclipse the bank from a planform view has been holding the bank boundary for many years.

Banklines were digitized at a scale of 1:2000 by one primary student analyst with minor assistance from a second student analyst. Both analysts digitized several banklines from years that were not used in this study to practice this process before digitizing the years of interest. The analysts also created separate shapefiles to indicate stretches of the river where bankline interpretation was difficult. These questionable areas were then looked at by multiple analysts to come to up with a final decision on where to digitize the bank.

After all the banklines were created for the years of interest, the centerlines were interpolated using a “Centerline Interpolation” tool in the National Center for Earth-Surface Dynamics’ (NCED) Planform Statistics Toolbox (Lauer 2006). This tool automates the process by creating center points at a user defined downstream distance (10 meters in this study) which is then adjusted to be equidistant to each bank (Figure 2.7; Aalto, Lauer, and Dietrich 2008). These lines were then inspected but no additional smoothing was necessary. For a detail regarding the NCED “Centerline Interpolation” tool (see Figure 2.8).

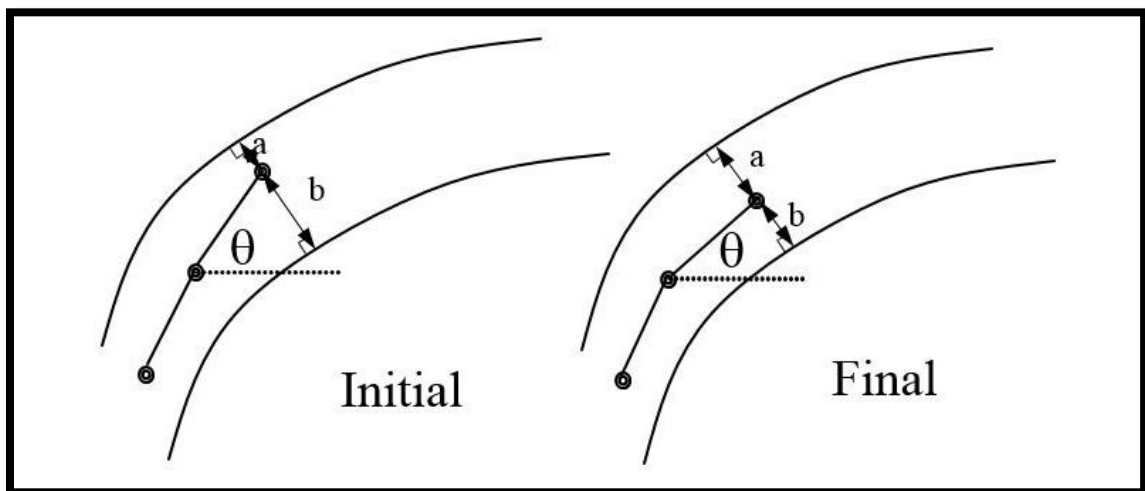


Figure 2.7: This figure is from (Lauer 2006) and shows how the algorithm creates the centerlines. In the initial phase, a new point is set at the user-defined distance from the prior point. The angle θ is then adjusted until the new point is equidistant between the nearest points on each bank line so $a = b$.

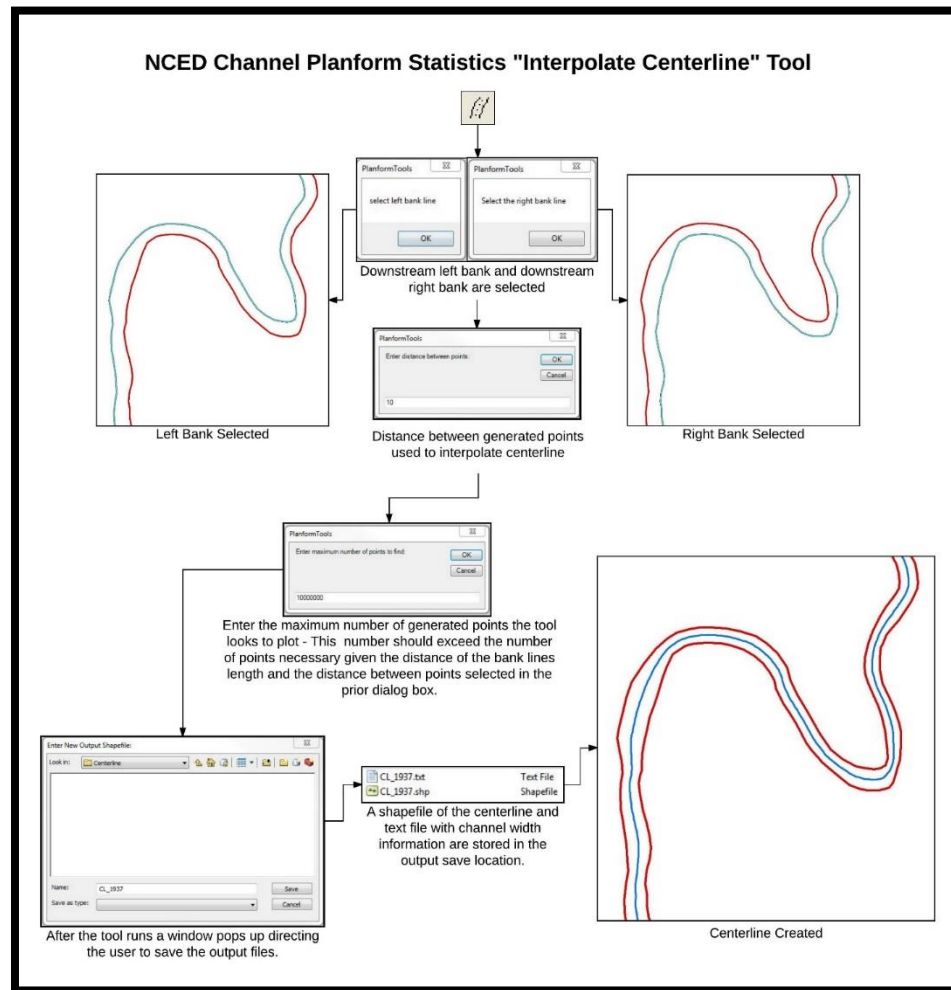


Figure 2.8: This workflow highlights the step-by-step process of working through the NCED Planform Statistics “Interpolate Centerline” tool.

2.2.5 Bank and Centerline Digitizing Error Assessment

Digitizing error can occur because of feature misidentification. This could be caused by visual obstructions (tree canopy, bridges, shadows, etc.), imagery resolution/scale, or simply by careless digitization. To assess this, a similar approach to Micheli, Kirchner, and Larsen (2004) was taken by repeating the digitization process multiple times. In theory, if banklines were perfectly identified and digitized multiple times for a given set of imagery, the subsequent collapsed centerlines would seamlessly

overlap each other. Therefore, if the same set of imagery is redigitized, any differences in centerlines will appear as “false migration” which is present from digitizing error (Figure 2.9).

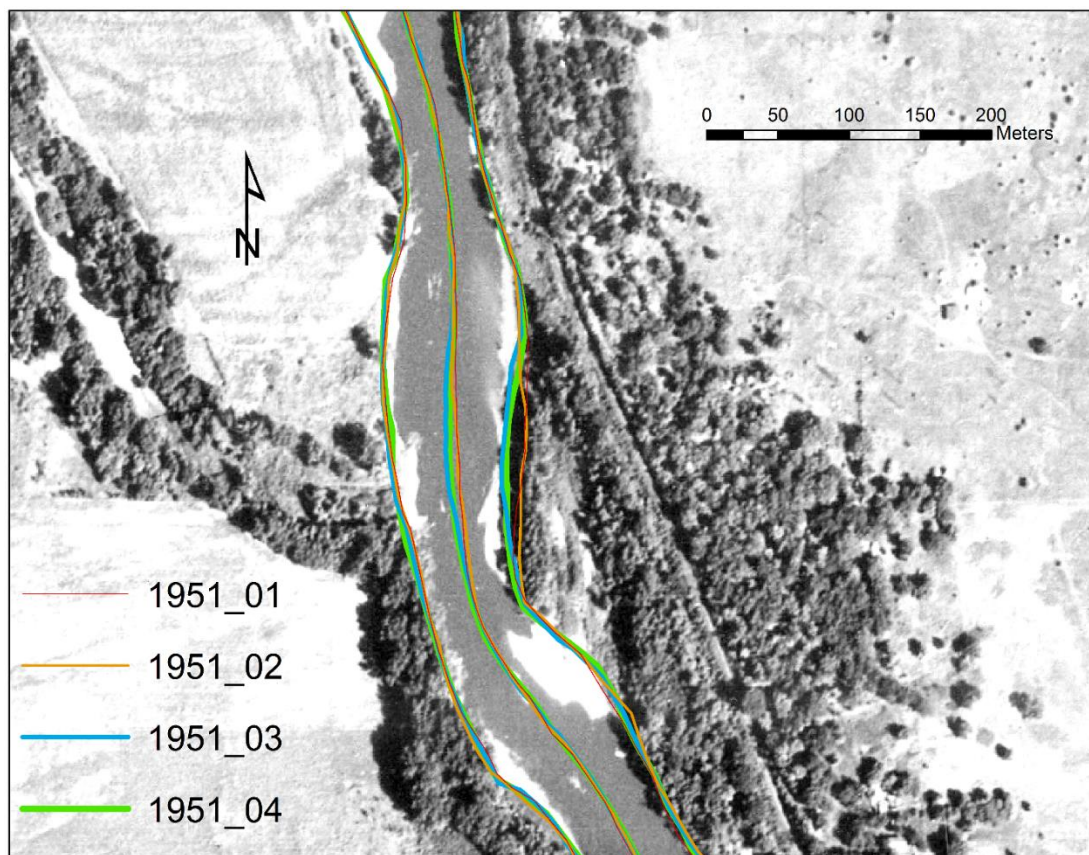


Figure 2.9: This figure displays a section of the four sets of banklines that were digitized for 1951 and subsequent collapsed centerlines that were created using the NCED “Interpolate Centerline” tool. The variations can be noticed between digitized banklines which subsequently changes the course of the centerline. These centerlines were then used to identify the digitization error present.

For this study, every year of imagery obtained was individually assessed. A 10 kilometer stretch of the Minnesota River was selected that was representative of the river. The stretch extended from the city of Mankato (urban) downstream into rural areas of both forested vegetation and farm land. For each year, the banklines for this stretch of river were digitized four times at a scale 1:2000 (same scale the banklines were digitized

at for the entire study area). It is important to note after each set of banklines was digitized, they were saved, and the layer was turned off to avoid influencing the next round of digitization.

Once the banklines were complete, The NCED Platform Statistics Toolbox “Channel Migration” tool was used to determine the false migration (i.e. digitizing error) present. This toolbox is also used in many channel migration studies (Aalto, Lauer, and Dietrich 2008; Belmont et al. 2011; Legleiter 2014; Lea and Legleiter 2016) and will also be used in Chapter 3 to calculate channel migration among the various time intervals. The steps used to complete this assessment are as follows:

1. Banklines were redigitized four times for every set/year of imagery used.
2. The NCED “Interpolate Center Line” tool was used to collapse the banklines to a centerline.
3. The NCED “Migration” tool was then used to make false migration measurements among all four centerlines (1-2, 1-3, 1-4, 2-3, 2-4, 3-4) for a total of six comparisons.
 - a. Measurements were taken at 10 meter intervals
 - b. Tables were exported as CSV’s for analysis
4. An R script (Appendix C) produced by Mitchell Donovan (Utah State) was modified and used to combine the CSV’s and create a box plot for comparative analysis among the time intervals considered.

2.3 Results

2.3.1 Image Collection, Registration, and Error Assessment

In total, 186 unreferenced aerial photographs were collected to create complete historical coverage of the Minnesota River study area (Figure 2.10). These photographs spanned four different time periods (1937, 1951, 1964, 1980) and were used in conjunction with the two time periods (1991, 2013 DOQs) previously referenced by the MnGeo WMS.

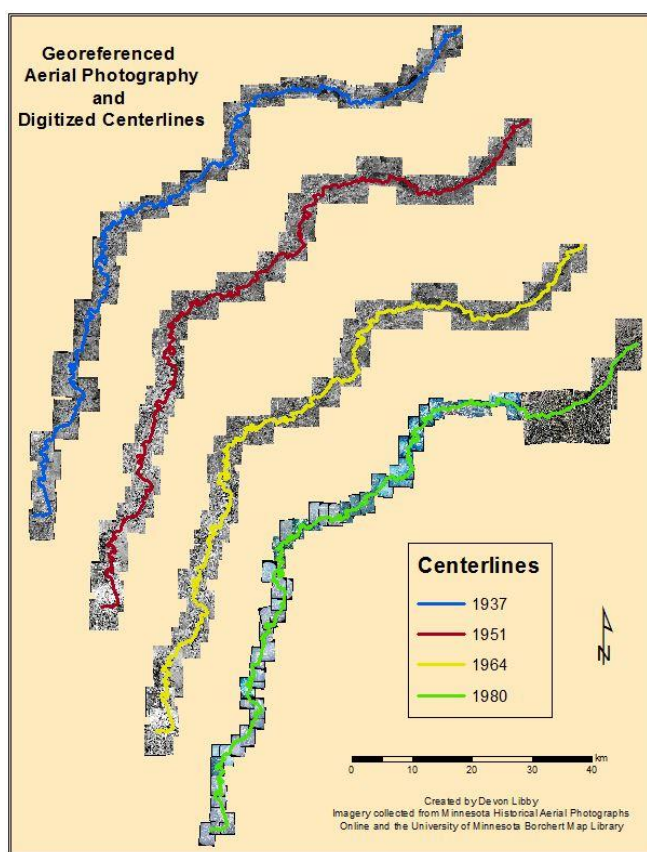


Figure 2.10: All georeferenced aerial photographs that were collected to get coverage of 1937, 1951, 1964, 1980.

As discussed in section 2.1.2, RMSE is ArcMap's built in error assessment for registered images. All 186 photographs had an RMSE under 1 (Appendix A). A summary of every time interval being used including: photograph dates, origin of the

photos, where they were obtained from, pixel resolution, and color type can be found in **Table 2**. The specific information on each individual photograph including: county and year, flight identification number, number of GCPs used, and RMSE can be found in Appendix A.

The image registration error that was assessed using independent GCPs was calculated in two different software packages and produced similar results. As mentioned in section 2.2.3, the first approach was a novel idea to use a spatial join in ArcMap to simply measure the linear offset distance of matching GCP pairs. Since this was a new idea, two analysts were used for every interval to see if results were uniform or if there was a major disparity that required further attention (Table 2.3). Results between analysts were quite similar validating the approach. The maximum mean discrepancy between analysts was 1.34 meters and was found to be as low as 0.20 meters (Table 2.3). Since these results between analysts proved to be reliable, the points were then combined for every interval to increase the amount of measurements made (Table 2.4). The maximum mean error was identified to be in the 1964-1980 interval at 10.83 meters and lowest error was in the 1991-2013 interval at 3.31 meters. The interval 1991-2013 has a significantly lower registration error than the other intervals because both these time periods imagery were DOQs from the WMS. DOQs by nature have a high degree of spatial accuracy but require specialties in software and skill and are time intensive to create (Hughes, McDowell, and Marcus 2006). All intervals where at least one-time period consisted of registered photographs had a mean error between 7.70-10.38 meters (Table 2.4).

Table 2.3: Data collected from two analysts for each time interval using the “Spatial Join” tool in ArcMap to calculate linear offset distances between GCP pairs for the two time periods being considered.

Time Interval	Analyst	# of GCP	Mean	Mean Difference Between Analysts	Maximum	Minimum	Standard Deviation
1937 to 1951	1	113	9.10	0.76	29.11	2.16	5.62
	2	120	8.34		38.62	0.87	6.55
1951 to 1964	1	122	7.56	0.84	47.34	0.73	6.03
	2	208	8.40		41.15	1.141	6.69
1964 to 1980	1	103	10.99	0.31	35.20	1.81	7.97
	2	106	10.68		46.00	1.57	7.73
1980 to 1991	1	162	8.14	1.34	33.46	0.36	5.98
	2	79	6.80		21.35	0.80	4.77
1991 to 2013	1	96	3.41	0.20	14.05	0.21	2.24
	2	108	3.21		17.01	0.02	2.22
1937 to 2013	1	76	6.39	1.27	24.58	0.55	5.21
	2	77	7.66		32.20	0.59	6.98

Table 2.4: The data from **Table 2.3** combined into one dataset for each time interval considered.

Time Interval	Number of GCP	Mean	Average RMSE Respectively	Maximum	Minimum	Standard Deviation
1937 to 1951	233	8.71	0.82 and 0.82	38.62	0.87	6.12
1951 to 1964	208	7.91	0.82 and 0.73	47.34	0.73	6.31
1964 to 1980	209	10.83	0.73 and 0.75	46.00	1.57	7.83
1980 to 1991	241	7.70	0.75 and (n/a)	33.46	0.36	5.64
1991 to 2013	204	3.31	n/a	17.01	0.02	2.23
1937 to 2013	153	7.03	0.83 and (n/a)	32.20	0.55	6.18

The independent GCPs were then reformatted in tabular form and moved into Lea and Legleiter's (2016) MATLAB script (Figure 2.6). The script produced a Microsoft Access Table (.mat) that stored generated variables from the script to use in the next script which determines whether migration measurements are statistically significant or insignificant (Chapter 3). Box plots (Figure 2.11-2.16) were also generated by the script providing another visual for each time interval which mirrored the results from the spatial join (Table 2.4) further validating the methods used.

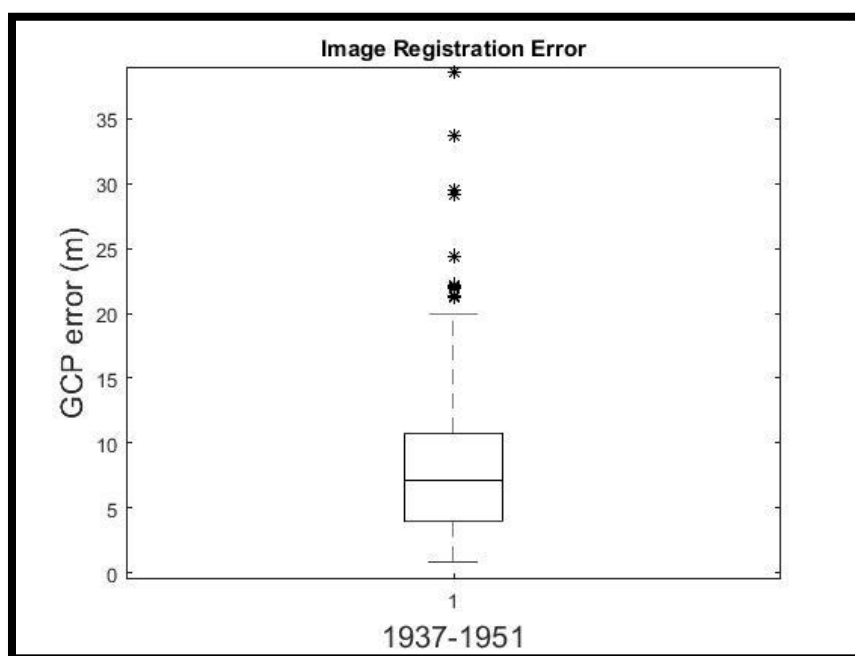


Figure 2.11: This displays the image registration error for the 1937-1951 time interval in a box plot generated from Lea and Legleiter's (2016) "QuantifyingRegistrationError" MATLAB script (Appendix B).

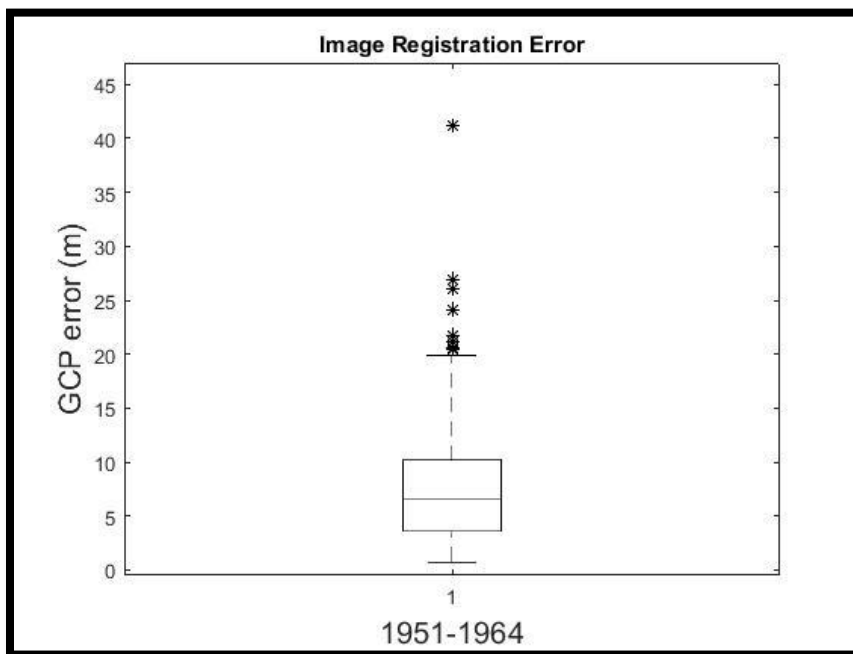


Figure 2.12: This displays the image registration error for the 1951-1964 time interval in a box plot generated from Lea and Legleiter’s (2016) “QuantifyingRegistrationError” MATLAB script (Appendix B).

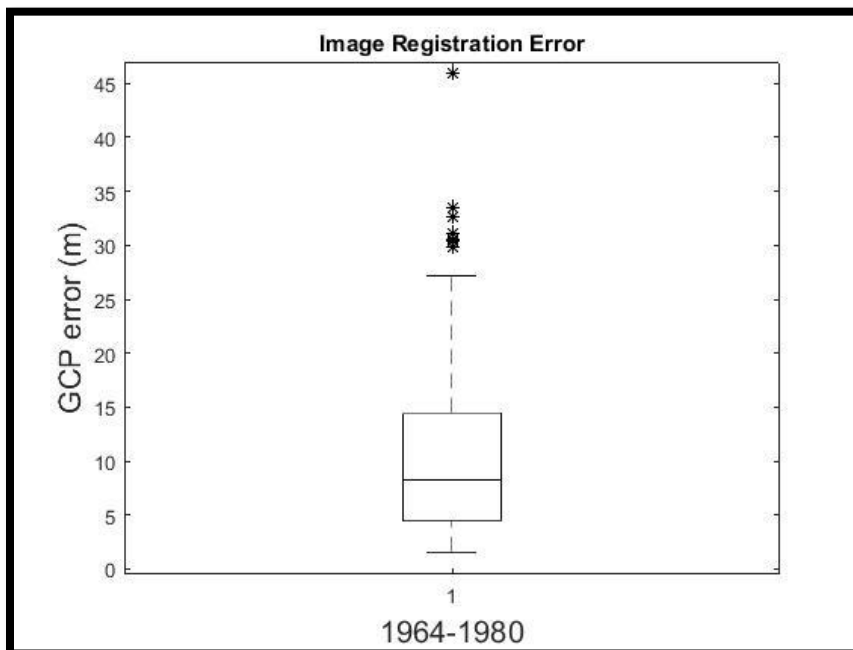


Figure 2.13: This displays the image registration error for the 1964-1980 time interval in a box plot generated from Lea and Legleiter’s (2016) “QuantifyingRegistrationError” MATLAB script (Appendix B).

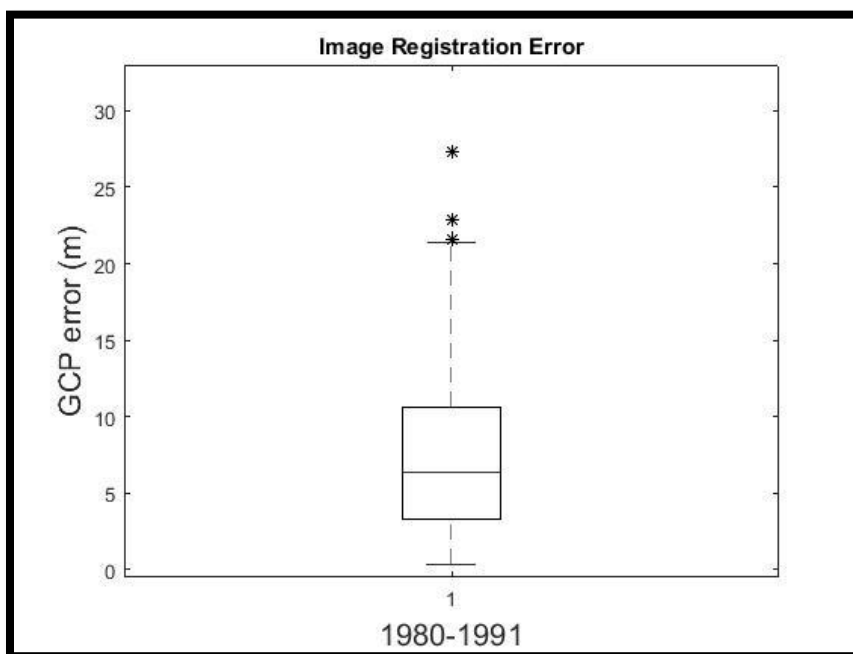


Figure 2.14: This displays the image registration error for the 1980-1991 time interval in a box plot generated from Lea and Legleiter’s (2016) “QuantifyingRegistrationError” MATLAB script (Appendix B).

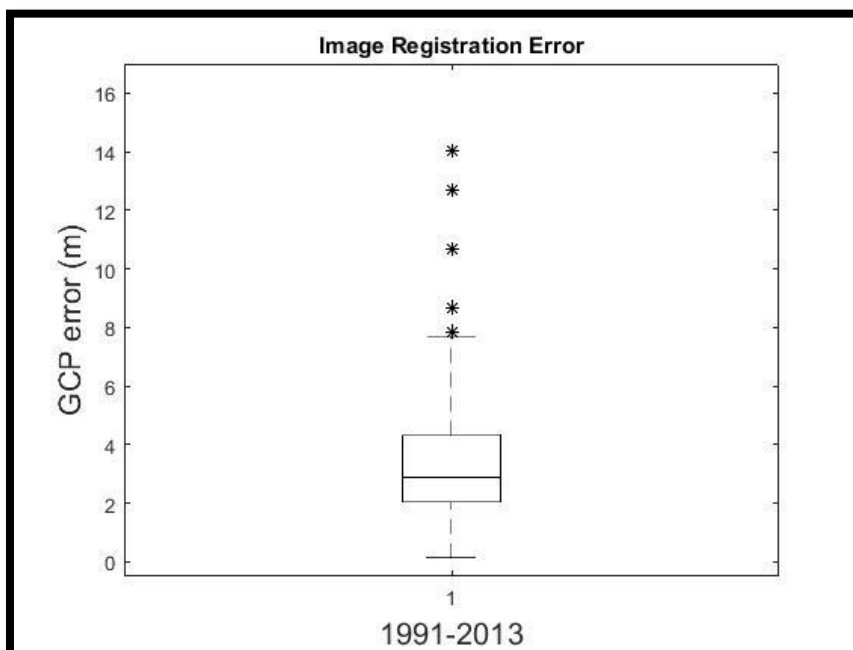


Figure 2.15: This displays the image registration error for the 1991-2013 time interval in a box plot generated from Lea and Legleiter’s (2016) “QuantifyingRegistrationError” MATLAB script (Appendix B).

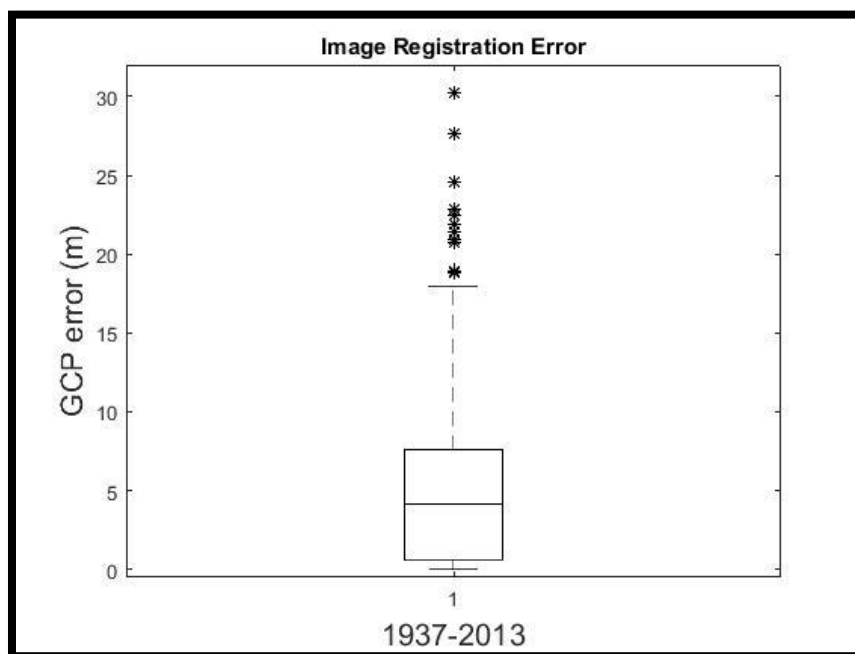


Figure 2.16: This displays the image registration error for the 1937-2013 time interval in a box plot generated from Lea and Legleiter’s (2016) “QuantifyingRegistrationError” MATLAB script (Appendix B).

2.3.2 Bank and Centerline Digitization and Error Assessment

Digitized banklines and collapsed centerlines which were created and used as input data in Chapter 3 are displayed in Figure 17-22. Error associated with the repeat digitization for every time period yielded relatively uniform results (Table 2.5). The range of averages was between 1.16 – 2.08 meters with a total of approximately 6000 measurements being made for every time period. Maximum error for the intervals ranged between 11.18 – 18.75 meters with minimums for every period being a few thousandths of a meter. Box plots (Appendix C) visually display the data for another cross comparison (Figure 2.23).

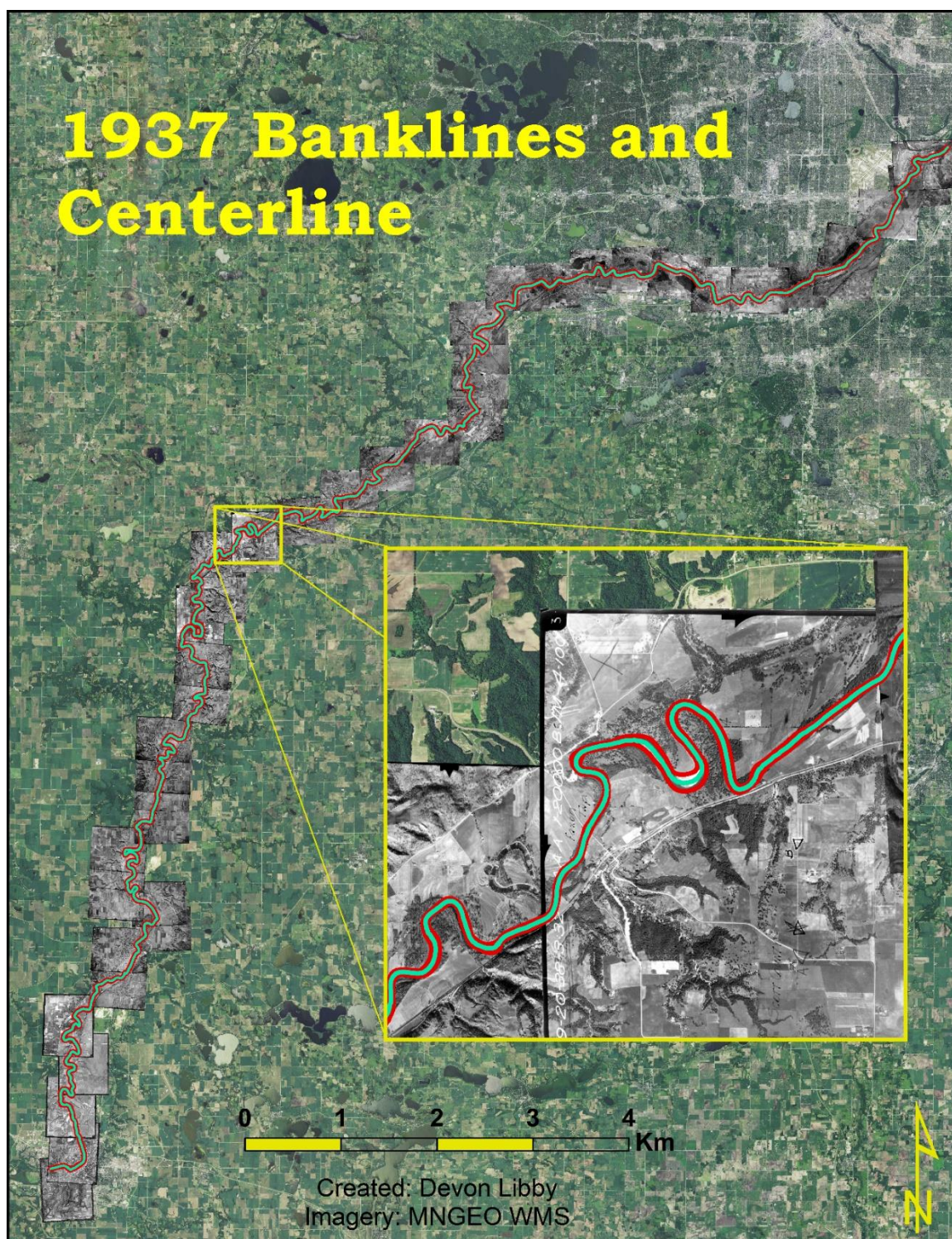


Figure 2.17: This map displays the digitized banklines and subsequently collapsed centerline for the 1937 time period overlaid on the 1937 georeferenced imagery from which it was digitized.

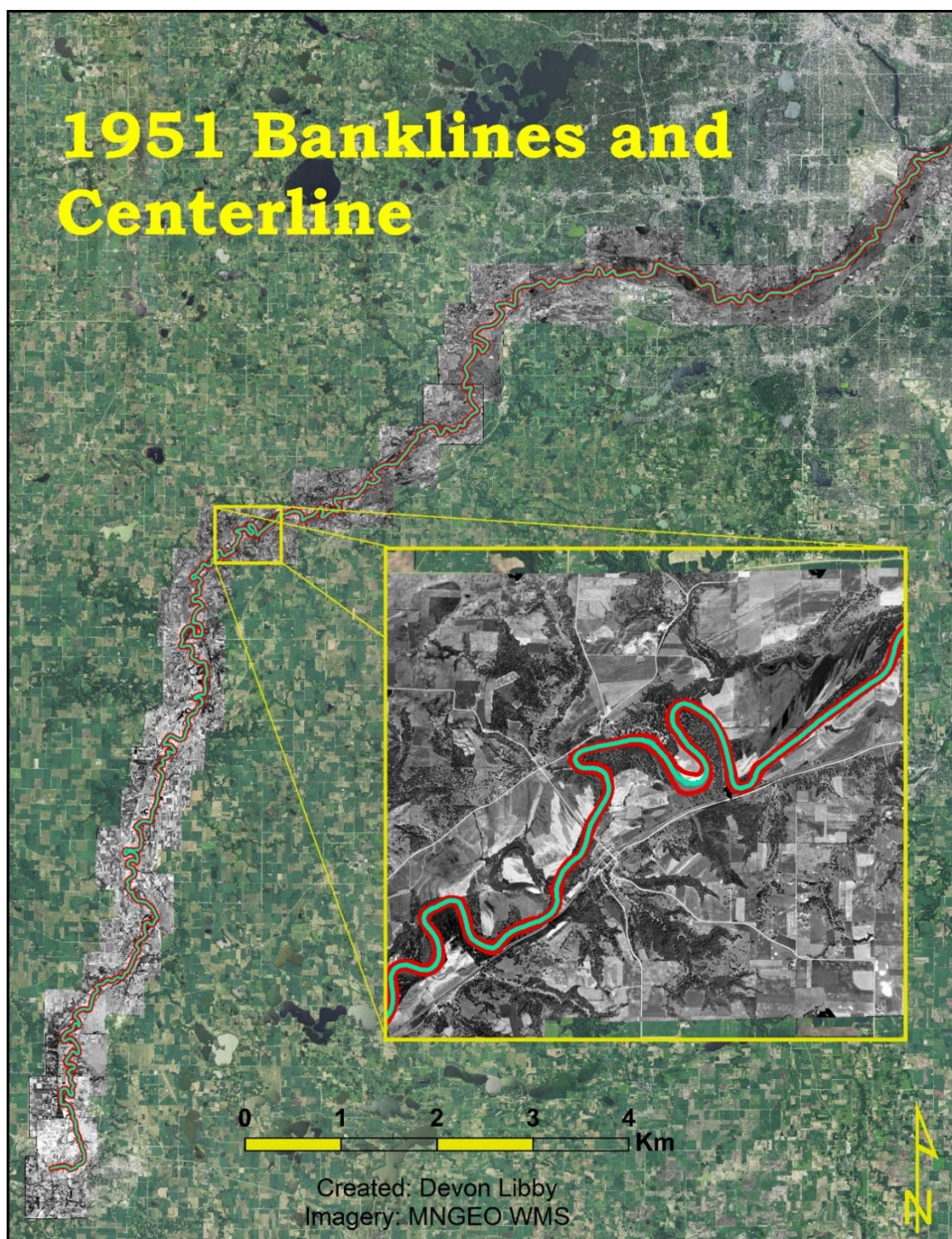


Figure 2.18: This map displays the digitized banklines and subsequently collapsed centerline for the 1951 time period overlaid on the 1951 georeferenced imagery from which it was digitized.

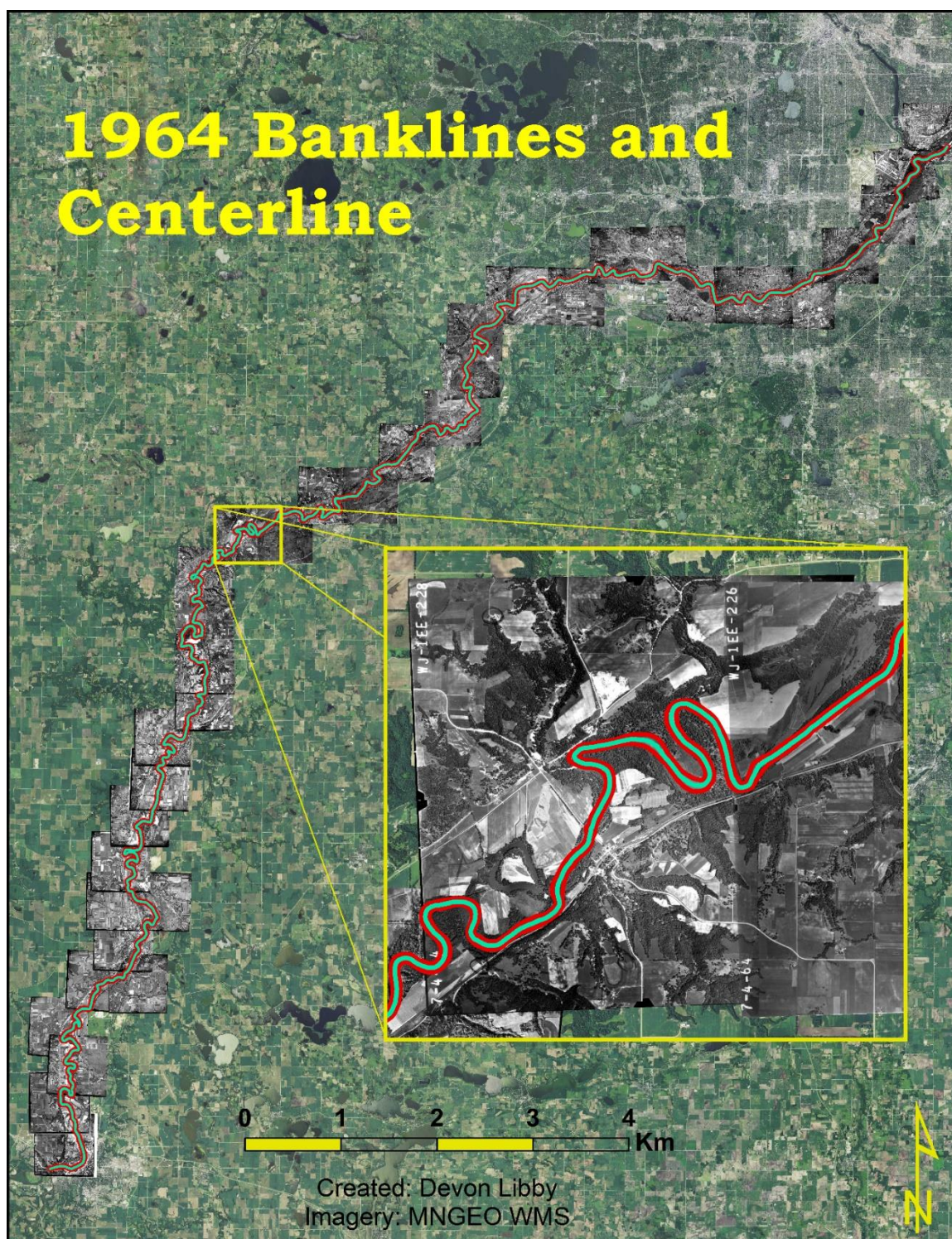


Figure 2.19: This map displays the digitized banklines and subsequently collapsed centerline for the 1964 time period overlaid on the 1964 georeferenced imagery from which it was digitized.

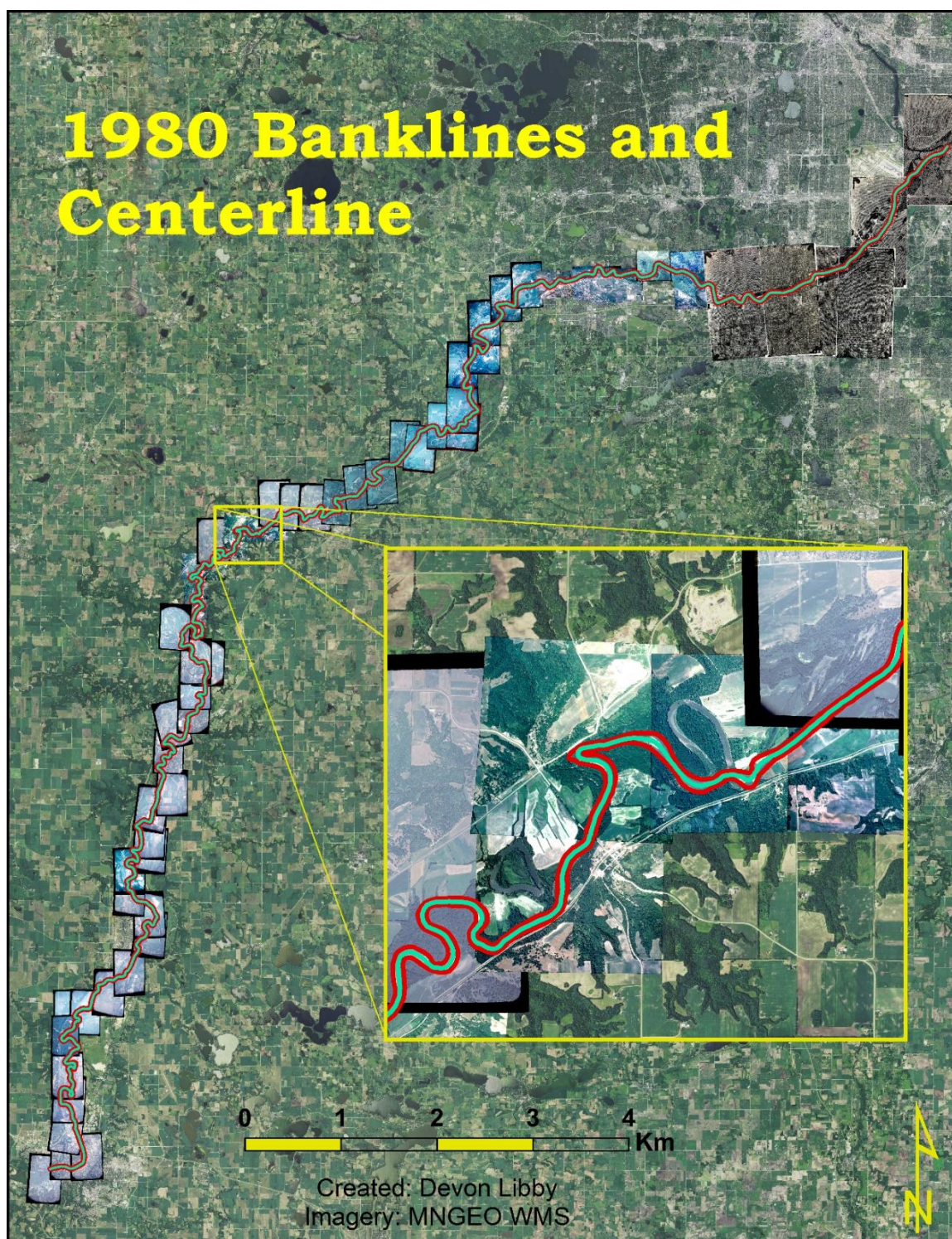


Figure 2.20: This map displays the digitized banklines and subsequently collapsed centerline for the 1980 time period overlaid on the 1980 georeferenced imagery from which it was digitized.

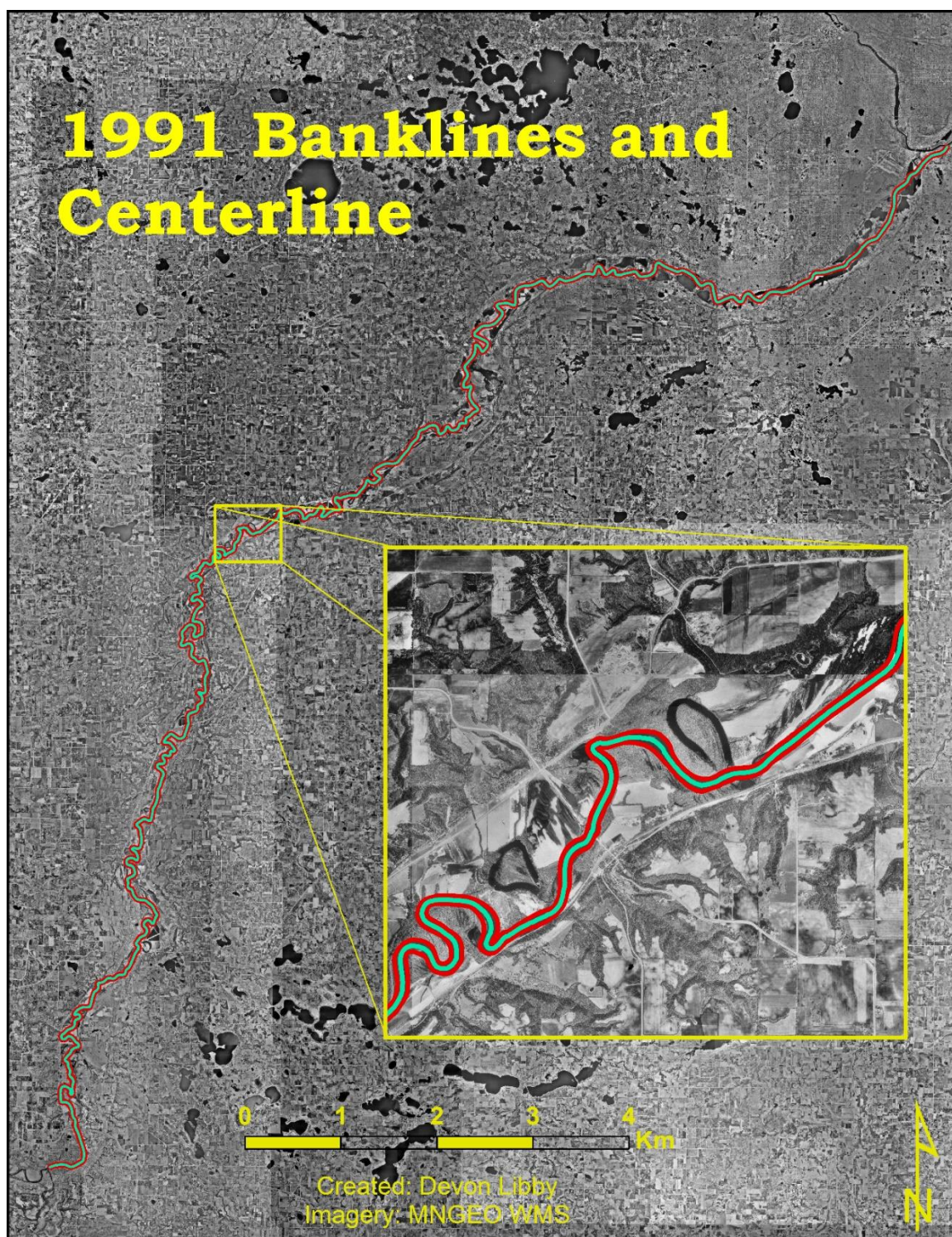


Figure 2.21: This map displays the digitized banklines and subsequently collapsed centerline for the 1991 time period overlaid on the 1991 MNGEO WMS DOQ from which it was digitized.

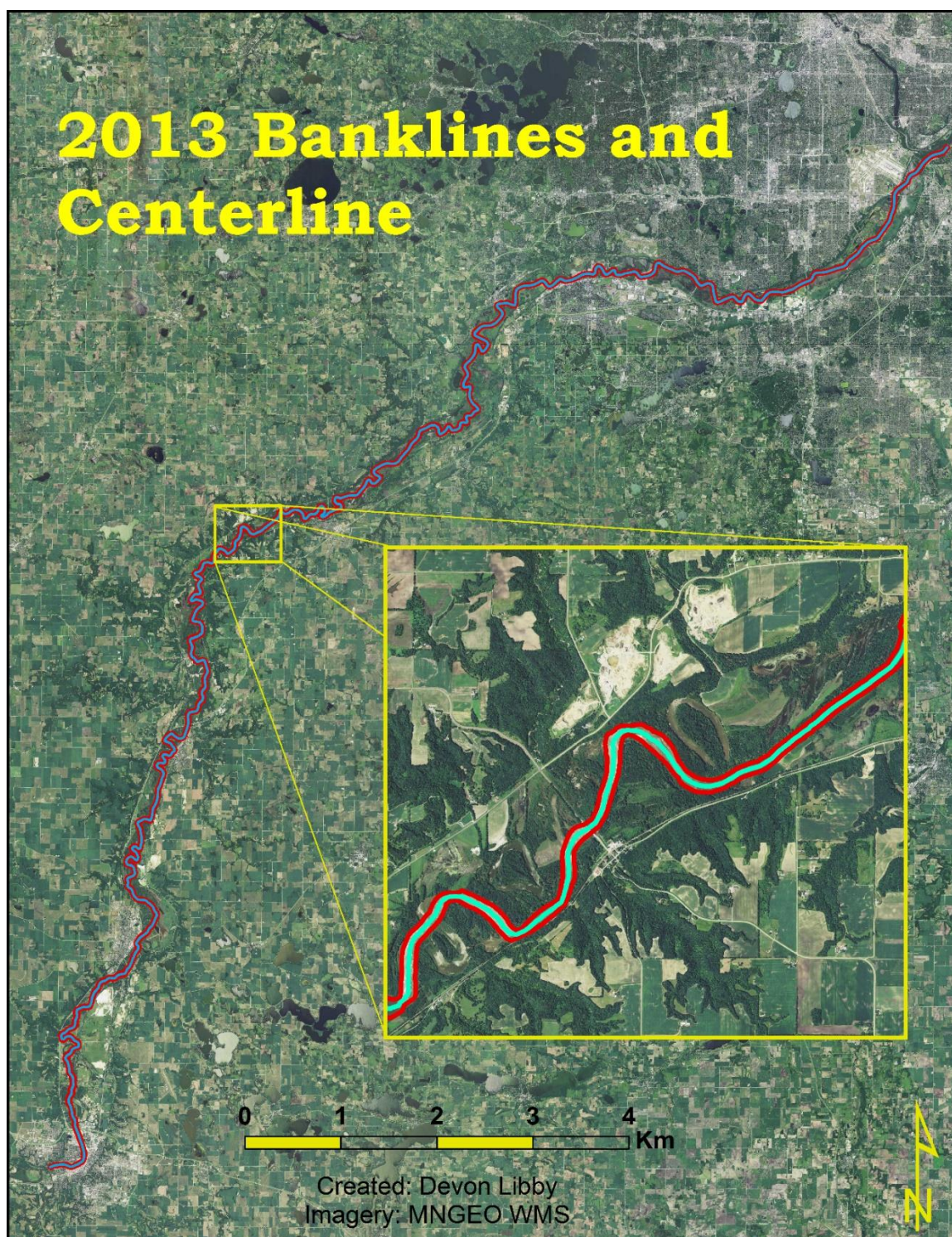


Figure 2.22: This map displays the digitized banklines and subsequently collapsed centerline for the 2013 time period overlaid on the 2013 MNGEO WMS DOQ from which it was digitized.

Table 2.5: Digitization Error Assessment

Year	Number of Measurements	Mean	Median	Maximum	Minimum	Standard Deviation
1937	6039	1.74	1.26	14.29	0.003	1.67
1951	5960	1.50	1.05	17.58	0.005	1.59
1964	6283	1.16	0.89	11.76	0.001	1.04
1980	6440	1.39	1.05	11.73	0.003	1.26
1991	5882	2.08	1.51	18.75	0.004	2.13
2013	5967	1.69	1.31	11.18	0.003	1.48

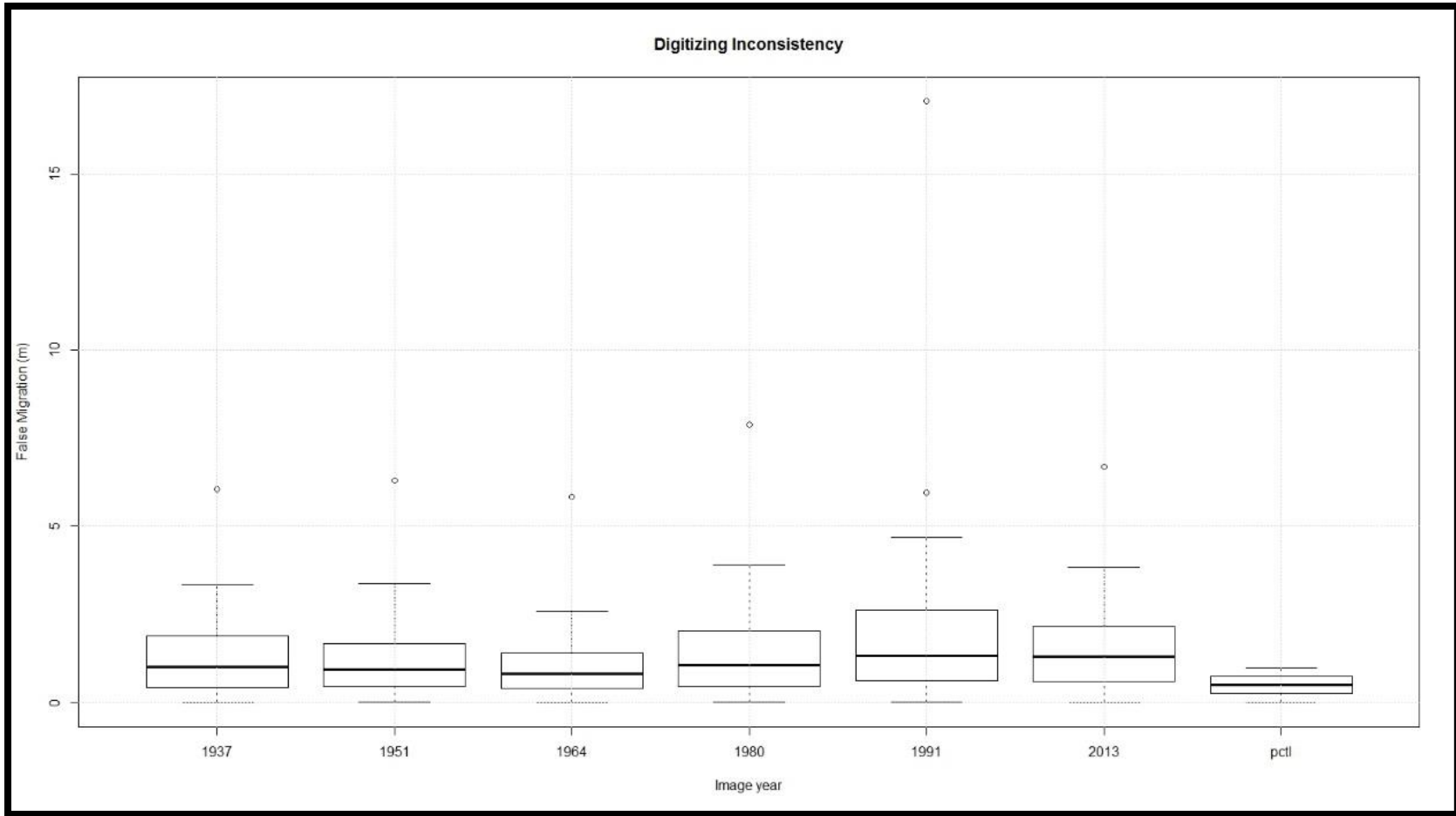


Figure 2.23: The box plot of digitizing error across the different time periods used for lateral channel migration. Although there are slight variations, the digitizing inconsistency is quite similar overall.

2.4 Discussion

The research presented in this chapter aimed to combine the methodologic approaches from past planform studies to thoroughly account for and minimize error and uncertainty, as well as, exposing pitfalls from past research. Both the temporal (six time periods four of which had to be registered) and spatial scale (~160 km of river) of this research on the Minnesota River, required significant data processing and offered insights into applying specific methodologies on large datasets.

The only existing data for this project was the aerial imagery which had to be collected, catalogued, and registered. The historical aerial photographs themselves originated from many sources (Table 2.2) and became a unique collection of registered imagery spanning the Minnesota River from Mankato to the Mississippi confluence. This newly created collection will hopefully aid future research projects outside the scope of this study and significantly save the next user time on imagery collection and registration. For this reason, Appendix A, Table 2.2, section 2.2.1, and section 2.2.2 were produced to provide sufficient documentation (metadata) for this research and for any future users.

2.4.1 Imagery

The parameters for registering aerial imagery to measure planform channel change was thoroughly investigated by Hughes, McDowell, and Marcus (2006) with many of the suggested optimal parameters being confirmed by Lea and Legleiter (2016). These studies guided the image registration in this research and should aid in

standardizing this aspect in future studies to minimize the initial error introduced into the data.

Once the images were registered, accuracy needed to be assessed to account for the remaining, unavoidable error present. By using the MATLAB script produced by Lea and Legleiter (2016) two things were accomplished:

- 1) Lateral migration measurements made chapter 3 can be determined as statistically significant or insignificant according to spatial variable error existing within the study area.
- 2) Standardization of error quantification in image registration can be repeated making comparative analysis among studies easily obtainable. In past studies, error analysis has been ignored or RMSE was used as the sole metric (e.g. Urban and Rhoads, 2004). This problem has been acknowledged as needing revision (Hughes, McDowell, and Marcus 2006). Unwin (1995) explains

“A common mistake when incorporating field data into a GIS is to assume that the error can be simply equated to the measurement error at the sampled points and quoted as a simple global statement such as ‘elevations accurate to 1 m’ or as a RMSE which gives an idea of the magnitude and variance of the errors but does not address their spatial variation” (p. 552).

Lea and Legleiter (2016) addressed and accomplished the short-comings of traditional error analysis (RMSE) with their MATLAB scripts. These scripts allow for two crucial considerations: 1) error needs to be considered in both magnitude and

direction (as a vector) 2) these vectors of error then need to be applied specifically to intervals being measured. It is necessary to analyze each interval's error vector (e.g. 1937-1951) separately since they are registered to a common base-image/DOQ (e.g. 1991), but do not have an expressed error metric output that relates them to one another. For instance, the 1937 imagery may have an error of 1 meter in a given location from the base DOQ and the 1951 imagery may have an error of 2 meters in this same location. Since these measurements are tied to the initial registration (base DOQ) without knowing the vector of the displacement, they have no relation to one another. By revisiting the 1937 imagery and 1951 imagery to find common GCP pairs, an error measured by the linear offset can be established that directly relates to measurements made between these two time periods. Another advantage of using two successive time periods (e.g. 1937 to 1951) is that there are many more common, unaltered features facilitating more reliable GCPs to be selected. For instance, streets, fences, etc. are much more likely to have remained static in the shorter span of time offering more points of comparison.

Lea and Legleiter (2016) script accounts for non-uniform error by using the X and Y coordinate pairs to assess the error vector in each location and interpolate an error surface for the whole reach of GCP coverage. Their script is intended to produce a visual of the error surface, but this portion had to be commented out (disabled) because the large number of GCPs in this research extended far beyond the disk space available needed for the computation. This is one recognized weak point when applying their methods to this larger dataset. However, the tabular output (used to create the visual) was still produced. This data serves as the input for the second MATLAB script that runs the migration

against the spatial variable error (SVE) and incorporates the digitization error. This is covered in Chapter 3 (see section 3.2.1.3).

The method presented by Lea and Legleiter (2016) should become the new standard for assessing registration error in lateral channel change studies. It not only assesses the error as being spatially variable but also automates the process of comparing error to lateral channel movement to detect if it is statistically significant. The downside of their method is that it requires the use of MATLAB. MATLAB has various costs depending on the capacity in which it is used but can cost as much as \$2,150 for industry use. MATLAB also has a proprietary programming language which has an associated learning curve, but Lea and Legleiter (2016) scripts are well commented so a user with relatively little programming background can use them.

Although Lea and Legleiter's (2016) script was used, a new approach had to be designed to handle the differences between the nature of their study and this study. Their study analyzed 6 images for 6 different dates over a 31 year span (1980 to 2011) for a 3 km stretch of river. This study analyzed 186 unreferenced images along with 2 DOQ sets of imagery over for 6 dates over a 76 year span (1937 to 2013) for a ~ 160 km stretch of the Minnesota River.

This study also differed from Lea and Legleiter (2016) by placing a new set of independent GCPs for every interval from which a measurement was made. This was done for several reasons. The image registration process can bias GCP placement in order to get an image to warp properly. This often involves distributing GCPs evenly throughout an area of interest to obtain "best results," but could also cause a user to

consciously or subconsciously skew point placement to achieve a better accuracy according since RMSE values appear within ArcMap as points are placed. If this is done, the GCP pair will then have an underestimated error measurement attached to it moving forward. This can be avoided by having different analysts, who have no invested interest in the overall study, place the new set of GCPs through the area. This creates a new, unbiased dataset to assess error that will inevitably include GCPs (new measurements) that were not used to in the image registration process. This will then include the warp error of areas that had a sparser amount of GCP placement in the image registration process which give a more accurate depiction of the error present.

Another reason for placing independent GCPs for each time interval is that it offers a greater amount of points for analysis. This is the same theory for using the 1991 DOQ for image registration that was discussed in section 2.2.2. Essentially, the closer two dates are to each other the higher the probability that there will be more static features to identify between the two sets of imagery.

Lea and Legleiter's (2016) scripts allow for comparing two centerlines where one is digitized from the base image, which has an assumed error of 0 meters, or two different centerlines that are registered to the same base image as reference where the error of both needs to be accounted for. With the method used in this study of placing independent GCPs for every interval, it is creating the condition of the earlier time having an assumed error of 0. This doesn't change the amount error in anyway, but rather is noted because when modifying the script it needs to be treated in this way. This is also a useful

approach if images were previously registered or if they were registered using several different base images.

Although Lea and Legleiter's (2016) analysis mainly focuses on handling spatial variation in image registration error, their scripts do require a input for digitization error. However, their study fails to refine how digitizing error should be handled which will be the focus of the next section.

2.4.2 Digitization

Digitizing banklines is a fairly straight-forward process. However, the way digitizing error has been assessed and reported has lacked a uniform approach. For instance, Aalto, Lauer, and Dietrich (2008) and Lauer and Parker (2008), used the movement of abandoned channels/oxbows which should remain stationary throughout sets of imagery as a proxy to evaluate the total geospatial error present (both registration and digitizing). This approach serves as a proxy for registration error but not for total error since the abandoned channels require additional subjective digitization.

Legleiter (2014) and Lea and Legleiter (2016) estimated digitizing error to be 2 meters by citing the digitizing error reported by Micheli and Kirchner (2002). This is often a poor approach because several determining factors may be different between studies. For instance, digitization error can be influenced by the scale of an aerial photograph, the scale digitized at in a GIS, the pixel resolution of the images, study specific obstructions/physical settings (e.g. heavy vegetation), shadows present in sets of imagery, the reliability of the analysts themselves, etc.

Micheli, Kirchner, and Larsen (2004) make the faulty assumption that in channel topography is uniform by digitizing a centerline from low flow water edges. Low flow

hydrology is incredibly complex with both natural and anthropogenic influences acting on the channel introducing new variables (Smakhtin 2001). For this reason, delineating bankfull edges is a better choice because it keeps the metric constant. However, the methodical approach used by Micheli, Kirchner, and Larsen (2004) of using repeated digitization to assess error will yield accurate, study-specific results, but should be done with a uniform metric like bankfull opposed to the edge of water. This was how digitizing error was analyzed in this study.

These are just a few examples that highlight the need for a standard procedure. Exploring the impacts these various factors have on digitization would be beneficial in future studies, but until then, it is suggested that a study specific test is run to evaluate digitization error on every set of imagery used. This will ensure the most accurate results and avoid over and under estimations of the error present. The mean digitizing error range in this study was between 1.16 to 2.08 meters (Table 2.5). Five of the six years analyzed were under 2 meters which indicates that assigning a 2 meter error based on previous studies would have been an over-estimation resulting in an unnecessary loss of measurements.

Another observation from this research is the superiority of the NCED “Interpolate Centerline” tool to the built-in ArcGIS cartography tool “Collapse Dual Lines To Centerline.” This is important because it is such a common practice to create a collapsed centerline to measure lateral migration (Lauer and Parker 2008; Nicoll and Hickin 2010; Giardino and Lee 2011; Lea and Legleiter 2016). Initially, the “Collapse Dual Lines to Centerline” was used and required extensive manual editing. Common

errors included extra lines that had to be deleted or gaps in the centerline that required an analyst to interpolate a small stretch of river using the banklines as a guide to connect the separated centerline (Figure 2.24). In rare cases, glitches were found that had created centerlines that did not accurately represent a line midway between banklines (Figure 2.24). As mentioned in section 2.2.4, the NCED “Interpolate Centerline” tool needed no user editing after being inspected which saved significant time and eliminated further errors that could be introduced from manual editing.

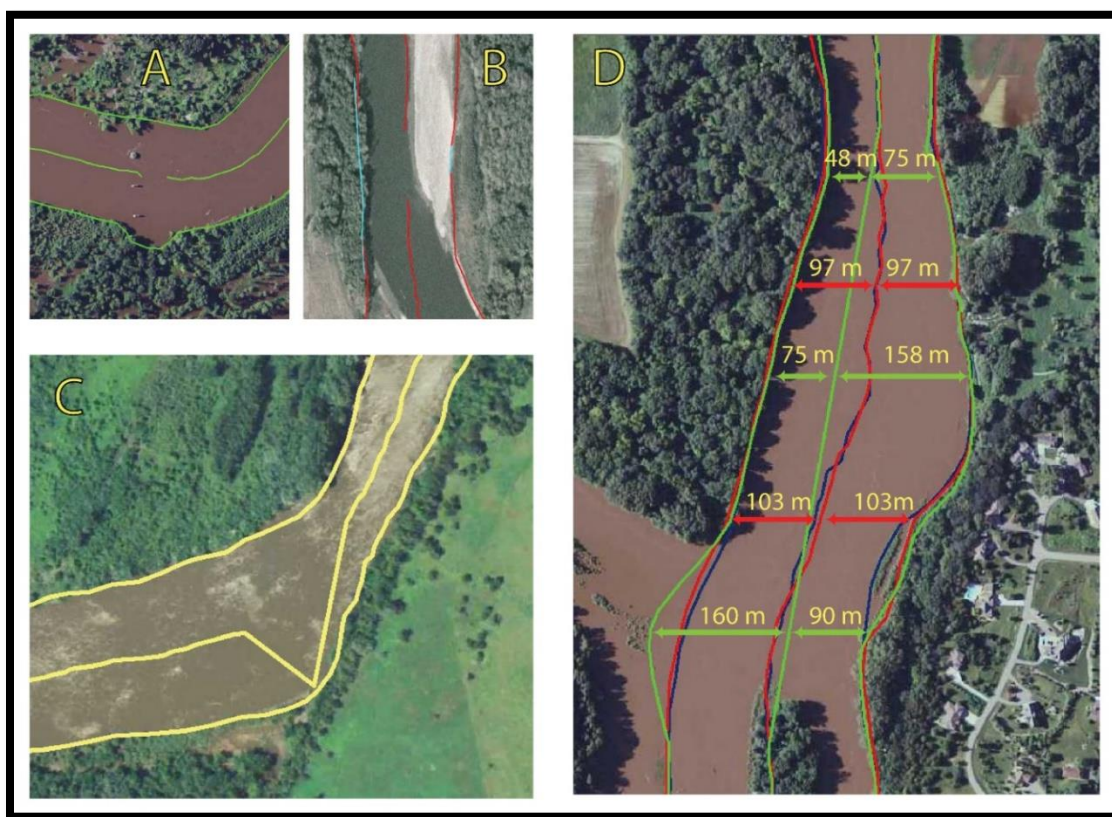


Figure 2.24: This figure displays the errors associated with the “Collapse Dual Lines To Centerline” tool. (A) Common gaps that require manual user interpolation. (B) Common line features highlighted in light blue which are not associated with the centerline but are created when the tool is run. These need to be selected and deleted. (C&D) Both show centerlines that did not get created correctly. While C is obvious, D is less obvious but can be seen through close inspection of the centerline and confirmed by quick measurements that highlight the error. In D the red and blue lines show correctly created centerlines while the green in this reach was incorrectly displayed.

2.5 Conclusion

Error and uncertainty has been recognized as needing attention in GIS studies for some time (Unwin 1995), but not until more recently has it gained attention by geomorphologists (Hughes, McDowell, and Marcus 2006) and specifically in fluvial channel change studies (Mount et al. 2003; Mount and Louis 2005; Lea and Legleiter 2016).

Shortcomings in past studies have included: ignoring certain aspects of error assessment, using metrics (e.g. RMSE) that have been deemed insufficient (Urban and Rhoads 2003; Giardino and Lee 2011), quantifying both digitizing and image registration error into one metric (Aalto, Lauer, and Dietrich 2008; Lauer and Parker 2008), and citing other studies' error results (Legleiter 2014; Lea and Legleiter 2016). Although these individual factors likely did not have major impacts on the results of past research, they do produce unnecessary uncertainty and methodological inconsistency. It is then difficult or impossible to do comparative analysis across planform channel change studies, severely hindering progress in understanding river planform dynamics.

This chapter aimed to not only assess and quantify the error and uncertainty for this specific research on the Minnesota River, but also evaluate the most appropriate and accurate way to accomplish this task to guide future research. Attention was given to image registration error and digitizing error individually since these have been widely recognized in past channel change studies as the primary sources of error (Gurnell, Downward, and Jones 1994; Hughes, McDowell, and Marcus 2006; Aalto, Lauer, and Dietrich 2008; Lauer and Parker 2008; Block 2014).

Lea and Legleiter's (2016) MATLAB scripts are by far the best advancement made to evaluate image registration error by viewing and accounting for the spatial variability of it. However, using independent GCPs for every interval considered within a study will offer a better overall evaluation of error present in the imagery along with the likely hood of having more points from which to draw from. It is also recommended to obtain study specific results from quantifying digitizing error as was outlined in this work. The error quantified in this chapter will be the basis for determining significant and insignificant lateral channel migration in Chapter 3.

Chapter 3 : Planform Channel Change of the Lower Minnesota River (1937-2013)

3.1 Introduction

In attempting to understand change within the fluvial system, temporal and spatial scales of analysis must be established (Schumm and Lichty 1965; Schumm 1977; Lawler 1993; Grabowski, Surian, and Gurnell 2014). In the case of temporal scale, Trimble and Cooke (1991) state “the recent past sets the stage for contemporary processes, which may not be fully intelligible without an appreciation of the past.” Thus, in order to understand the contemporary fluvial system, it is crucial to assess historical change within the system (Winterbottom 2000; Rhoads 2003), particularly when trying to understand channel planform dynamics (Hickin and Nanson 1984; Jones 1994; Hooke 1995; Gurnell 1997; Winterbottom 2000; Urban and Rhoads 2003; Gurnell, Downward, and Hughes, McDowell, and Marcus 2006; Block 2014).

In addition to establishing a temporal framework of study, an appropriate spatial scale needs to be considered for the research. In fluvial systems, this can range anywhere from drainage pattern networks to an individual grain of sediment. Schumm (1985) states that reach scale analysis is of most interest to geomorphologists who are concerned with what the pattern of the river reveals about its history and behavior. Since this is the primary purpose of the research in this thesis, most of the focus in this chapter is at the reach scale; however, it should be noted that both larger and smaller scale elements and processes need to be given credence to make reach-scale interactions fully intelligible.

The purpose of the research in this chapter is take the error and uncertainty analysis from Chapter 2 and apply it to the planform measurements calculated in a GIS. These measurements on the Minnesota River will then aid in filling the gap of knowledge that currently exists on the main stem Minnesota River. Since discharge and sediment have significantly increased from various anthropogenic activities, primarily linked to land use and climate change, the following research questions will be explored:

- 5) Have the channel migration rates remained stable over the past 76 years of aerial photographic record (1937-2013), or are increases or decreases seen? If the latter, do these increases and decreases show any spatial or temporal patterns?
- 6) Does channel width fluctuate over this similar time frame? If so, are there spatial or temporal patterns related to this change?
- 7) How have human modification on the river (e.g. bridges, flood control structures, etc.) effected planform channel change in the upstream and downstream directions?
- 8) In relation to the invasive carp problem, are there controlled reaches of the Minnesota River that exhibit very little change and could potentially be suitable for invasive carp barriers?

Specifically, these research questions will be applied on the last 160 km (100 mi) of the Minnesota River, extending from the Blue Earth/Minnesota River confluence down the Minnesota/Mississippi River confluence (Figure 3.1). This stretch of river is of interest for stopping the advancement of invasive carp along with being the end of the primary

transfer corridor adjusting to increasing discharge and sediment yields from the MRB before entering the Mississippi (Engstrom, Almendinger, and Wolin 2009; Belmont et al. 2011; Kelly et al. 2017).

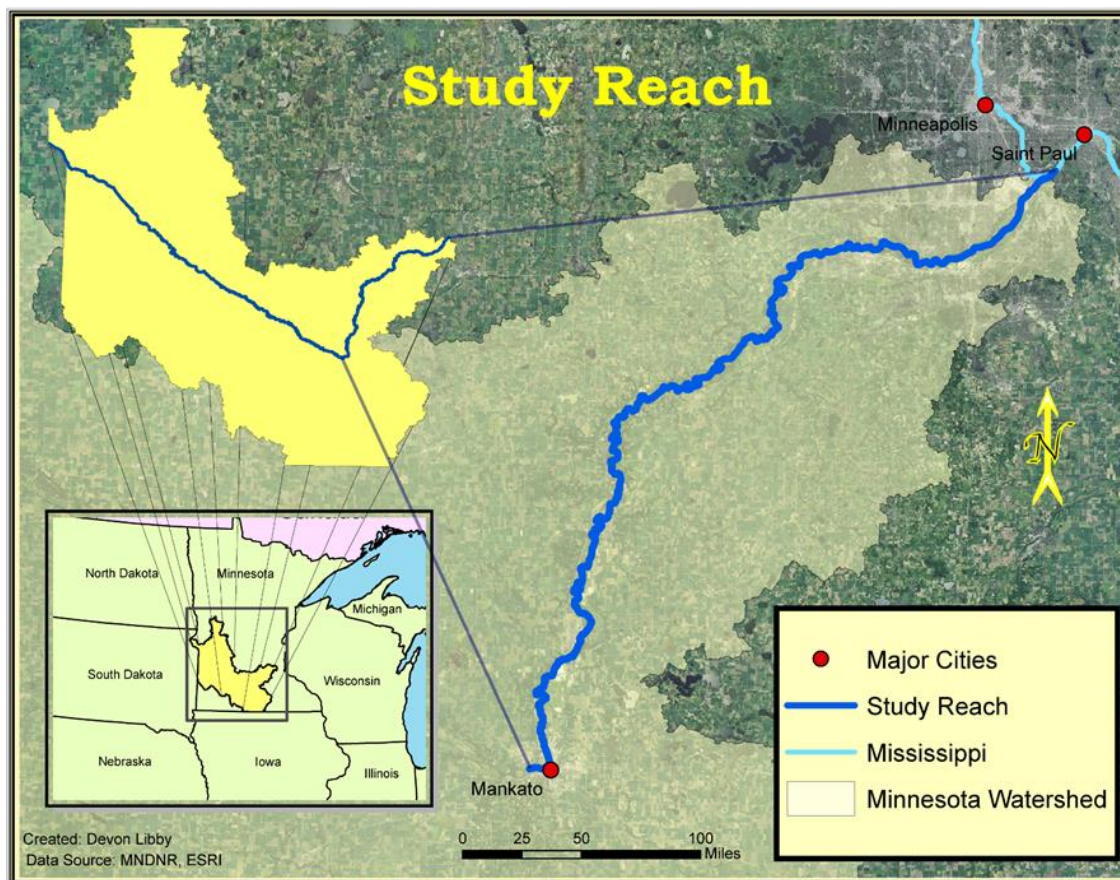


Figure 3.1: The study reach for this research is the 160 km (100 mi) of the Minnesota River beginning in Mankato and ending with the confluence with the Mississippi River.

3.1.1 Study Area

The Minnesota River Basin (MRB) is a dynamic, transient landscape because of ongoing landscape-scale adjustment due to the retreat of continental glacial ice that covered much of the landscape ~12,000 14,000 years BP (Clayton and Moran 1982; Fenton et al. 1983; Teller, Leverington, and Mann 2002). The Des Moines Lobe of the Laurentide Ice Sheet flowed over much of the MRB leaving behind a thick package of

glacial and glacio-fluvial sediments (Hallberg and Kemmis 1986; Patterson 1997; Patterson and Wright 1998;). As climate warmed at the end of the last glacial maximum (~11,000 years BP; Ojakangas and Matcsh 1982) meltwater pooled in pro-glacial lakes in many ice-marginal locations. One such proglacial lake, Lake Agassiz (Upham 1896; Teller, Leverington, and Mann 2002; Fisher 2003), was formed in the northwestern Minnesota, eastern North Dakota, and extended into Canada nearly to the Hudson Bay and was dammed behind the Big Stone Moraine of west central Minnesota (Thorleifson 1996; Fisher 2004). Eventually, Lake Agassiz breached its basin through several spillways including the Gulf of Mexico, Arctic Ocean, North Atlantic Ocean, and Hudson Bay (Thorleifson 1996; Teller, Leverington, and Mann 2002). The initial breach of meltwater occurred in west central Minnesota as Lake Agassiz meltwater either overtopped (i.e. spillover) or flowed through (as a result of moraine dam failure) the Big Stone Moraine sometime before (Wright Jr, Lease, and Johnson 1998; Teller, Leverington, and Mann 2002; Lepper et al. 2007). This breaching event carved the present-day Minnesota River Valley which is nearly 8km (5 mi) wide in certain areas (Upham 1896; Thorleifson 1996; Teller, Leverington, and Mann 2002; Fisher 2003, 2004; Lepper et al. 2007). Following recession of the flood waters, the Minnesota River Valley became the new base level for tributary streams flowing into the valley. As a result, the tributaries of the modern Minnesota River are still responding to this abrupt, 40 (mouth) 300 (downstream) meter, base level change (Clayton Moran 1982; Moran 1982; Ojakangas and Matcsh 1982; Gran et al. 2009; Gran, Belmont, Day, Jennings, et al. 2011). This, in turn, has resulted in a landscape prone to high sediment yields as these

tributaries incise through the landscape (Figure 1.10; Fisher 2004; Belmont et al. 2011; Gran, Belmont, Day, Finnegan, et al. 2011).

However, this geologically-young system and its evolution has experienced further perturbation through anthropogenic alteration of land cover and hydrology following European settlement (Engstrom, Almendinger, and Wolin 2009; Belmont et al. 2011; Schottler et al. 2014). The MRB was historically a landscape dominated by wetlands (Musser, Kudelka, and Moore 2009), which are vital for water and sediment retention in the uplands of this landscape (Mitsch and Gosselink 2000). However, starting in the early 1900's the landscape began to be drained to more effectively cultivate the landscape (Lenhart et al. 2011). Currently, 78% of the MRB is row crop agriculture largely occupied by corn and soybean fields (Musser, Kudelka, and Moore 2009; Belmont et al. 2011).

In addition, artificial forms of surface and subsurface drainage have dramatically altered hydrology and erosional processes in the MRB (Kelley and Nater 2000; Kelley et al. 2006; Engstrom, Almendinger, and Wolin 2009; Mulla and Sekely 2009; Schottler 2012; Schottler et al. 2014). One of the most prevalent forms of drainage is subsurface tiling. Tiling is a network of tubes with small perforations below the soil surface used to capture and pipe infiltrating water off the landscape (Schottler 2012; Fofoula-Georgiou et al. 2015). This system of drainage changes flow patterns, rainfall-runoff timing, and landscape storage driving new hydrologic regimes (Fofoula-Georgiou et al. 2015). The hydrology of the region is further impacted by shifting climatic conditions. In Minnesota an increase in mean annual precipitation, number of days receiving precipitation, and

amount of intense rainfall events per year cause increased frequency and magnitude of peak discharges throughout the region's fluvial systems (Novotny and Stefan 2007; Gran, Belmont, Day, Jennings, et al. 2011; Yuan and Mitchell 2014; Kelly et al. 2017;).

Ultimately, anthropogenic perturbations (e.g. climate, land use, and modification of hydrology) have resulted in more erosive rivers (Schottler et al. 2014). Lake Pepin, a naturally dammed lake located just downstream of the confluences of the Minnesota and Mississippi River, has received a ten-fold increase (85,000 mg/year prior to 1830's to as high as 850,000 mg/year between 1950-2008) in sediment since European settlement (Engstrom, Almendinger, and Wolin 2009; Belmont et al. 2011). Significantly, the Minnesota River plays a primary role in this ongoing sediment accumulation as 90% of the sediment comes from the Minnesota River which only contributes 38% of the discharge to lake (Kelley and Nater 2000; Kelley et al. 2006; Belmont et al. 2011). Prior to this period, sediment contributions remained static to the lake for nearly 10,000 years (Kelley et al. 2006; Engstrom, Almendinger, and Wolin 2009; Blumentritt, Engstrom, and Balogh 2013; Belmont and Fofoula-Georgiou 2017).

Of this increase in sediment loads, near-channel sources have shown to be major contributors in the MRB especially from the tall bluffs below the knick-zones on Minnesota River tributaries (Belmont et al. 2011; Schottler et al. 2014; Belmont and Fofoula-Georgiou 2017). In the 1950's a large portion of the sediment load shifted to field sources which was combatted with various conservation efforts and tillage practices reducing this sediment source, yet the sediment rates did not decline (Belmont and Fofoula-Georgiou 2017). This is explained from the shift going back to near channel

sources due to the altered hydrology from the prevalence of various forms of artificial drainage, and increased precipitation events (Novotny and Stefan 2007; Fofoula-Georgiou et al. 2015; Belmont and Fofoula-Georgiou 2017; Kelly et al. 2017).

3.1.2 Significance of the Study Area

Rivers are naturally dynamic features but will quickly change morphological characteristics because of anthropogenic and climatic forces acting within or on a watershed (Schumm 1977; VanLooy and Martin 2005). Channel morphology change or stability is the result of prevailing hydrological conditions of which runoff and sediment yield are the most influential (Knox 1977). Given the drastic hydrologic change and sediment load increase over the past century and a half within the MRB (Engstrom, Almendinger, and Wolin 2009; Fofoula-Georgiou et al. 2015; Groten, Ellison, and Hendrickson 2016; Kelly et al. 2017), further study of channel change is necessary to better understand how the river is responding through time in the context of both landscape and ecological management.

3.1.2.1 Fluvial Geomorphology and River Management

Several equations predicting channel behavior from Schumm (1969) were discussed in Chapter 1 (see section 1.2), but notably an increase in discharge, which is observed on the Minnesota River, can be exemplified using the following equation.

Equation 3.1

$$Q^+ \cong \frac{w^+ d^+ (w/d)^+ \lambda^+}{s^-}$$

Where discharge (Q), channel width (w), depth (d), width-depth ratio (w/d), meander wave length (λ), channel slope (s), and sinuosity (S). Plus signs (+) indicate an increase while negative signs (-) indicate a decrease in that variable. Using these general relationships, it is likely that given what we know about the ongoing change in the MRB, we can expect to see an increase in channel width (Lauer et al. 2017), width depth ratio, and channel wavelength, and a decrease in sinuosity. Increased sediment loads (Engstrom, Almendinger, and Wolin 2009; Belmont et al. 2011; Groten, Ellison, and Hendrickson 2016) and subsequent turbidity impairment (Belmont and Foufoula-Georgiou 2017) have plagued the Minnesota River and much of the Upper Mississippi River Basin (UMRB) resulting in unhealthy ecosystems (Foufoula-Georgiou et al. 2015) and increasing sand deposition/aggradation in the farthest downstream portions of the Lower Minnesota River (Jennings 2016). Recently, Groten, Ellison, and Hendrickson (2016) have shown that sediment yield from Mankato to Jordan increases by two and half times. However downstream of Jordan, a significant decrease is seen revealing a sediment sink. The erosional processes of channel migration and channel width change are contributing to these sediment dynamics as near channel sources. Therefore, quantification of channel planform change on the Minnesota River will aid in spatially identifying areas of acute concern (i.e. greatest near-channel sediment contributions).

This increase in sedimentation in certain reaches of the fluvial system has led to the need to dredge parts of the Minnesota River for it to remain navigable for barges. This is also true for Lake Pepin and the Mississippi, which has seen a ten-fold increase in sediment post-European settlement (USACE 2007; Engstrom, Almendinger, and Wolin

2009; Belmont et al. 2011). The Minnesota River's portion of the inland barge navigation network is important with several of the world's largest grain marketing companies operating terminals to provide to both domestic and foreign markets. These terminals serve as the most cost-effective distribution routes for areas of the upper Midwest. The estimated 4 million tons of product moving annually on the Minnesota River saves an estimated \$50,000,000 in costs opposed to using other transportation routes (e.g. Great Lakes, rail, etc.). In the event that the Minnesota River is no longer navigable, these are costs that would be passed on to the producer (i.e. the farmer) in the form of lower prices offered by the grain companies (USACE 2007). The USACE admits that projecting future dredging maintenance on the Minnesota River is difficult with the many unknowns and variables effecting channel maintenance (USACE 2007), prompting the need for a better understanding of the planform channel adjustments of the river.

A better understanding of migration and width adjustment extends beyond dredging to all existing and future infrastructure in the Minnesota River Valley. This region is heavily occupied with many cities abutting the river and personal residences near the river which are susceptible to the erosional forces of the river (Johannesson and Parker 1985). Therefore, if geomorphic trends in the river planform change are seen, informed decisions can also be made to protect current structures and guide how to better engineer future structures to handle any anticipated trending changes (Kondolf, Piégay, and Landon 2002). The benefits of this knowledge are of monetary value but also are of safety concern to protect human life.

With all that is known about the issues facing the MRB, little is known on how the primary drainage of the MRB, the Minnesota River, has adjusted in response to these changes. Therefore, this research aims to fill an essential gap by revealing historic temporal and spatial trends of planform channel change on the lower Minnesota River (Figure 3.1), in a period dominated by anthropogenic modification of the fluvial system. Specifically, the lower Minnesota is of interest since the last 15 river miles are currently being actively dredged (USACE 2007). A large majority of this sediment comes from the Le Sueur River which contributes 24-30% of the total suspended solid load despite the watershed occupying only 7% of the MRB. This load enters the Minnesota River via the Blue Earth River in Mankato which marks the beginning of the study area (Figure 3.1).

3.1.2.2 Ecological/Biological Management

In addition to helping understand ongoing change in the fluvial system, assessment of channel change can aid in ecological and biological management practices within the riparian corridor (Bunn and Arthington 2002; Foufoula-Georgiou et al. 2015). In the case of the Minnesota River, feasibility of an instream barrier, to hinder the upstream advancement of invasive carp, is not well understood. Planform channel change analysis is essential to this assessment. Not only does a stretch of the river need to be stable in terms of migration and width to place a barrier, but it also needs to be in a location where it will not be cut-off from the main channel during a flood. In addition, if channel form change occurs (i.e. lateral migration, translation sinuosity, width, pattern change, etc.), a barrier could be rendered ineffective as the river is no longer the same as what the barrier was designed for. Without this understanding, an uninformed decision

of placement could lead to millions of tax payer dollars being wasted if a barrier was compromised in any of the aforementioned ways.

In terms of instream barriers, the lower Minnesota River is a preferred location since urban development in the river valley has created several stretches of river that are already controlled (e.g. Mankato's Flood Walls). It is also of concern to block the advancement of invasive carp from travelling any farther upstream than necessary to avoid threatening other basins like the Red River Basin.

3.2 Methods

To conduct planform channel change analysis of the lower Minnesota River, we apply a method of measuring channel migration, width, and sinuosity using GIS analysis to assess channel change dynamics through historical time. This analysis incorporates both image registration and bankline digitization error (Chapter 2) which will collectively be referred to as total spatial error.

Total spatial error considers both the registration and digitizing error present in a GIS-based methodology. Block (2014) offers an exemplary approach to quantifying the total spatial error margin for GIS planform studies based on data derived from DOQs and georectified aerial photographs. The total spatial error for channels digitized based of DOQs is as follows:

Equation 3.2

$$\text{Total Spatial Error} = \sqrt{(\text{average RMSE of the DOQ})^2 + (\text{digitization error})^2}$$

The total spatial error for channels digitized based on georeferenced imagery need to not only account the RMSE of the aerial photograph but also the RMSE of the DOQ (source error) used to derive the GCPs during the image registration process. This formula is as follows:

Equation 3.3

Total Spatial Error =

$$\sqrt{(\text{average RMSE of the DOQ} + \text{average RMSE of the aerial photograph})^2 + (\text{digitization error})^2}$$

Lea and Legleiter (2016) use this same premise in their methods, but instead of using RMSE, they use the error vectors from the GCPs displacement discussed in section 2.1.2 to assess the spatial variable error (SVE) in image registration. The SVE is then compared to the x and y coordinates of the migration line end points to see if the measurement exceeds the error in that location. This process is done in the second MATLAB script covered in this chapter. As with any research focus, there are shifts that take place in hopes of advancement, and in channel planform studies as well as other remotely conducted studies, geospatial error is becoming an independent subject matter. SVE is the new standard for how error should be viewed and calculated in future channel migration studies.

3.2.1 Channel Migration

The banklines and centerlines that were created in Chapter 2 served as the inputs for measuring channel planform change in this chapter. Lateral channel movement, channel width change, and sinuosity/channel length were calculated throughout the 1937-

2013 temporal scale of this analysis. To accomplish calculating channel migration four main steps were followed:

- 1) The National Center for Earth-Surface Dynamics (NCED) Planform Statistics Toolbox was used to create trajectory files measuring lateral channel movement along with a file storing width measurements. From this point forward, the term “trajectory” will be used to define lateral channel migration measurements.
- 2) The newly created data from the prior step was entered into a custom, created ArcMap tool in order to update and correct measurements as well as add required fields (x and y coordinates, paired ID’s) so it can be seamlessly integrated into MATLAB
- 3) The output data from step 2 and the previously created error analysis in Chapter 2 is entered into Lea and Legleiter’s (2016) “ChannelChangSignF” MATLAB script (Appendix D) in order to determine which measurements are statistically significant (exceed the amount of error).
- 4) The tabular output data from step 3 was entered into another custom created ArcMap tool to automate the process of tying the tabular data to the spatial data along with updating fields.

3.2.1.1 National Center for Earth Surface Dynamics Planform Statistics Toolbox

Lateral channel movement was calculated using the NCED Planform Statistics toolbox (Lauer 2006). The time intervals analyzed were 1937-1951, 1951-1964, 1964-1980, 1980-1991, and 1991-2013. These intervals were selected based on the availability of imagery and based on a similar temporal scale (~10-20 years). The following steps

were used to calculate lateral channel movement for the intervals of interest. This detailed step by step process will allow any future studies to exactly replicate the methods of this study.

Step 1: Add two centerlines for a given interval into ArcMap.

Step 2: Select the “Lateral Measurement” from the NCED toolbox which prompts the user to select the “to” (later date) and “from” (earlier date) centerlines from each time interval.

Step 3: After the lines are selected, a dialog box opens prompting “Y” to be entered if apex lines are to be considered. Apex lines are user generated lines within ArcMap that can be used to aid the program in correctly identifying lateral migration for bends in the river that are translated (see Figure 1.5) downstream (Lauer 2006). Based on the suggestion of other researchers, this was left empty in this study indicating no apex lines should be considered, but could be investigated further for future studies.

Step 4: The program creates trajectory graphic lines which provide a visual in ArcMap from which lateral migration are derived. It should be noted that these lines are just graphics and not a shapefile. When this process is complete a window will open directing the user to select a location on the computer for a new polygon shapefile to be created and stored along with a file name.

Step 5: After the file is named and stored, another dialog box opens prompting the user to select a lateral offset distance from the centerline for the new polygon shapefile dimensions.

Step 6: This polygon shapefile is then created and stores the lateral migration measurements within its attribute table. This step is intended to be the terminal point for the tool, however the following steps are needed for editing errors (Figure 3.2) and for the future MATLAB script to be compatible with the shapefiles.

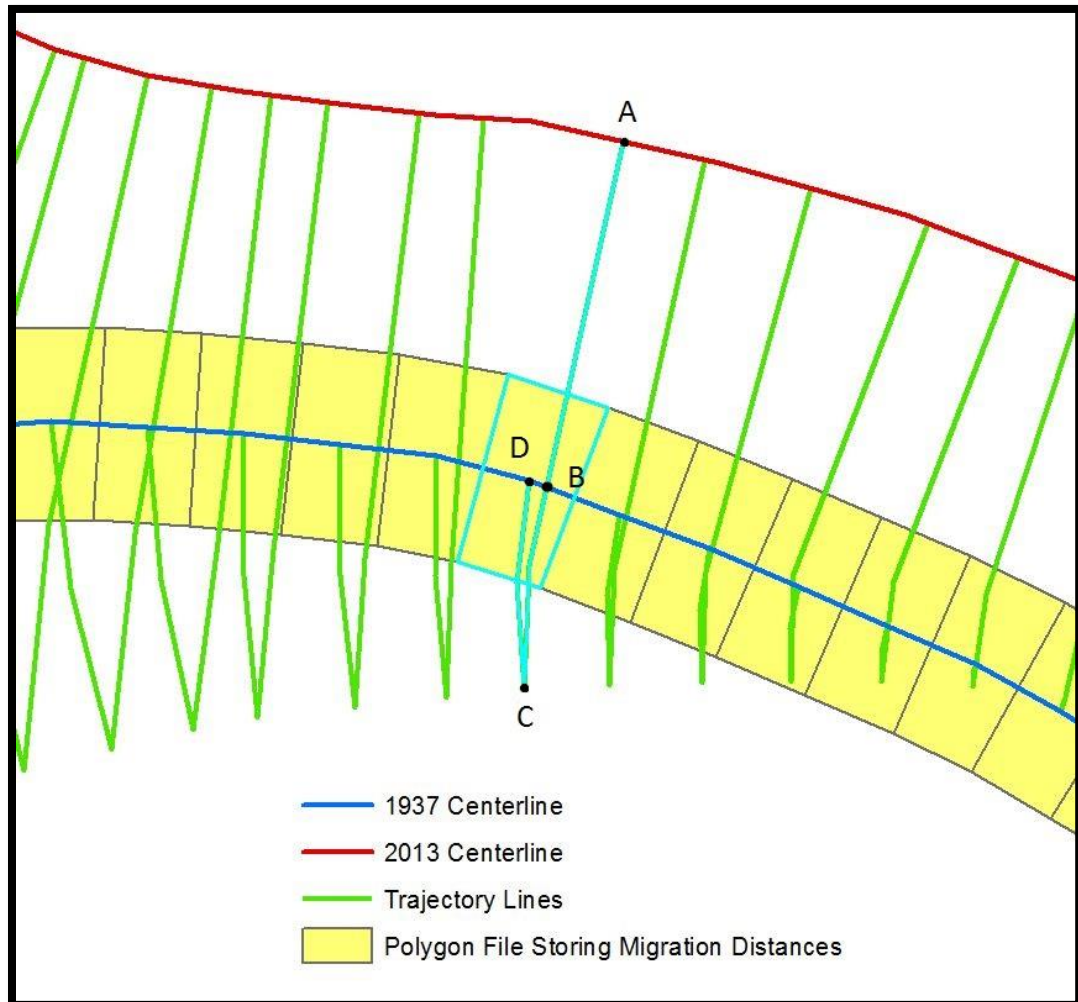


Figure 3.2: This figure shows inaccurate migration measurements made from the “Lateral Migration” tool. The polygon file (yellow rectangles) are what the tool uses to store the migration information based on the trajectory line graphics (green lines). The measurement from point A to point B is 36.6 meters and would be an accurate measurement for lateral channel movement. However, the highlighted polygon indicates a migration distance of 79.7 meters which is the measurement of the entire highlighted trajectory line (point A-B-C-D). For this reason, it is imperative to save and edit the trajectory graphics to recalculate correct measurements.

Step 7: The graphics files discussed in step 4 need to be saved as a shapefile. This can be accomplished by right-clicking the layer and selecting “Convert Feature to Graphic”. By doing this, spatial data is created for the trajectory lines (lateral migration lines) which can be manipulated by editing and recalculating measurements if needed.

Step 8: Once “Convert Feature to Graphic” is selected, a dialog box appears where the shapefile name and storage location is selected by the user. Note a check box for “Automatically delete graphics after conversion” must be selected to avoid ArcMap from crashing.

Step 9: The newly created trajectory line shapefile is added to ArcMap, and three lines running the longitudinal length of the river need to be selected and deleted in an editing session so only the lateral migration trajectory lines remain.

Step 10: Finally, all trajectory lines need to be inspected and edited to catch any errors made by the tool. This is most commonly seen where cut-offs occur (Figure 3.3). In this study, the lines were first edited by students from an upper-division fluvial geomorphology class and then inspected and further edited by myself. This methodology for running the NCED “Lateral Migration” tool and creating the trajectory lines is summarized in Figure 3.4 with images showing the step by step processes of the tool.

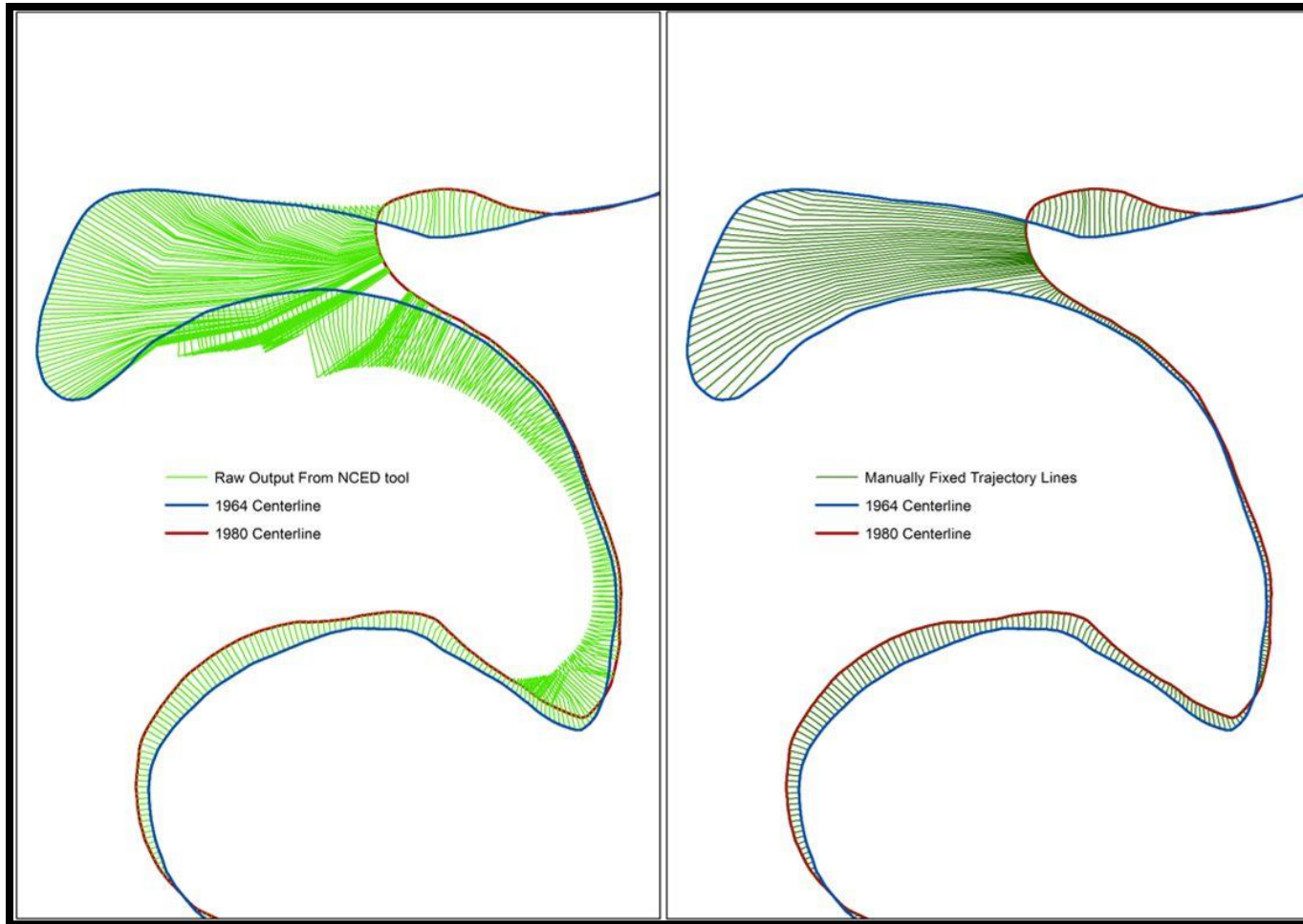


Figure 3.3: The first image (left) shows the raw trajectory lines from the NCED “Migration Tool.” These lines clearly create false measurements much larger than what they should be by extending outside the 1964 centerline and then back in to connect to the 1980 centerline. In these cases, it was often easiest to delete the lines and manually digitize a more natural trajectory between the two centerline (right).

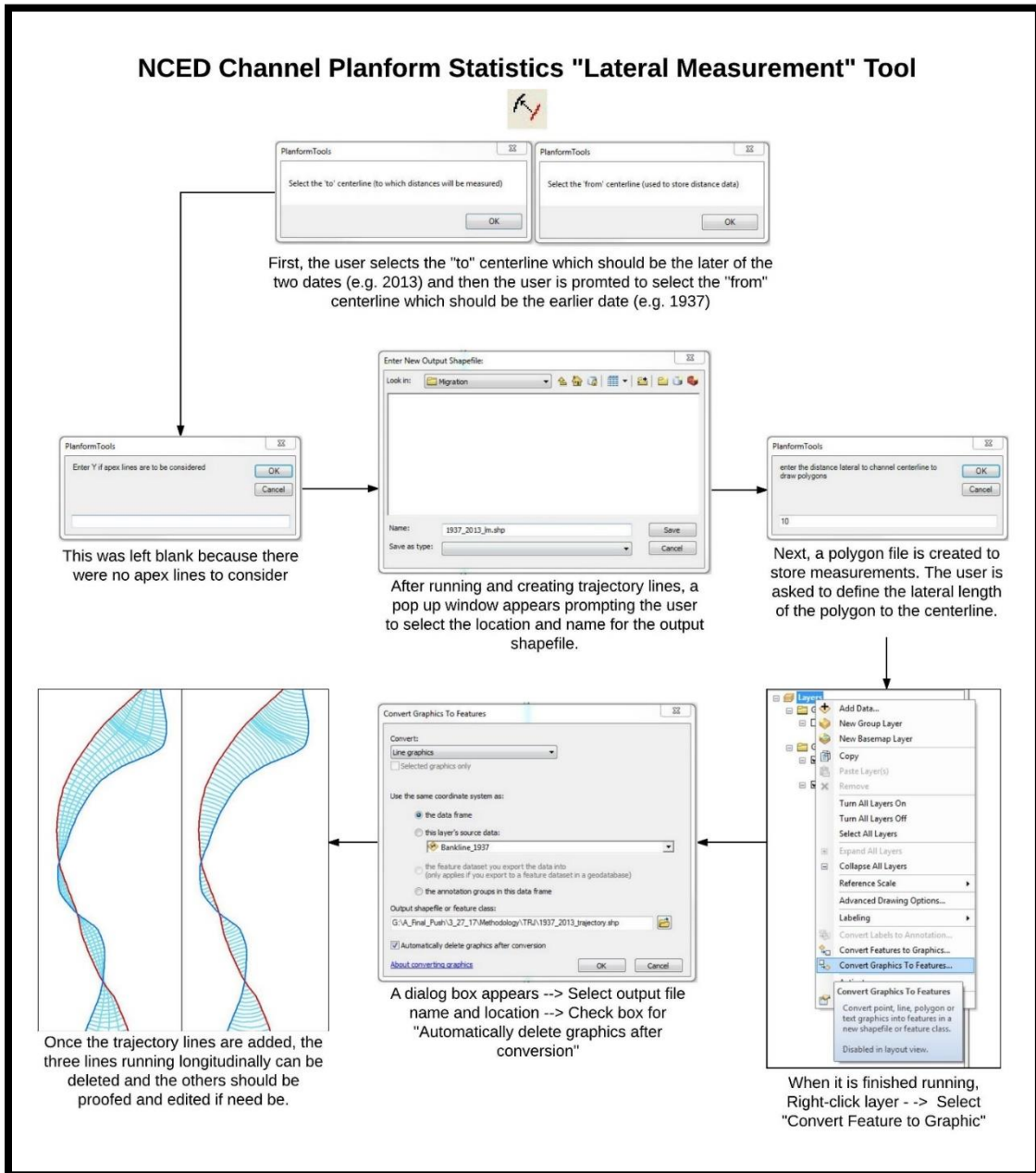


Figure 3.4: The NCED Channel Planform Statistics “Lateral Measurement” tool has various steps required to successfully complete the process beginning to end. The figure above shows the work flow with visuals and descriptors.

3.2.1.2 Pre MATLAB Processing

Once all trajectory lines were edited to accurately display the lateral migration of the river for each interval, a model (Figure 3.5) was created to set the structure for writing a python script (Appendix E) to automate the process to prepare the data so it could be entered into the “ChannelChangeSignif” MATLAB script from Lea and Legleiter (2016). This script was written and turned into a custom ArcGIS tool (Figure 3.6; Appendix E) making the automation capabilities accessible to those with no programming knowledge. The script/ArcGIS tool will be referred to as “Pre MATLAB Processing” script or tool from here on out. It is important to realize these two things are doing the exact same thing. The tool simply creates a Graphical User Interface (GUI) so the “Pre MATLAB Processing” script can be run without any code ever being seen by the user.

The “Pre MATLAB Processing” script (Figure 3.6; Appendix E) accomplished two main goals:

- 1) It gave every trajectory line a correct measurement identifying downstream-left channel migration as positive and downstream-right channel migration as negative. This was necessary because the measurements provided with the initial NCED “Migration Tool” had inaccurate (errored) lines (Figure 3.2 and Figure 3.3) resulting in false measurements.

- 2) It gave every trajectory line XY coordinates on each end of the line and all coordinate pairs were exported as an .xls file with a common ID field linking each pair to its respective trajectory line. This file was necessary for the “ChannelChangeSignif” MATLAB script (Lea and Legleiter, 2016) to determine if the distance between the

coordinate pair exceeds the error present in that location, thereby evaluating whether measurement exceeds the error in that given location or not.

The “Pre MATLAB Processing” ArcGIS tool is simplistic in that it only requires the user to set a location for storing created files, input the edited trajectory polyline shapefile, and input the centerline for the earlier year of the interval considered (Figure 3.6). A detailed explanation for the tool and every selection was also added in the “Show Help” portion of the tool to make it user friendly. Although the tool requires only three inputs, a series of processes run within the script and all the intermediate files are stored in a temporary folder that the script then deletes at the end in order to minimize unnecessary clutter. The “Pre MATLAB Processing” script with detailed explanation can be seen in Appendix E.

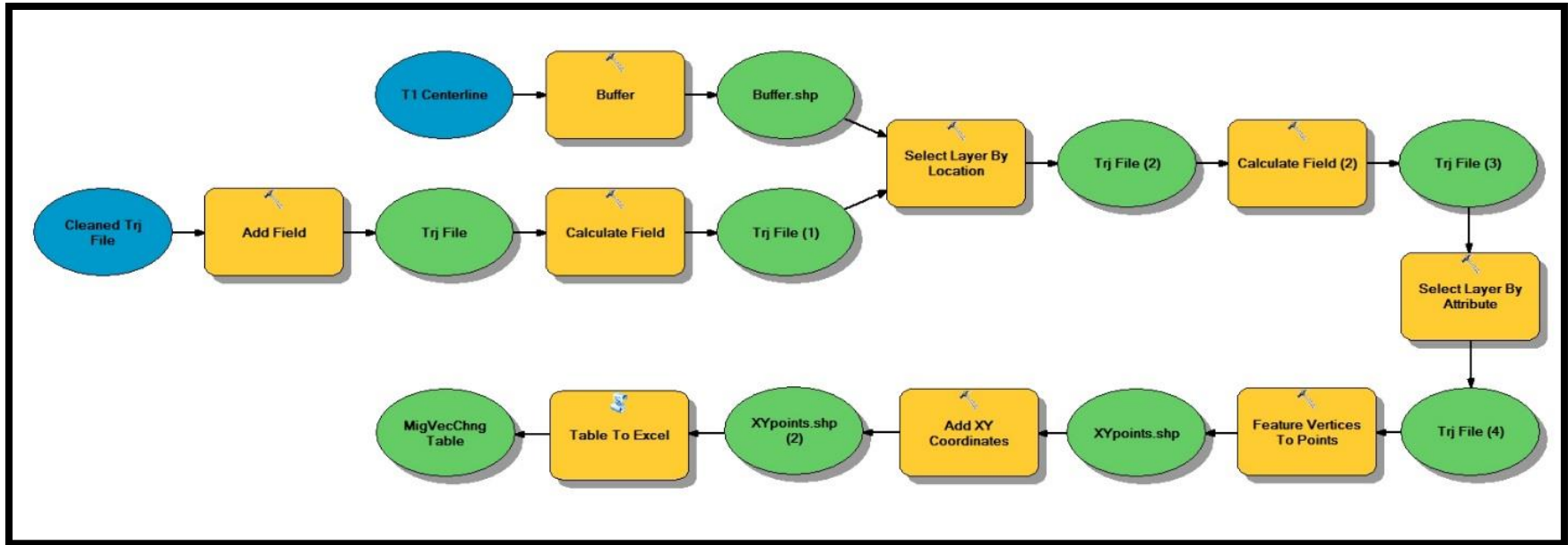


Figure 3.5: This model takes the edited trajectory lines and calculates the length of each line (lateral migration) and assigns negative values to migration occurring in the downstream-right direction. Each individual line is then given an XY coordinate on each end which the MATLAB script then uses to determine with the distance between the pair of points exceeds the error present in that location. The script (**Appendix E**) written from this model is much more robust and fully details all the processes in the comments. This model served for a framework to initially conceptualize the main workflow of the tool.

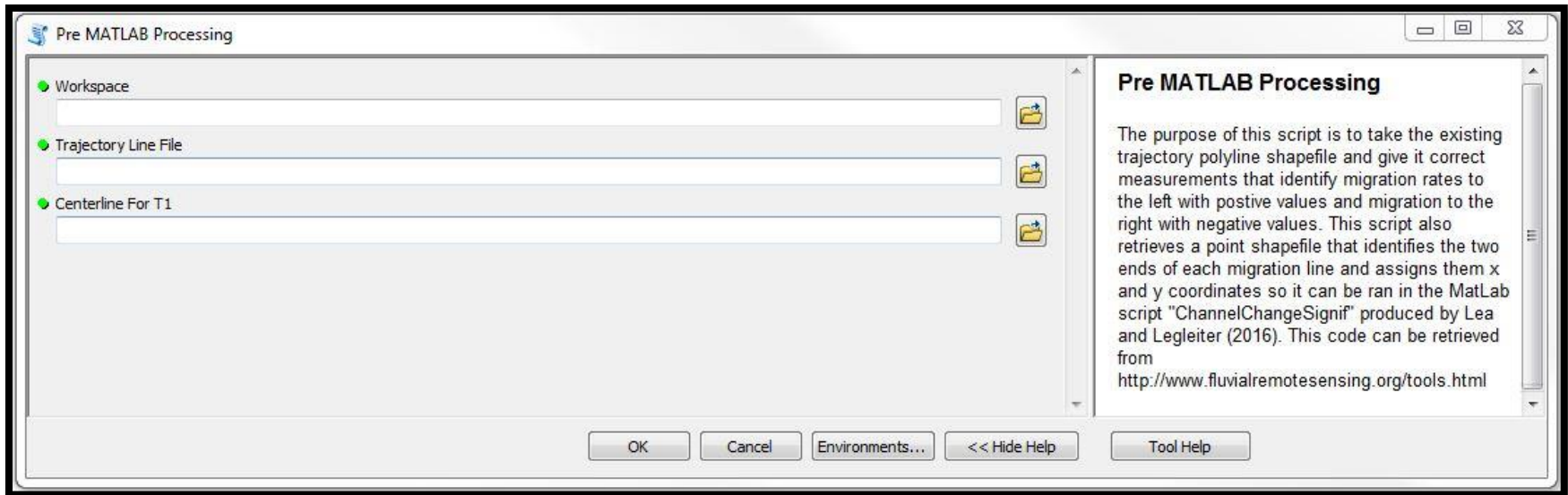


Figure 3.6: The Graphical User Interface (GUI) for the Pre MATLAB Processing tool has three user required inputs along with tool help descriptors defining the overall function of the tool and each input. The input and descriptors are as follows: 1) Workspace - Enter the workspace that contains the trajectory polyline file and centerline for time 1. This will be the folder where the output files will be written as well. 2) Trajectory Line File - Select the trajectory polyline file for the interval of interest. 3) Centerline for T1 - Select the polyline file for the river centerline for time 1 (the earlier of the two years in the interval).

3.2.1.3 MATLAB “ChannelChangeSignif”

The data stored in the .xls file from “Pre MATLAB Processing” script along with the error analysis output (RegErrorResults.mat) from the “QuantifyinRegistrationError” script in Chapter 2 in were used at inputs into Lea and Legleiter’s (2016) “ChannelChangeSignif” MATLAB script (Appendix D). This script evaluates the lateral migration distances to the total spatial error (registration error and digitizing error) to determine if the measurements exceed the error and are significant or if they do not and are insignificant. The modifications and user supplied inputs for the “ChannelChangeSignif” script are as follows:

1. The easting and northing were both changed to zero since UTM coordinates were used in the “QuantifyingRegistrationError” script and no adjustments were needed. The easting and northing serve to match the coordinates from the error analysis GCPs to the trajectory line coordinates if necessary, but since the GCPs used in Chapter 2 already were input in the same coordinate system that the trajectory lines (UTM), no adjustment was needed.
2. Digitizing error was input to correctly match the results from the digitizing error assessment done in Chapter 2 (Table 2.5). For every interval, the average digitizing error for each year of the interval was averaged and input into the script. For instance, if year 1 had an average digitizing error of 2.00 and year 2 had an average digitizing error of 2.50, the interval average would be 2.25 and serve as the input digitizing error. The inputs used were:
 - a. 1937-1951 = 1.620 meters

- b. 1951-1964 = 1.330 meters
 - c. 1964-1980 = 1.275 meters
 - d. 1980-1991 = 1.730 meters
 - e. 1991-2013 = 1.885 meters
 - f. 1937-2013 = 1.715 meters
3. As directed in Lea and Legleiter's instructions a new variable was created in MATLAB and named "MigVecChng." This variable is n x 5 matrix (n being the number of migration measurements from the study and 5 being the columns a-e below) was populated using the information created in the XLS file from the "Pre MATLAB Processing" tool. The information input is as follows:
- a. Column 1 = ID
 - b. Column 2 = Pair ID
 - c. Column 3 = Migration Distances
 - d. Column 4 = X Coordinate
 - e. Column 5 = Y Coordinate

This transposed the variables into column-vector format so the script could run.

4. A section of the script calculates significant and insignificant migration based off RMSE. This portion of the script had to be manually changed to the time frame specific averaged RMSE value. This section of the script also has two different equations to choose from depending on whether the periods in a given interval were warped to separate base images or if the base image itself was used as one of the periods in the interval considered.

5. Custom lines of script were added to further automate the processes by automatically creating the .csv file that original script required to be manually created through copy and pasting matrices out of MATLAB into Excel. The added script and comments are as follows:

```

% Devon Libby's additions to simplify and automate the process of creating a
% csv file containing the information of significant and nonsignificant
% migration.

% Creating the header names in an array
ColumnNames = {'FID','Sig_SVE','Sig_RMSE','Sig90'}
% Creating the ID field which will serve as the foreign key in
% to join the significant/insignificant table with the migration
% measurement table in ArcMap. This is accomplished by selecting every
% other entry from column two in the MigVecChng variable and moving it
% into a standalone matrix
ID = MigVecChng(1:2:end,2:2);
% This concatenates the ID field, SVE, RMSE, and 90th percentile
% significant/insignificant tables into one.
sigList_All = [ID sigList_SVE sigList_RMSE sigList_90];
% This function was downloaded from
% https://www.mathworks.com/matlabcentral/fileexchange/29933-csv-with-
column-headers
% (credit: Keith Brady) and allows a csv file to be written from the newly
% concatenated list and given the header from "ColumnNames".
csvwrite_with_headers('MATLABoutput.csv',sigList_All,ColumnNames)

```

Once the script has completed running, all files that reside in the folder are prepared for processing through the “Post MATLAB Processing” tool. A script function “csvwrite_with_headers” written by Keith Brady was used and his script for the function can be seen in Appendix F.

It should be noted that when the “ChannelChangeSignif” script was first executed, an error occurred in the “scatteredInterpolant” command within the script. The error message specified “Input data point values must be specified in column-vector format.”

In order to fix this two lines were added to the code immediately before the “scatteredInterplant” command

```
Xresid = Xresid';
```

```
Yresid = Yresid';
```

This transposed (flipped the columns and rows) the data and fixed the error. For more information see Appendix D.

3.2.1.4 Post MATLAB Processing

After the tabular data stored in the .csv was created in MATLAB to discern between statistically significant and insignificant data, it had to be brought back into ArcMap, joined to the trajectory line shapefile, and given new downstream measurements. The new downstream measurements were necessary since the shapefile was manually edited negating the usefulness of the original downstream measurements from the Planform Toolbox. This was accomplished by creating another model (Figure 3.7) to set the conceptual framework for the necessary processes. A script (Appendix G) was then written in order to create another custom ArcMap tool (Figure 3.8) that seamlessly integrated the output .csv of the “ChannelChangeSignif” MATLAB script with the already existing files created from prior tools. The custom script/tool to accomplish this was named “Post MATLAB Processing” and will be referred to as such moving forward. The ArcGIS tool requires the user to:

1. Set the workspace
2. Input the trajectory polyline shapefile
3. Input the newly created .csv that was created and properly formatted in the “ChannelChangeSignif” MATLAB script

4. Enter the number of years separating the two periods in the interval being considered. This is done so a new field can be populated with an annual migration.
5. Set the coordinate priority from which measures will be accumulated for linear referencing i.e. calculating new downstream measurements. For this stretch of river, LOWER_LEFT was selected since that is where the direction of flow begin. LOWER_LEFT could be thought of as south west as well.
6. Input the centerline for the earlier period in the time interval

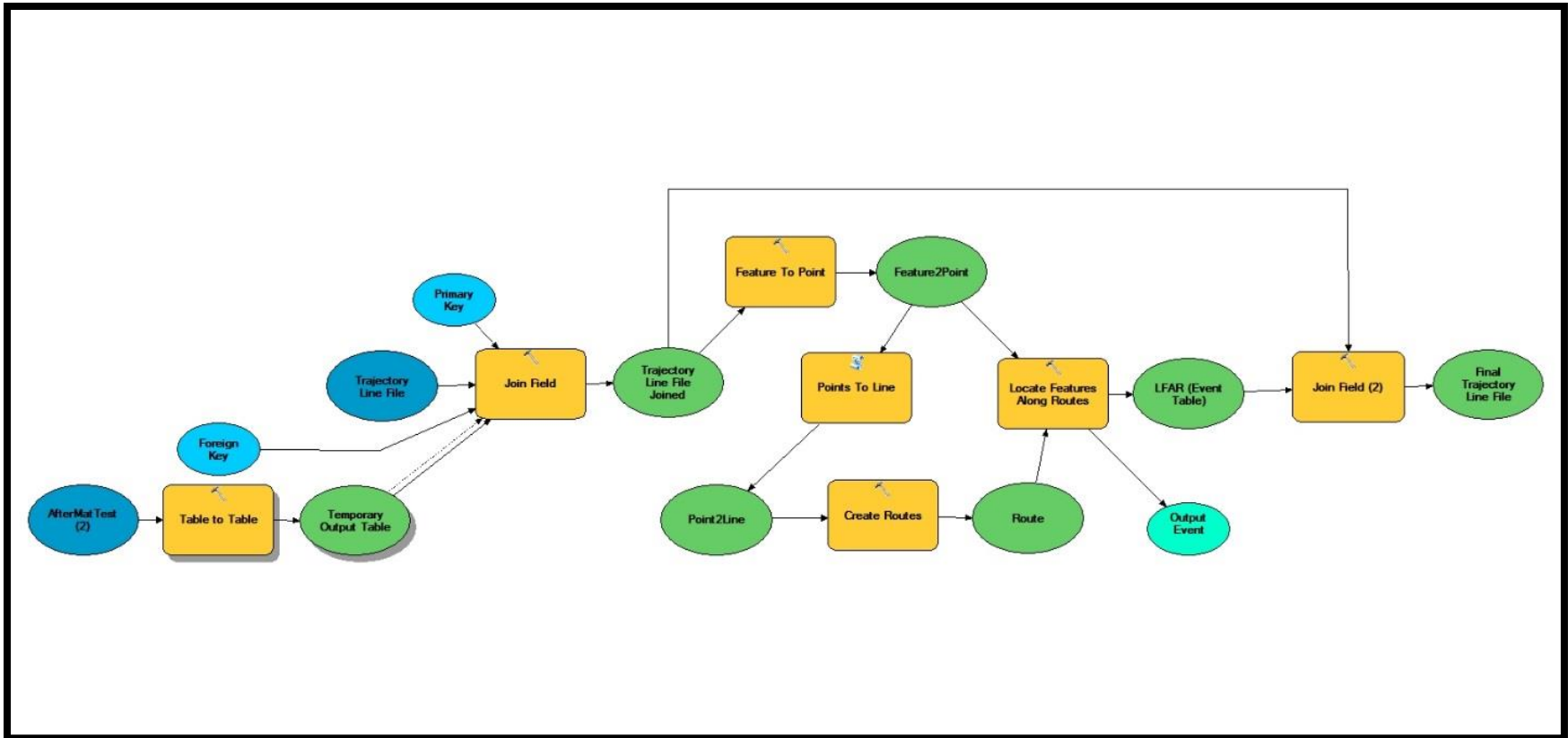


Figure 3.7: This model takes the newly created CSV that was output from the “ChannelChangeSignif” MATLAB script and joins the data back to the trajectory line shapefile. Once this is completed the tool recalculates downstream measurements through a series of tools and then joins the new up to date measurements to the trajectory line file. The script (Appendix 3D) written from this model is much more robust and fully details all the processes in the comments. This model served for a framework to initially conceptualize the main workflow of the tool.

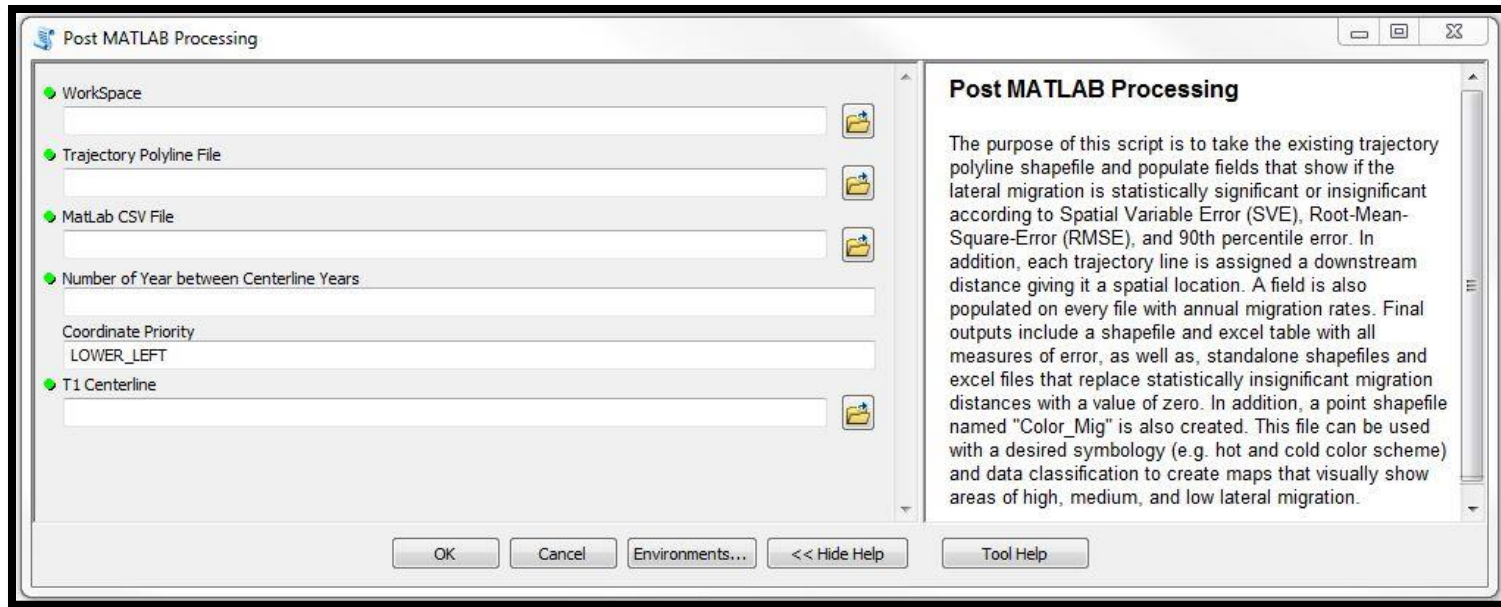


Figure 3.8: The GUI for the Post MATLAB Processing tool has six user required inputs along with tool help descriptors defining the overall function of the tool and each input. The input and descriptors are as follows: 1) Workspace - Set the workspace to the folder containing the appropriate trajectory polyline file and CSV file containing significant and insignificant measurements that are used as the next two inputs 2) Trajectory Polyline File - Select the appropriate trajectory polyline file. 3) MatLab CSV File - Select the appropriate CSV file containing significant and insignificant measurements. Note: this CSV file must contain only four columns with headings "FID", "SVE", "RMSE", "Ninety" respectively. If these aren't spelled and capitalized correctly the script will fail to run. 4) Number of Years between Centerline Years - Enter the number of years (interval) between the two centerlines. Example: Time 1 centerline is 1937 and Time 2 centerline is 1951. The number entered would be 14. 5) Coordinate Priority - The position from which measures will be accumulated for each output route during the linear referencing process. Options include: UPPER_LEFT — Measures will be accumulated from the point closest to the minimum bounding rectangle's upper left corner. This is the default. LOWER_LEFT — Measures will be accumulated from the point closest to the minimum bounding rectangle's lower left corner. UPPER_RIGHT — Measures will be accumulated from the point closest to the minimum bounding rectangle's upper right corner. LOWER_RIGHT — Measures will be accumulated from the point closest to the minimum bounding rectangle's lower right corner. 6) T1 Centerline - Select a polyline shapefile for the earlier of the two time periods for the interval considered.

The “ChannelChangeSignif” MATLAB script calculates significant and insignificant measures based on three metrics (SVE, RMSE, 90th percentile – for more information on these see Appendix D). The “Post MATLAB Processing” script was written to create unique shapefiles and Excel tables for each of metrics (Figure 3.9). In creation of the files, an update cursor uses fields which denotes insignificant measurements as 0’s significant measurements as 1’s to then update the total migration and annual migration fields. If a measurement is insignificant (denoted by 0) the cursor changes the total migration and annual migration fields to 0 since they do not exceed the error present. The trajectory shapefile used to parse (separate) this data into individual files is also updated but stores all the information for the three metrics along with all migration measurements regardless of whether they are significant or insignificant. This preserves all of the original data and can always be referred back to by the user. An Excel table is also created from the newly updated shapefile as well. Another output is a point shapefile named “Color_Mig”. This file can be used in combination with a desired symbology (e.g. hot and cold color scheme) and data classification to create maps visually displaying the amount of channel mobility. All intermediate files created in this script are stored in a temporary folder which are automatically deleted at the end of the script to avoid unnecessary clutter.

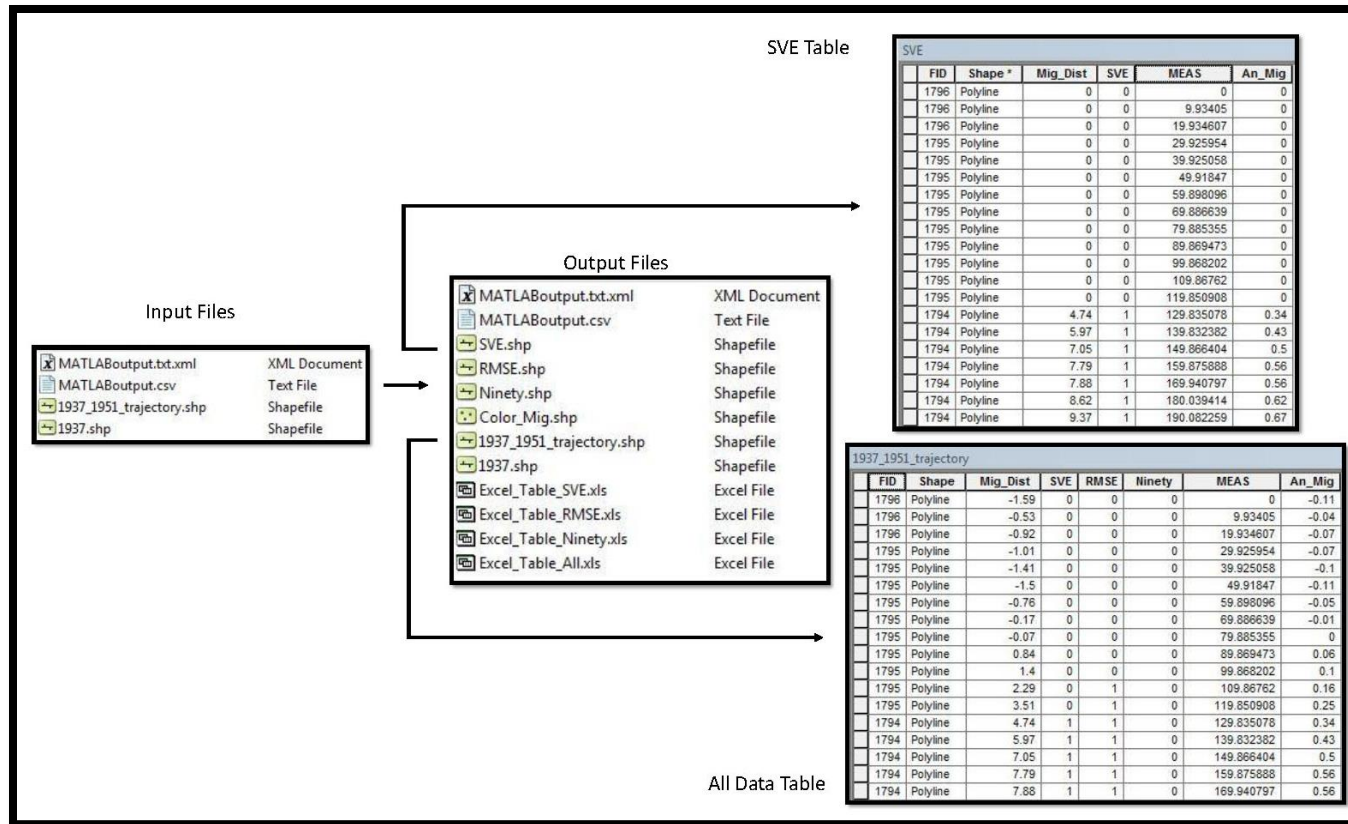


Figure 3.9: Only three files are required as inputs into the “Post MATLAB Processing” tool. The output files created from the tool include: 1) the input trajectory shapefile with new fields showing statistically significant and insignificant measurement denoted by 1’s and 0’s respectively along with downstream measurements and annual migration. 2) Three new polyline shapefiles (SVE, RMSE, Ninety) that show only the fields pertinent to the specific error metric and reduce insignificant measurements to 0’s in the total migration and annual migration fields. 3) Excel tables for all the shapefiles in order to increase efficiency for data analysis. 4) A point shapefile named "Color_Mig" that can be used in combination with a desired symbology (e.g. hot and cold color scheme) and data classification to create maps that visually represent channel mobility.

Once all the data was run through the tool, it was manually inspected. A minor problem was noticed when “Sort Ascending” was applied to the measurement field in ArcMAP. In a couple of the intervals a handful of trajectory lines were reporting a downstream measurement of “0”. Upon closer inspection, it was discovered that these trajectory lines lacked measurements because they were not connected to the T1 centerline (earlier time period centerline) which the tool used to create a route in order to assign measurements to the trajectory line (Figure 3.10). This issue could have been handled in multiple ways, but it was decided that the intervals affected by this problem would be corrected by fixing the trajectory lines and rerunning the data through the “Post MATLAB Tool.” This was done to ensure the highest degree of accuracy with the data. Another alternative would be to manually type in the downstream measurements by using the “Identify Route Locations” tool within ArcMap. However, the main issue with this approach is that every excel table (4 total) and shapefile (5 total) would have to be opened and edited which could introduce user error along with being a time consuming and tedious process.

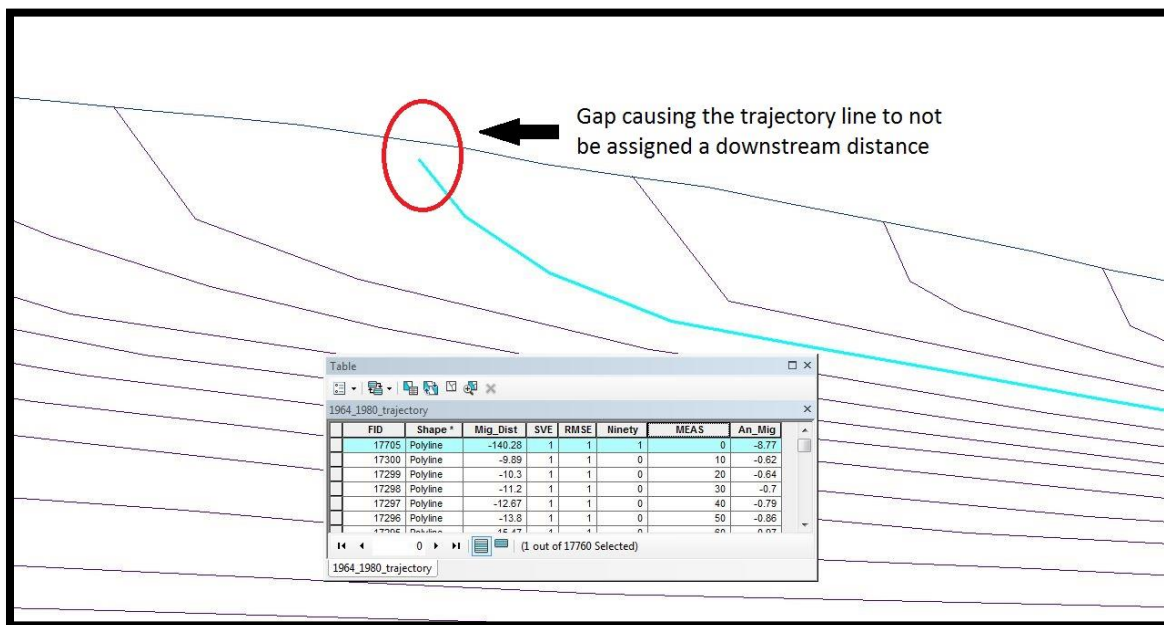


Figure 3.10: The trajectory was not connected to the T1 centerline. Since this centerline was converted to a route to assign downstream distances to the individual trajectory lines, the gap caused it to be passed over.

3.2.1.5 Cutoff vs Non-Cutoff Datasets

The definition used in this study for a “cutoff” needs to be explained since cutoffs were not included as channel migration in the reach analysis. These measurements were not included because a cutoff is not eroding and reworking sediment between the old channel and new channel. However, there were instances in this study where an old channel was rapidly abandoned but reworked or fully eroded all the land between the old channel and new channel. In these instances, the measurements were considered as “non-cutoff migration” since erosion and subsequent sediment reworking occurred over the area between the old and new channel (Figure 3.11). The channel migration data also becomes heavily weighted by cutoff measurements when they are included alongside non cutoff migration measurements. In some cases on the Minnesota River, a cutoffs old channel location to new channel location is over thousand meters away. Although the

primary focus moving forward is on channel migration without cutoff measurements, the presence of cutoffs within reaches will be discussed since they do show spatial and temporal trends that can be used to interpret the results. Cutoffs are also important to note since they are directly tied to reductions in stream sinuosity.

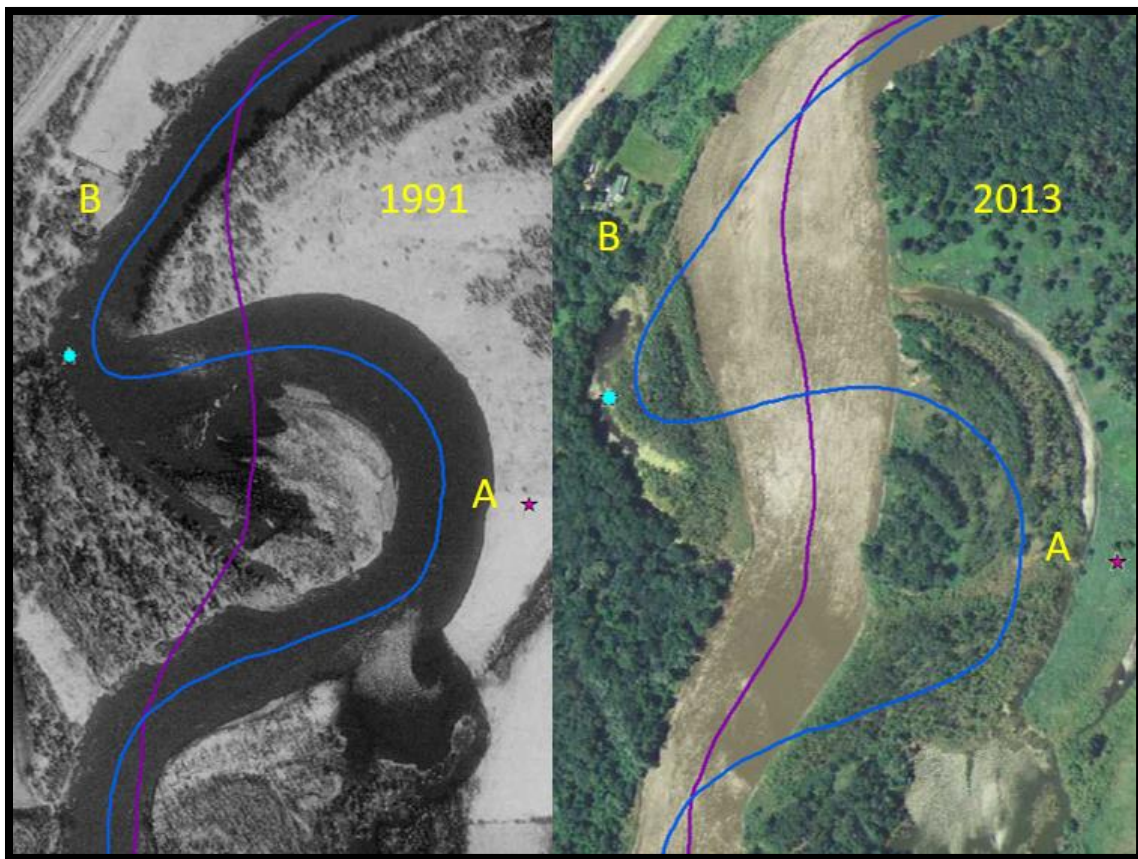


Figure 3.11: This figure displays the difference in cutoffs that were not considered in migration measurements (A) and “cutoffs” that were considered as migration. In cutoff A, there is clearly uneroded land that was left behind when the cutoff occurred, whereas, cutoff B eroded all the land when establishing the new channel route. The blue dot shows where an oxbow lake is forming which would cause some to call this a cutoff, but it is not in this study.

3.2.2 Width Change and Sinuosity/Stream Length

Width measurements were calculated and stored in a text file when the centerlines were created in the NCED “Centerline Interpolation” tool (see section 2.2.4; Figure 2.8).

In order to make these files usable in ArcMap, the text files were converted to dBASE (.dbf) tables using the “Table to dBase” tool. This process is necessary so ArcMap can handle the large amount of entries contained in the file opposed to just trying to bring the text files into ArcMap. The dBase contains the xy coordinates for the left and right side of each measurement so the “XY to Line” tool was then used to create a shapefile of the width measurements. One shortcoming of this tool is that it does not transfer all the attributes contained in the original dBASE table so it is necessary to use the ID field (optional to transfer in the “XY to Line” tool) to join the newly created shapefile back to the dBASE table in order to access width measurements and downstream distances. This can be done many ways but in order to permanently join the necessary fields the “Join Field” data management tool was used. Another option would be to create a new width measurement field using the “Calculate Geometry” function within ArcMap to populate it.

Sinuosity is simply the relationship between channel length divided by valley length. To calculate these measurements, the geometry of the centerlines was calculated in ArcMap to get channel lengths then a separate shapefile was created and digitized for the valley length. These measurements were then joined to a single table and the field calculator was used to populate a new field storing the sinuosity measurements alongside the channel lengths.

3.2.3 River Reach and Pinch Point Analysis

Once all the calculations and analysis were complete, the data was broken down into river reaches based on geomorphic breaks (Figure 3.12) for longitudinal spatial analysis. These reaches were defined based on geomorphic characteristics of the channel

(sinuosity, meander wavelength, depositional features, etc.) and river valley width as well as any influencing anthropogenic features (urban areas, bridges, flood control structures, etc.). For detail on the how the geomorphic breaks were determined see Appendix H. This was accomplished by adding a new “River_Reach” field to the shapefile of interest (e.g. 1937-1951 migration shapefile) and overlaying a polyline shapefile with 16 segments matching the spatial extent of each break. Another way to accomplish this is by creating a polygon shapefile for the geomorphic breaks and using a “select by location” to then edit and populate fields to the respective geomorphic break.

A secondary, river reach break system (Figure 3.13) was used for displaying the shapefile named “Color_Mig” that visually displays channel mobility using intuitive color schemes to represent the data (discussed in section 3.2.1.4). These river reaches were based solely on providing an appropriate extent to best qualitatively display the data and were not used for any further analysis.

Since the placement of invasive carp barriers are primary consideration of this research, several “pinch points” or areas where structures are presently controlling the stream were selected and planform change was analyzed. First, Mankato’s reach of river controlled by a flood control structure is looked at followed by four bridges. These pinch points were analyzed to see if any discernable trends could be seen in the evolution of upstream vs downstream morphology over the years of record.

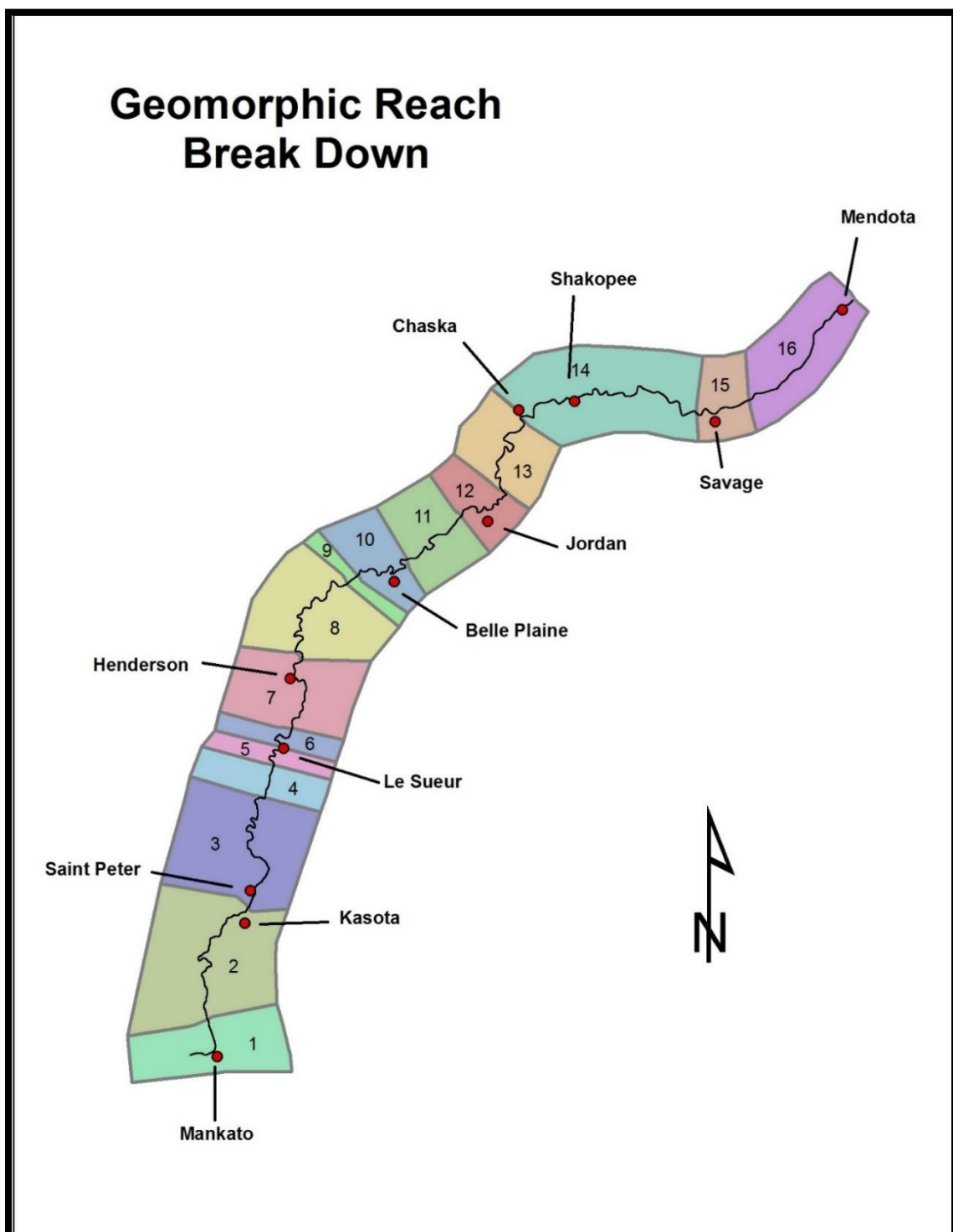


Figure 3.12: Displayed are the 16 geomorphic breaks that the study area was broken down into.

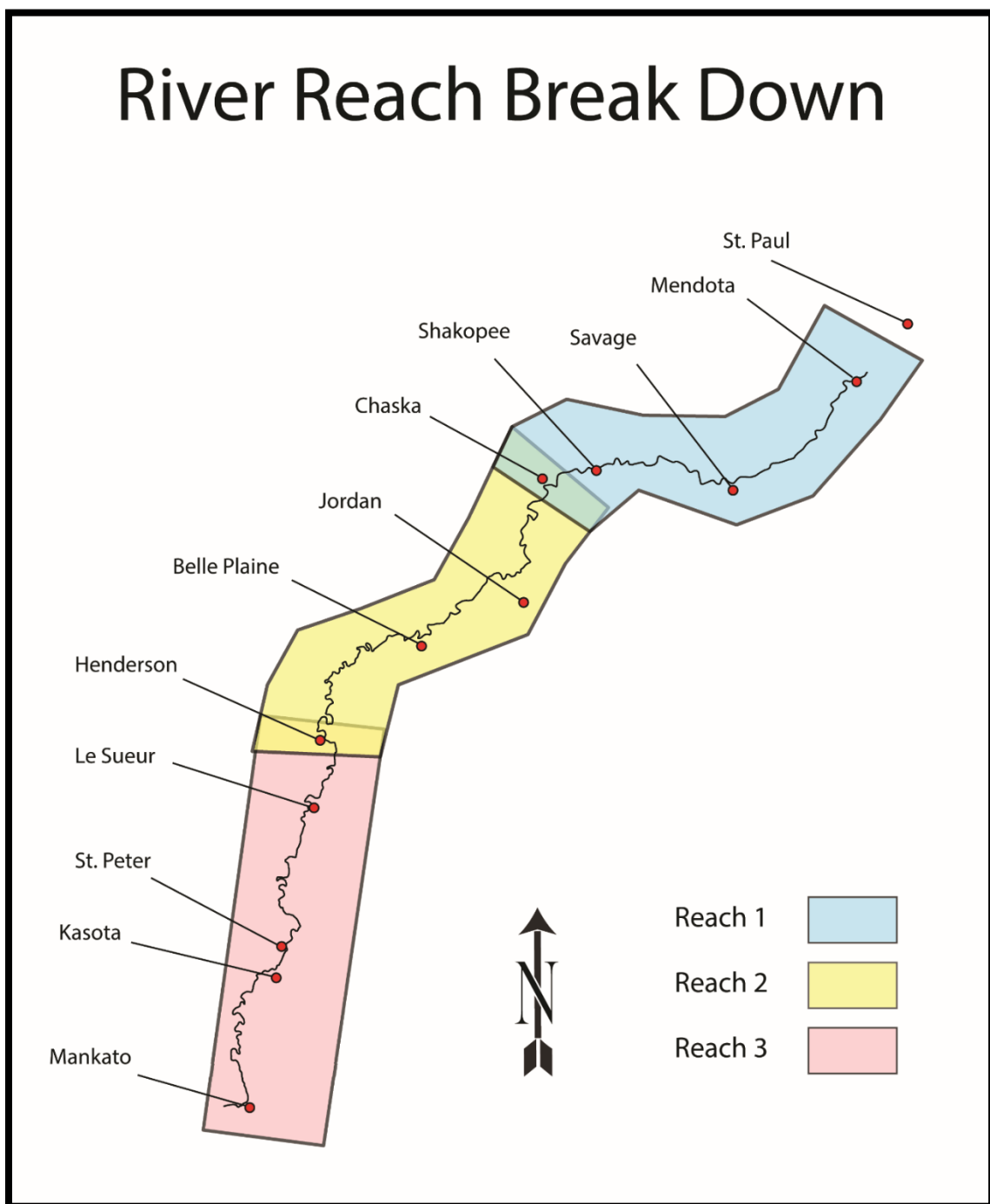


Figure 3.13: These are the three break points used to offer a spatial extent appropriate for viewing the “Color Migration” maps which are an output of the “Post MATLAB Processing” tool

3.3 Results

3.3.1 Channel Migration

Channel migration can be analyzed at various scales. This section will first look at the study area as whole to see large scale spatial and temporal longitudinal trends exist. Attention will then be given to color migration maps which are also viewed at a larger scale but offer a unique view of the data by maintaining the spatial characteristics of the river. These maps are especially powerful in conveying migration to viewers without a scientific or mathematic background since graphical views of data are not necessarily intuitive to all viewers. Finally, a smaller scale focus will be given through reach analysis. Schumm (1985) states that reach scale analysis is of most interest to geomorphologists who are concerned with what the pattern of the river reveals about its history and behavior. Reach analysis also offers a higher resolution revealing if larger scale patterns are distributed over many reaches, or if acute activity or stability is seen within larger trends.

3.3.1.1 Large Scale Data Analysis

When viewing the data for channel migration for the lower Minnesota River at a large scale (Figure 3.14, Figure 3.15) the first ~115-120 river kilometers (Mankato to a little past Jordan) are historically more actively migrating than the downstream ~40-60 kilometers (measurements vary due to changing stream length for a given interval). Sixteen of the nineteen cutoffs of the entire temporal scale of the study appear in the upstream 90 kilometers (Figure 3.14). Although the next 25-30 kilometers are still active without cutoffs, a break is seen after this point where the channel migration decreases (Figure 3.14, Figure 3.15). Viewing the data at this scale shows broad patterns that are

primarily spatial. Appendix I displays every interval's annual channel migration in a standalone graph.

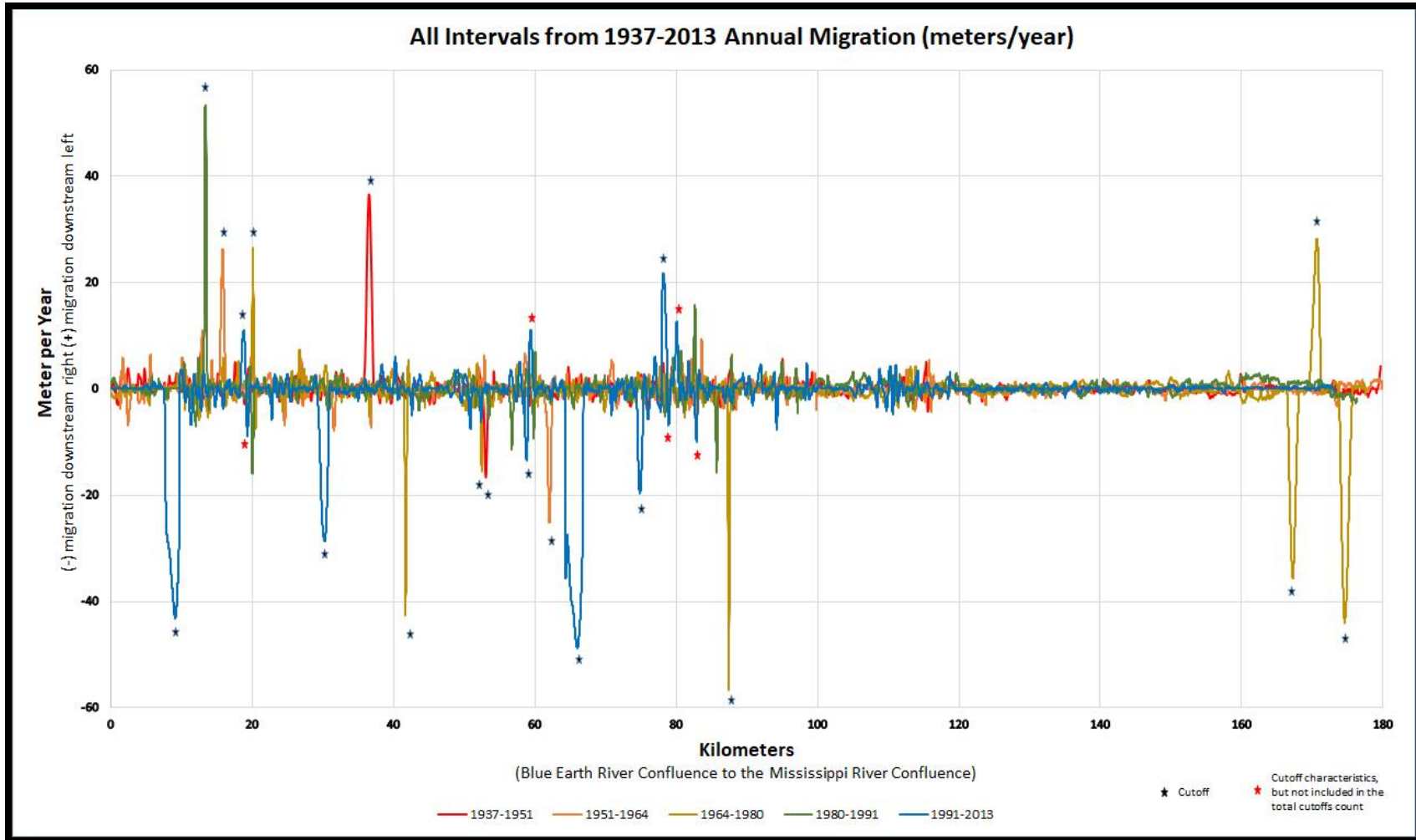


Figure 3.14: Graphical results for annual migration for all intervals related to downstream distance from the Blue Earth River confluence to the Mississippi River confluence with cutoff measurements included. These cutoffs are denoted on the graph with stars.

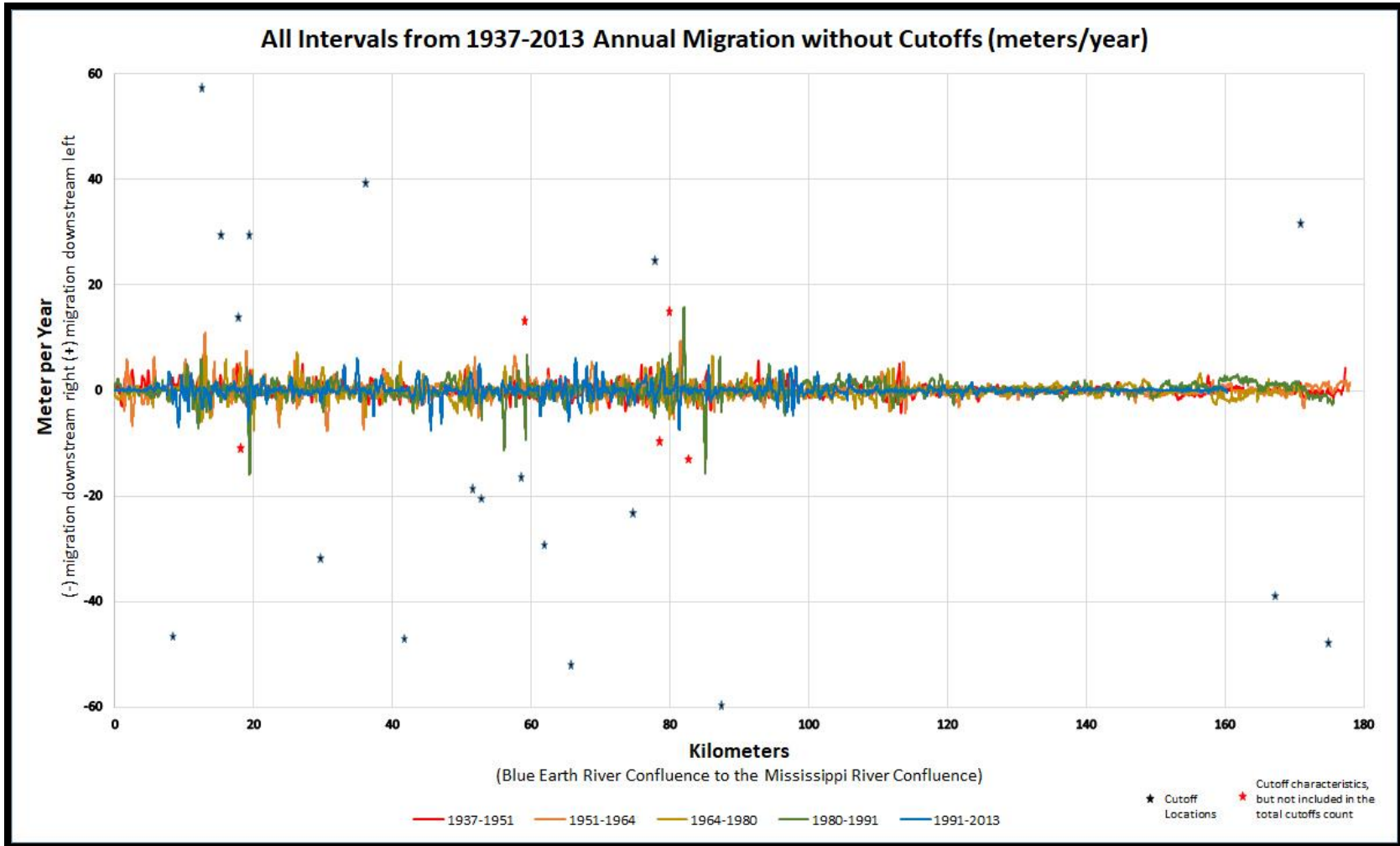


Figure 3.15: Graphical results for annual migration for all intervals related to downstream distance from the Blue Earth River confluence to the Mississippi River confluence with cutoffs measurements removed, however cutoff locations are denoted on the graph with stars.

3.3.1.2 Color Migration Maps (Preserving Spatial Attributes of the Data)

The results of the output “Color_Mig” shapefile produced in the Post MATLAB Script (Figure 3.16- Figure 3.18) reveal the same spatial trends as the graphical (Figure 3.14, Figure 3.15) view, however more detail is distinguishable. For instance, the first third of the study area (Figure 3.16) displays stretches of relative stability mixed within the more active reaches – a trend not evident in the graphical view. The area immediately downstream of the city of Henderson has also been a very active stretch of river in all the intervals considered (Figure 3.17). These output shapefiles demonstrate another way to display same data while maintaining spatial characteristics and applying an intuitive “hot and cold” color scheme. This view of the data shows the high degree of variability in the Minnesota River’s channel migration prompting the need for more detailed reach analysis.

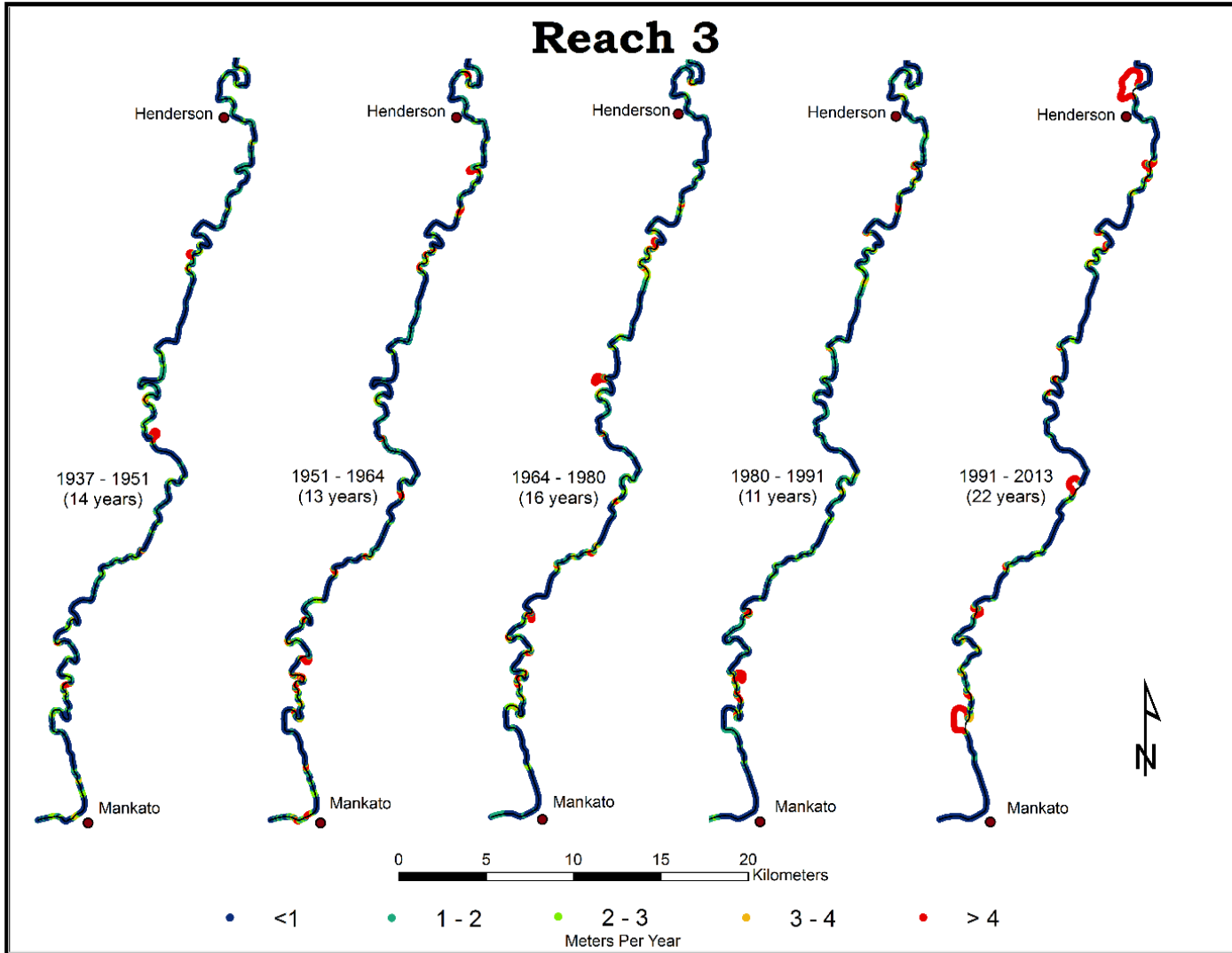


Figure 3.16: Displays the output for the “Color_Mig” shapefile from the Post MATLAB script in Reach 3 (Mankato to Henderson).

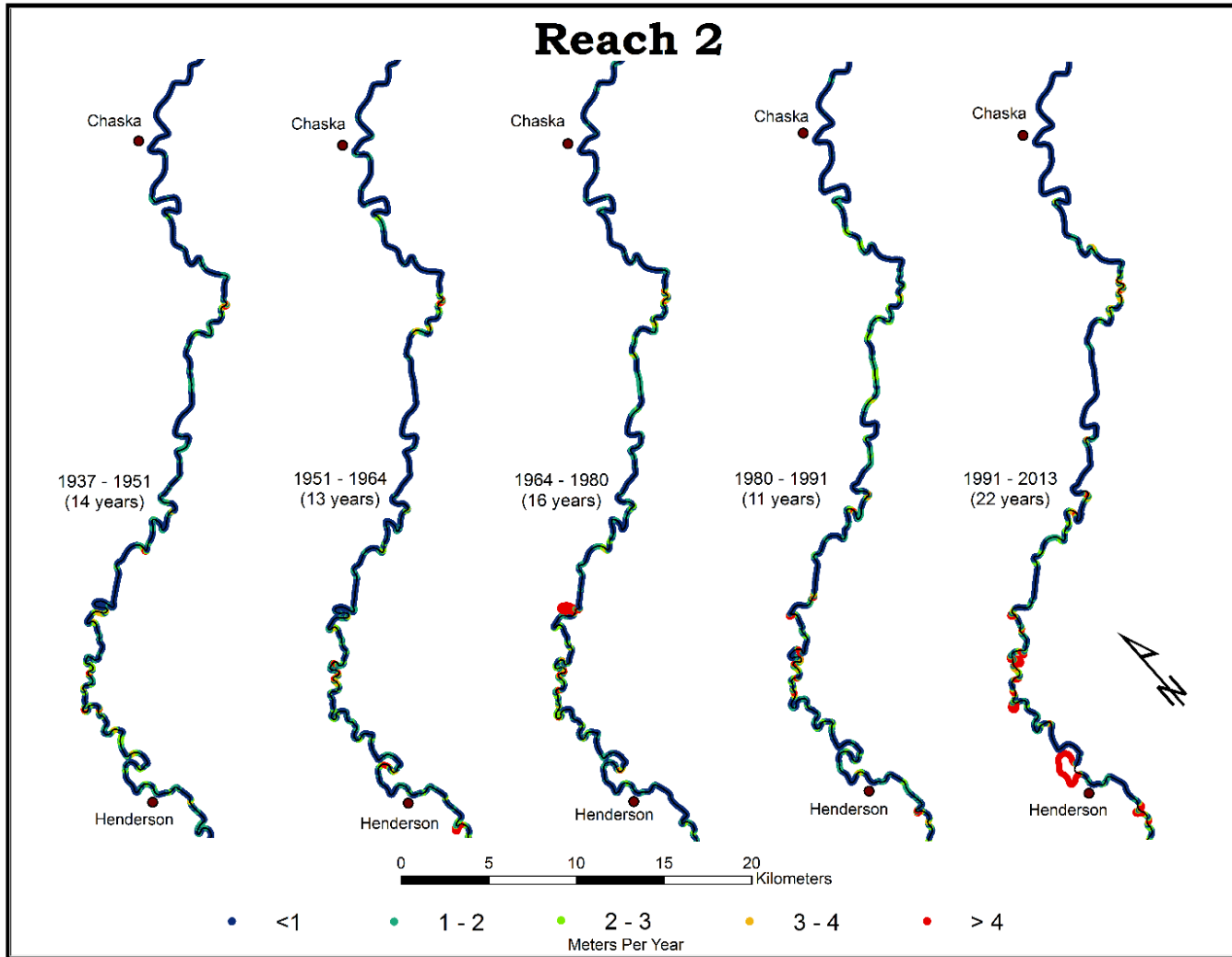


Figure 3.17: Displays the output for the “Color_Mig” shapefile from the Post MATLAB script in Reach 2 (Henderson to Chaska).

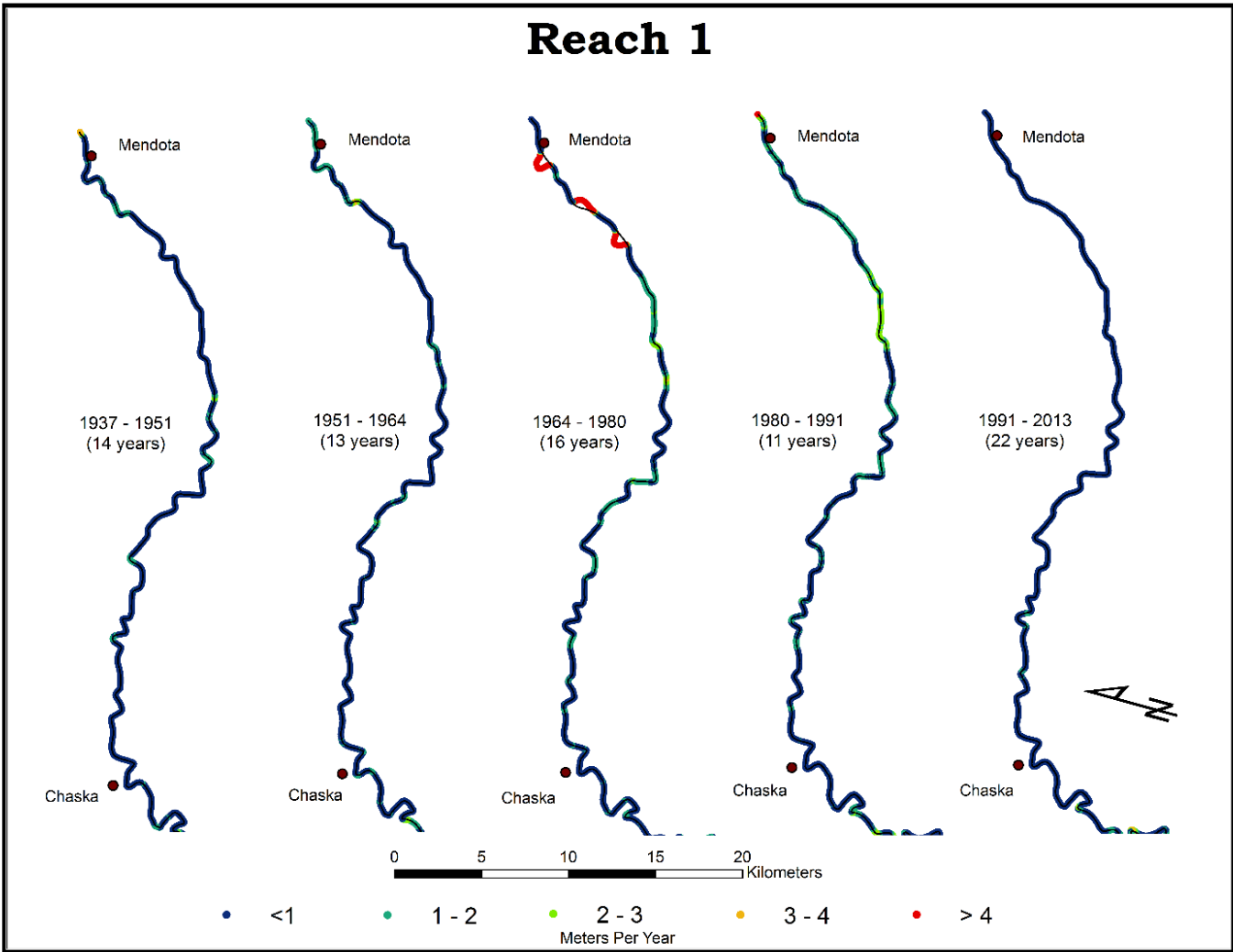


Figure 3.18: Displays the output for the “Color_Mig” shapefile from the Post MATLAB script in Reach 1 (Chaska to Mendota).

3.3.1.3 Geomorphic Break Reach Analysis

Geomorphic break (Figure 3.12) analysis revealed further temporal and spatial trends that were not intelligible in the prior forms of analysis. Considerations were given to:

- 1) Average annual channel migration (AACM) for each reach in each interval
- 2) The overall AACM for each reach (1937-2013)
- 3) The overall AACM for each interval for the whole river (Reach 1-16)
- 4) The maximum annual channel migration (MACM) measurement for each reach in each interval
- 5) The average MACM measurement for each reach
- 6) The MACM for each interval for the whole river (Reach 1-16)
- 7) Cutoff locations relation to 1-6

Minimums values for individual reaches of a given interval were not considered since they all contain measurements of zero. Any measurement that did not exceed the error present (termed by Lea and Legleiter (2016) as statistically insignificant) was assigned the value of zero for this analysis. This was done because these measurements were almost exclusively smaller measurements, and to simply exclude them would bias the AACM measurements to appear higher than they are. Conversely, this has the potential to bias the AACM measurements to appear lower than they are, if actual migration took place, but was not enough to exceed the error in that location. The data was initially analyzed both with the insignificant measurements excluded and included as zero's. It was decided the latter analysis more accurately displayed the data.

3.3.1.3.1 Average Annual Channel Migration (AACM)

Reach 5 in the 1964-1980 interval had the highest AACM of 2.43 meters per year (m/y) (Table 3.1, Figure 3.19). Reach 5 also had the highest overall reach AACM rate with a reach average of 1.86 m/y (Table 3.1, Figure 3.20). Aside from Reach 5, Reach 2, 3, 7, 8, and 12 have been historically active reaches, all having AACM rates above the 50th percentile (median or 2nd quantile) throughout all the intervals considered (Table 3.1, Figure 3.20). Reach 10 has also been quite active with only one interval (1951-1964) being slightly under the 50th percentile. Reach 9 in the 1980-1991 interval had the lowest AACM of 0.11 (m/y) (Table 3.1, Figure 3.19). Reach 9 also had the lowest overall reach AACM rate with a reach average of 0.31 m/y (Table 3.1, Figure 3.20). Aside from Reach 9, Reach 6, 13, 14 and 15 have been historically inactive reaches, all having AACM rates below the 50th percentile throughout all the intervals considered (Table 3.1, Figure 3.19). Reach 4 and 11 have also remained inactive with the interval 1980-1991 being the exception for both.

The most recent interval of 1991-2013 interestingly marks the highest migration rates for Reach 7, 8, 10, and 12 and the lowest migration rates for Reach 1, 3, 4, 15, and 16 (Table 3.1). This interval also has three reach measurements in the 90th percentile and six measurements in the 10th percentile of all 80 AACM measurements considered (Table 3.1). This is nearly three times the amount of extreme (top and bottom 10%) values expected in a normal distribution. This is an indication that the present fluvial conditions are undergoing a change from those that historically existed. Reach 13-16 compose a little less than third of the total study area, and only contain two AACM measurements above the 50th percentile (both found in Reach 16) (Table 3.1). This indicates an overall

spatial trend of decreasing channel migration on the lower Minnesota moving in the downstream direction (Figure 3.20) however variability is seen throughout the reaches (Figure 3.19, Figure 3.20).

Table 3.1: Average Annual Channel Migration

Average Annual Channel Migration by Reach and Interval (m/yr)						
Reach	1937-1951	1951-1964	1964-1980	1980-1991	1991-2013	Average
1	1.07	1.46	0.61	0.45	0.24	0.76
2	1.05	1.37	1.41	1.21	1.39	1.29
3	0.98	0.81	1.00	0.93	0.79	0.90
4	0.35	0.69	0.61	0.89	0.18	0.54
5	1.53	1.98	2.43	1.36	2.01	1.86
6	0.55	0.63	0.74	0.68	0.69	0.66
7	0.89	1.14	0.86	1.33	1.51	1.15
8	1.28	1.13	1.26	1.57	1.75	1.40
9	0.41	0.31	0.53	0.11	0.19	0.31
10	0.84	0.74	0.78	0.90	1.27	0.90
11	0.66	0.33	0.76	1.10	0.39	0.65
12	1.03	1.15	1.32	1.08	1.41	1.20
13	0.39	0.56	0.44	0.48	0.48	0.47
14	0.26	0.38	0.58	0.49	0.27	0.40
15	0.78	0.37	0.54	0.69	0.23	0.52
16	0.40	0.63	0.83	1.39	0.16	0.68
Average	0.77	0.84	0.91	0.99	0.81	0.86
10th Percentile						
Quartile 1		Quartile 2		Quartile 3		90th percentile
0.27		0.48		1.20		1.45
< 0.27	>0.27 & <0.48	>0.48 & <0.78	>0.78 & <1.20	>1.20 & <1.45	>1.45	

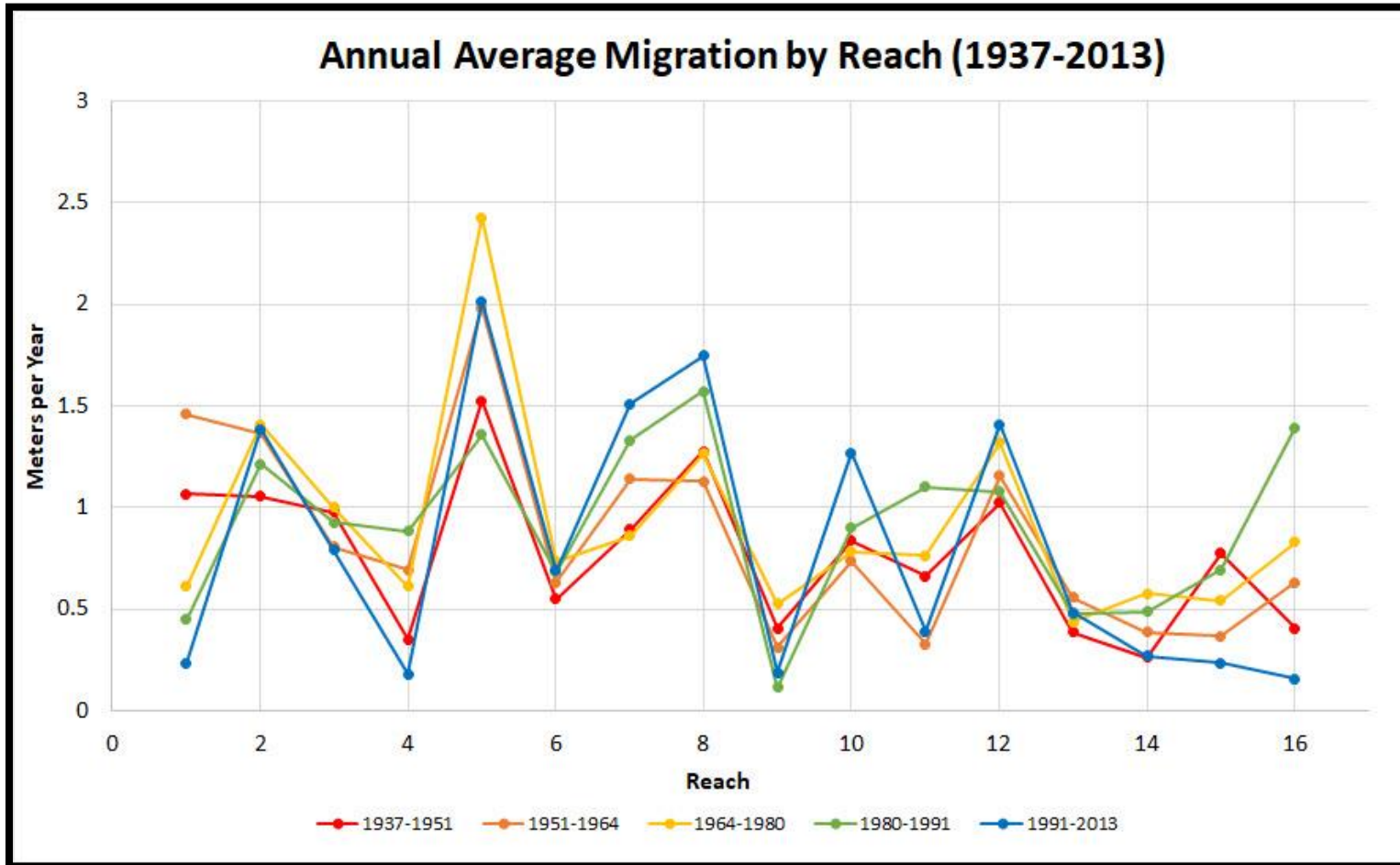


Figure 3.19: Graphical results for annual average migration for all intervals grouped by river reach. Reach one begins at the Blue Earth River confluence and Reach 16 ends at the Mississippi River confluence.

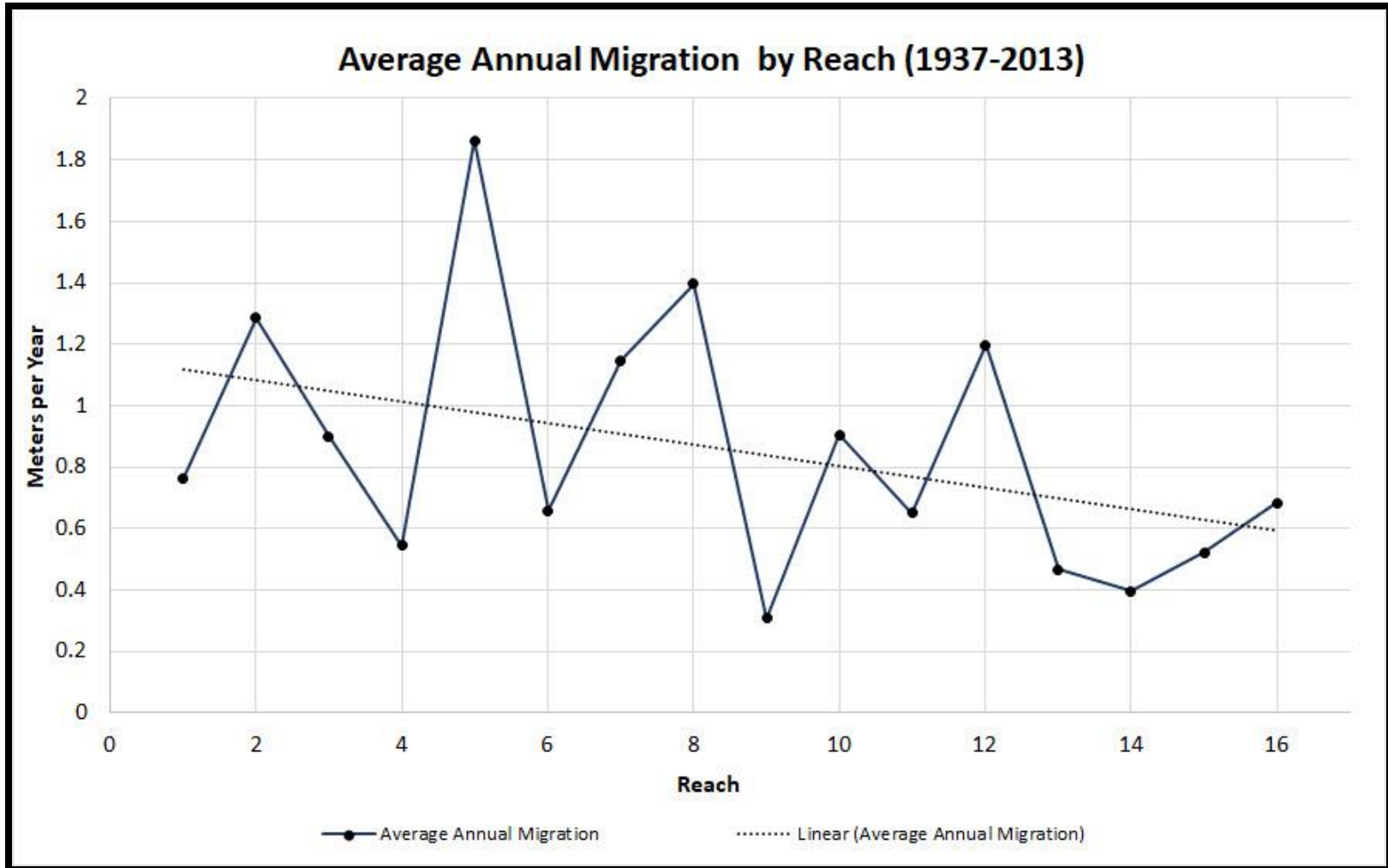


Figure 3.20: Graphical results showing the average migration of all years by reach. Reach 1 begins at the Blue Earth River confluence and Reach 16 ends at the Mississippi River confluence.

3.3.1.3.2 Maximum Annual Channel Migration (MACM)

Although Reach 5 had the greatest reach/interval AACM and the overall highest reach AACM, it did not rank among the highest reaches in terms of MACM (Table 3.1, Table 3.2). Reach 2 in the 1980-1991 interval had the highest MACM of any reach/interval with a measurement of 15.86 m/y or a total of 174.48 meters (Figure 3.21, Table 3.2). Reach 2 also had the highest average MACM of the reaches at 10.42 m/y (Table 3.2). Reach 7 and 8 also had high MACM rates with an average of 7.57 m/y and 9.95 m/y (Table 3.2). Reach 4, 9, 11, and 13-16 all averaged MACM measurements under 3 meters per year (Table 3.2). Reach 9, a reach characterized by an unusually long, straight length of channel, had lowest averaged MACM at 0.88 m/y and the lowest reach/interval measurement of 0.49 m/y in the 1991-2013 interval. Every MACM measurement in this reach fell in the 10th percentile (Table 3.2).

Reach 2, 7, and 8 contained all the 90th percentile MACM measurements revealing a strong relationship between these spatial locations over the entire temporal range of the study. In the prior section, low AACM measurements were seen in Reach 13-16 which is also the case for MACM. In these reaches, all but one MACM measurement is above the 50th percentile. Of the other nineteen measurements, eight of them are in the 25th percentile, two of which fall in the 10th percentile. This affirms another spatial/temporal trend that less channel migration is historically seen in the downstream reaches. The 1991-2013 interval show an unproportioned amount of extreme values (top and bottom 10%) relative to the other intervals much like it did in AACM. Four 10th percentile measurements and three 90th percentile measurements were recorded which is slightly under 50% of all extreme values.

Table 3.2: Maximum Annual Channel Migration by Reach and Interval

Maximum Annual Channel Migration by Reach and Interval (m/yr)						
Reach	1937-1951	1951-1964	1964-1980	1980-1991	1991-2013	Total
1	3.93	6.63	2.97	2.45	1.37	3.47
2	7.13	11.01	7.49	15.86	10.63	10.42
3	4.09	7.80	5.49	4.12	7.44	5.79
4	1.13	1.55	2.72	3.58	0.67	1.93
5	4.12	6.34	4.61	3.42	7.47	5.19
6	1.49	6.42	3.20	5.58	6.08	4.55
7	4.17	6.69	4.67	11.21	11.09	7.57
8	5.34	9.40	6.6	15.75	12.64	9.95
9	0.97	0.93	1.04	0.98	0.49	0.88
10	5.69	3.83	3.27	5.10	7.46	5.07
11	1.97	1.28	2.17	3.27	4.82	2.70
12	5.12	5.53	4.25	3.28	4.59	4.55
13	2.37	3.00	1.73	3.04	3.49	2.73
14	1.60	2.20	2.17	2.04	1.60	1.92
15	2.87	2.00	3.35	1.76	0.77	2.15
16	4.31	3.27	2.63	3.04	0.78	2.81
Max	7.13	11.01	7.49	15.86	12.64	10.83
10th Percentile						
10th Percentile		Quartile 1	Quartile 2	Quartile 3	90th Percentile	
1.05		2.07	3.53	5.98	9.24	
< 1.05	>1.05 & <2.07	>2.07 & <3.53	>3.53 & <5.98	>5.98 & <9.24	>9.24	

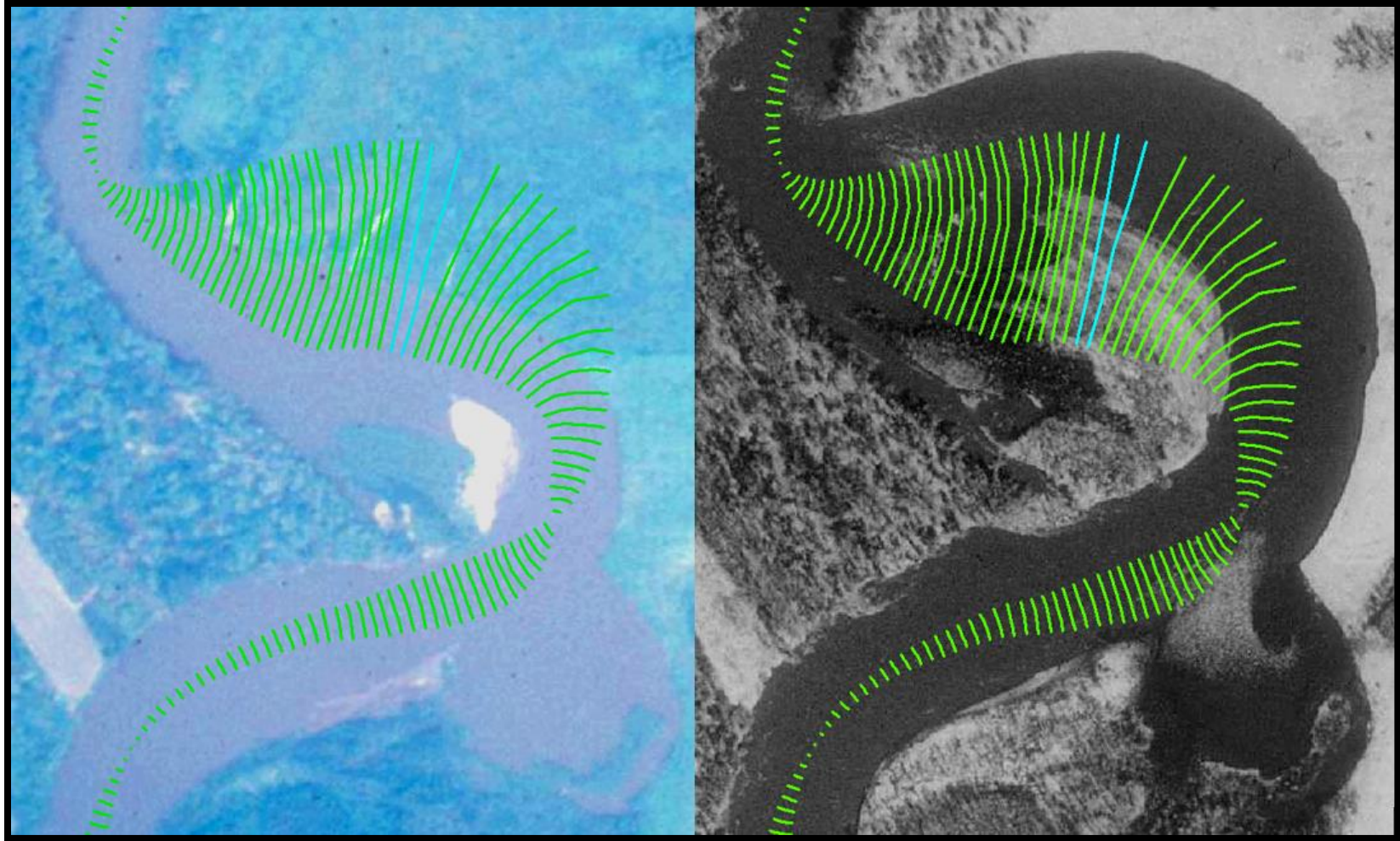


Figure 3.21: Reach 2 in the 1980 (left) to 1991 (right) had the the highest MACM of any reach/interval. This figure has the two measurements of 15.86 m/y (total 174.48 m) highlighted in light blue

3.3.1.3.2 Cutoff location relation to AACM and MACM

Although cutoffs measurements were removed from the reach analysis (Figure 3.19, Figure 3.20), Figure 3.22 displays cutoff locations with an embedded table showing the cutoffs by reach and by interval. Most cutoffs are in the upstream half of the study area (Reach 1-8) except for three cutoffs that occurred in Reach 16 in the 1964-1980 interval. Reach 2 had the most cutoffs with five total and the intervals 1964-1980 and 1991-2013 had the most cutoffs with seven a piece.

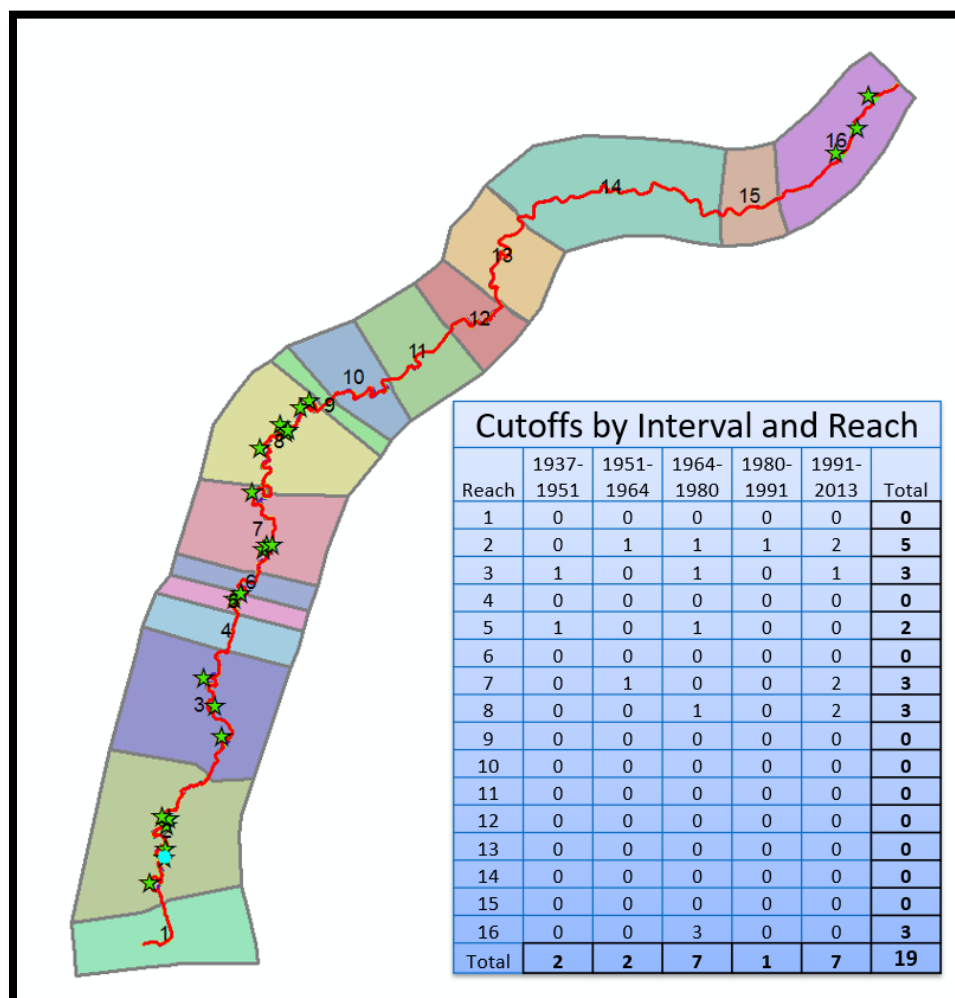


Figure 3.22: Stars denote cutoff locations. The embedded table shows the cutoffs by reach and by interval.

3.3.2 Channel Width Change

When viewing the data for channel width for the lower Minnesota River at a large scale (Figure 3.23) two trends were evident. Temporally, overall channel width increased from 1937-2013 (Figure 3.24). Spatially, the increase in channel width observed in the upstream was greatest with a gradual decrease moving in the downstream direction (Figure 3.24). Appendix J shows each period (1937-2013) in separate graphs. Beyond these general trends, not much else can be seen in the data at this scale. However, reach analysis revealed more spatial and temporal trends with considerations given too:

- 1) Average channel width (ACW) for each reach in each period
- 2) The overall ACW for each reach (1937-2013)
- 3) The overall ACW for each period for the whole river (Reach 1-16)
- 4) The maximum channel width (MaxCW) measurement for each reach in each period
- 5) The MaxCW measurement for each reach
- 6) The MaxCW for each period for the whole river (Reach 1-16)
- 7) The minimum channel width (MinCW) measurement for each reach in each period
- 8) The MinCW measurement for each reach
- 9) The MinCW for each period for the whole river (Reach 1-16)

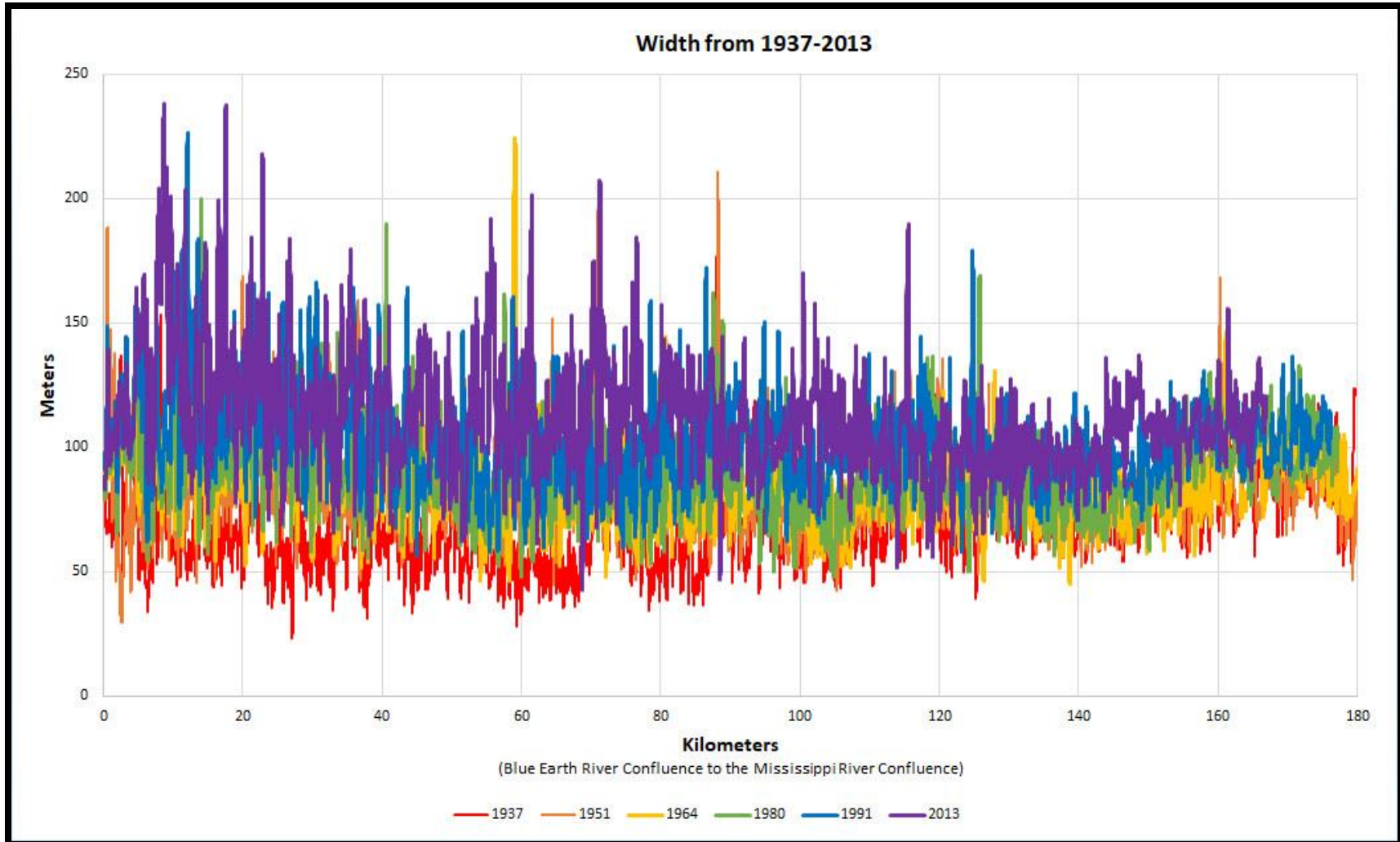


Figure 3.23: Graphical results for width measurements for all years related to downstream distance from the Blue Earth River confluence to the Mississippi River.

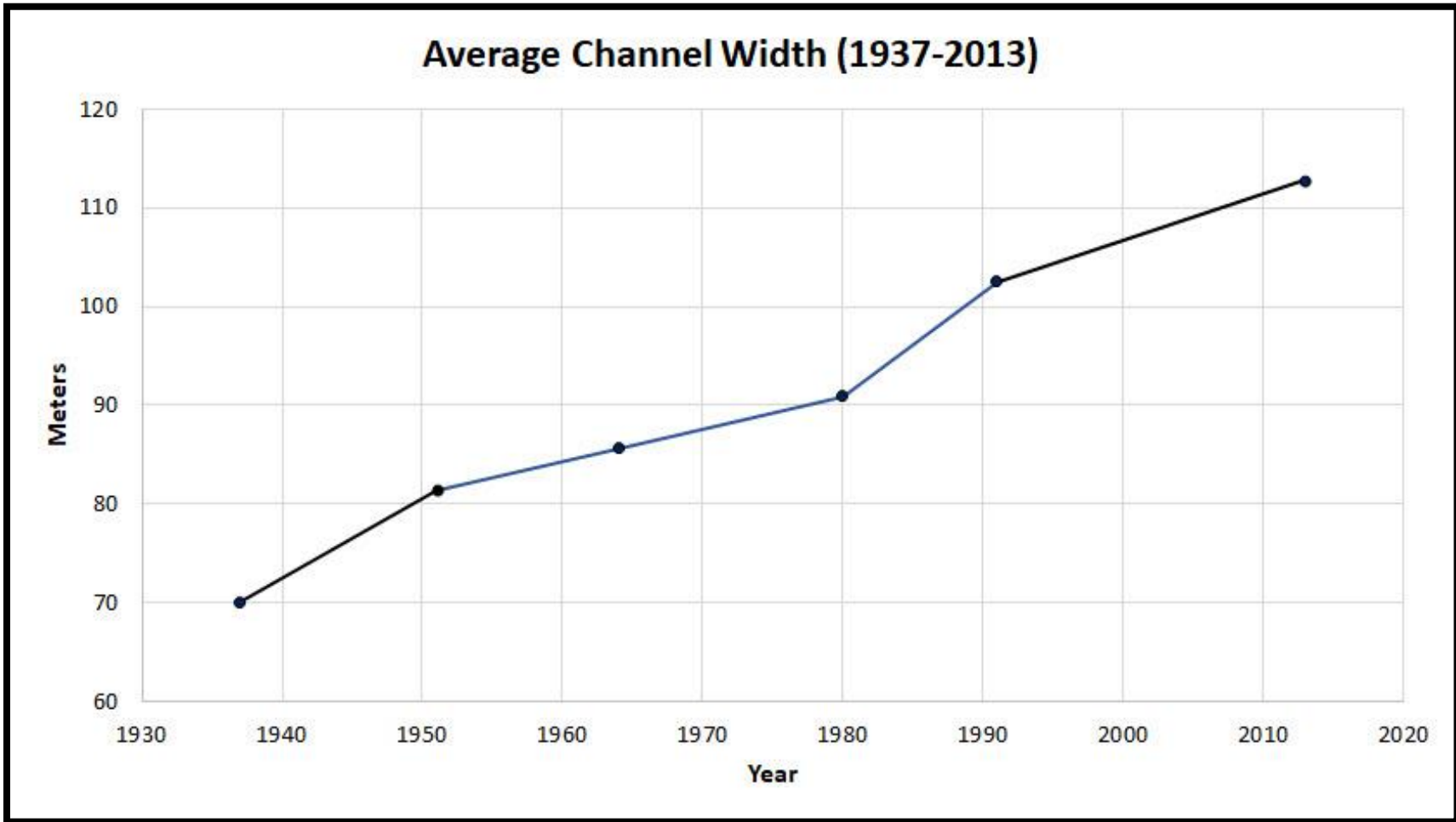


Figure 3.24: Graphical results for channel width change for all years. Throughout the time of record in this study a clear increase is seen.

3.3.2.1 Average Channel Width (ACW)

Reach 2-9 and 11 in 1937 contained all the ACW measurements below the 10th percentile with Reach 6 being the lowest at 53.94 m, while the 2013 period contained all but one (Reach 2 in 1991) of the measurements above the 90th percentile with Reach 2 being the highest at 139.05 m (Table 3.3, Figure 3.25). Reach 2 also had the highest overall ACW of any of the reaches at 100.19 m, and Reach 6 had the lowest overall ACW at 77.21 m (Table 3.3, Figure 3.25). An incremental increase in ACW of ~ 5-10 m was seen in each successive interval from 1937-2013. Reach analysis further demonstrated both the temporal increase in ACW, but also a spatial/temporal shift from channel width being greater in the downstream reaches to channel width being greater in the upstream reaches (Table 3.3, Figure 3.25).

Table 3.3: Average Channel Width by Reach and Interval

Average Channel Width by Reach and Interval (m/yr)							
Reach	1937	1951	1964	1980	1991	2013	Average
1	72.66	79.91	98.87	99.87	114.90	118.74	97.49
2	65.48	87.20	94.63	99.17	115.58	139.05	100.19
3	62.03	81.92	86.92	95.17	109.72	117.67	92.24
4	65.32	77.21	79.05	85.26	92.41	103.68	83.82
5	58.42	89.17	87.51	80.88	100.98	123.90	90.14
6	53.94	71.01	80.60	74.17	86.84	96.69	77.21
7	60.00	84.20	86.13	88.71	98.82	122.45	90.05
8	66.50	79.83	82.13	90.80	97.98	117.31	89.09
9	62.35	67.10	80.64	84.67	95.48	99.26	81.59
10	69.79	78.45	81.82	88.14	105.90	116.47	90.10
11	65.37	70.87	75.70	76.15	92.39	101.92	80.40
12	76.06	87.86	85.09	91.77	102.20	114.93	92.99
13	73.30	82.69	82.91	92.44	100.63	100.79	88.79
14	76.21	77.18	78.56	80.73	93.55	96.37	83.77
15	82.26	86.37	90.00	104.96	109.72	113.75	97.85
16	86.93	84.51	92.06	99.61	104.94	109.33	96.23
Average	70.05	81.45	85.65	90.89	102.54	112.84	89.50
10th Percentile							
Quartile 1		Quartile 2		Quartile 3		90th Percentile	
66.92		87.36		99.81		114.91	
<66.92		>66.92 & <78.68		>78.68 & <87.36		>87.36 & <99.81	
						>99.81 & <114.91	
						>114.91	

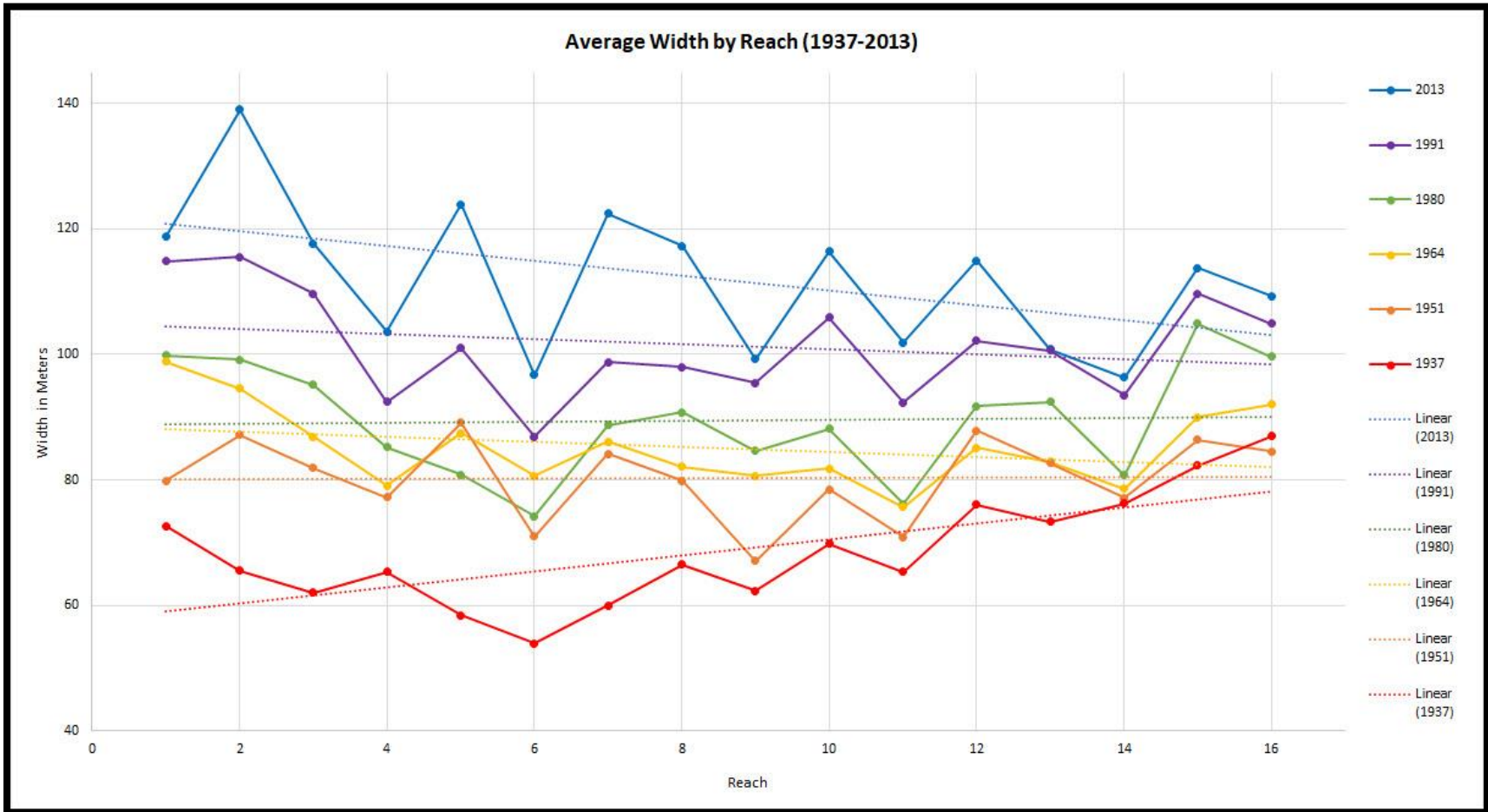


Figure 3.25: Graphical results for average channel width for all years grouped by river reach. Reach 1 begins at the Blue Earth River confluence and Reach 16 ends at the Mississippi River confluence.

3.3.2.2 *Maximum Channel Width (MaxCW)*

The greatest (>90th percentile) MaxCW measurements were relatively evenly distributed temporally (two in 1951, two in 1964, one in 1980, one in 1991, and three in 2013), yet were concentrated within Reaches 2 and 6-8. The highest recorded width measurement was 238.03 m for Reach 2 in 2013 (Table 3.4). The smallest (<10th percentile) MaxCW measurements were concentrated both temporally in the earlier time periods (four in 1937, three in 1951, one in 1964, and one in 1980) and spatially in Reaches 4-6, 9, and 11 (Table 3.4). All six of the MaxCW measurements in Reach 2 were above the median of which five were greater than the 75th percentile and three of those above the 90th percentile (Table 3.4). Whereas, all six of the MaxCW measurements in Reach 9 were below the 25th percentile of which four were in the bottom 10th percentile (Table 3.4).

Table 3.4: Maximum Channel Width by Reach and Interval

Maximum Channel Width by Reach and Interval (m/yr)							
Reach	1937	1951	1964	1980	1991	2013	Average
1	136.85	188.44	134.18	145.63	163.10	169.75	156.32
2	153.42	185.94	164.37	200.09	226.61	238.03	194.75
3	94.56	159.49	152.21	189.83	166.64	183.92	157.78
4	89.36	91.17	93.69	118.76	115.28	132.63	106.82
5	79.09	128.91	109.34	115.15	146.81	149.23	121.42
6	77.37	104.38	213.13	147.32	127.70	146.08	136.00
7	135.29	197.62	224.27	161.43	160.38	201.33	180.05
8	176.83	210.69	144.37	162.41	172.12	207.25	178.94
9	83.38	80.88	89.48	93.62	103.12	109.21	93.28
10	118.98	124.00	115.75	128.04	150.72	157.26	132.46
11	95.54	89.17	95.35	96.23	116.42	144.02	106.12
12	134.55	140.72	112.98	119.34	137.87	169.90	135.89
13	121.62	135.82	131.04	168.94	179.31	190.10	154.47
14	106.59	107.69	106.22	112.46	121.92	133.16	114.67
15	125.52	168.37	146.90	130.19	130.61	137.24	139.80
16	123.82	105.47	117.11	132.76	136.71	156.01	128.65
Average	176.8349	210.6944	224.2744	200.0937	226.6119	238.03	139.84
10th Percentile							
Quartile 1		Quartile 2		Quartile 3		90th Percentile	
93.67		113.52		134.92		162.93	
192.35		162.93		192.35		192.35	
<93.67	>93.67 & <113.52	>113.52 & <134.92	>134.92 & <162.93	>162.93 & <192.35	>192.35		

3.3.2.2 *Minimum Channel Width (MinCW)*

The greatest (>90th percentile) MinCW measurements were concentrated in 1980 (one measurement), 1991 (5), and 2013 (4) and distributed among Reach 1, 5, 9, 12, 15, 16 (Table 3.5). The smallest (<10th percentile) MinCW measurements were concentrated temporally in Reach 1-8 in 1937 and Reach 1 in 1951. The lowest recorded width measurement was 23.66 m for Reach 2 in 1937 (Table 3.5). Although it is no surprise the smallest MinCW measurements are found in 1937 and 1951 and the highest MinCW measurements are found 1980, 1991, and 2013, it is interesting to see an inversion from the from the lowest falling in Reach 1-8 and the highest being concentrated downstream (Reach 9,12, 15,16) (Table 3.5).

Table 3.5: Minimum Channel Width by Reach and Interval

Minimum Channel Width by Reach and Interval (m/yr)							
Reach	1937	1951	1964	1980	1991	2013	Average
1	34.13	30.04	57.71	55.41	61.97	83.44	53.78
2	23.66	45.97	52.74	54.46	63.15	74.05	52.34
3	31.64	47.15	51.94	55.73	56.87	64.84	51.36
4	39.47	62.59	62.12	59.72	60.80	69.48	59.03
5	38.01	60.64	46.77	59.25	77.52	87.17	61.56
6	35.61	53.02	46.92	52.54	58.64	62.64	51.56
7	28.25	44.91	48.05	48.38	58.38	61.72	48.28
8	34.54	47.15	52.97	53.40	60.11	42.80	48.50
9	46.67	53.91	68.30	75.88	85.96	87.65	69.73
10	41.84	47.20	53.42	50.35	62.81	47.45	50.51
11	43.52	42.80	51.90	48.39	69.75	76.08	55.41
12	44.42	63.95	55.38	66.44	77.55	73.29	63.50
13	39.51	49.74	46.18	50.37	58.40	52.18	49.40
14	54.11	52.17	45.10	56.66	63.85	56.41	54.72
15	56.22	58.40	56.99	83.24	86.82	81.97	70.61
16	52.85	46.84	70.97	76.86	86.81	77.27	68.60
	23.66	30.04	45.10	48.38	56.87	42.80	56.81
10th Percentile							
Quartile 1		Quartile 2		Quartile 3		90th Percentile	
39.50		47.15		55.39		63.67	
77.53							
<39.50	>39.50 & <47.15	>47.15 & <55.39		> 55.39 & <63.67		>63.67 & <77.53	
						>77.53	

3.3.3 Sinuosity and Channel Length

An overall decrease in sinuosity and stream length has been seen from 1937 to 2013 (Figure 3.26, Figure 3.27, Table 3.6). From 1937 to 1964 stream length slightly increased (< 2 kilometers) but then decreased drastically from 1964 to 2013 losing ~14 kilometers (9 kilometers from 1991 to 2013; Figure 3.27). However, reach analysis shows that this significant decrease in overall stream length is not occurring in all locations. Reach 5, 10, 11, and 12 are exceptions experiencing an increase in sinuosity from 1937 to 2013, and Reach 1, 4, 9, 13, 14, 15 have remained completely or almost completely static (Figure 3.26, Table 3.6). Therefore, the majority of stream length/sinuosity decrease has been concentrated in Reach 2, 3, 6, 7, 8, and 16 (Figure 3.26, Figure 3.27, Table 3.6)

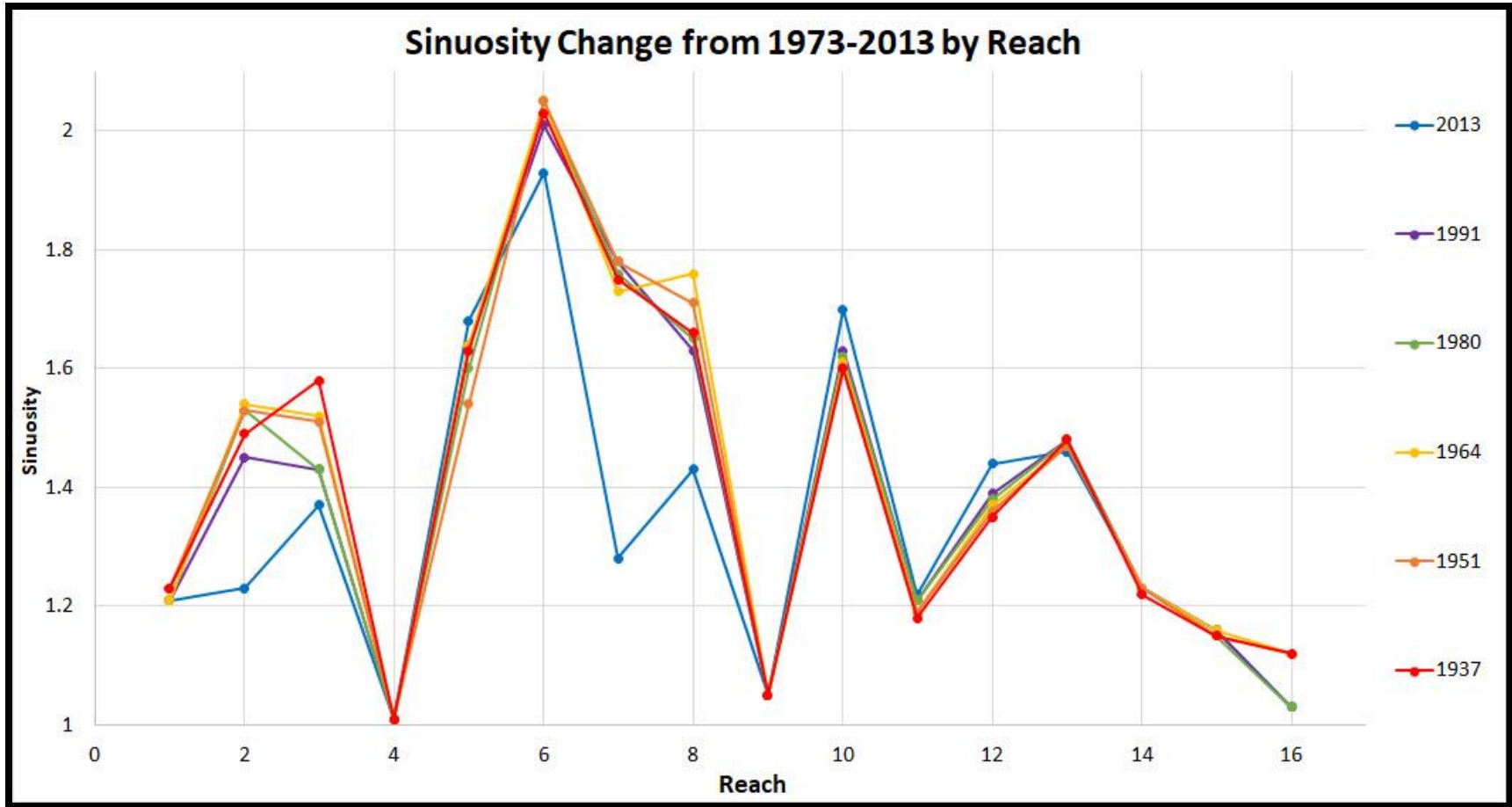


Figure 3.26: Sinuosity by river reach. Reach 1 begins at the Blue Earth River confluence and Reach 16 ends at the Mississippi River confluence.

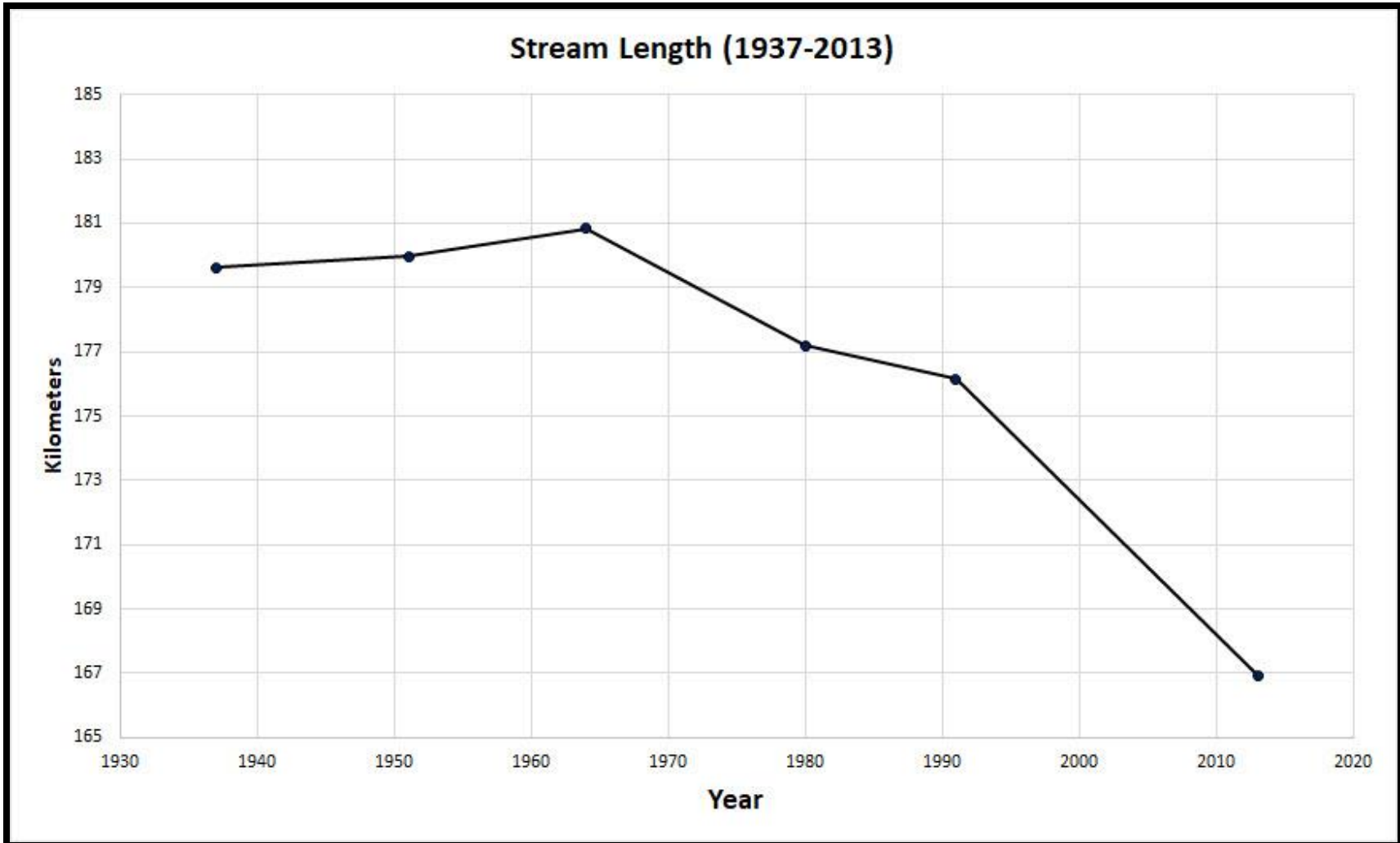


Figure 3.27: Stream length from 1937 to 2013. For the record of time, a significant decline in stream length has been seen.

Table 3.6: Sinuosity by Reach and Interval

Sinuosity by Reach and Interval (m/yr)							
Reach	1937	1951	1964	1980	1991	2013	
1	1.23	1.23	1.21	1.21	1.21	1.21	
2	1.49	1.53	1.54	1.53	1.45	1.23	
3	1.58	1.51	1.52	1.43	1.43	1.37	
4	1.01	1.01	1.01	1.01	1.01	1.01	
5	1.63	1.54	1.64	1.60	1.64	1.68	
6	2.03	2.05	2.05	2.05	2.01	1.93	
7	1.75	1.78	1.73	1.76	1.78	1.28	
8	1.66	1.71	1.76	1.65	1.63	1.43	
9	1.05	1.05	1.05	1.05	1.05	1.05	
10	1.60	1.60	1.61	1.62	1.63	1.70	
11	1.18	1.19	1.19	1.21	1.21	1.22	
12	1.35	1.36	1.37	1.38	1.39	1.44	
13	1.48	1.47	1.47	1.48	1.48	1.46	
14	1.22	1.23	1.23	1.23	1.23	1.23	
15	1.15	1.15	1.16	1.15	1.16	1.16	
16	1.12	1.12	1.12	1.03	1.03	1.03	
10th Percentile							
1.04		Quartile 1 1.16		Quartile 2 1.38		Quartile 3 1.61	
1.04		1.16		1.38		1.61	
≤1.05	>1.04 & <1.16	>1.16 & <1.38	>1.38 & <1.61	>1.61 & <1.76	>1.76		

3.3.4 Pinch Points and the Consideration of Invasive Carp Barriers

3.4.2.1 Mankato

Mankato's floodwall and riprap-controlled river stretch (Figure 3.28) has been a location of interest since it has large area of river that has been heavily engineered. The results show that since the Mankato flood walls were installed in the mid-1960's a significant decrease (~ 3 m/y) in channel migration occurred (Figure 3.29), which is uncharacteristic to other less controlled river reaches which show static or increases in migration (Figure 3.15). However, width did not immediately stabilize in this reach (Figure 3.30) and continued to rise in a manner characteristic with other river reaches (Figure 3.25), but recently (1991-2013) has seen its first, although minor, decrease in channel width.

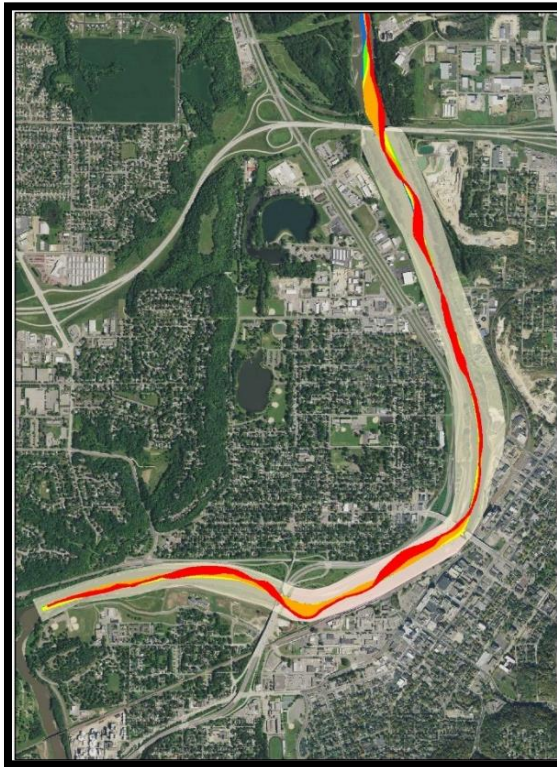


Figure 3.28: Mankato's floodwall and riprap-controlled river stretch.

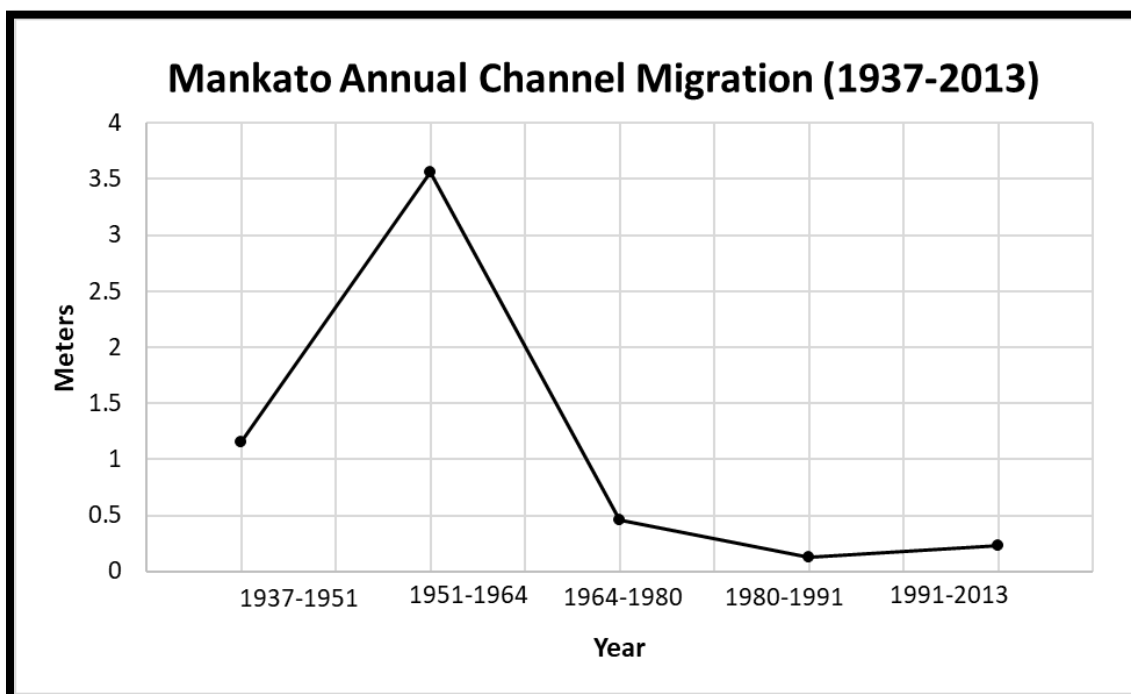


Figure 3.29: Average annual channel migration in Mankato's floodwall and riprap controlled river stretch.

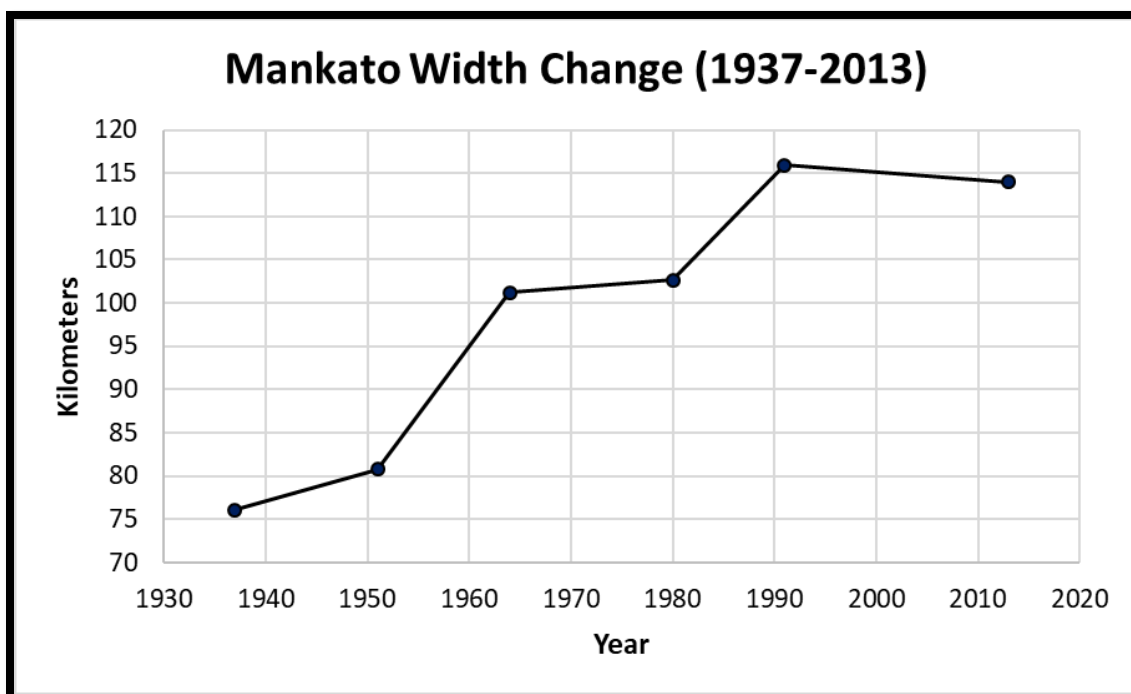


Figure 3.30: Width change in Mankato's floodwall and riprap controlled river stretch.

3.4.2.2 Highway 14 Bridge (Mankato)

The highway 14 bridge (Figure 3.31) was built in 1976 which offered a location to see pre and post bridge planform characteristics. Channel migration was consistently greater downstream than upstream except for 1991-2013. It should be noted that the upstream did not change much compared to the prior interval (1980-1991), but rather the downstream became less active. Width flipped from downstream being greater to upstream being greater post-bridge occupation. The width on both sides of the bridge nearly tripled in size over the period of record (Table 3.7).

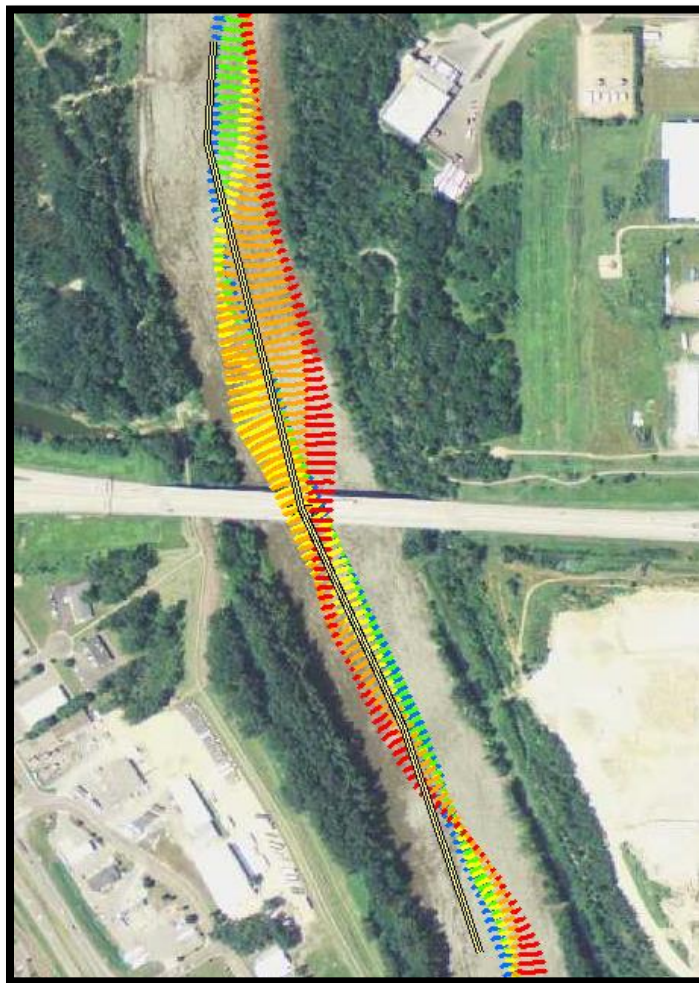


Figure 3.31: Highway 14 bridge on the edge of Mankato/North Mankato, MN.

Table 3.7: Highway 14 bridge upstream vs downstream migration and width change. The red box shows the years after the bridge was built. 1991-2013 was the only time upstream migration was greater than downstream. Width was traditionally greater downstream, but reversed after the bridge was built.

		Migration (meters)						
		1937-1951	1951-1964	1964-1980	1980-1991	1991-2013	Average	
Upstream		0.71	0.91	0.94	0.60	0.61	0.75	
Downstream		0.90	3.42	1.23	1.13	0.22	1.38	
		Width						
		1937	1951	1964	1980	1991	2013	Average
Upstream		56.25	77.52	91.89	105.03	132.3	141.91	100.82
Downstream		60.99	78.73	96.99	92.99	126.14	154.43	101.71

3.4.2.3 Highway 22 Bridge (St. Peter)

The Highway 22 Bridge in St. Peter (Figure 3.32) is ~ 20 km downstream from the Highway 14 Bridge. This river crossing existed over the record of time considered in this study. The upstream portion migration has been on average five times greater than that of downstream measurements (Table 3.8). Interestingly, this pinch point also experienced a switch in width change being greater in the downstream to the upstream following 1964, like the Highway 14 Bridge. Therefore, this measurement indicates that Highway 14's switch in width change post-bridge construction may only be a correlation and not a cause of the structure's presence since this same switch was experienced from a bridge established over the entire time scale.

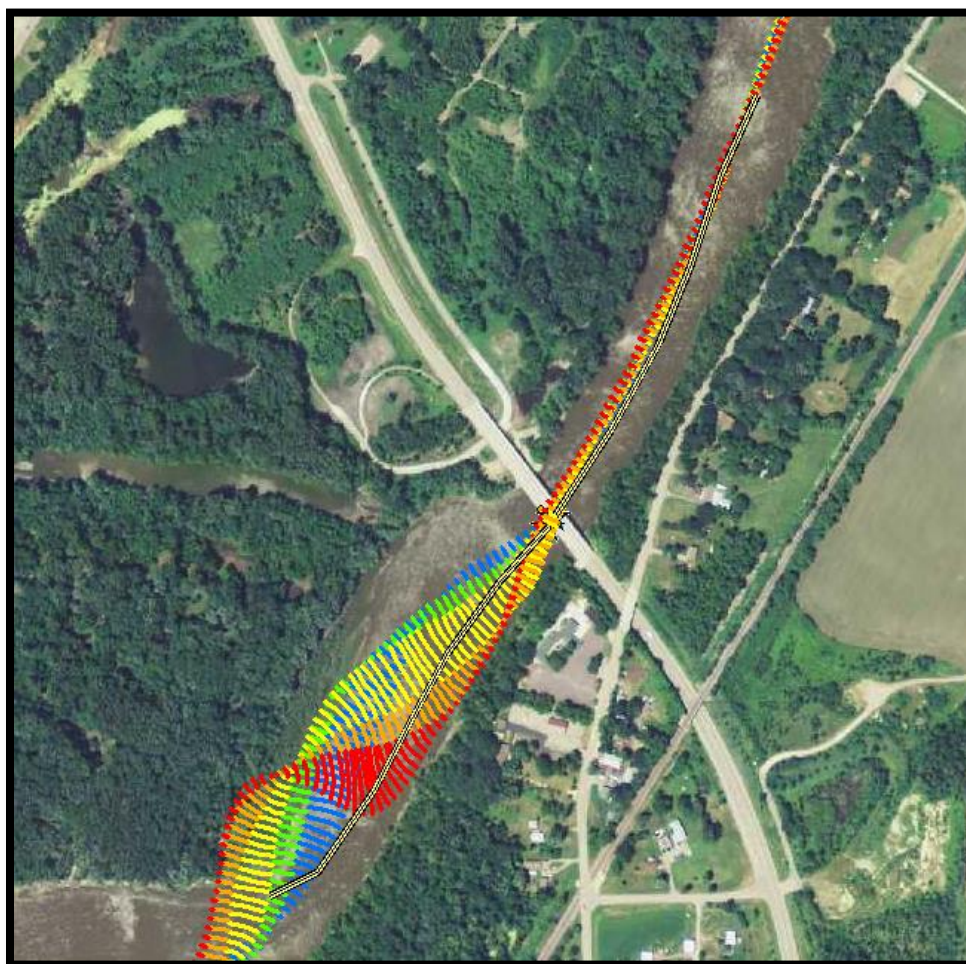


Figure 3.32: Highway 22 bridge on the edge of St. Peter, MN.

Table 3.8: Highway 22 bridge upstream vs downstream migration and width change. The red line in the migration measurements indicated the distinct break in a highly active upstream and inactive downstream. Width measurements switched from being greater downstream to upstream after the 1964 measurement.

	Migration (meters)					Average	
	1937-1951	1951-1964	1964-1980	1980-1991	1991-2013		
Upstream	1.40	1.32	2.24	1.27	1.25	1.50	
Downstream	0.44	0.31	0.46	0.24	0.08	0.31	
	Width						
	1937	1951	1964	1980	1991	2013	Average
Upstream	40.91	84.36	85.43	107.31	122.23	119.60	93.31
Downstream	80.38	99.88	91.02	92.52	103.53	97.00	94.06

3.4.2.4 Highway 169 Bridge (Le Sueur)

The Highway 169 Bridge (Figure 3.33) near the city of Le Sueur, MN, has been fairly active in terms of migration with the most recent interval of time (1991-2013) being the least active both upstream and downstream of the bridge (Table 3.9). Width change has shown unsteady trends in terms of upstream vs. downstream but overall has experienced an increase in channel width with the upstream increasing from 52.48 meters to 105.01 meters and the downstream increasing from 45.86 meters to 125.88 meters (Table 3.9). However, 1964 had the greatest width of record with the upstream averaging 151.72 meters and the downstream averaging 163.75 meters (Table 3.9).

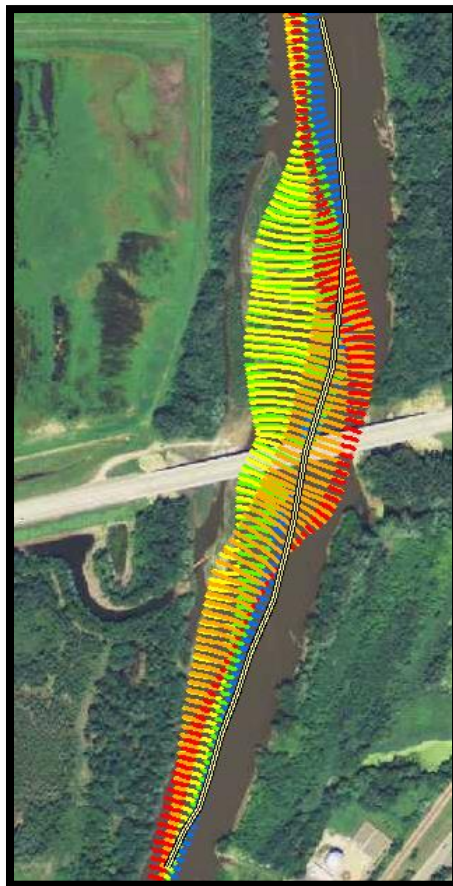


Figure 3.33: Highway 169 bridge on the edge of Le Sueur, MN.

Table 3.9: Highway 169 bridge upstream vs downstream migration and width change.

	Migration (meters)					Average	
	1937-1951	1951-1964	1964-1980	1980-1991	1991-2013		
Upstream	0.68	3.16	1.65	1.36	0.40	1.45	
Downstream	1.48	2.98	2.51	5.85	0.66	2.70	
			Width				
	1937	1951	1964	1980	1991	2013	Average
Upstream	52.48	85.38	151.72	94.96	88.54	105.01	96.35
Downstream	45.86	83.28	163.75	95.52	81.80	125.88	99.35

3.4.2.5 Dan Patch Line Bridge (Savage)

The Dan Patch Line Bridge (Figure 3.34) offers a look at a pinch point where the Minnesota River is actively managed to maintain barge traffic (USACE 2007; Groten, Ellison, and Hendrickson 2016). This stretch has experienced relatively stable channel migration conditions with overall temporal decrease, and the most recent interval (1991-2013) marking the lowest migration rates both upstream and downstream of the bridge (Table 3.10). The width has been consistently greater in the downstream side of the bridge by ~5-17 meters. It should be noted that the downstream measurements are located on a meander bend (Figure 3.34) which likely introduce channel geometry effects on bank shear stress as well. The width has increased temporally with the upstream increasing by ~30 meters and the downstream by just under 40 meters (Table 3.10)

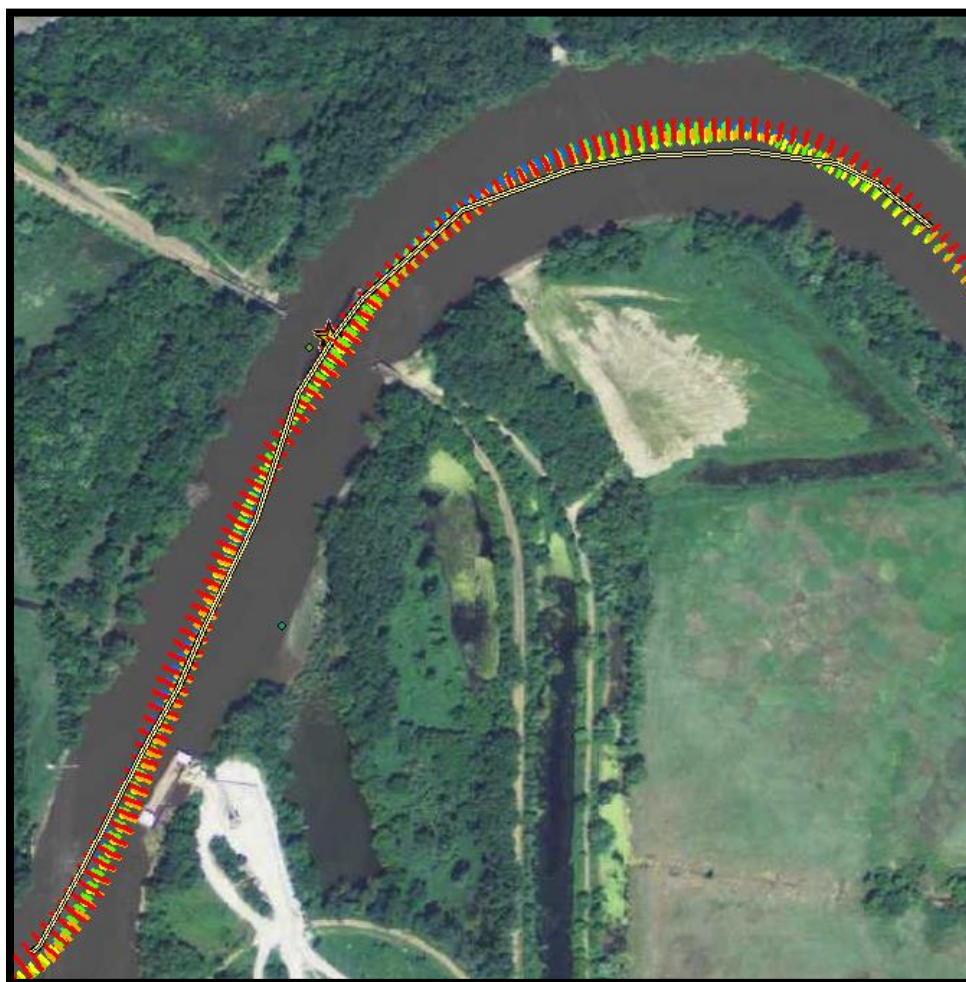


Figure 3.34: Dan Patch Line Bridge in Savage, MN.

Table 3.10: Dan Patch Line Bridge upstream vs downstream migration and width change.

	Migration (meters)					Average	
	1937-1951	1951-1964	1964-1980	1980-1991	1991-2013		
Upstream	1.47	0.79	0.24	0.60	0.20	0.66	
Downstream	0.92	0.53	0.48	0.95	0.19	0.61	
	Width					Average	
	1937	1951	1964	1980	1991		2013
Upstream	69.39	72.85	72.01	93.16	101.92	100.29	84.94
Downstream	79.45	77.81	83.61	106.24	112.72	117.23	96.18

3.4 Discussion

3.4.1 Methodological Considerations

3.4.1.1 Trajectory Method vs Polygon Method

To accomplish the objectives of this research, a complete assessment of the appropriate methodologies in published literature was conducted. In that assessment a comparison between the two most commonly used methods, the Trajectory Method and the Polygon Method, was made. Consistency in quantifying channel change is important so comparative analysis among various studies can be easily made. If a uniform approach is adopted, the science of understanding planform channel adjustments will drastically improve since direct river to river comparisons can be made.

In the Polygon Method (Urban and Rhoads 2003; Giardino and Lee 2011), a series of polygons are created by two intersecting centerlines from different years. The area of each polygon is then divided by the length of the earlier year centerline to get a migration rate (Figure 3.35). The quotient is then divided by the number of years between the two centerlines to get an annual migration rate. The equation is as follows:

Equation 3.4

$$Rm = \frac{A}{L}/y$$

Where Rm is the migration rate, A is the area of the polygon, L is the length of the centerline length of the earlier years bordering the polygon, and y is the number of years between the channel centerlines used in the interval.

To test the Polygon Method, a model was built to automate this process in ArcMap (Figure 3.36). Figure 3.37 shows an example output of this methodology, and

Figure 3.38 is the output from the methodology discussed in section 3.2 from the NCED Planform Statistics toolbox (the method that was ultimately used in this study).

Graphically, the two outputs look similar. However, upon closer analysis the polygon method underestimates the migration rates and drastically generalizes them. In this comparison, the polygon method created ~400 measurements while a 10 m interval was used with the Trajectory Method (NCED Planform) which produced ~17,500 measurements in Figure 3.38. The Polygon Method simply does not have enough measurements for the resolution required to do planform channel change analysis, especially on smaller reaches or pinch points like those done within this study (Figure 3.39). For these reasons, the polygon method is discouraged as a method of measuring channel migration. However, the framework for creating polygons (Figure 3.36) could be used and extended into studies focused sediment budgets and on quantifying erosion.

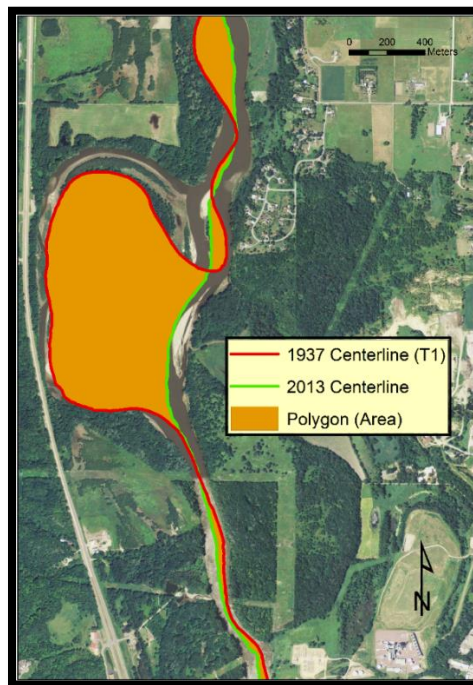


Figure 3.35: The required inputs to calculate migration using the Polygon Method

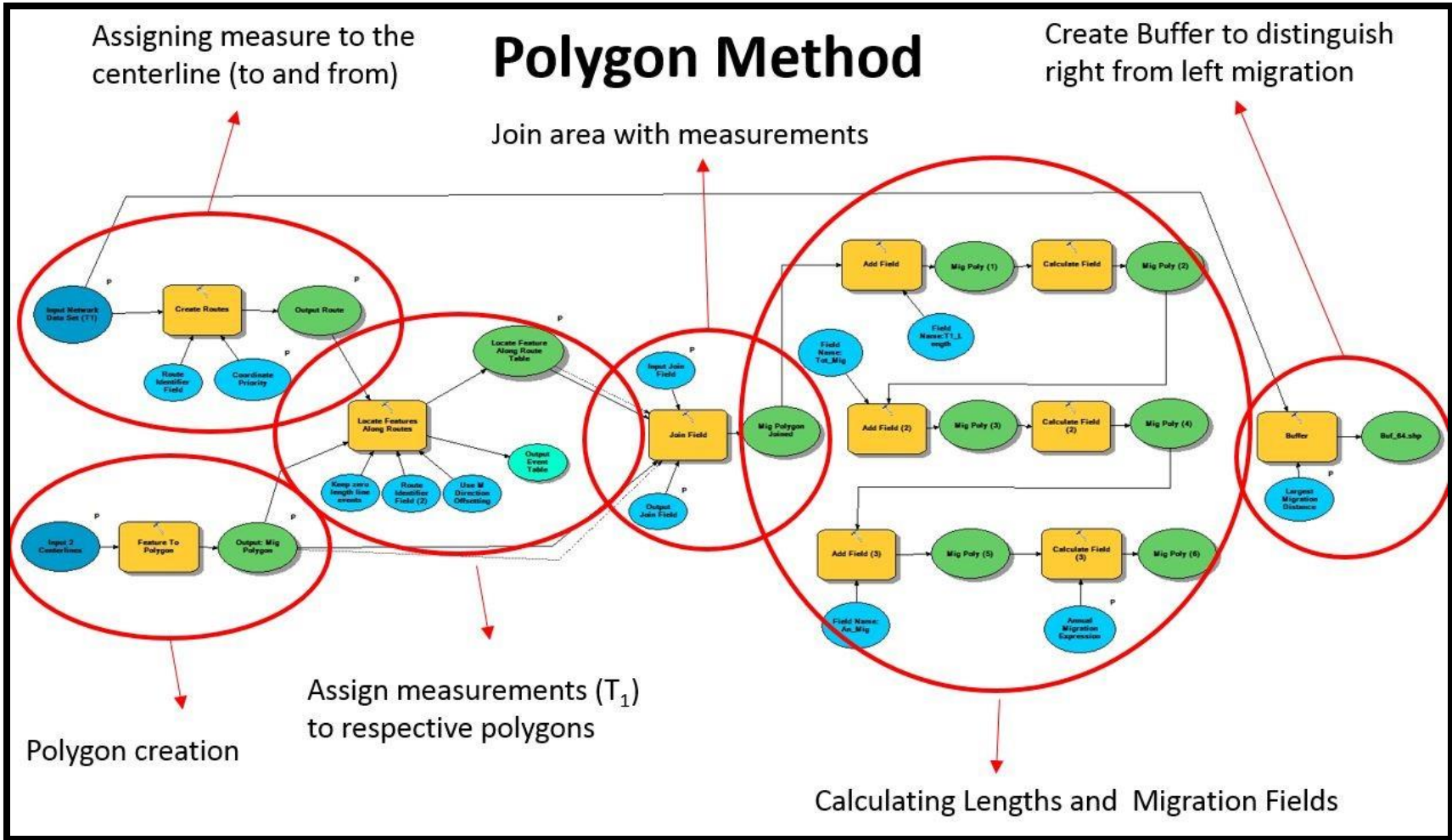


Figure 3.36: Polygon Method model

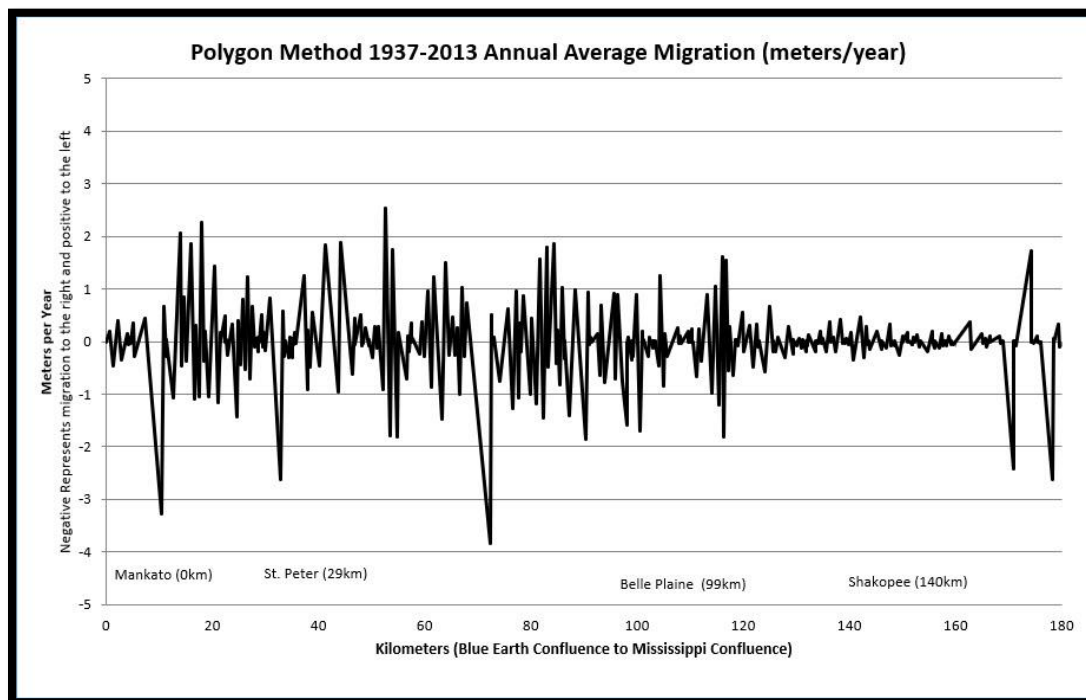


Figure 3.37: Output data from the Polygon Method

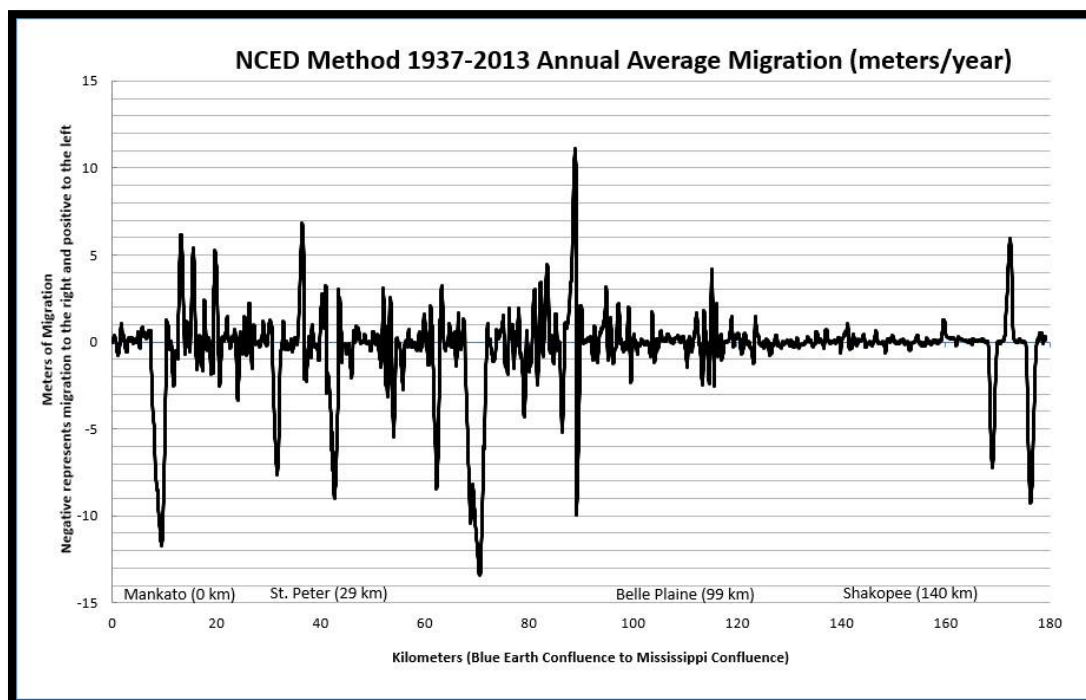


Figure 3.38: Output data from the NCED Planform Statistics Tools

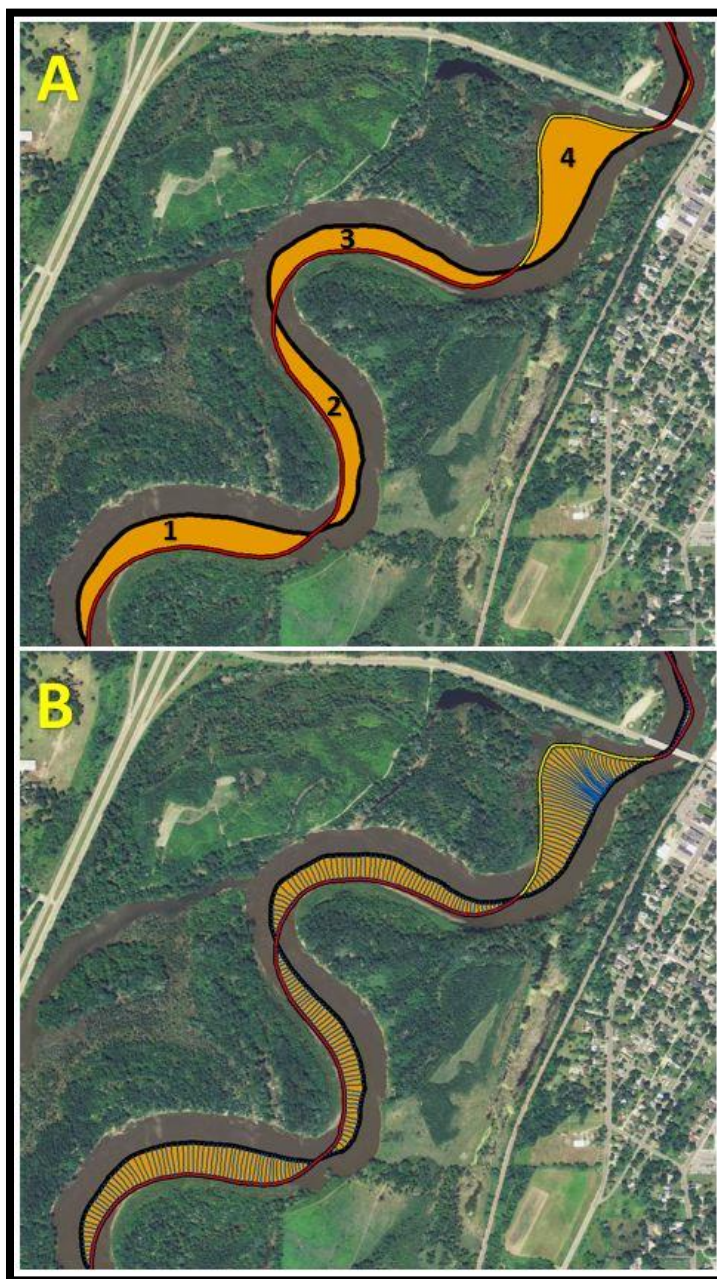


Figure 3.39: A) This figure displays the inputs needed in order to calculate channel migration using the polygon method. For each orange polygon (1-4), the red centerline (T1) length is used to divide the area of the polygon. Polygon has this measurement highlighted in yellow. This number is then divided by the number of years between the centerlines. In the example above, twenty-two would be used since the two input centerlines are 1991 (Red) and 2013 (Black). B) This shows an example of the trajectory lines (Blue lines) created using the planform statistics toolbox. The user defined intervals selected was ten meters therefore a new trajectory line or measurement is generated laterally between the centerlines for every 10 meters in the downstream distance.

3.4.1.2 Error Metrics

Lea and Legleiter's (2016) MATLAB scripts produce three error metrics: SVE, RMSE, and 90th Percentile. One of the ArcGIS tools created in this research (Figure 3.7 and Figure 3.8), specifically created separate excel and shapefile outputs (Figure 3.9) so a user can see study specific results for each metric. The outputs from this research were plotted spatially (Figure 3.40) and graphically (Figure 3.41) to compare differences. After comparison it is evident that the 90th percentile error metric considers measurements as statistically insignificant which are in fact real-world migration. On the other hand, RMSE likely considers too many measurements as statistically significant, since the overall RMSE measurements were so low in this study. As shown in Chapter 2, independent GCPs showed a much higher variability in error than RMSE shows. Therefore, RMSE is applying a generalized error value to an incredibly broad study area which contains localized areas that far exceed RMSE. SVE's ability to account for the spatial variability of the error makes it the most preferred error metric of the three.

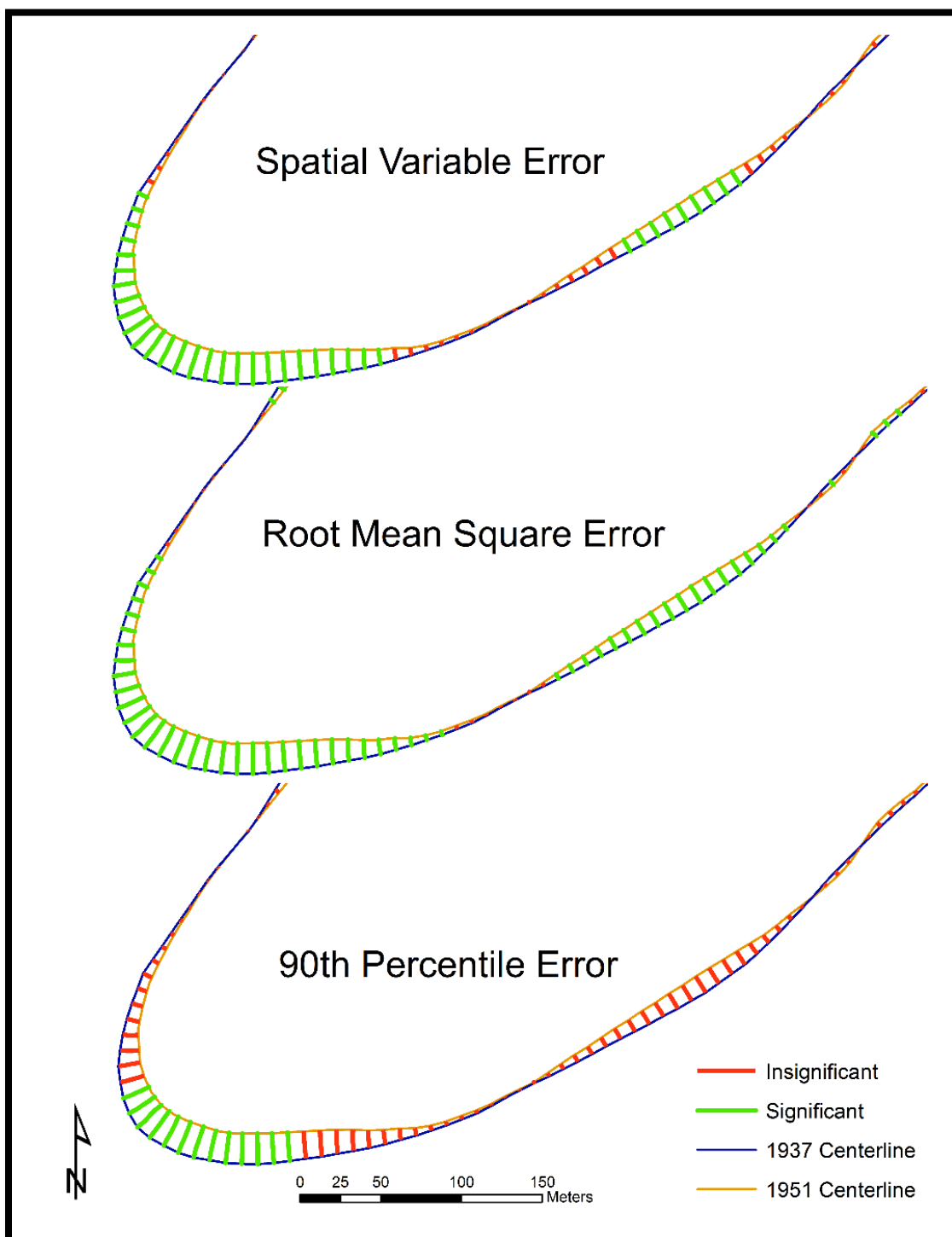


Figure 3.40: Spatial comparison of differing error metrics significant vs insignificant measurements.

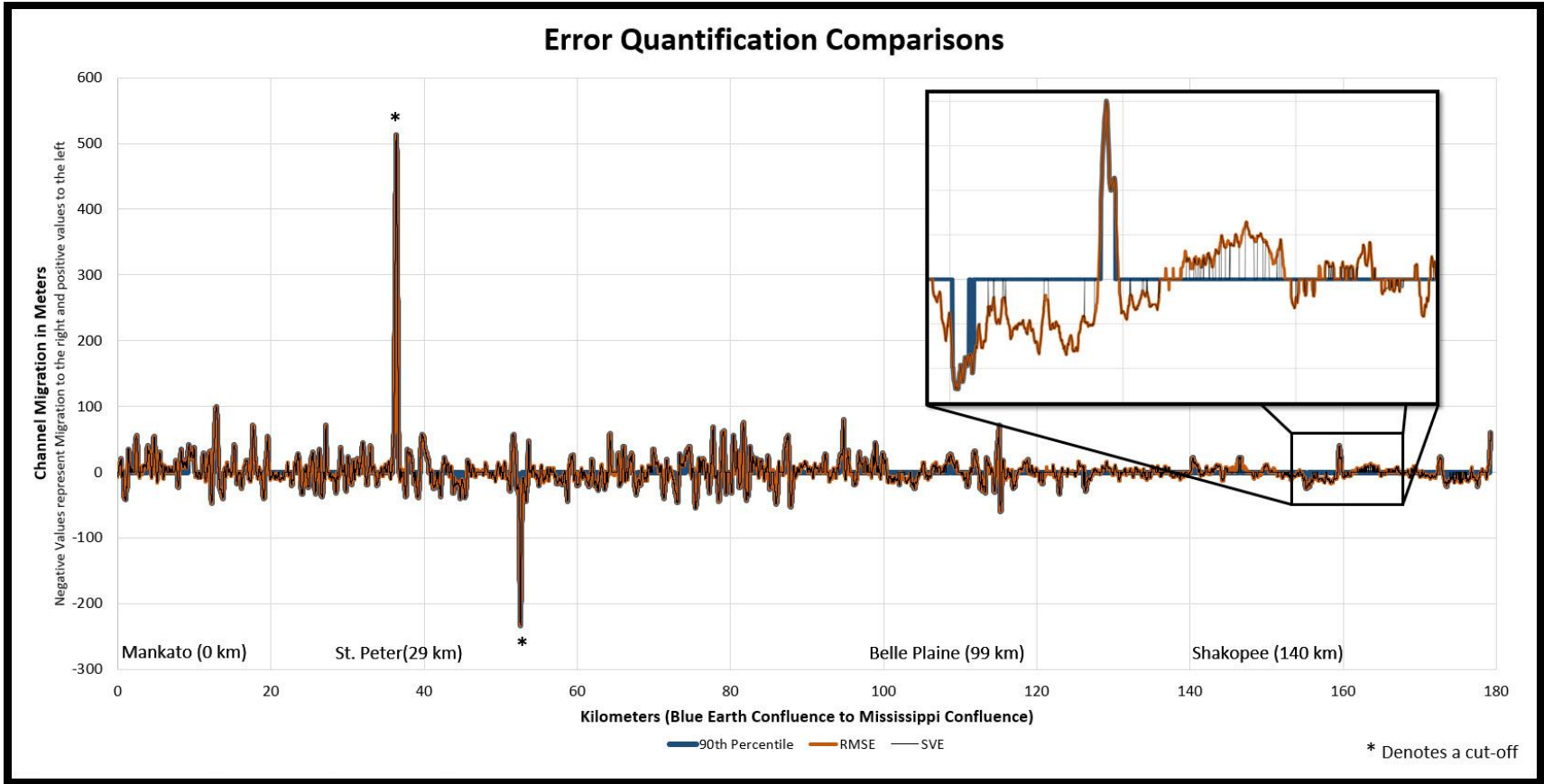


Figure 3.41: Graphical comparison of differing error metrics significant vs insignificant measurements.

3.4.1.3 Problems Overcome

The following two sections outline a few methodological problems that were overcome throughout the analysis of the research. First, an error issue running the MATLAB script “ChannelChangeSignif” will be discussed followed the considerations for handling errored trajectory lines output from the NCED Planform Statistics toolbox.

3.4.1.3.1 MATLAB “ChannelChangeSignif”

When running the “ChannelChangeSignif” script the scattered interpolant function raised the following exception – “The number of data point locations should equal the number of data point values.” This was corrected by going back to the “ErrorQuantification” MATLAB script and tracing the root of the problem back to the original GCP text file. The issue originated from an extra blank entry at the end of the shapefiles from which they were derived creating an extra or “unequal” amount of lines in the GCP text file. Once these blank lines were deleted the data point location and data point values were equal in the matrices created in MATLAB which corrected this problem.

3.4.1.3.2 Errored Trajectory File Lines

The issues with errored trajectory lines (discussed in section 3.2.1.1) which are used for measuring lateral migration (Figure 3.2) caused several issues throughout this research. At first, a method of using the clip function within ArcMap was formulated to automate cleaning up errored lines by using the centerlines as a bound since all migration should be contained within the two centerlines for each interval. This seemed to work well at first, however; it was unsuccessful because it would leave an extra vertex

associated with the line. This gave the clipped lines three endpoints opposed to two which caused issues when trying to extract the XY coordinates to use in the MATLAB “ChannelChangeSignf” script. Instead of the two sets of coordinates a third XY set was added for the extra vertex. For this reason, this methodology was abandoned, and all the trajectory lines were manually checked and edited.

In some cases (especially on cutoffs), hundreds of trajectory lines would be incorrect. In this case it was easiest to delete these lines all together and digitize new lines for the trajectory measurements. This, however, created a new set of problems for the “Post MATLAB Processing” script that was written for this research. Part of this scripts job was too recalculate the trajectory lines measurements and then assign new downstream distances to each line measurement since they were manually edited and had no attributes associated with them. When the new shapefiles came out of the script, it was obvious the downstream distances were far from accurate, so the script was run a single line at a time until the error was identified. When the following lines of code were run the problem became evident.

```
# Feature To Point - This take the center of ever line in the trajectory file and creates a point
```

```
arcpy.FeatureToPoint_management(TrjLF, F2Point, "CENTROID")
```

```
# Points To Line - This takes the points generated in the last tool and creates a line from them
```

```
arcpy.PointsToLine_management(F2Point, P2Line, "", "", "NO_CLOSE")
```

```
# Create Routes - This takes the line created in the last tool and converts it to a route in order to give it measure
```

```
arcpy.CreateRoutes_lr(P2Line, "Id", Route, "LENGTH", "", "", CoordPriority, "1", "0", "NO_IGNORE", "INDEX")
```

```

# Locate Features Along Routes - This takes the points that were created and assigns
them downstream measure which will inturn give the
# trajectory lines measure in the next step
arcpy.LocateFeaturesAlongRoutes_lr(F2Point, Route, "Id", "1 Meters", LFAR, OETP,
"FIRST", "NO_DISTANCE", "ZERO", "FIELDS", "M_DIRECTON")
# Join Field - This steps permanently joins the downstream measurements from the point
file to the corresponding trajectory line
arcpy.JoinField_management(TrjLF, PKey, LFAR, "ORIG_FID", "MEAS")

```

The output line in the “Point to Line” function was created so measurements for downstream distances could be calculated. However, this line skipped around according to the trajectory lines object ids from which the line was derived in the prior function, “Feature to Point” (Figure 3.42). The trajectory lines object ids were not in order since many were manually created in the editing process to fix errored trajectory lines originally output from the NCED “Lateral Migration” tool. To overcome this problem the script was edited to the following.

```

# Intersect Analysis - This creates points at the intersection of the TRJ polyline file and
the T1 centerline
arcpy.Intersect_analysis([T1, TrjLF], IntPoint, "ALL", "0.1 Meters", "POINT")

```

```

# Create Routes - This takes the line created in the last tool and converts it to a route in
order to give it measure
arcpy.CreateRoutes_lr(T1, "Id", Route, "LENGTH", "", "", CoordPriority, "1", "0",
"NO_IGNORE", "INDEX")

```

```

# Locate Features Along Routes - This takes the points that were created and assigns
them downstream measure which will inturn give the
# trajectory lines measure in the next step
arcpy.LocateFeaturesAlongRoutes_lr(IntPoint, Route, "Id", "1 Meters", LFAR, OETP,
"FIRST", "NO_DISTANCE", "ZERO", "FIELDS", "M_DIRECTON")

```

```

# Wildcard is needed in order to automate selection of the foreign key since it inserts the
shapefiles name and could vary among users
fid_year = arcpy.ListFields(LFAR, "FID_*_1")[0].name

```

Join Field - This steps permanently joins the downstream measurements from the point file to the corresponding trajectory line
 arcpy.JoinField_management(TrjLF, PKey, LFAR, fid_year, "MEAS")

This required the extra user inputs of a centerline from the earlier time in the interval considered and the “coordinate priority” so it the script could know the proper direction for accumulating distance. By doing this, the tool can be used on any river no matter which direction it flows.

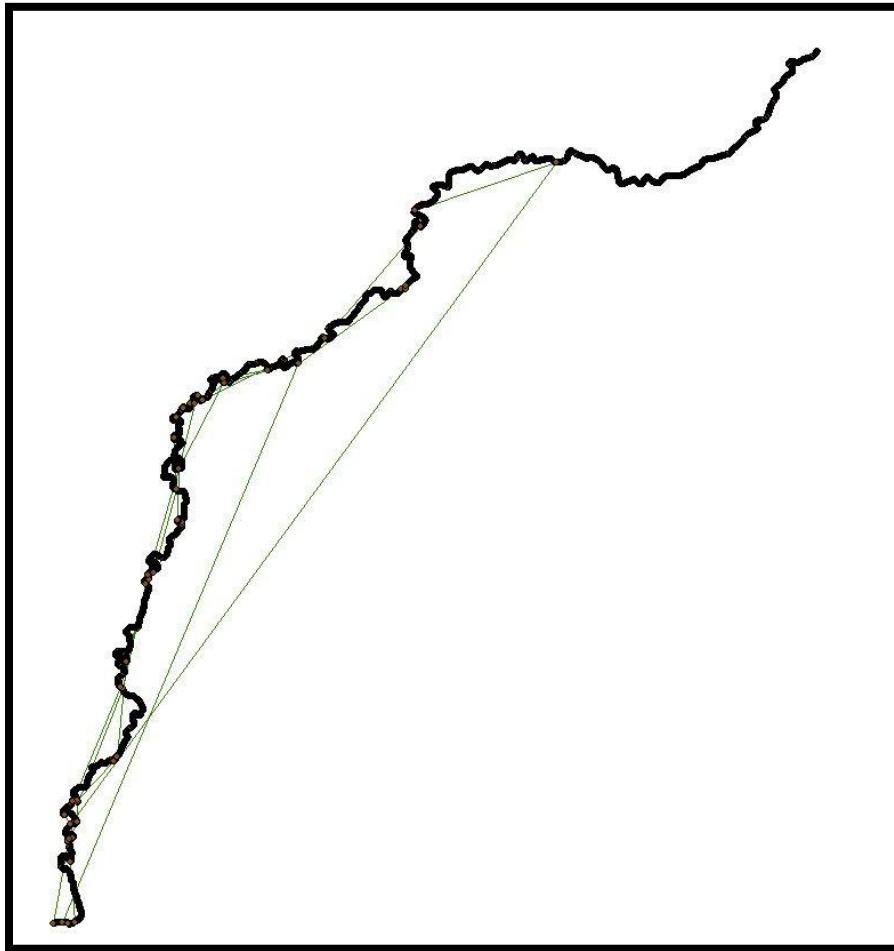


Figure 3.42: This shows the line created by the script from which downstream distances were being calculated. It was not immediately evident that this was the problem since this file was an intermediary file that was created and then deleted before the script terminated. The line was created according to the object id field for the points which caused a problem since many new lines were added to the original file to correct errored trajectory lines.

3.4.2 Planform Channel Change

As expected, the changing hydrologic and sediment regimes in the MRB has created changing planform characteristics on the Minnesota River (Lenhart et al. 2013; Lauer et al. 2017). The two most notable trends include an overall increase in channel width and decreased channel length/sinuosity. Channel migration has shown change, but not as pervasively as the other two planform characteristics. Since this study was conducted on a large stretch of river it was essential to break the data into reaches to see if the generalized trends for the entire study reach were uniform throughout, or if localized temporal and spatial differences could be observed (Figure 3.43 and Figure 3.44). Although the attention in this section will be on general spatial and temporal trends and the most and least dynamic reaches of the river, Appendix K contains an aerial view and graphs for annual channel migration, channel width, sinuosity for every reach investigated in this study.

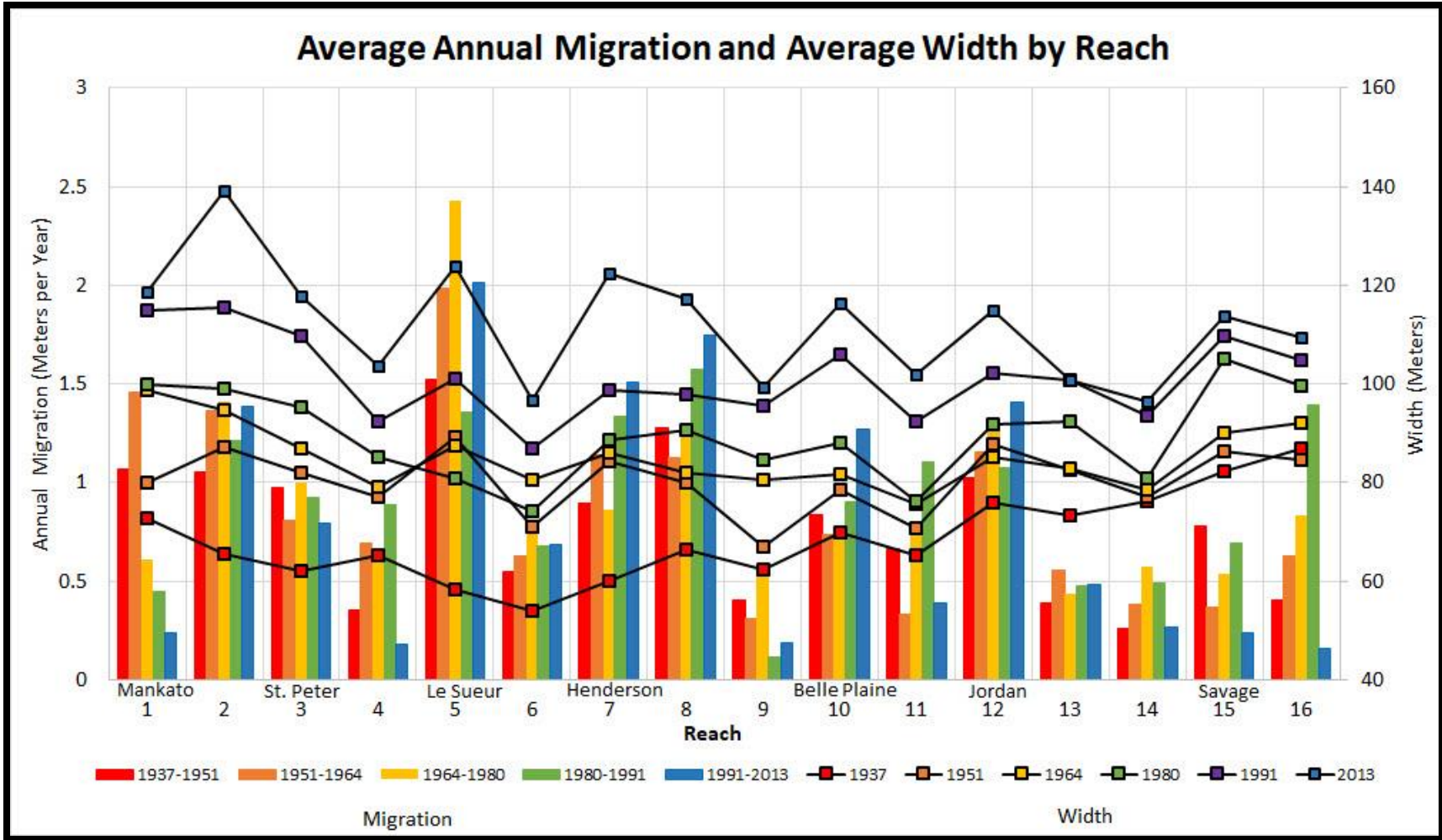


Figure 3.43: Annual migration and width of the lower Minnesota River channel through the delineated Reaches (Figure 3.12).

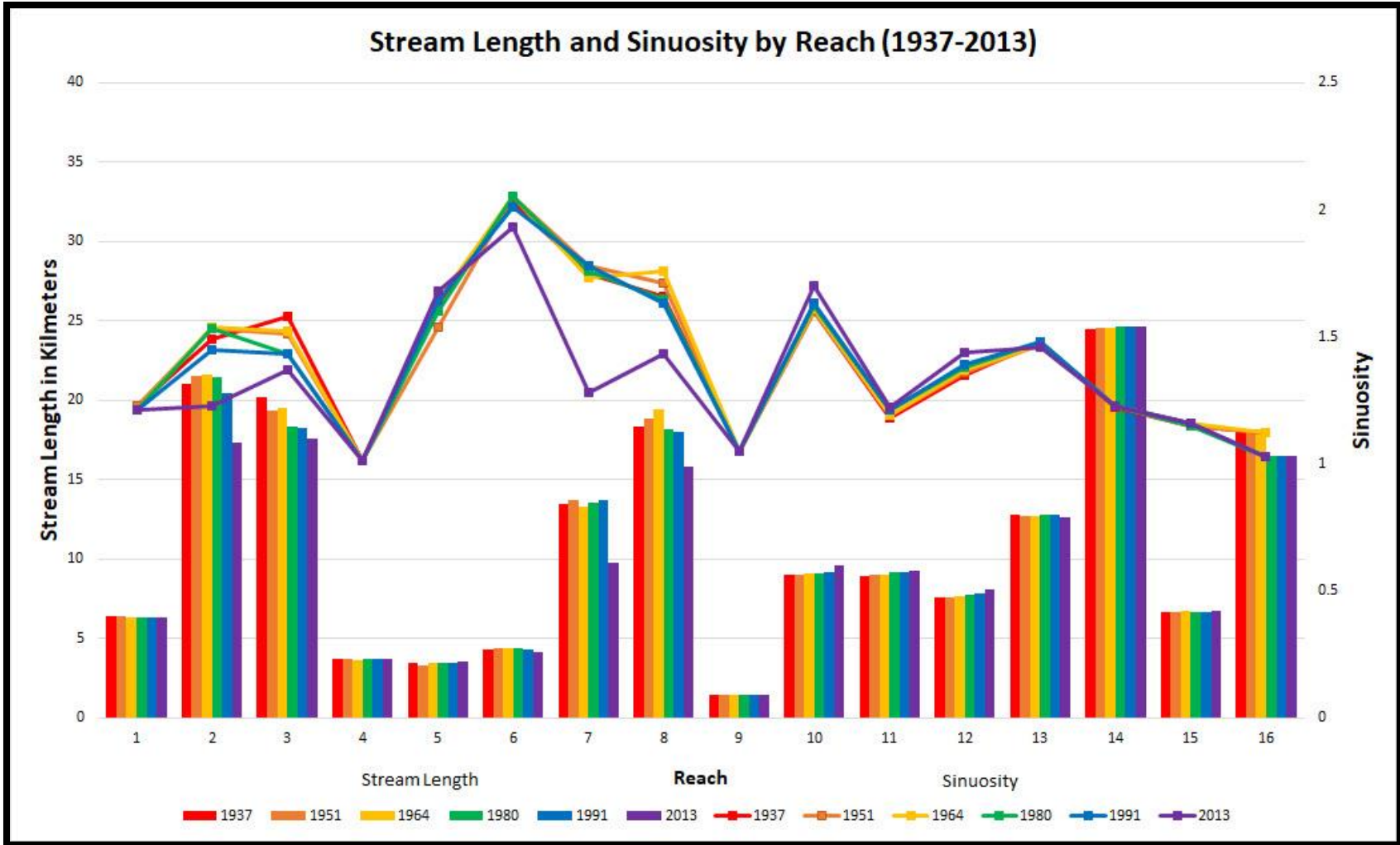


Figure 3.44: Stream length and sinuosity of lower Minnesota River Reaches

3.4.2.1 Channel Migration

Spatially, the Minnesota River has exhibited greater channel migration in the upstream reaches (1-12; Figure 3.12) over ~115 km between Mankato and Jordan with a marked decrease just downstream Jordan (Figure 3.14, Figure 3.15, Table 3.1, Table 3.2, Appendix I). This spatial trend is likely seen for several reasons. Groten et al. (2016), found that the stretch of Minnesota River from Mankato to Jordan is a major sediment contributor with the USGS gauging data in Jordan displaying a sediment yield that is two and half times greater than that of Mankato. However, the stretch of the Minnesota River from Jordan to Fort Snelling reveals sediment yields significantly lower than those reaches just upstream. This suggests that the reach from Jordan to Fort Snelling is a sediment sink. In addition, and as to be expected, they also found that median bedload size decreases downstream from Mankato as well.

The downstream changes are interpreted because of a flattening stream gradient. Although the stretch of Minnesota River from Mankato to the confluence has a gentle gradient, slope significantly decreases in the most downstream reaches of the river (Figure 3.45). Notably, Mankato to Jordan has a slope of 0.0002 or 0.16 m/km (10 in/mi) and Jordan to Fort Snelling (near the Mississippi confluence) has a slope of 0.00006 or 0.06 m/km (3.8 in/mi) (Ellison 2015). This change in slope marks a change stream power on the Minnesota River which is why we see less channel migration in the downstream reaches as well as a sediment sink.

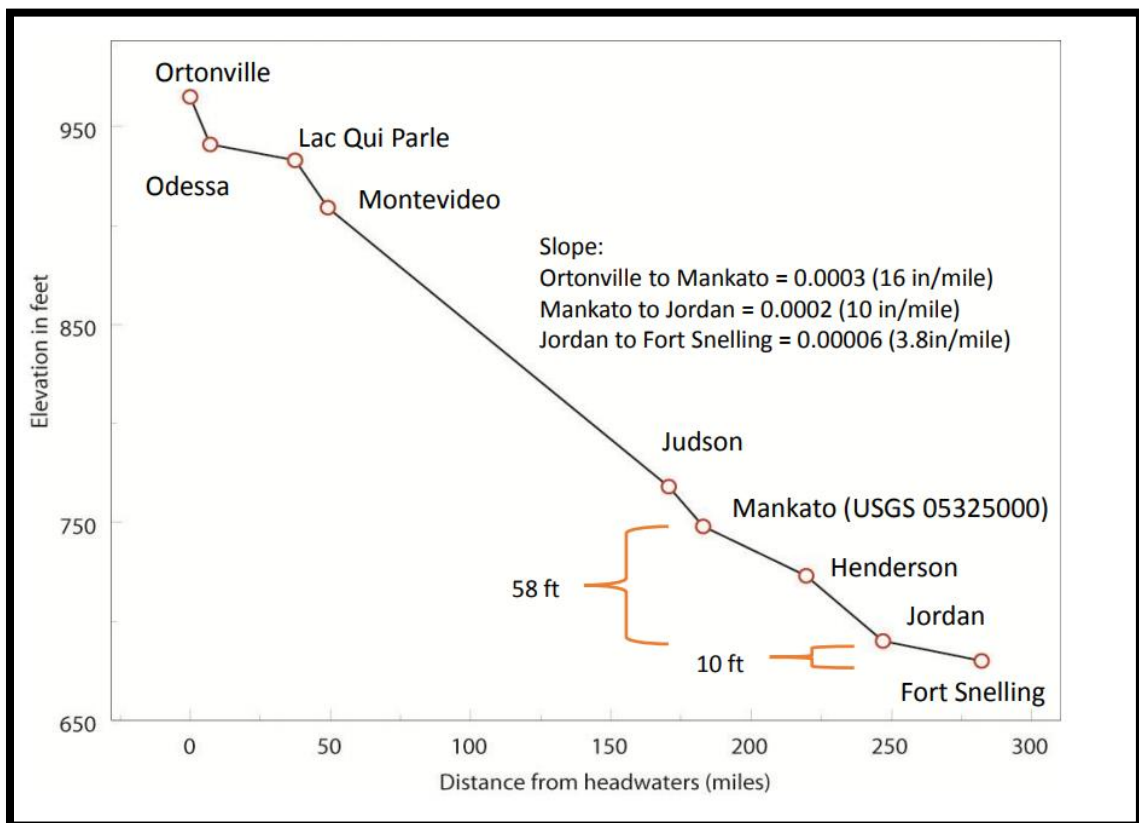


Figure 3.45: The Minnesota has a very low stream gradient, yet noticeable breaks are still present effecting the morphology of the river. Graphic from (Ellison 2015).

The upstream reaches have several large tributaries which contribute a great deal of sediment to the Minnesota River (Belmont et al. 2011; Gran, Belmont, Day, Jennings, et al. 2011; Groten, Ellison, and Hendrickson 2016). Among these are the Le Sueur River Watershed which has the highest sediment yield of any tributary in the MRB, contributing up to 30% of the sediment load to the Minnesota River while only occupying 7% of the MRB (Belmont et al. 2011). Groten et al. (2016) identify High Island Creek as the next highest contributor of sediment yield. This tributary enters the Minnesota River just downstream of the city of Henderson (Reach 7). Visual inspection of aerial imagery also shows several other tributaries with significant depositional features (e.g. large slumping bluffs, wide in-channel sandbars) within the tributaries themselves and large

alluvial fans deposited in the Minnesota River. Among these are Seven Mile Creek, Le Sueur Creek, Rush River, and Beavens Creek, with the latter two also exhibiting large, exposed bluffs abutting the river much like the Le Sueur River.

Based on the findings of Groten et al. (2016) sediment, primarily transported in suspension, in the upstream reaches begins to fall out after Jordan, which coincides with the aforementioned reduction in slope (Figure 3.45). This transition falls half way through Reach 12, which is dominated by high migration rates from the channel translating downstream (Figure 3.46). Reach 12 marks the last reach to show any significant annual channel migration, except for Reach 16 in the 1980-1991 interval. The “Instability Concept” (discussed in 1.3.2.1; Dey 2014) suggests that irregularities or perturbations in the upstream relate to modified structure in the downstream flow and sediment regime causing a river channel to meander. These upstream perturbations/irregularities include sediment deposition on the bed (Griggs 1906), velocity changes due to turbulence (Hjulström 1957), or oblique entry of flow in a channel (Friedkin 1945) all of which are seen in Reach 12 Figure 3.46.

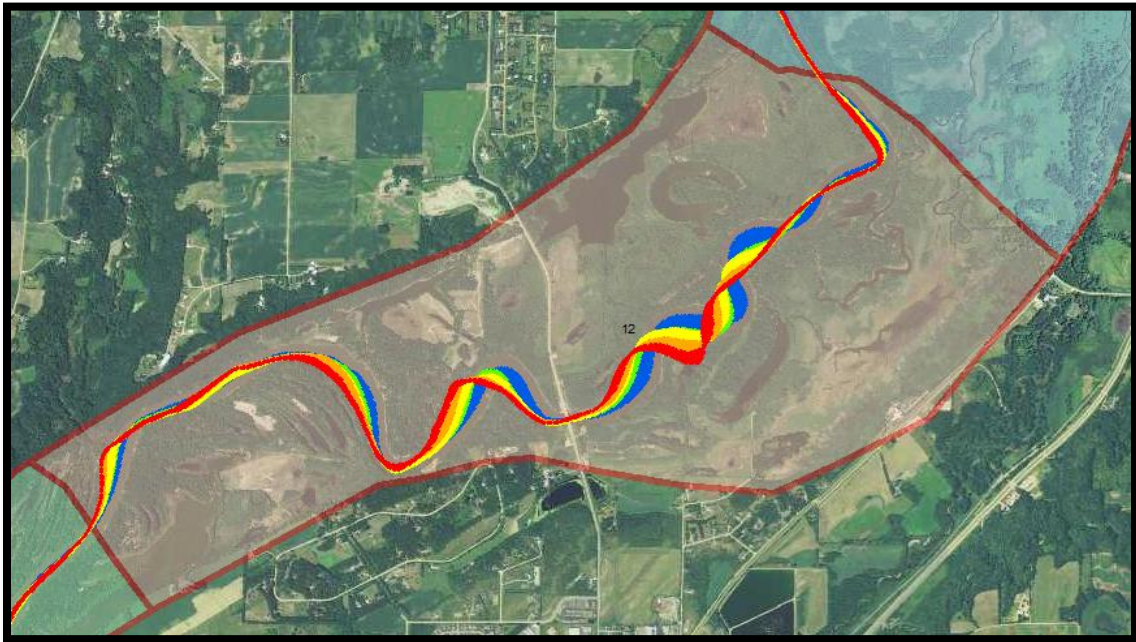


Figure 3.46: Reach 12 with migration displayed (Red = 1937-1951, Orange = 1951-1964, Yellow = 1964-1980, Green = 1980-1991, Blue = 1991-2013)

The highest AACM was seen in Reach 5 and the lowest AACM was seen in Reach 9, these were both short reaches and need to be viewed as such in terms of data analysis. These reaches were defined (Appendix H) based on geomorphic characteristics of the channel (sinuosity, meander wavelength, depositional features, etc.) and river valley width as well as any influencing anthropogenic features (urban areas, bridges, flood control structures, etc.). Reach 4, 6, and 9 were significantly shorter than most of other reaches and had uncharacteristically low AACM (Table 3.1) which created breaks in the data. In hindsight, these reaches should be combined with surrounding reaches to better display the data for AACM. However, they do show the areas of highest stability on the river which was part of the objectives in this research.

Temporally, the entire study reach has seen an increasing AACM except for the most recent interval (1991-2013) which has decreased (Table 3.1). The increased AACM

was expected given the higher stream flows, increased frequency of high flow events, and increased precipitation within the watershed (Figure 1.11; Novotny and Stefan 2007; Gran, Belmont, Day, Jennings, et al. 2011; Yuan and Mitchell 2014; Kelly et al. 2017). This overall increase in discharge is expected to increase the stream power of the river enabling greater amounts of channel migration/bank erosion. However, one explanation from this could be the influence of river management. Despite 1991-2013 showing a decrease in AACM, three Reaches (5, 7, and 8) are all above the 90th percentile for AACM (Table 3.1). This, however, is offset by 6 Reaches being below the 10th percentile and mostly found in urban areas. For instance, Reach 1 is Mankato's heavily engineered river stretch containing riprap, earthen levees, and cement flood walls, which has drastically reduced AACM measurements. Also Reaches 14, 15, and 16 are in the Minneapolis-St. Paul Metropolitan Area which has portions of the channel that are actively managed for barge traffic (USACE 2007, Jennings 2016). This is likely not the only reason, but can explain, in part, the observed trends in AACM.

As expected, these locations and intervals strongly correlate to the reaches and intervals experiencing the highest AACM and MACM. This reveals another form of dynamism in these reaches that not only relates to high erosional channel migration, but also to the rivers ability to change course rapidly, occupying great extents of the river valley.

3.4.2.2 Channel Width

Channel width has steadily increased from 1937 – 2013 (Figure 3.24). All reaches show an increase in channel width, but the upstream reaches increased at a higher rate than that of the downstream reaches (Figure 3.25). This disproportionate increase has

changed the linear trend from the downstream having greater channel widths in 1937 to the upstream having greater widths by 2013 (Figure 3.25). This could be a result of higher channel migration in the upstream reaches enlarging the banks more rapidly than that of the lower downstream reaches.

This behavior was expected given the increase in discharge in the MRB over this period (Novotny and Stefan 2007; Yuan and Mitchell 2014; Kelly et al. 2017).

Schumm's (1969) Equation 3.1 associates both an increase in channel width and an increase in width/depth ratio resulting from an increase in discharge. Given the increased need for channel dredging in the lower reaches of the Minnesota River to maintain barge traffic (Groten, Ellison, and Hendrickson 2016), it can be assumed that naturally (i.e. without modification) channel depth would be decreasing, supporting an increasing width/depth ratio.

An increased width/depth ratio is generally characterized with a higher shear stress being placed on the outer bank which increases and accelerates bank erosion. Reach 2 had the highest overall ACW and the greatest ACW of any reach in 1991 and 2013 (Table 3.1). Reach 2 also had the 2nd highest overall AACM and historically high MACM, with the greatest MACM of all reach/intervals in 1991 (Table 3.1, Table 3.2). On the other hand, Reaches with low ACW (e.g. Reach 4, 6, 9,) showed low AACM (Figure 3.43, Table 3.1, Table 3.2).

3.4.2.3 Channel Sinuosity/Stream Length

The decrease in channel sinuosity and stream length observed is interpreted as a result of cutoffs occurring from 1937-2013 (Figure 3.22). However, the magnitude of the cutoffs is increasing resulting in an accelerated loss of sinuosity and stream length

(Figure 3.26, Figure 3.27). The 1964-1980 and 1991-2013 intervals both experienced seven cutoffs (Figure 3.22), yet the decrease in stream length (Figure 3.27) was far greater in the 1991-2013 interval, especially in Reach 2, 7, and 8 (Figure 3.26). Figure 3.47 shows two different cutoffs from the 1991-2013 interval, the first (Figure 3.47A) resulting in ~2 km of stream length lost, and the second (Figure 3.47B) resulting in ~3 km of stream length lost. These large cutoffs are likely due to several factors. First, they are near a major highway (HWY 169) inhibiting further migration. Second, the increase in discharge (Figure 1.11) leads to more frequent floodplain inundation, increasing the likelihood for cutoffs. Notably, the cutoff in Figure 3.47A is in Reach 2, which had the highest amount of cutoffs of any reach (Figure 3.22) demonstrating the high geomorphic activity in this reach.

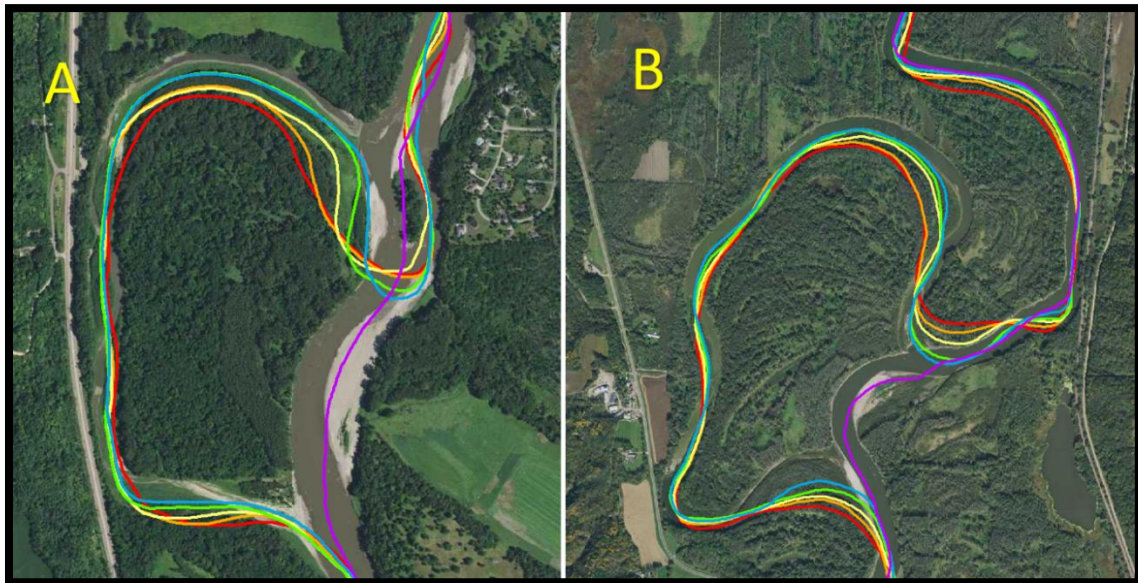


Figure 3.47: Displayed are two different cutoffs from the 1991-2013 interval. (A) resulted in ~2 km of stream length lost, and (B) resulting in ~3 km of stream length lost.

3.5 Conclusion

The Minnesota River is a highly dynamic system undergoing morphological planform channel adjustment as observed in the historical, aerial photograph record. This adjustment is likely linked to the MRB experiencing increased discharge from increased agricultural drainage practices and a changing climate resulting in more precipitation. Channel migration has been historically more active from Mankato to Jordan. Although the overall trend has revealed an increase in average annual migration (1937 to 1951 = 0.77 m/y, 1951 to 1964 = 0.84 m/y, 1964 to 1980 = 0.91 m/y, 1980 to 1991 = 0.99 m/y), the most recent interval analyzed, 1991-2013, has shown a slight decline (0.81 m/y). However, maximum annual channel migration is increasing with the highest recorded annual measurements being in 1980-1991 (15.86 m/y) and 1991-2013 (12.64 m/y). Despite an increasing trend in AACM and MACM, several areas of the Minnesota River showed historical migration stability (Reach 6 and 9).

Channel width has nearly doubled, on average throughout the lower Minnesota River, with every channel subsection, or reach, showing an increase. Reach 2 also had the highest overall ACW of any of the reaches at 100.19 m, and Reach 6 had the lowest overall ACW at 77.21 m (Table 3.3, Figure 3.25). An incremental increase in ACW of ~ 5-10 m was seen in each successive interval from 1937-2013. Reach analysis further demonstrated both the temporal increase in ACW, but also a spatial/temporal shift from channel width being greater in the downstream reaches to channel width being greater in the upstream reaches (Table 3.3, Figure 3.25). The increase in channel width has been

greater in the upstream reaches, and there has been a longitudinal shift from increasing width in the downstream direction to decreasing width (Figure 3.25).

Sinuosity is variable on the reach scale, but the overall trend reveals a decrease in sinuosity and, thereby, stream length. This is interpreted to be the result of recent cutoffs. The 1964-1980 and 1991-2013 intervals both experienced seven cutoffs (Figure 3.22), however; the decrease in stream length (Figure 3.27) was far greater in the 1991-2013 interval, especially in Reach 2, 7, and 8 (Figure 3.26) due to an increase in the magnitude of the cutoffs size.

Pinch points show a great deal of variability in planform change due to the unique features of different infrastructure. The stretch of river passing through Mankato (Figure 3.28) showed the greatest increase in migration stability following the floodwall and riprap-controlled being constructed in the mid-1960's leading to a decrease (~ 3 m/y) in channel migration (Figure 3.29). However, width did not immediately stabilize in this reach (Figure 3.30) and continued to rise in a manner characteristic with other river reaches (Figure 3.25), but recently (1991-2013) has seen its first, although minor, decrease in channel width.

The understanding of both spatial and temporal historic planform changes can now help aid decision makers in deciding if an area is potentially suitable for an invasive carp barrier. In addition, various lower Minnesota River Valley communities and residents can use this information to assess erosional hazards to property and infrastructure. Lastly, this information helps us better understand the historical impact of anthropogenic activities on the behavior of this fluvial system.

References

- Aadland, L. 2015. Barrier effects on native fishes of Minnesota. Minnesota Department of Natural Resources. <http://files.dnr.state.mn.us/eco/streamhab/barrier-effects.pdf> (accessed May 1, 2015).
- Aalto, R., J. W. Lauer, and W. E. Dietrich. 2008. Spatial and temporal dynamics of sediment accumulation and exchange along Strickland River floodplains (Papua New Guinea) over decadal-to-centennial timescales. *Journal of Geophysical Research: Earth Surface* 113 (F1). doi:10.1029/2006JF000627.
- Amhar, F., J. Jansa, and C. Ries. 1998. The generation of true orthophotos using a 3D building model in conjunction with a conventional DTM. *International Archives of Photogrammetry and Remote Sensing* 32:16-22.
- ArcGIS for Desktop. 2016. Fundamentals of georeferencing a raster dataset. <http://desktop.arcgis.com/en/arcmap/10.3/manage-data/raster-and-images/fundamentals-for-georeferencing-a-raster-dataset.htm>. (accessed January 27, 2017).
- Arora, V. K., and G. J. Boer. 2001. Effects of simulated climate change on the hydrology of major river basins. *Journal of Geophysical Research: Atmospheres* 106 (D4):3335-3348.
- Baker, V. R. 2013. Sinuous rivers. *Proceedings of the National Academy of Sciences of the United States of America* 110 (21):8321-8322. doi: 10.1073/pnas.1306619110.
- Belmont, P., and E. Foufoula-Georgiou. 2017. Solving water quality problems in agricultural landscapes: New approaches for these nonlinear, multiprocess,

multiscale systems. *Water Resources Research* 53 (4):2585-2590.

doi:10.1002/2017WR020839.

Belmont, P., K. B. Gran, S. P. Schottler, P. R. Wilcock, S. S. Day, C. Jennings, J. W.

Lauer, E. Viparelli, J. K. Willenbring, D. R. Engstrom, and G. Parker. 2011.

Large shift in source of fine sediment in the Upper Mississippi River.

Environmental Science & Technology 45 (20):8804-8810.

doi:10.1021/es2019109.

Black, E., C. E. Renshaw, F. J. Magilligan, J. M. Kaste, W. B. Dade, and J. D. Landis.

2010. Determining lateral migration rates of meandering rivers using fallout radionuclides. *Geomorphology* 123 (3-4):364-369.

doi:10.1016/j.geomorph.2010.08.004

Block, D. 2014. Historical channel-planform change of the Little Colorado River near Winslow, Arizona. Scientific Investigations Report 2014-5112., US Geological Survey, Reston, Virginia.

Blumentritt, D. J., D. R. Engstrom, and S. J. Balogh. 2013. A novel repeat-coring approach to reconstruct recent sediment, phosphorus, and mercury loading from the upper Mississippi River to Lake Pepin, USA. *Journal of Paleolimnology* 50 (3):293-304. doi:10.1007/s10933-013-9724-8.

Booth, D. B., and C. R. Jackson. 1997. Urbanization of aquatic systems: Degradation thresholds, stormwater detection, and the limits of mitigation. *JAWRA Journal of the American Water Resources Association* 33 (5):1077-1090.

doi:10.1111/j.1752-1688.1997.tb04126.x.

- Bradley, C., and D. G. Smith. 1984. Meandering channel response to altered flow regime: Milk River, Alberta and Montana. *Water Resources Research* 20 (12):1913-1920. doi:10.1029/WR020i012p01913.
- Brewer, P., and J. Lewin. 1998. Planform cyclicity in an unstable reach: Complex fluvial response to environmental change. *Earth Surface Processes and Landforms* 23 (11):989-1008.
- Brezonik, P. L., K.W. Easter, L. Hatch, D. Mulla, and J. Perry. 1999. Management of diffuse pollution in agricultural watersheds: Lessons from the Minnesota River Basin. *Water Science and Technology* 39 (12):323-330.
- Bristow, C. S., and J. L. Best. 1993. Braided rivers: perspectives and problems. *Geological Society, London, Special Publications* 75 (1):1-11. doi:10.1144/GSL.SP.1993.075.01.01.
- Buckingham, S. E., and J. W. Whitney. 2007. GIS methodology for quantifying channel change in Las Vegas, Nevada. *Journal of American Water Resources Association* 43 (4):888- 898. doi:10.1111/j.1752-1688.2007.00073.x.
- Bunn, S. E., and A. H. Arthington. 2002. Basic principles and ecological consequences of altered flow regimes for aquatic biodiversity. *Environmental Management* 30 (4):492-507. doi:10.1007/s00267-002-2737-0.
- Burkham, D. 1972. Channel changes of the Gila River in Safford valley, Arizona, 1846-1970. Geologic Survey Professtional Paper 655-G. US Geological Survey, Washington D.C.

- Carlson, A. K., and B. Vondracek. 2014. Synthesis of ecology and human dimensions for predictive management of bighead and silver carp in the United States. *Reviews in Fisheries Science & Aquaculture* 22 (4):284-300.
doi:10.1080/23308249.2014.967747.
- Carlston, C. W. 1965. The relation of free meander geometry to stream discharge and its geomorphic implications. *American Journal of Science* 263 (10):864-885.
doi:10.2475/ajs.263.10.864.
- Carpenter, S. R., N. F. Caraco, D. L. Correll, R. W. Howarth, A. N. Sharpley, and V. H. Smith. 1998. Nonpoint pollution of surface waters with phosphorus and nitrogen. *Ecological Applications* 8 (3):559-568. doi:10.1890/1051-0761(1998)008[0559:NPOSWW]2.0.CO;2.
- Carson, M. A., and M. F. Lapointe. 1983. The inherent asymmetry of river meander planform. *The Journal of Geology* 91 (1):41-55. doi:10.1086/628743.
- Carson, M. A., and G. A. Griffiths. 1987. Bedload transport in gravel channels. *Journal of Hydrology (New Zealand)* 26 (1):1-151.
- Chang, K. T. 2014. *Introduction to geographic information systems*. 7th ed. New York, NY: McGraw-Hill.
- Charlton, R. 2007. *Fundamentals of fluvial geomorphology*. New York, NY: Routledge.
- Chatley, H. 1938. Hydraulics of large rivers. *J. Junior Inst. Eng* 48: 401-416
- Chick, J. H., and M. A. Pegg. 2001. Invasive carp in the Mississippi River Basin. *Science* 292 (5525):2250-2251. doi:10.1126/science.292.5525.2250.

- Chrisman, N. 1982. Theory of cartographic error and its measurement in digital data bases. American Society of Photogrammetry and Remote Sensing. Falls Church, VA.
- Clayton, L., and S. R. Moran. 1982. Chronology of late Wisconsinan glaciation in middle North America. *Quaternary Science Reviews* 1 (1):55-82. doi:10.1016/0277-3791(82)90019-1.
- Comiti, F., M. Da Canal, N. Surian, L. Mao, L. Picco, and M. A. Lenzi. 2011. Channel adjustments and vegetation cover dynamics in a large gravel bed river over the last 200 years. *Geomorphology* 125 (1):147-159. doi:10.1016/j.geomorph.2010.09.011.
- Constantine, J. A., T. Dunne, J. Ahmed, C. Legleiter, and E. D. Lazarus. 2014. Sediment supply as a driver of river meandering and floodplain evolution in the Amazon Basin. *Nature Geoscience* 7 (12):899-903. doi:10.1038/ngeo2282.
- Crowell, M., S. P. Leatherman, and M. K. Buckley. 1991. Historical shoreline change: Error analysis and mapping accuracy. *Journal of Coastal Research* 7 (3):839-852.
- Daniels, J. M. 2003. Floodplain aggradation and pedogenesis in a semiarid environment. *Geomorphology* 56 (3-4):225-242. doi:10.1016/S0169-555X(03)00153-3.
- Darby, S. E., M. Rinaldi, and S. Dapporto. 2007. Coupled simulations of fluvial erosion and mass wasting for cohesive river banks. *Journal of Geophysical Research: Earth Surface* 112 (F3). doi:10.1029/2006JF000722.
- Davis, W. M. 1889. The rivers and valleys of Pennsylvania. *National Geographic Society* 1:183-252.

- . 1902. Baselevel, grade and peneplain. *The Journal of Geology* 10 (1):77-111.
- Dawson, H. A., U. G. Reinhardt, and J. F. Savino. 2006. Use of electric or bubble barriers to limit the movement of Eurasian ruffe (*Gymnocephalus cernuus*). *Journal of Great Lakes Research* 32 (1):40-49. doi:10.3394/03801330(2006)32[40:UOE0BB]2.0.CO;2.
- Day, S. S., K. B. Gran, P. Belmont, and T. Wawrzyniec. 2013a. Measuring bluff erosion part 1: Terrestrial laser scanning methods for change detection. *Earth Surface Processes and Landforms* 38 (10):1055-1067. doi:10.1002/esp.3353.
- . 2013b. Measuring bluff erosion part 2: Pairing aerial photographs and terrestrial laser scanning to create a watershed scale sediment budget. *Earth Surface Processes and Landforms* 38 (10):1068-1082. doi:10.1002/esp.3359.
- DeGrandchamp, K. L., J. E. Garvey, and R. E. Colombo. 2008. Movement and habitat selection by invasive Asian carps in a large river. *Transactions of the American Fisheries Society* 137 (1):45-56. doi:10.1577/T06-116.1.
- Dey, S. 2014. *Fluvial hydrodynamics*. Berlin, Heidelberg: Springer.
- Dodds, W. K. 2006. Nutrients and the “dead zone”: the link between nutrient ratios and dissolved oxygen in the northern Gulf of Mexico. *Frontiers in Ecology and the Environment* 4 (4):211-217. doi:10.1890/15409295(2006)004[0211:NATDZT]2.0.CO;2.
- Downward, S. R., A. M. Gurnell, and A. Brookes. 1994. A methodology for quantifying river channel planform change using GIS. *IAHS Publications-Series of Proceedings and Reports-Intern Assoc Hydrological Sciences* 224:449-456.

- Dunne, T., and L. B. Leopold. 1978. *Water in environmental planning*. New York, NY: W.H Freeman and Company.
- Dury, G. H. 1964. Principles of underfit streams. Geologic Survey Professional Paper 452-A. US Geological Survey, Washington D.C.
- Eakin, H. M. 1910. The influence of the earth's rotation upon the lateral erosion of streams. *The Journal of Geology* 18 (5):435-447.
- Einstein, A. 1926. The cause of the formation of meanders in the Courses of Rivers and of the So-Called Baer's Law. *Die Naturwissenschaften* 14 (11):223-224.
- Ellison, C. A. 2015. Sediment concentrations, loads, particle-size fractions, and hydroacoustics in the lower Minnesota River, 2011-2014. US Geologic Survey PowerPoint Presentation prepared in conjunction with the US Army Corps of Engineers. September 9.
- Engstrom, D. R., J. E. Almendinger, and J. A. Wolin. 2009. Historical changes in sediment and phosphorus loading to the upper Mississippi River: Mass-balance reconstructions from the sediments of Lake Pepin. *Journal of Paleolimnology* 41 (4):563-588. doi:10.1007/s10933-008-9292-5.
- Everitt, B. L. 1968. Use of the cottonwood in an investigation of the recent history of a flood plain. *American Journal of Science* 266 (6):417-439.
doi:10.2475/ajs.266.6.417.
- Faulkner, D. J., P. H. Larson, H. M. Jol, G. L. Running, H. M. Loope, and R. J. Goble. 2016. Autogenic incision and terrace formation resulting from abrupt late-glacial

- base-level fall, lower Chippewa River, Wisconsin, USA. *Geomorphology* 266:75-95. doi:10.1016/j.geomorph.2016.04.016.
- Fenton, M. M., S. Moran, J. T. Teller, and L. Clayton. 1983. Quaternary stratigraphy and history in the southern part of the Lake Agassiz basin. Special Paper 26 – Lake Agassiz, Geologic Association of Canada.
- Fisher, T. G. 2003. Chronology of glacial Lake Agassiz meltwater routed to the Gulf of Mexico. *Quaternary Research* 59 (2):271-276. doi:10.1016/S0033-5894(03)00011-5.
- . T. G. 2004. River Warren boulders, Minnesota, USA: Catastrophic paleoflow indicators in the southern spillway of glacial Lake Agassiz. *Boreas* 33 (4):349-358. doi:10.1111/j.1502-3885.2004.tb01245.x.
- Florsheim, J. L., J. F. Mount, and A. Chin. 2008. Bank erosion as a desirable attribute of rivers. *Bioscience* 58 (6):519-529. doi:10.1641/B580608.
- Forsberg, D. C. 1992. Minnesota Wetland Conservation Act of 1991: Balancing public and private interests. *William Mitchell Law Review* 18 (4):1021-1071.
- Foufoula-Georgiou, E., Z. Takbiri, J. A. Czuba, and J. Schwenk. 2015. The change of nature and the nature of change in agricultural landscapes: Hydrologic regime shifts modulate ecological transitions. *Water Resources Research* 51 (8):6649-6671. doi:10.1002/2015WR017637.
- Friedkin, J. F. 1945. Laboratory study of the meandering of alluvial rivers. US Army Corp of Engineers,, Vicksburg, Mississippi.

- Garofalo, D. 1980. The influence of wetland vegetation on tidal stream channel migration and morphology. *Estuaries* 3 (4):258-270. doi:10.2307/1352081.
- Gay, G. R., H. H. Gay, W. H. Gay, H. A. Martinson, R. H. Meade, and J. A. Moody. 1998. Evolution of cutoffs across meander necks in Powder River, Montana, USA. *Earth Surface Processes and Landforms* 23 (7):651-662.
- Giardino, J. R., and A. A. Lee. 2011. Rates of channel migration on the Brazos River. Contract No. 0904830898, Department of Geology & Geophysics, Texas A&M University, College Station, Texas.
- Gilbert, G. K. 1877. Report on the geology of the Henry Mountains. US Geological Survey, Washington D.C.
- . 1884. The Sufficiency of Terrestrial Rotation for the Deflection of Streams. *American Journal of Science (1880-1910)* 27 (162):427.
- Gilroy, K. L., and R. H. McCuen. 2012. A nonstationary flood frequency analysis method to adjust for future climate change and urbanization. *Journal of Hydrology* 414-415:40-48. doi:10.1016/j.jhydrol.2011.10.009.
- Gilvear, D., S. Winterbottom, and H. Sichingabula. 2000. Character of channel planform change and meander development: Luangwa River, Zambia. *Earth Surface Processes and Landforms* 25 (4):421-436. doi:10.1002/(SICI)1096-9837(200004)25:4<421::AID-ESP65>3.0.CO;2-Q.
- Goudie, A. S. 2006. Global warming and fluvial geomorphology. *Geomorphology* 79 (3-4):384-394. doi:10.1016/j.geomorph.2006.06.023.

- Grabowski, R. C., N. Surian, and A. M. Gurnell. 2014. Characterizing geomorphological change to support sustainable river restoration and management. *Wiley Interdisciplinary Reviews: Water* 1 (5):483-512. doi:10.1002/wat2.1037.
- Graf, W. L. 2000. Locational probability for a dammed, urbanizing stream: Salt River, Arizona, USA. *Environmental Management* 25 (3):321-335. doi:10.1007/s002679910025.
- Gran, K., P. Belmont, S. Day, C. Jennings, J. W. Lauer, E. Viparelli, P. Wilcock, and G. Parker. 2011. An integrated sediment budget for the Le Sueur River Basin. Report wq-iw7-29o, Minnesota Pollution Control Agency.
- Gran, K. B., P. Belmont, S. S. Day, N. Finnegan, C. Jennings, J. W. Lauer, and P. R. Wilcock. 2011. Landscape evolution in south-central Minnesota and the role of geomorphic history on modern erosional processes. *GSA Today* 21 (9):7-9. doi:10.1130/G121A.1.
- Gran, K. B., P. Belmont, S. S. Day, C. Jennings, A. Johnson, L. Perg, and P. R. Wilcock. 2009. Geomorphic evolution of the Le Sueur River, Minnesota, USA, and implications for current sediment loading. *Geological Society of America Special Papers* 451:119-130.
- Gran, K. B., N. Finnegan, A. L. Johnson, P. Belmont, C. Wittkop, and T. Rittenour. 2013. Landscape evolution, valley excavation, and terrace development following abrupt postglacial base-level fall. *Geological Society of America Bulletin* 125 (11-12):1851-1864. doi:10.1130/B30772.1.

- Griggs, R. F. 1906. The Buffalo River: An interesting meandering stream. *Bulletin of the American Geographical Society* 38 (3):168-177. doi:10.2307/197916.
- Groten, J. T., C. A. Ellison, and J. S. Hendrickson. 2016. Suspended-sediment concentrations, bedload, particle sizes, surrogate measurements, and annual sediment loads for selected sites in the lower Minnesota River Basin, water years 2011 through 2016. Scientific Investigations Report 2016-5174, US Geological Survey. Reston, Virginia. doi: 10.3133/sir20165174.
- Gurnell, A. M. 1997. Channel change on the River Dee meanders, 1946–1992, from the analysis of air photographs. *River Research and Applications* 13 (1):13-26. doi:10.1002/(SICI)1099-1646(199701)13:1<13::AID-RRR420>3.0.CO;2-W.
- Gurnell, A. M., S. R. Downward, and R. Jones. 1994. Channel planform change on the River Dee meanders, 1876–1992. *River Research and Applications* 9 (4):187-204. doi:10.1002/rrr.3450090402.
- Hallberg, G. R., and T. J. Kemmis. 1986. Stratigraphy and correlation of the glacial deposits of the Des Moines and James lobes and adjacent areas in North Dakota, South Dakota, Minnesota, and Iowa. *Quaternary Science Reviews* 5:65-68. doi:10.1016/0277-3791(86)90175-7.
- Haque, C. E., and M. Q. Zaman. 1989. Coping with riverbank erosion hazard and displacement in Bangladesh: Survival strategies and adjustments. *Disasters* 13 (4):300-314. doi:10.1111/j.1467-7717.1989.tb00724.x.
- Harvey, M. D., and C. C. Watson. 1986. Fluvial processes and morphological thresholds in incised channel restoration. *JAWRA Journal of the American Water Resources*

Association 22 (3):359-368. doi: 10.1111/j.1752-1688.1986.tb01890.x.

He, Q., and D. E. Walling. 1996. Interpreting particle size effects in the adsorption of ¹³⁷Cs and unsupported ²¹⁰Pb by mineral soils and sediments. *Journal of Environmental Radioactivity* 30 (2):117-137. doi:10.1016/0265-931X(96)89275-7.

Hereford, R. 1984. Climate and ephemeral-stream processes: Twentieth-century geomorphology and alluvial stratigraphy of the Little Colorado River, Arizona. *GSA Bulletin* 95 (6):654-668. doi:10.1130/0016-7606(1984)95<654:CAEPTG>2.0.CO;2.

Hession, W. C., J. E. Pizzuto, T. E. Johnson, and R. J. Horwitz. 2003. Influence of bank vegetation on channel morphology in rural and urban watersheds. *Geology* 31 (2):147-150. doi:10.1130/0091-7613(2003)031<0147:IOBVOC>2.0.CO;2.

Hickin, E. J., and G. C. Nanson. 1984. Lateral migration rates of river bends. *Journal of Hydraulic Engineering* 110 (11):1557-1567. doi:10.1061/(ASCE)0733-9429(1984)110:11(1557).

Hjulström, F. 1957. A study of the meander problem. *Bulletin*. Institute of Hydraulics, Royal Institute of Technology. Stockholm, Sweden.

Hooke, J. 2003. River meander behaviour and instability: A framework for analysis. *Transactions of the Institute of British Geographers* 28 (2):238-253. doi:10.1111/1475-5661.00089.

- . 1995. River channel adjustment to meander cutoffs on the River Bollin and River Dane, northwest England. *Geomorphology* 14 (3):235-253.
doi:10.1016/0169-555X(95)00110-Q.
- . 2007. Spatial variability, mechanisms and propagation of change in an active meandering river. *Geomorphology* 84 (3-4):277-296.
doi:10.1016/j.geomorph.2006.06.005.
- Huang, H. Q., and G. C. Nanson. 1997. Vegetation and channel variation; a case study of four small streams in southeastern Australia. *Geomorphology* 18 (3-4):237-249.
doi:10.1016/S0169-555X(96)00028-1.
- Hughes, M. L., P. F. McDowell, and W. A. Marcus. 2006. Accuracy assessment of georectified aerial photographs: Implications for measuring lateral channel movement in a GIS. *Geomorphology* 74 (1-4):1-16.
doi:10.1016/j.geomorph.2005.07.001.
- Inglis, C. C., and G. Lacey. 1947. Meanders and their bearing on river training. Maritime and Waterways Engineering Division. *The Institution of Civil Engineers Engineering Division Papers* 5 (17):3-24. doi:10.1680/idivp.1947.13075.
- Jennings, C. 2016. Why so much sand in the lower Minnesota River? *Open Rivers* Fall Edition. ISSN 2471-190X
- Johannesson, H., and G. Parker. 1985. Computer simulated migration of meandering rivers in Minnesota. Project Report No. 242 Universtiy of Minnesota, St. Anthony Falls Hydraulic Laboratory., Minneapolis, MN.

- Keller, E. A. 1972. Development of alluvial stream channels: A five-stage model. *Geological Society of America Bulletin* 83 (5):1531-1536. doi:0.1130/0016-7606(1972)83[1531:DOASCA]2.0.CO;2.
- Kelley, D. W., and E. A. Nater. 2000. Historical sediment flux from three watersheds into Lake Pepin, Minnesota, USA. *Journal of Environmental Quality* 29 (2):561-568. doi:10.2134/jeq2000.00472425002900020025x.
- Kelley, D. W., S. A. Brachfeld, E. A. Nater, and H. E. Wright Jr. 2006. Sources of sediment in Lake Pepin on the upper Mississippi River in response to Holocene climatic changes. *Journal of Paleolimnology* 35 (1):193-206. doi:10.1007/s10933-005-8686-x.
- Kelly, S. A., Z. Takbiri, P. Belmont, and E. Foufoula-Georgiou. 2017. Human amplified changes in precipitation–runoff patterns in large river basins of the Midwestern United States. *Hydrology and Earth System Sciences* 21 (10):5065-5088. doi:10.5194/hess-21-5065-2017.
- Kimmerling, A., A. Buckley, P. Muehrcke, and J. Muehrcke. 2011. *Map use: Reading, analysis, interpretation*. Redlands, CA: Esri Press Academic.
- Kleinhans, M. G. 2010. Sorting out river channel patterns. *Progress in Physical Geography: Earth and Environment* 34 (3):287-326. doi:10.1029/2005WR004674.
- Knighton, D. 2014. *Fluvial forms and processes: A new perspective*. New York, NY: Routledge.

- Knox, J. C. 1977. Human impacts on Wisconsin Stream Channels. *Annals of the Association of American Geographers* 67 (3):323-342. doi:10.1111/j.1467-8306.1977.tb01145.x.
- Koel, T. M., K. S. Irons, and E. N. Ratcliff. 2000. Asian carp invasion of the upper Mississippi River System. Project Status Report 2000-05, US Department of the Interior, US Geological Survey, Upper Midwest Environmental Sciences Center, La Crosse, WI.
- Kolar, C. S., D. C. Chapman, W. R. Courtenay, C. M. Housel, J. D. Williams, and D. P. Jennings. 2007. *Bigheaded carps: A biological synopsis and environmental risk assessment*. Bethesda, MD: American Fisheries Society
- Kondolf, G. M., H. Piégay, and N. Landon. 2002. Channel response to increased and decreased bedload supply from land use change: contrasts between two catchments. *Geomorphology* 45 (1-2):35-51. doi:10.1016/S0169-555X(01)00188-X.
- Kovacic, D. A., M. B. David, L. E. Gentry, K. M. Starks, and R. A. Cooke. 2000. Effectiveness of constructed wetlands in reducing nitrogen and phosphorus export from agricultural tile drainage. *Journal of Environmental Quality* 29 (4):1262-1274. doi:10.2134/jeq2000.00472425002900040033x.
- Lacey, J. M. 1923. Some problems connected with the rivers and the canals in southern India. *Minutes of the Proceedings of the Institution of Civil Engineers* 216 (1923): 150-160. doi.org/10.1680/imotp.1923.14469.

- Lane, E. W. 1955. Importance of fluvial morphology in hydraulic engineering. *Proceedings (American Society of Civil Engineers)* 81 (745).
- Larsen, E. W., E. H. Girvetz, and A. K. Fremier. 2007. Landscape level planning in alluvial riparian floodplain ecosystems: using geomorphic modeling to avoid conflicts between human infrastructure and habitat conservation. *Landscape and Urban Planning* 79 (3-4):338-346. doi:10.1016/j.landurbplan.2006.04.003.
- Lauer, J. W., C. Echterling, C. Lenhart, P. Belmont, and R. Rausch. 2017. Air-photo based change in channel width in the Minnesota River basin: Modes of adjustment and implications for sediment budget. *Geomorphology* 297:170-184. doi:10.1016/j.geomorph.2017.09.005.
- Lauer, J. W., and G. Parker. 2008. Net local removal of floodplain sediment by river meander migration. *Geomorphology* 96 (1-2):123-149. doi:10.1016/j.geomorph.2007.08.003.
- Lauer, W. 2006. NCED Stream restoration toolbox-channel planform statistics and ArcMap project. *National Center for Earth-Surface Dynamics (NCED)*. https://repository.nced.umn.edu/browser.php?current=author&author=35&dataset_id=15. (accessed April 5, 2018).
- Lawler, D. M. 1993. The measurement of river bank erosion and lateral channel change: A review. *Earth Surface Processes and Landforms* 18 (9):777-821. doi:10.1002/esp.3290180905.

- Lea, D. M., and C. J. Legleiter. 2016. Refining measurements of lateral channel movement from image time series by quantifying spatial variations in registration error. *Geomorphology* 258:11-28. doi: 10.1016/j.geomorph.2016.01.009.
- Legleiter, C. J. 2014. Downstream effects of recent reservoir development on the morphodynamics of a meandering channel: Savery Creek, Wyoming, USA. *River Research and Applications* 31 (10):1328-1343. doi:10.1002/rra.2824.
- Leliavsky, S. 1966. *Introduction to Fluvial Hydraulics*. New York, NY: Dover Publications
- Lenhart, C., E. S. Verry, K. N. Brooks, and J. A. Magner. 2011. Adjustment of prairie pothole streams to land-use, drainage and climate changes and consequences for turbidity impairment. *River Research and Applications* 28 (10):1609-1619. doi:10.1002/rra.1549.
- Lenhart, C. F., M. L. Titov, J. S. Ulrich, J. L. Nieber, and B. J. Suppes. 2013. The role of hydrologic alteration and riparian vegetation dynamics in channel evolution along the lower Minnesota River. *Transactions of the ASABE* 56 (2):549-561. doi:10.13031/2013.42686.
- Leopold, L. B., and W. B. Langbein. 1966. River meanders- theory of minimum variance. *Scientific American* 214 (6):60-73.
- Leopold, L. B., and T. Maddock Jr. 1953. The hydraulic geometry of stream channels and some physiographic implications. Professional Paper 252, US Geological Survey, Washington D.C.

- Leopold, L. B., and M. G. Wolman. 1957. River channel patterns: braided, meandering, and straight. Professional Paper 282-B, US Geological Survey, Washington, D.C.
- . 1960. River meanders. *Geological Society of America Bulletin* 71 (6):769-793. doi:10.1130/0016-7606(1960)71[769:RM]2.0.CO;2.
- Lepper, K., T. G. Fisher, I. Hajdas, and T. V. Lowell. 2007. Ages for the Big Stone Moraine and the oldest beaches of glacial Lake Agassiz: Implications for deglaciation chronology. *Geology* 35 (7):667-670. doi:10.1130/G23665A.1.
- Leung, Y., and J. Yan. 1998. A locational error model for spatial features. *International Journal of Geographical Information Science* 12 (6):607-620. doi:10.1080/136588198241699.
- Little, W. C., C. R. Thorne, and J. B. Murphey. 1982. Mass bank failure analysis of selected Yazoo Basin streams. *Transactions of the ASAE* 25 (5):1321-1328. doi:10.13031/2013.33721.
- Mackin, J. H. 1948. Concept of the graded river. *Geological Society of America Bulletin* 59 (5):463-512. doi:10.1130/0016-7606(1948)59[463:COTGR]2.0.CO;2.
- Macklin, M. G., and J. Lewin. 1989. Sediment transfer and transformation of an alluvial valley floor: the River South Tyne, Northumbria, UK. *Earth Surface Processes and Landforms* 14 (3):233-246. doi:10.1002/esp.3290140305.
- Magdalene, S. C. C. 2004. From field to stream: Rapid runoff through agricultural tile drainage systems within the Minnesota River basin. Thesis, University of Minnesota.

- Matisoff, G., and P. J. Whiting. 2012. Measuring soil erosion rates using natural (^{7}Be , ^{210}Pb) and anthropogenic (^{137}Cs , $^{239,240}\text{Pu}$) radionuclides. *Handbook of Environmental Isotope Geochemistry*, 1:487-519. doi:10.1007/978-3-642-10637-8_25.
- Matsch, C. 1983. River Warren, the southern outlet to glacial Lake Agassiz. Special Paper 26 – Lake Agassiz, Geologic Association of Canada 26:231-244.
- Micheli, E. R., and J. W. Kirchner. 2002. Effects of wet meadow riparian vegetation on streambank erosion. 1. Remote sensing measurements of streambank migration and erodibility. *Earth Surface Processes and Landforms* 27 (6):627-639. doi:10.1002/esp.338.
- Micheli, E., J. W. Kirchner, and E. W. Larsen. 2004. Quantifying the effect of riparian forest versus agricultural vegetation on river meander migration rates, Central Sacramento River, California, USA. *River Research and Applications* 20 (5):537-548. doi:10.1002/rra.756.
- Miller, J. R. 1997. The role of fluvial geomorphic processes in the dispersal of heavy metals from mine sites. *Journal of Geochemical Exploration* 58 (2-3):101-118. doi:10.1016/S0375-6742(96)00073-8.
- Mitsch, W. J., and J. G. Gosselink. 2000. The value of wetlands: Importance of scale and landscape setting. *Ecological economics* 35 (1):25-33. doi:10.1016/S0921-8009(00)00165-8.
- MNDNR. 2014. DNR explains environmental DNA. <http://www.dnr.state.mn.us/invasive-carp/faq.html> (accessed April 14, 2015)

- MnGeo. 2014. Composite image service WMS, Minnesota. http://www.mngeo.state.mn.us/chouse/metadata/composite_wms.html (accessed April, 20, 2015).
- Montgomery, D. R., and J. M. Buffington. 1997. Channel-reach morphology in mountain drainage basins. *Geological Society of America Bulletin* 109 (5):596-611. doi:10.1130/0016-7606(1997)109<0596:CRMIMD>2.3.CO;2.
- Moore, M. T., R. Kröger, M. A. Locke, R. F. Cullum, R. W. Steinriede Jr., S. Testa III, R. E. Lizotte Jr., C. T. Bryant, and C. M. Cooper. 2010. Nutrient mitigation capacity in Mississippi Delta, USA drainage ditches. *Environmental Pollution* 158 (1):175-184. doi:10.1016/j.envpol.2009.07.024.
- Morgan, J. L., S. E. Gergel, and N. C. Coops. 2010. Aerial photography: A rapidly evolving tool for ecological management. *Bioscience* 60 (1):47-59. doi:10.1525/bio.2010.60.1.9.
- Motta, D., J. D. Abad, E. J. Langendoen, and M. H. Garcia. 2012. A simplified 2D model for meander migration with physically-based bank evolution. *Geomorphology* 163-164:10-25. doi:10.1016/j.geomorph.2011.06.036.
- Mount, N., and J. Louis. 2005. Estimation and propagation of error in measurements of river channel movement from aerial imagery. *Earth Surface Processes and Landforms* 30 (5):635-643. doi:10.1002/esp.1172.
- Mount, N. J., J. Louis, R. M. Teeuw, P. M. Zukowskyj, and T. Stott. 2003. Estimation of error in bankfull width comparisons from temporally sequenced raw and corrected aerial photographs. *Geomorphology* 56 (1-2):65-77. doi:10.1016/S0169-555X(03)00046-1.

- MPCA. 1998. Bacteria in the Minnesota River. [cited 5/2/2015. <http://www.pca.state.mn.us/index.php/view-document.html?gid=9962>. (accessed May 2, 2015).
- . 2002. Minnesota River Basin plan. <http://www.pca.state.mn.us/index.php/view-document.html?gid=9947> (accessed May 1, 2015).
- . 2008. Nutrients: Phosphorus, nitrogen sources, impact on water quality - A general overview. <http://www.pca.state.mn.us/index.php/view-document.html?gid=7939> (accessed May 2, 2015).
- MRBDC. 2003. Minnesota River profile. http://mrbdc.mnsu.edu/mnbasin/fact_sheets/river_profile (accessed April, 15, 2015)
- . 2004. Minnesota River Valley formation. <http://mrbdc.mnsu.edu/minnesota-river-valley-formation> (accessed May 1, 2015).
- . 2011 Minnesota River Basin fast facts. <http://mrbdc.mnsu.edu/minnesota-river-basin-fast-facts> (accessed April 20, 2015).
- Mulla, D. J., and A. C. Sekely. 2009. Historical trends affecting accumulation of sediment and phosphorus in Lake Pepin, upper Mississippi River, USA. *Journal of Paleolimnology* 41 (4):589-602. doi:10.1007/s10933-008-9293-4.
- Musser, K., S. Kudelka, and R. Moore. 2009. *Minnesota River Basin trends*. Mankato, MN: Minnesota State University, Mankato, Water Resources Center.
- Naden, P. S. 2010. The fine-sediment cascade. In *Sediment cascades: An integrated approach*, ed. T. Burt and R. Allison, 271-3-306. Oxford, UK: John Wiley & Sons.

- Nanson, G. C., and E. J. Hickin. 1983. Channel migration and incision on the Beatton River. *Journal of Hydraulic Engineering* 109 (3):327-337.
doi:10.1061/(ASCE)0733-9429(1983)109:3(327).
- . 1986. A statistical analysis of bank erosion and channel migration in western Canada. *Geological Society of America Bulletin* 97 (4):497-504.
doi:10.1130/0016-7606(1986)97<497:ASAOBE>2.0.CO;2.
- Neu, H. A. 1967. Transverse flow in a river due to earth's rotation. *Journal of the Hydraulics division* 93 (5):149-166.
- Nicoll, T. J., and E. J. Hickin. 2010. Planform geometry and channel migration of confined meandering rivers on the Canadian prairies. *Geomorphology* 116 (1-2):37-47. doi:10.1016/j.geomorph.2009.10.005.
- NOAA. 2015. Gulf of Mexico dead zone 'above average'. <http://www.noaanews.noaa.gov/stories2015/080415-gulf-of-mexico-dead-zone-above-average.html> (accessed November, 11, 2017).
- Noatch, M. R., and C. D. Suski. 2012. Non-physical barriers to deter fish movements. *Environmental Reviews* 20 (1):71-82. doi:10.1139/a2012-001.
- Novotny, E. V., and H. G. Stefan. 2007. Stream flow in Minnesota: Indicator of climate change. *Journal of Hydrology* 334 (3-4):319-333.
doi:10.1016/j.jhydrol.2006.10.011.
- O'Connor, J. E., M. A. Jones, and T. L. Haluska. 2003. Flood plain and channel dynamics of the Quinault and Queets Rivers, Washington, USA. *Geomorphology* 51 (1-3):31-59. doi: 10.1016/S0169-555X(02)00324-0.

- Odgaard, A. J. 1987. Streambank erosion along two rivers in Iowa. *Water resources research* 23 (7):1225-1236. doi:10.1029/WR023i007p01225.
- Ojakangas, R. W., and C. L. Matcsh. 1982. *Minnesota's geology*. Minneapolis, MN: University of Minnesota Press.
- Onishi, Y., S. C. Jain, and J. F. Kennedy. 1976. Effects of meandering in alluvial streams. *Journal of the Hydraulics division* 102 (HY7):899-917.
- Osman, A. M., and C. R. Thorne. 1988. Riverbank stability analysis. I: Theory. *Journal of Hydraulic Engineering* 114 (2):134-150. doi:10.1061/(ASCE)0733-9429(1988)114:2(134).
- Osterkamp, W. R., M. L. Scott, and G. T. Auble. 1998. Downstream effects of dams on channel geometry and bottomland vegetation: Regional patterns in the Great Plains. *Wetlands* 18 (4):619-633. doi:10.1007/BF03161677.
- Patterson, C., and H. Wright. 1998. Contributions to Quaternary studies in Minnesota. Report of Investigations 48 ISSN 0076-9177, Minnesota Geological Survey, St. Paul, MN.
- Patterson, C. J. 1997. Southern Laurentide ice lobes were created by ice streams: Des Moines Lobe in Minnesota, USA. *Sedimentary Geology* 111 (1-4):249-261. doi:10.1016/S0037-0738(97)00018-3.
- Patton, P. C., and S. A. Schumm. 1975. Gully erosion, Northwestern Colorado: A threshold phenomenon. *Geology* 3 (2):88-90. doi:10.1130/0091-7613(1975)3<88:GENCAT>2.0.CO;2.

- Pegg, M. A., and J. H. Chick. 2004. An evaluation of barriers for preventing the spread of bighead and silver carp to the Great Lakes. Illinois Natural History Survey. <http://www.iisgcp.org/research/ais/pegg.html> (accessed May 1, 2015).
- Pereira, W. E., and F. D. Hostettler. 1993. Nonpoint source contamination of the Mississippi River and its tributaries by herbicides. *Environmental Science & Technology* 27 (8):1542-1552. doi:10.1021/es00045a008.
- Petrolia, D. R., and P. H. Gowda. 2006. Missing the boat: Midwest farm drainage and Gulf of Mexico hypoxia. *Review of Agricultural Economics* 28 (2):240-253. doi:10.1111/j.1467-9353.2006.00284.x.
- Pimentel, D., L. Lach, R. Zuniga, and D. Morrison. 2000. Environmental and economic costs of nonindigenous species in the United States. *Bioscience* 50 (1):53-65. doi:10.1641/0006-3568(2000)050[0053:EAECON]2.3.CO;2.
- Pizzuto, J. E. 1994. Channel adjustments to changing discharges, Powder River, Montana. *Geological Society of America Bulletin* 106 (11):1494-1501. doi:10.1130/0016-7606(1994)106<1494:CATCDP>2.3.CO;2.
- Professional Aerial Photographers Association. 2015. History of aerial photography. http://professionalaerialphotographers.com/content.aspx?page_id=22&club_id=808138&module_id=158950 (accessed March, 31, 2015).
- Prus-Chacinski, T. M. 1954. Patterns of motion in open channel bends. *Association International d'Hydrologie* 3 (38):311-318.
- Quraishy, M. S. 1943. River meandering and the earth's rotation. *Current Science* 12 (10):278-278.

- Rabalais, N. N., R. E. Turner, and D. Scavia. 2002. Beyond Science into Policy: Gulf of Mexico Hypoxia and the Mississippi River: Nutrient policy development for the Mississippi River watershed reflects the accumulated scientific evidence that the increase in nitrogen loading is the primary factor in the worsening of hypoxia in the northern Gulf of Mexico. *BioScience* 52 (2):129-142. doi:10.1641/0006-3568(2002)052[0129:BSIPGO]2.0.CO;2.
- Rasmussen, J. 2011. Regulations as a tool in Asian carp management. In *Invasive Asian carps in North America*. ed. D. C. Chapman and M. H. Hoff, 175-190. Bethesda, Maryland: American Fisheries Society.
- Rhoades, E. L., M. A. O'Neal, and J. E. Pizzuto. 2009. Quantifying bank erosion on the South River from 1937 to 2005, and its importance in assessing Hg contamination. *Applied Geography* 29 (1):125-134. doi:10.1016/j.apgeog.2008.08.005.
- Rhoads, B.L. 2003. Protocols for Geomorphic Characterization of Meander Bends in Illinois.
- Rhoads, B. L. 2003. Protocols for geomorphic characterization of meander bends in Illinois. Prepared for Illinois Department of Natural Resources, Conservation 2000 Ecosystems Project – Embarras River 001-98, Department of Geography, University of Illinois, Urbana.
- Richard, G. A., P. Y. Julien, and D. C. Baird. 2005. Statistical analysis of lateral migration of the Rio Grande, New Mexico. *Geomorphology* 71 (1-2):139-155. doi:10.1016/j.geomorph.2004.07.013.

- Richardson, J. M., and I. C. Fuller. 2010. Quantification of channel planform change on the lower Rangitikei River, New Zealand, 1949-2007: response to management? *GeoScience* ISSN 1179-4968.
- Ritchie, J. C., and J. R. McHenry. 1990. Application of radioactive fallout cesium-137 for measuring soil erosion and sediment accumulation rates and patterns: A review. *Journal of Environmental Quality* 19 (2):215-233.
doi:10.2134/jeq1990.00472425001900020006x.
- Robert, A. 2014. *River processes: An introduction to fluvial dynamics*. New York, NY: Routledge.
- Rogers, T., M. Mitchell, C. Kim, and T. Loesch. 2006. Determining orthophotograph accuracy. *Geospatial Solutions* 16 (3):26-29.
- Rubey, W. W. 1952. Geology and mineral resources of the Hardin and Brussels Quadrangles in Illinois. Paper 201. US Geological Survey, Washington D.C.
- Ruebush, B. C. 2011. In-situ tests of sound-bubble-strobe light barrier technologies to prevent the range expansions of Asian carp. Thesis, University of Illinois at Urbana-Champaign.
- Sampson, S. J., J. H. Chick, and M. A. Pegg. 2009. Diet overlap among two Asian carp and three native fishes in backwater lakes on the Illinois and Mississippi rivers. *Biological Invasions* 11 (3):483-496. doi:10.1007/s10530-008-9265-7.
- Schaffernak, F. 1950. *Grundriss der Flussmorphologie und des Flussbaues*: Vienna, Austria: Springer-Verlag.

- Schoklitsch, A. 1937. *Hydraulic structures: a text and handbook*. New York, NY: The American Society of Mechanical Engineers.
- Schottler, S. P., D. Engstrom, D. Blumentritt, C. Jennings, and L. Triplett. 2010. Fingerprinting sources of sediment in large agricultural river systems. *Final Report to Minnesota Pollution Control Agency, St. Paul* 68.
- Schottler, S. P. 2012. Intensified tile drainage evaluation. Science Museum of Minnesota, Environmental and Natural Resources Trust Fund, Marine, MN.
- Schottler, S. P., J. Ulrich, P. Belmont, R. Moore, J. W. Lauer, D. R. Engstrom, and J. E. Almendinger. 2014. Twentieth century agricultural drainage creates more erosive rivers. *Hydrological Processes* 28 (4):1951-1961. doi:10.1002/hyp.9738.
- Schumm. 1969. River metamorphosis. *Journal of the Hydraulics Division* 95 (1):255-274.
- . 1977. *The fluvial system*. New York, NY: Wiley-Interscience.
- . 1979. Geomorphic thresholds: The concept and its applications. *Transactions of the Institute of British Geographers* 4 (4):485-515. doi:10.2307/622211.
- . 1985. Patterns of alluvial rivers. *Annual Review of Earth and Planetary Sciences* 13 (1):5-27. doi:10.1146/annurev.ea.13.050185.000253.
- Schumm, S. A., and R. W. Licity. 1965. Time, space, and causality in geomorphology. *American Journal of Science* 263 (2):110-119. doi:10.2475/ajs.263.2.110.
- Severinghaus, L. L., and L. Chi. 1999. Prayer animal release in Taiwan. *Biological Conservation* 89 (3):301-304. doi:10.1016/S0006-3207(98)00155-4.

- Shields Jr., F. D., A. Simon, and L. J. Steffen. 2000. Reservoir effects on downstream river channel migration. *Environmental Conservation* 27 (1):54-66.
- Simon, A. 1989. A model of channel response in disturbed alluvial channels. *Earth Surface Processes and Landforms* 14 (1):11-26. doi:10.1002/esp.3290140103.
- Simon, A., and A. J. C. Collison. 2002. Quantifying the mechanical and hydrologic effects of riparian vegetation on streambank stability. *Earth Surface Processes and Landforms* 27 (5):527-546. doi:10.1002/esp.325.
- Simon, A., and C. R. Thorne. 1996. Channel adjustment of an unstable coarse-grained stream: opposing trends of boundary and critical shear stress, and the applicability of extremal hypotheses. *Earth Surface Processes and Landforms* 21 (2):155-180. doi:10.1002/(SICI)1096-9837(199602)21:2<155::AID-ESP610>3.0.CO;2-5.
- Simons, D. B., and M. L. Albertson. 1960. Uniform water conveyance channels in alluvial materials. *Journal of the Hydraulics division* 86 (5):33-71.
- Sin, S. N., H. Chua, W. Lo, and L. M. Ng. 2001. Assessment of heavy metal cations in sediments of Shing Mun River, Hong Kong. *Environment International* 26 (5-6):297-301. doi:0.1016/S0160-4120(01)00003-4.
- Slama, C. C., C. Theurer, and S. W. Henriksen. 1980. *Manual of photogrammetry*. Falls Church, VA: American Society of photogrammetry.
- Smakhtin, V. U. 2001. Low flow hydrology: A review. *Journal of Hydrology* 240 (3-4):147-186. doi:10.1016/S0022-1694(00)00340-1.

- Smith, M. L. 2017. Minnesota's largest invasive carp caught in Redwood Falls. *Star Tribune*. <http://www.startribune.com/minnesota-s-largest-invasive-carp-caught-in-redwood-falls/427263551/> (accessed April, 5 2018).
- Smith, N. D., and D. G. Smith. 1984. William River: An outstanding example of channel widening and braiding caused by bed-load addition. *Geology* 12 (2):78-82. doi:10.1130/0091-7613(1984)12<78:WRAOEO>2.0.CO;2.
- Spangler, T. 2014. \$18 billion would keep Asian carp out of Great Lakes. *USA Today*. <https://www.usatoday.com/story/news/nation/2014/01/06/asian-carp-report-great-lakes/4348241/> (accessed April 5, 2018).
- Steil, M. 2007. NOAA says Dead Zone could be largest ever. *MPR News*. <https://www.mprnews.org/story/2007/07/17/deadzonesize> (accessed April, 5, 2018).
- Steinberg, S. L., and S. J. Steinberg. 2015. *Gis research methods: Incorporating spatial perspectives*. Redlands, CA: Esri Press.
- Strupczewski, W. G., V. P. Singh, and W. Feluch. 2001. Non-stationary approach to at-site flood frequency modelling I. Maximum likelihood estimation. *Journal of Hydrology* 248 (1-4):123-142. doi:10.1016/S0022-1694(01)00397-3.
- Surian, N., and A. Cisotto. 2007. Channel adjustments, bedload transport and sediment sources in a gravel-bed river, Brenta River, Italy. *Earth Surface Processes and Landforms* 32 (11):1641-1656. doi:10.1002/esp.1591.

- Surian, N., L. Mao, M. Giacomini, and L. Ziliani. 2009. Morphological effects of different channel-forming discharges in a gravel-bed river. *Earth Surface Processes and Landforms* 34 (8):1093-1107. doi:10.1002/esp.1798.
- Tal, M., K. Gran, A. B. Murray, C. Paola, and D. M. Hicks. 2004. Riparian vegetation as a primary control on channel characteristics in multi-thread rivers. *Riparian Vegetation and Fluvial Geomorphology* 1:43-58. doi:10.1029/008WSA04.
- Tal, M., and C. Paola. 2007. Dynamic single-thread channels maintained by the interaction of flow and vegetation. *Geology* 35 (4):347-350. doi:10.1130/G23260A.1.
- Teller, J. T., D. W. Leverington, and J. D. Mann. 2002. Freshwater outbursts to the oceans from glacial Lake Agassiz and their role in climate change during the last deglaciation. *Quaternary Science Reviews* 21 (8-9):879-887. doi:10.1016/S0277-3791(01)00145-7.
- Thorleifson, L. 1996. Review of Lake Agassiz history. *Sedimentology, Geomorphology, and History of the Central Lake Agassiz Basin*. Geological Association of Canada Field Trip Guidebook B 2:55-84.
- Thorne, C., C. Alonso, D. Borah, S. Darby, P. Diplas, P. Julien, D. Knight, J. Pizzuto, M. Quick, and A. Simon. 1998. River width adjustment. I: Processes and mechanisms. *Journal of Hydraulic Engineering* 124 (9): 881-902. doi:10.1061/(ASCE)0733-9429(1998)124:9(881).

- Thorne, C., J. Murphey, and W. Little. 1981. Bank stability and bank material properties in the bluffline streams of northwest Mississippi. *Appendix D, Report to the Corps of Engineers, Vicksburg District under Section 32.*
- Thorne, C. R., A. P. G. Russell, and M. K. Alam. 1993. Planform pattern and channel evolution of the Brahmaputra River, Bangladesh. *Geological Society, London, Special Publications 75* (1):257-276. doi:10.1144/GSL.SP.1993.075.01.16.
- Thorne, C. R., and N. K. Tovey. 1981. Stability of composite river banks. *Earth Surface Processes and Landforms* 6 (5):469-484. doi:10.1002/esp.3290060507.
- Tip of the Mitt Watershed Council. 2014. How to Identify bighead, silver, black, and grass carp. <http://www.watershedcouncil.org/learn/aquatic%20invasive%20species/asian-carp/how-to-identify-bighead-and-silver-carp/> (accessed April 25, 2015)
- Trimble, S. W., and R. U. Cooke. 1991. Historical sources for geomorphological research in the United States. *The Professional Geographer* 43 (2):212-228. doi:10.1111/j.0033-0124.1991.00212.x.
- U.S. Department of the Interior. 1996. National Mapping Program Technical Instructions, Part 2. Reston, Virginia.
- Unwin, D. J. 1995. Geographical information systems and the problem of 'error and uncertainty'. *Progress in Human Geography* 19 (4):549-558.
- Upham, W. 1896. *The glacial lake agassiz*. US Geological Survey, Washington D.C.
- Urban, M. A., and B. L. Rhoads. 2003. Catastrophic human-induced change in stream-channel planform and geometry in an agricultural watershed, Illinois, USA.

Annals of the Association of American Geographers 93 (4):783-796.

doi:10.1111/j.14678306.2003.09304001.x.

USACE. 2007. Minnesota River 9-foot channel project - Dredged material management plan/environmental assessment - Minnesota River about I-35W bridge. US Army Corps of Engineers, St. Paul, MN

———. 2014. GLMRIS Report: Great Lakes and Mississippi River Interbasin Study. cited 4/15/2015. US Army Corps of Engineers.

VanLooy, J. A., and C. W. Martin. 2005. Channel and vegetation change on the Cimarron River, southwestern Kansas, 1953–2001. *Annals of the Association of American Geographers* 95 (4):727-739. doi:10.1111/j.1467-8306.2005.00483.x.

Vogel, R. M., C. Yaindl, and M. Walter. 2011. Nonstationarity: Flood magnification and recurrence reduction factors in the United States. *Journal of the American Water Resources Association* 47 (3):464-474. doi:10.1111/j.1752-1688.2011.00541.x.

Vörösmarty, C. J., M. Meybeck, B. Fekete, K. Sharma, P. Green, and J. P. M. Syvitski. 2003. Anthropogenic sediment retention: Major global impact from registered river impoundments. *Global and Planetary Change* 39 (1-2):169-190. doi:10.1016/S0921-8181(03)00023-7.

Wang, D., and M. Hejazi. 2011. Quantifying the relative contribution of the climate and direct human impacts on mean annual streamflow in the contiguous United States. *Water Resources Research* 47 (10). doi:10.1029/2010WR010283.

- Wellmeyer, J. L., M. C. Slattery, and J. D. Phillips. 2005. Quantifying downstream impacts of impoundment on flow regime and channel planform, lower Trinity River, Texas. *Geomorphology* 69 (1-4):1-13.
doi:10.1016/j.geomorph.2004.09.034.
- Wickert, A. D., J. M. Martin, M. Tal, W. Kim, B. Sheets, and C. Paola. 2013. River channel lateral mobility: metrics, time scales, and controls. *Journal of Geophysical Research: Earth Surface* 118 (2):396-412.
doi:10.1029/2012JF002386.
- Williams, G. P. 1978. Bank-full discharge of rivers. *Water Resources Research* 14 (6):1141-1154. doi:10.1029/WR014i006p01141.
- Winterbottom, S. J. 2000. Medium and short-term channel planform changes on the Rivers Tay and Tummel, Scotland. *Geomorphology* 34 (3-4):195-208.
doi:10.1016/S0169-555X(00)00007-6.
- Wishart, D., J. Warburton, and L. Bracken. 2008. Gravel extraction and planform change in a wandering gravel-bed river: The River Wear, Northern England. *Geomorphology* 94 (1-2):131-152. doi: 10.1016/j.geomorph.2007.05.003.
- Wohl, E. 2012. Identifying and mitigating dam-induced declines in river health: Three case studies from the western United States. *International Journal of Sediment Research* 27 (3):271-287. doi:10.1016/S1001-6279(12)60035-3.
- Wright Jr, H., K. Lease, and S. Johnson. 1998. Glacial River Warren, Lake Pepin, and the environmental history of southeastern Minnesota. In *Contributions to quaternary*

- studies in Minnesota*. ed. C.J. Patterson and H.E. Wright Jr., 131-140.
Minneapolis, MN: Minnesota Geological Survey Report on Investigations.
- Yalin, M. S., and A. F. Da Silva. 2001. *Fluvial processes*. London, England: CRC Press.
- Yang, C. T. 1971. On river meanders. *Journal of Hydrology* 13:231-253.
doi:10.1016/0022-1694(71)90226-5.
- Yao, Z., J. Xiao, W. Ta, and X. Jia. 2013. Planform channel dynamics along the Ningxia–Inner Mongolia reaches of the Yellow River from 1958 to 2008: Analysis using Landsat images and topographic maps. *Environmental Earth Sciences* 70 (1):97-106. doi:10.1007/s12665-012-2106-0.
- Yuan, F., P. Larson, R. Mulvihill, D. Libby, J. Nelson, T. Grupa, and R. Moore. 2017. Mapping and Analyzing Stream Network Changes in Watonwan River Watershed, Minnesota, USA. *International Journal of Geo-Information* 6 (11):369. doi:10.3390/ijgi6110369.
- Yuan, F., and M. Mitchell. 2014. Long-term climate change at four rural stations in Minnesota, 1920-2010. *Journal of Geography and Geology* 6 (3):228.
- Zanoni, L., A. Gurnell, N. Drake, and N. Surian. 2008. Island dynamics in a braided river from analysis of historical maps and air photographs. *River Research and Applications* 24 (8):1141-1159. doi:10.1002/rra.1086.
- Zapata, F. 2003. The use of environmental radionuclides as tracers in soil erosion and sedimentation investigations: recent advances and future developments. *Soil and Tillage Research* 69 (1-2):3-13. doi:10.1016/S0167-1987(02)00124-1.

Appendix

Appendix A

Full registry of every collected aerial photograph used in this study sorted by year and county.

County & Year	Photo I.D. Number	Number of GCPs Used	Total RMS Error	
Blue Earth 1937	BJG-1-3**	8	0.943136	
	BIP-5-92**	8	0.718186	
	BIP-9-9**	8	0.661759	
	BIP-9-35**	9	0.936103	
Le Sueur 1937	BJG-2-25**	8	0.803199	
	WF-5-338	8	0.748209	
	WF-5-341	8	0.715205	
	WF-5-396	8	0.915635	
	WF-5-398	8	0.991539	
	WF-5-345	8	0.475706	
	WF-5-347	8	0.635866	
	WF-5-348	10	0.978789	
	WF-5-404	8	0.853785	
	WF-5-406	9	0.889252	
	WF-5-407	8	0.771299	
	WF-5-409	8	0.923454	
	WF-5-356	8	0.867018	
	WF-5-354	9	0.931321	
	Scott 1937	BJM-3-83**	9	0.891791
		WJ-9-395	8	0.615319
WJ-9-393		8	0.809855	
WJ-9-392		8	0.854515	
BJM-4-100**		8	0.859631	
WJ-7-326		8	0.927112	
WJ-7-305		8	0.803489	
WJ-5-255		8	0.776959	
WJ-5-227		8	0.778667	
WJ-5-217		9	0.568294	
WJ-5-219		8	0.863107	
WJ-5-221		8	0.865138	
WJ-5-223		9	0.85996	
WJ-5-178		9	0.917537	
WJ-4-172		9	0.88825	
WJ-4-123		8	0.968202	

	WJ-5-268	8	0.985806
	WJ-3-78	9	0.913501
	WJ-3-73	8	0.835747
	WK-10-752	8	0.552281
Dakota 1937	WK-6-490	8	0.647758
	WK-8-650	9	0.892791
	WK-8-648	8	0.788822
	WK-5-368	8	0.959985
	WK-8-642	8	0.918655
	WN-2-146	8	0.393456
Blue Earth 1951	BIP-2G-209*	9	0.921057
	BIP-1G-144*	10	0.891252
	BIP-2G-130*	8	0.699735
	BIP-2G-160*	8	0.627338
Le Sueur 1951	WF-01H-150	9	0.6684
	WF-02H-048	9	0.994594
	WF-02H-057	8	0.971867
	WF-05H-018	8	0.782464
	WF-04H-004	8	0.775642
	WF-04H-102	8	0.951251
	WF-04H-109	8	0.708532
	WF-02H-203	8	0.823723
	WF-02H-124	9	0.668544
	WF-02H-117	8	0.735107
Scott 1951	WJ-3H-3	10	0.948917
	WJ-3H-115	8	0.96663
	WJ-3H-120	9	0.9747
	WJ-3H-122	9	0.744484
	WJ-5H-173	8	0.99068
	WJ-5H-171	8	0.708331
	WJ-4H-51	8	0.964089
	WM-4H-79	9	0.926328
	WM-5H-74	12	0.641114
	WM-2H-119	8	0.636515
	WM-2H-193	9	0.760185
	WJ-2H-191	10	0.86426
	WJ-2H-189	8	0.83109
	WJ-5H-124	8	0.376638
	WJ-5H-126	9	0.823913

	WJ-2H-183	8	0.834361
	WJ-2H-182	9	0.782781
	WJ-2H-180	10	0.961046
Dakota 1951	WK-2H-178	9	0.845294
	WK-5H-136	8	0.9113
	WK-5H-181	8	0.820057
	WK-5H-204	8	0.8903
Carver 1964	WJ-3EE-64	8	0.846215
	WJ-5EE-117	8	0.889534
	WJ-1EE-228	8	0.49325
	WJ-1EE-226	8	0.467654
	WJ-4EE-159	8	0.632615
	WJ-4EE-157	8	0.825204
	WJ-2EE-108	8	0.700044
	WJ-5EE-14	9	0.788962
	WJ-2EE-205	8	0.410915
	WJ-4EE-148	8	0.999628
Hennepin 1964	WN-1EE-8	8	0.535465
	WN-1EE-5	8	0.725886
	WN-1EE-4	8	0.459552
	WN-1EE-30	8	0.857565
	WN-1EE-26	8	0.558263
	WN-1EE-2	8	0.999143
	WN-1EE-16	8	0.245725
	WN-1EE-14	8	0.61563
	WK-4EE-69	8	0.560000
	WK-3EE-122	9	0.736709
	WJ-5EE-9	8	0.985039
	WJ-5EE-8	8	0.928404
	WJ-5EE-6	8	0.839852
Nicollet 1964	BIP-1EE-44	10	0.877704
	BIP-1EE-74	9	0.65574
	WF-4EE-91	10	0.892792
	WF-1EE-128	9	0.888442
	WF-4EE-94	8	0.805539
	WF-4EE-96	9	0.577345
	WF-2EE-27	8	0.489471
	WF-5EE-190	8	0.769535
	WF-5EE-192	10	0.918159

	WF-2EE-124	9	0.759734
	WF-5EE-48	8	0.627846
	WF-5EE-59	9	0.880104
	WF-5EE-194	8	0.934425
	WF-4EE-32	8	0.734137
	WF-1EE-5	8	0.987944
Blue Earth 1980	AS-BE-SO-14-79	8	0.817416
	AS-BE-MAN-MA-12	8	0.648751
	AS-BE-MAN-MB-7	8	0.866059
	AS-BE-MAN-MA-1	8	0.895093
	AS-BE-LIME-LM-25	8	0.994281
	AS-BE-LIME-LM-24	8	0.707572
Nicollet 1980	AS-NIC-BEL-BD-12**	8	0.82821
	AS-NIC-OSH-OW-06_E*	8	0.659469
	AS-NIC-OSH-OW-06*	8	0.533789
Le Sueur 1980	AS-LES-KAS-KA-32	9	0.595707
	AS-LES-KAS-KA-28	8	0.500884
	AS-LES-KAS-KA-15	8	0.756206
	AS-LES-KAS-KA-10	8	0.779874
	AS-LES-KAS-KA-04	9	0.559004
	AS-LES-OTT-OT-33	8	0.566047
	AS-LES-OTT-OT-27	8	0.528658
	AS-LES-OTT-OT-22	8	0.864734
	AS-LES-OTT-OT-15	8	0.530746
	AS-LES-OTT-OT-11	8	0.944928
Sibley 1980	AS-SIB-HEN-35	8	0.528763
	AS-SIB-HEN-26	8	0.875494
	AS-SIB-HEN-24	8	0.798729
	AS-SIB-HEN-13*	8	0.824433
	AS-SIB-HEN-13	8	0.978362
	AS-SIB-HEN-12	8	0.989861
	AS-SIB-JESS-35	8	0.906574
	AS-SIB-FAX-07	8	0.627286
	AS-SIB-FAX-34	8	0.666664
	AS-SIB-FAX-35	8	0.798153
	AS-SIB-FAX-36	8	0.844069
Scott 1980	AS-SCO-BLA-R26-36	8	0.77532
	AS-SCO-BLA-R26-25	8	0.960128

	AS-SCO-BLA-R26-24	8	0.889988
	AS-SCO-BLA-R26-13	8	0.951592
	AS-SCO-BLA-R25-18	8	0.927822
	AS-SCO-BLA-R25-8	8	0.933821
	AS-SCO-BLA-R25-5	8	0.537953
	AS-SCO-BLA-R25-4	8	0.572957
	AS-SCO-BLA-R25-3	8	0.927834
	AS-SCO-JACK-02	8	0.759419
	AS-SCO-SHA-T115-R23-01	9	0.848379
	AS-SCO-SHA-T115-R22-06	8	0.277945
	AS-SCO-SHA-T115-R22-05	8	0.425829
	AS-SCO-SHA-T115-R22-04	8	0.419313
	AS-SCO-SAV-06	9	0.93885
	AS-SCO-SAV-08	8	0.872587
	AS-SCO-SHA-T115-R22-01	8	0.787476
Carver 1980	AS-CAR-SANF-T114-R24-31**	8	0.979884
	AS-CAR-SANF-T114-R24-29**	8	0.887107
	AS-CAR-SANF-T114-R24-28**	8	0.763447
	AS-CAR-SANF-T114-R24-15**	8	0.767714
	AS-CAR-SANF-T114-R24-14*	8	0.475768
	AS-CAR-SANF-T114-R24-12*	8	0.63236
	AS-CAR-SANF-T114-R23-7E*	8	0.730462
	AS-CAR-SANF-T114-R23-6E*	8	0.89166
	AS-CAR-CAR-30*	8	0.702322
	AS-CAR-CAR-20*	8	0.825718
	AS-CAR-CAR-17*	8	0.749966
	AS-CAR-CHA-T115-R23-9*	8	0.802729
	AS-CAR-CHA-T115-R23-3*	8	0.891705
Hennepin 1980	AS-HEN-EP-35**	8	0.802236
	AS-HEN-EP-36**	9	0.818521
Dakota 1980	SCAN-L-10-WestHalf	8	0.985676
	SCAN-L-10-EastHalf	8	0.648762
	SCAN-L-11-WestHalf	8	0.344481

	SCAN-L-11-EastHalf	8	0.60665
	SCAN-K-12-WestHalf	8	0.796727
	SCAN-J-12-EastHalf	8	0.680568

Aerial photographs were obtained from the University of Minnesota online Aerial Index or scanned at the Borchert Library. Labeling contains type of image (aerial slide, scanned), county, township, subsection within township, and the corresponding number of the individual photos. *Not all Townships contain subsections.

*= Photo from previous year

**= Photo from following year

Appendix B

“QuantifyingRegistrationError” Script from Lea and Legleiter (2016) with modifications by Mitchell Donovan (Doctoral Candidate at Utah State University).

```
%% Quantifying spatial variations in image registration error
% Devin M. Lea and Carl J. Legleiter
% 'Refining measurements of lateral channel movement from image time
% series by quantifying spatial variations in registration error'
% Correspondance to: Devin Lea (dlea@uoregon.edu)
% Last modified: 11-30-15

%% NOTES:
% This script uses MATLAB functions to iteratively calculate error vectors
% (\epsilon) and the components of the error vectors (\epsilon_x and
% \epsilon_y, sometimes referred to as E_x and E_y) using leave-one-out
% cross-validation for a set of ground control point (GCP) coordinates
% supplied by the user. Eight transformation equations are available to
% the user with the cp2tform function for calculating registration errors
% between the base image coordiantes and the matching predicted image
% coordinates on the warped image. After the error residuals have been
% calculated, the script creates an interpolated surface of error values
% using one of five chosen algorithms. A separate script
% (ChannelChangeSignif.m) uses the error surfaces to compared the
% endpoints of channel migration vectors supplied by the user to determine
% if observed lateral channel migration exceeds local registration error.

% The code and its comments are written with the assumption the user is
% supplying one input image to be registered to a single base image;
% however, the script can be easily modified if more than one input image
% will be registered to the base image.

% Comments with two spaces after the % sign indicate pre-script info
% Comments with one space indicate description of what script is doing
% Comments with zero spaces indicate code that is currently commented out
% but could be used. Comments above the code should note when the code that
% is commented out is suitable to use.

%% CREDITS:
% Devin M. Lea - University of Wyoming, Department of Geography
% Now at University of Oregon, Department of Geography
% dlea@uoregon.edu
% Carl J. Legleiter - Department of Geography, University of Wyoming
% Carl.Legleiter@uwoyo.edu
```



```
%% LICENSE:
% Copyright (C) 2015 Devin M. Lea and Carl J. Legleiter
%
% This program is free software: you can redistribute it and/or modify
% it under the terms of the GNU General Public License as published by
% the Free Software Foundation, either version 3 of the License, or
% any later version.
%
% This program is distributed in the hope that it will be useful,
% but WITHOUT ANY WARRANTY; without even the implied warranty of
% MERCHANTABILITY or FITNESS FOR A PARTICULAR PURPOSE. See the
% GNU General Public License for more details.
%
% For the full GNU General Public License, please see:
% <http://www.gnu.org/licenses/>.
%
% This software is made available to potential users AS IS, without any
% promise of technical support. The user is solely responsible for
% implementing the code for use in his/her own project, without
% assistance from the authors.

%% Manual inputs required from the user + possible changes
% THIS SCRIPT REQUIRES THE FOLLOWING USER INPUTS:
% 1) Base image and warp image GCP locations for each warp and base image
% pair. Locations are provided using image coordinates in a n x 2 matrix,
% where n is the number of GCPs. See the Import ground control points
% section for more details.
% ADDITIONALLY, THE USER MAY WISH TO CHANGE THE FOLLOWING:
% 1) The maximum error value displayed on the y axis for the boxplot in the
% section 'Create boxplot for visualizing error distribution'. The error is
% currently calculated as the rounded 90th percentile error value for the
% transformation method with the largest maximum error. However, this
% inherently will leave out some outlier error values that are off the
% display. The user should change this value (set by the equation
% (round(max(prctile(XYresid_all,90)))) ) dependent on their distribution
% of error and error visualization needs.
% 2) Error residuals used for error surface interpolation. The script is
% set up to create an interpolated surface for E_x and E_y using the
% residual error from the 2nd order polynomial transformation. If error
% from another transformation method is desired, changes need to be made to
% griddata and the caxis in the section 'Create interpolated surface of
% error values'
% 3) The user may wish to edit caxis in the section 'Create interpolated
% surface of error values' to make the positive and negative values on the
```

% colorbar equal in magnitude. Similarly, xlim and ylim could be edited.

```
%% Import ground control points
% After matching locations in an input image and base image with ground
% control points (GCPs) using appropriate software (e.g. Erdas Imagine,
% ENVI), export the GCP coordinates for the input and base images from that
% software to a text file. The coordinates will be saved as image
% coordinates. For the easiest transfer to MATLAB, open the text file in
% Microsoft Excel so that each column represents an X or Y coordinate for
% the base or warp image. In MATLAB, create two new variables in your
% workspace called 'b_GCPs' (for base image GCPs) and 'i_GCPs' (for input
% image GCPs). Copy and paste the X and Y coordinates for the input image
% from Microsoft Excel (or equivalent program) to the variable 'i_GCPs' in
% MATLAB; do the same for the X and Y coordinates from the base image to
% paste into the variable 'b_GCPs'. When you have finished, both 'i_GCPs'
% and 'b_GCPs' variables should be n x 2 double matrices, where n is the
% number of GCPs you matched between the input and base images.

% NOTE: This analysis assumes you are only using two images (base and
% warp). If you have more than one input image you want to register to your
% base image, you will want to edit the variable names to avoid confusion.
% For example, in the Lea and Legleiter study for which this code was
% developed, five input images were registered to the (sixth) base image.
% To avoid confusion, the year of each input image was added to the end of
% its associated 'i_GCPs' and 'b_GCPs' variables.
% Example:
% In the Lea and Legleiter study, the base image was acquired in 2012. One
% of the input images to be registered was acquired in 1980. Thus:
% 'b_GCPs_1980' refers to GCPs placed on the 2012 base that are matched to
% GCPs placed on the 1980 input image
% 'i_GCPs_1980' refers to GCPs placed on the 1980 input image

%% Set up working directory
% Tell MATLAB where to look for any functions we might call
workDir = 'F:\Devon_Thesis\Final_ArcWork\MatLab\MatScript\1964_1980';
cd(workDir);
files = dir('*gcp.txt'); %searching for all files ending in gcp.txt, representing the image
files other than the base/reference image.
baseFile = '1964_1980gcp.txt'; %specify a name for the base file that will be loaded for
b_GCPs.
gcpData = struct; %Sets gcpData up as a structured data variable so it can store the
information efficiently.
```

```

for i = 1:length(files)

yr = files(i).name(1:4);
fprintf(yr);
fprintf('\n');

varNames = {'Id','POINT_X','POINT_Y'}; % variable names I want to keep
gcp2015table = readtable(baseFile,'ReadVariableNames',1,'Delimiter',','); % load base
GCP table
Id = gcp2015table.(varNames{1}); % store Id
POINT_X = gcp2015table.(varNames{2}); % store x coords
POINT_Y = gcp2015table.(varNames{3}); % store y coords
gcp2015table = table(Id,POINT_X,POINT_Y); % replace table by creating new table
with only these vars
gcp2015table = sortrows(gcp2015table,'Id'); % sort table at end because sorting the initial
large table is slower

gcptable = readtable(files(i).name,'ReadVariableNames',1,'Delimiter',','); % load GCP
table for other images
Id = gcptable.(varNames{1}); % store Id
POINT_X = gcptable.(varNames{2}); % store x coords
POINT_Y = gcptable.(varNames{3}); % store y coords
gcptable = table(Id,POINT_X,POINT_Y); % replace table by creating new table with
only these vars
gcptable = sortrows(gcptable,'Id'); % sort table at end because sorting the initial large
table is slower

% intersect the two tables together, keeping only
% ids that appear in both tables
gcpTable = innerjoin(gcptable,gcp2015table,'key','Id');
format long % use this to stop matlab from truncating. default is "format short"
gcpTable;

%Converting table to an array so that I can work with the data.
gcpCoords = table2array(gcpTable);

gcpData(i).year = yr;
gcpData(i).b_GCPs = gcpCoords(:,4:5);
gcpData(i).i_GCPs = gcpCoords(:,2:3);

b_GCPs = gcpCoords(:,4:5);
i_GCPs = gcpCoords(:,2:3);

% If you have more than one input image to be warped as in the Lea and

```

```

% Legleiter study, note you will need to alter the following code for each
% warp and base pair for which you want to assess georegistration error.

% To make sure the GCPs coordinates are generally located correctly in
% space, use a simple scatter plot:
% Scatter plot for base image GCPs
% figure
% scatter(b_GCPs(:,1),b_GCPs(:,2),'b')
% set(gca,'YDir','reverse'); axis equal; box on
% xlabel('Image X coordinate')
% ylabel('Image Y coordinate')
% title('Base Image GCPs','fontsize',14)
% % Scatter plot for input image GCPs
% figure
% scatter(i_GCPs(:,1),i_GCPs(:,2),'r')
% set(gca,'YDir','reverse'); axis equal; box on
% xlabel('Image X coordinate')
% ylabel('Image Y coordinate')
% title('Input Image GCPs','fontsize',14)
% NOTE: The Y-axis is called and reversed in the second command for these
% scatter plots because the origin of image coordinates is usually in the
% top left corner, as opposed to a traditional grid where the origin is
% placed at the bottom left corner (assuming x and y are positive values).

%% Leave-one-out cross-validation for geometric transformation of GCPs
% This section uses a for loop to iteratively withhold one GCP pair,
% transform map coordinates from the input image to the base image using
% the remaining n-1 GCP pairs and one of eight chosen transformation
% equations, and predict the x and y coordinate values of the withheld
% GCP on the resulting warped image by inputting the withheld base GCP
% coordinates into the fit transformation equation.

% Start loop to withhold the j'th pair of input and base GCPs per iteration
for j = 1:length(i_GCPs)
    % Get all GCP x coordinate values from input image
    Xi = i_GCPs(:,1);
    % Set j'th x coordinate equal to new variable and remove the chosen
    % coordinate from the list of all x coordinate values
    Xi_h = Xi(j);
    Xi(j) = [ ];
    % Get all GCP y coordinate values from input image
    Yi = i_GCPs(:,2);
    % Set j'th y coordinate equal to new variable and remove the chosen
    % coordinate from the list of all y coordinate values

```

```

Yi_h = Yi(j);
Yi(j) = [ ];
% Combine Xi and Yi into a single matrix
XYi = [Xi Yi];
% Get all GCP x coordinate values from base image
Xb = b_GCPs(:,1);
% Set j'th x coordinate equal to new variable and remove the chosen
% coordinate from the list of all x coordinate values
Xb_h = Xb(j);
Xb(j) = [ ];
% Get all GCP y coordinate values from base image
Yb = b_GCPs(:,2);
% Set j'th y coordinate equal to new variable and remove the chosen
% coordinate from the list of all y coordinate values
Yb_h = Yb(j);
Yb(j) = [ ];
% Combine Xb and Yb into a single matrix
XYb = [Xb Yb];
% Combine the withheld points from the input and base image into two
% matrices
XYi_h = [Xi_h Yi_h];
XYb_h = [Xb_h Yb_h];
% Fit transformation equations to base image and input image GCP pairs.
% NOTE: Values are divided (and later multiplied) by 1000 in the code
% because large input values sometimes cause an error. This method was
% adopted from a discussion found here:
% http://www.mathworks.com/matlabcentral/newsreader/view\_thread/30091
% tform_sim = cp2tform((XYb/1000),(XYi/1000),'similarity');
% tform_aff = cp2tform((XYb/1000),(XYi/1000),'affine');
% tform_proj = cp2tform((XYb/1000),(XYi/1000),'projective');
% tform_2poly = cp2tform((XYb/1000),(XYi/1000),'polynomial',2);
% tform_3poly = cp2tform((XYb/1000),(XYi/1000),'polynomial',3);
% tform_4poly = cp2tform((XYb/1000),(XYi/1000),'polynomial',4);
% tform_pwl = cp2tform((XYb/1000),(XYi/1000),'piecewise linear');
% tform_lwm = cp2tform((XYb/1000),(XYi/1000),'lwm');
% Predict x and y coordinate values of withheld input image GCP using
% transformation equations & combine coordinates into a matrix
% 2nd Order Polynomial
% [xm4, ym4] = [Xi_h/1000, Yi_h/1000];
BPred = [Xi_h Yi_h];

% Calculate residual vector distance XY (i.e., Euclidian distance, also
% referred to as error vector /epsilon in the manuscript) and its x and
% y components for each transformation method

```

```

% 2nd Order Polynomial
Xresid(j) = (Xb_h - (Xi_h));
Yresid(j) = (Yb_h - (Yi_h));
XYresid(j) = pdist2(XYb_h,(BPred));

end

% Transpose vectors containing error residuals
gcpData(i).Xresid = Xresid';
gcpData(i).Yresid = Yresid';
gcpData(i).XYresid = XYresid';

% Calculate maximum error, minimum error, and root-mean-square error for
% the residual vector distances from each transformation method
%maxE = max(XYresid');
%minE = min(XYresid');
XY2resid = XYresid'.^2;
RMSE = sqrt(((sum(XY2resid))/(length(XY2resid))));

% clearvars Xresid Yresid XYresid b_GCPs i_GCPs

end

%% Plot histograms of error vectors
% Use the histograms to understand the distribution of error for each
% transformation method

hist(Xresid)
hist(Yresid)
hist(XYresid)

%% Create boxplot for visualizing error distribution

% Create the boxplot
boxplot(XYresid,'colors','k','symbol','k*')
% The user may wish to change the maximum error displayed on the y axis;
% see Manual inputs + possible changes section for more details
axis([0.5,1.5,-0.5,(round(max(prctile(XYresid,100))))])
x1 = xlabel('Transformation Type','FontSize',15);
ylabel('GCP error (m)','FontSize',15);

%% ANOVA test

```

```

% Tests statistical difference between means of eight transformation
% methods
% [p,table,stats] = anova1(XYresid_all);
% c = multcompare(stats);

% %% Create interpolated surface of error values
% %% Create meshgrid for calculating interpolated surface. Meshgrid size is
% %% set by the minimum and maximum x and y values. A value 10% the size of
% %% the range of all x and y values is added or subtracted to the meshgrid to
% %% provide a buffer of space around the area of interest.
% [X,Y] = meshgrid((round(min(b_GCPs(:,1)))+0.5)-(round(range(b_GCPs(:,1))/10)):...
% 1:(round(max(b_GCPs(:,1)))+0.5)+(round(range(b_GCPs(:,1))/10)),...
% (round(min(b_GCPs(:,2)))+0.5)-(round(range(b_GCPs(:,2))/10)):...
% 1:(round(max(b_GCPs(:,2)))+0.5)+(round(range(b_GCPs(:,2))/10)));
% %% Translate values of base GCPs so they plot correctly with meshgrid
% bGCPs_trans = [(b_GCPs(:,1)-(min(b_GCPs(:,1)))+range(b_GCPs(:,1))/10) ...
% (b_GCPs(:,2)-(min(b_GCPs(:,2)))+range(b_GCPs(:,2))/10)];
% %% Use griddata to create an interpolated surface of error for E_y and E_x
% %% (Vqy and Vqx, respectively) across the area defined by the convex hull of
% %% the GCPs
% Vqy = griddata(b_GCPs(:,1),b_GCPs(:,2),Yresid,X,Y,'linear');
% Vqx = griddata(b_GCPs(:,1),b_GCPs(:,2),Xresid,X,Y,'linear');
%
% %% Create figure to show interpolated error surface for E_y
% %% NOTE: This does NOT show error and image coordinates in their true
% %% location in space; the images are designed just to help the user
% %% visualize areas of higher and lower error.
% figure
% kk = image(Vqy,'CDataMapping','scaled');
% %% Set x and y axes limits
% xlim([0 round(range(b_GCPs(:,1))+((round(range(b_GCPs(:,1))/10)*2)))]
% ylim([0 round(range(b_GCPs(:,2))+((round(range(b_GCPs(:,2))/10)*2)))]
% xlabel('Image X coordinate')
% ylabel('Image Y coordinate')
% title('Interpolated \epsilon_y surface','fontsize',14)
% %% Set all nan values outside the interpolated error surface to white
% set(kk,'alphadata',~isnan(Vqy))
% %% Set colormap
% colormap('jet')
% %% Colorbar, axes, and labeling
% h = colorbar;
% caxis([(min(Yresid)-(range(Yresid)/20)) ...
% (max(Yresid)+(range(Yresid)/20))])
% ylabel(h, '\epsilon_y','fontsize',16)

```

```

% % Keep figure and use scatterplot to show locations of base GCPs on
% % interpolated surface
% hold on
% hh = scatter(bGCPs_trans(:,1),bGCPs_trans(:,2),50);
% set(hh,'MarkerEdgeColor','k','LineWidth',1.2)
%
% % Create figure to show interpolated error surface for E_x
% % NOTE: This does NOT show error and image coordinates in their true
% % location in space; the images are designed just to help the user
% % visualize areas of higher and lower error.
% figure
% kk = image(Vqx,'CDataMapping','scaled');
% % Set x and y axes limits
% xlim([0 round(range(b_GCPs(:,1))+((round(range(b_GCPs(:,1))/10))*2))])
% ylim([0 round(range(b_GCPs(:,2))+((round(range(b_GCPs(:,2))/10))*2))])
% xlabel('Image X coordinate')
% ylabel('Image Y coordinate')
% title('Interpolated \epsilon_x surface','fontsize',14)
% % Set all nan values outside the interpolated error surface to white
% set(kk,'alphadata',~isnan(Vqx))
% % Set colormap
% colormap('jet')
% % Colorbar, axes, and labeling
% % Colorbar axes set by min and max error values +/- 5% of range of error
% h = colorbar;
% caxis([(min(Xresid)-(range(Xresid)/20)) ...
% (max(Xresid)+(range(Xresid)/20))])
% ylabel(h, '\epsilon_x','fontsize',16)
% % Keep figure and use scatterplot to show locations of base GCPs on
% % interpolated surface
% hold on
% hh = scatter(bGCPs_trans(:,1),bGCPs_trans(:,2),50);
% set(hh,'MarkerEdgeColor','k','LineWidth',1.2)

%% End QuantifyRegistrationError.m
% For determining statistical significance of migration vectors, use
% ChannelChangeSignif.m
% Save a .mat file of the variables generated in this script and load them
% for use with ChannelChangeSignif.m
save RegErrorResults.mat

```


Appendix C

R script written by Mitchell Donavan from Utah State University and modified Devon Libby to fit the data used in this study

```
library("MASS") #required for 'calibrate'
#install.packages("G:/F_Drive_Arc_BU/Final_ArcWork/Error_Calc/Digitizing_Error/CSV/Library/calibrate_1.7.2.zip")
library(calibrate) #Required for textxy that labels points.
```

```
years = c(1937,1951,1964,1980,1991,2013)
```

```
setwd("G:/F_Drive_Arc_BU/Final_ArcWork/Error_Calc/Digitizing_Error/CSV")
```

```
for (year in years){
  files = list.files(pattern= paste(year,"_*",sep=""))
  for (curr_file in files){
    for (j in (1:length(files))) {
      err_data = read.csv(curr_file)

      err_df=data.frame(matrix(NA, nrow = length(err_data[,1]), ncol = length(files)))
      colnames(err_df)=c("er_1_2","er_1_3","er_1_4","er_2_3','er_2_4','er_3_4')

      assign(paste('err',j,sep="), abs(err_data$Mig_dist))
    }
    assign(paste('err',year,'_tot',sep="), c(err1, err2, err3, err4, err5, err6))
  }
}
```

```
#-----
```

```
#calculating quantiles
```

```
x = seq(from=0,to=1,by=.05)
```

```
quant.table= data.frame(matrix(NA, nrow = length(x), ncol = length(years)))
```

```
colnames(quant.table)=c('1937','1951','1964','1980','1991','2013')
```

```
quant.table$pctl= x
```

```
i=1
```

```
for (n in x){
```

```
  q1937 = round(quantile(err1937_tot,n),2)
```

```
  q1951 = round(quantile(err1951_tot,n),2)
```

```
  q1964 = round(quantile(err1964_tot,n),2)
```

```

q1980 = round(quantile(err1980_tot,n),2)
q1991 = round(quantile(err1991_tot,n),2)
q2013 = round(quantile(err2013_tot,n),2)

qtot=c(q1937,q1951,q1964,q1980,q1991,q2013)
j=1
for (k in qtot){
  quant.table[i,j] = k
  j=j+1
}
i=i+1
}

#plotting the quantile distritbutions for each year
for (j in 1:7){
  if (j==1){
    plot(x,quant.table[,j],type='l',lty=j,ylim=c(0,18),
         xlab='Quantile',ylab='Digitizing Error (m)',main='Image Digitizing Error')
  }
  else{
    par(new=T)
    plot(x,quant.table[,j],type='l',lty=j,ylim=c(0,18),xlab="",ylab="")
  }
}

grid(nx=NULL)
legend(.1,15,c('1937','1951','1964','1980','1991','2013'),lty=c(1,2,3,4,5,6))

boxplot(quant.table, main ='Digitizing Inconsistency', ylab='False Migration
(m)',xlab='Image year')
grid(nx=NULL)
dev.copy2pdf(file='G:/F_Drive_Arc_BU/Final_ArcWork/Error_Calc/Digitizing_Error/C
SV Boxplots.pdf.', width = 12, height = 8)

```

Appendix D

“ChannelChangeSignif” MATLAB script created by Lea and Legleiter (2016) with additional lines of code added by Devon Libby.

```

%% Assess statistical significance of lateral channel change
% Devin M. Lea and Carl J. Legleiter
% 'Refining measurements of lateral channel movement from image time
% series by quantifying spatial variations in registration error'
% Correspondance to: Devin Lea (dlea@uoregon.edu)
% Last modified: 11-30-15

%% NOTES:
% This script is used to assess the statistical significance of
lateral
% migration vectors. After interpolated surfaces are generated using
% QuantifyRegistrationError.m, this script uses the endpoint verticies
of
% lateral migration vectors to create an error ellipse around the
vertex
% on the time 1 channel centerline and determines if the vertex on the
% time 2 channel cenerline is inside or outside the error ellipse
polygon.
% If the vertex in time 2 is outside the error ellipse, the migration
is
% statistically significant, while if the vertex in time 2 is
contained in
% the error ellipse polygon the migration distance does not exceed the
% error threshold and the change is not statistically significant.

% The code and its comments are written with the assumption the user
is
% supplying one set of migration vectors from the registration of one
% input image to a base image; however, comments describe where the
script
% can be modified if more than one set of migration vectors are being
% assessed for significant channel change.

% Comments with two spaces after the % sign indicate pre-script info
% Comments with one space indicate description of what script is doing
%Comments with zero spaces indicate code that is currently commented
out
%but could be used. Comments above the code should note when the code
that
%is commented out is suitable to use.

%% CREDITS:
% Devin M. Lea - University of Wyoming, Department of Geography
% Now at University of Oregon, Department of Geography
% dlea@uoregon.edu
% Carl J. Legleiter - Department of Geography, University of Wyoming
% Carl.Legleiter@uwyo.edu

```

```

%% LICENSE:
% Copyright (C) 2015 Devin M. Lea and Carl J. Legleiter
%
% This program is free software: you can redistribute it and/or modify
% it under the terms of the GNU General Public License as published by
% the Free Software Foundation, either version 3 of the License, or
% any later version.
%
% This program is distributed in the hope that it will be useful,
% but WITHOUT ANY WARRANTY; without even the implied warranty of
% MERCHANTABILITY or FITNESS FOR A PARTICULAR PURPOSE. See the
% GNU General Public License for more details.
%
% For the full GNU General Public License, please see:
% <http://www.gnu.org/licenses/>.
%
% This software is made available to potential users AS IS, without
any
% promise of technical support. The user is solely responsible for
% implementing the code for use in his/her own project, without
% assistance from the authors.

%% Manual inputs required from the user + possible changes

% THIS SCRIPT REQUIRES THE FOLLOWING USER INPUTS:
% 1) Variables calculated in QuantifyRegistrationError.m. Load them
here if
% needed.
load RegErrorResults.mat
% 2) Migration vector distances, endpoint coordinates, and ID numbers
for
% each endpoint coordinate and for each migration vector. See TestData
% Excel file for an example and 'Calculate statistical significance of
% migration vectors' section of this script for more details.
% 3) Real world coordinates from the top left corner of your base
image.
% This is needed to convert the GCP coordinates in 'b_GCPs' from image
% coordinates to real world coordinates. This study assumes you will
use
% UTM coordinates. In ArcGIS you can find the real world coordinate
% information about the top, left, right, and bottom pixel columns or
rows
% by right-clicking your raster base image in the table of contents and
% selecting Properties -> Source. Find the values and set the
coordinate
% for the x direction (i.e., easting for UTM) equal to the easting
variable
% in this section. Similarly, set the coordinate for the y direction
(i.e.,
% northing for UTM) equal to the northing variable.
easting = 0;
northing = 0;
% 4) Digitizing error. This is the estimated error associated with the

```

```
% user's channel bankline digitizing. The Lea and Legleiter study
assumed
% this error was 2 meters based on precedence (set by Micheli and
Kirchner,
% 2002; see reference in Lea and Legleiter) and based on image
resolution
% of the images used in Lea and Legleiter. However, this variable will
% change based on the user and image resolution and should be changed
% accordingly in this section before error and statistical significance
of
% change is assessed.
digError = 1.62;
% ADDITIONALLY, THE USER MAY WISH TO CHANGE THE FOLLOWING:
% 1) The type of interpolation calculated for scatteredInterpolant in
the
% section 'Calculate statistical significance of migration vectors'.
See
% MATLAB help on scatteredInterpolant for more information of the types
of
% interpolation available.
% 2) If more than one pair of images are being analyzed for
statistically
% significant change, the user might need to use different equations.
The
% locations where these changes would be made is noted throughout the
% script.

%% Generating lateral migration vectors in ArcGIS
% In this section, real-world coordinates from the endpoints of lateral
% channel migration vectors (x_m1, y_m1; x_m2, y_m2 from Fig. 3) are
pasted
% into a matrix called MigVecChng. This matrix also will contain a
specific
% ID for each migration vector, a pair ID linking the two coordinates
that
% define the migration vector, and the calculated migration vector
% distance. All of these variables making up the matrix are created and
% calculated in ArcGIS using the Planform Statistics Tools developed by
Wes
% Lauer (currently at Seattle University). These tools are available
for
% download at the National Center for Earth-Surface Dynamics website
% through the University of Minnesota at this webpage:
% http://www.nced.umn.edu/content/stream-restoration-toolbox

% The following section provides a detailed description of the steps
that
% must be completed before the code at the end of the section can be
run to
% calculate significant and not significant migration vectors.

% Visit the NCED website noted above, open the Planform Statistics tab,
and
% download the ArcMap addin called PlanformTools2.0.esriAddIn to your
```

```

% working folder. You can also download other useful files, such as the
% powerpoint file named PlanformStatisticsTools_v2.0 for ArcGIS 10,
which
% shows how all addin tools can be used.
% Launch ArcMap and from the main menu select Customize -> Add-In
Manager
% to verify Planform Tools have installed successfully. Click on the
% Customize button and then New to set up a new toolbar from which you
can
% access the tools. Give the toolbar a name like Planform Stats and
click
% OK; a new, empty toolbar should be added to your ArcMap window. Place
the
% tools on the toolbar by going to Commands tab of the Customize dialog
and
% look under Add-In Controls, where you should see the three tools
listed
% in the Commands panel. Highlight each of these tools in turn and drag
it
% onto your new toolbar.

% Now you can digitize the bankfull channel for each image. Create a
% shapefile (polyline) for each image. Load the bankline shapefiles
into
% ArcMAP and used the Editor Toolbar to start an editing session.
Again,
% define the bankfull channel, which will not necessarily correspond to
the
% edge of the water, especially if the image was acquired at low-flow
% conditions. The edge of continuous vegetation is generally a good
% indicator of bankfull stage. For each image date, create separate
left
% and right banklines. Always digitize all banklines in the same
direction,
% from upstream to downstream. Also, terminate your two banklines at
the
% same position along the channel (i.e., don't extend one bankline
further
% downstream on one side of the channel than on the other side). If
your
% channel splits into multiple channels, interpret which is the main
active
% channel and define your banklines for that channel alone.
% NOTE: the digitizing can also be performed in other software packages
% (e.g., ENVI); just export your vectors as shapefiles and load them
into
% ArcMAP when you are finished digitizing.

% When you have digitized both banklines along your reach of interest,
you
% can use the Centerline Interpolation tool in the Planform Statistics
% tools to create a channel centerline based on the banklines. See the
% associated PowerPoint for more details on the tool. To use the tool,

```

```

% click on the icon with two parallel lines and a series of dots
between
% the lines. You will be prompted to select the left bankline (left
side of
% the channel when facing downstream) - click OK then on the
appropriate
% bankline, which should be highlighted in blue. Repeat this process
for
% the right bankline. Next, you will be asked to specify a distance
between
% centerline points; a value of ~20% of the mean bankfull width is
% recommended. Enter the maximum number of points to find - set this to
a
% very large value, like 10,000. After the tool runs, you will be
prompted
% to enter a new output shapefile name. You can now load the centerline
% into ArcMap and compare it to the position of your two banklines.
Repeat
% this process for each image and its pair of right and left digitized
% bankfull lines to acquire a bankfull centerline. Along with each
channel
% centerline shapefile, the Centerline Interpolation tool also produces
a
% separate text file. Refer to the PowerPoint for information on the
% contents of the shapefile and text file.

% After you have created an interpolated centerline for your images you
can
% move on to measuring lateral channel migration. To do so, use the
Lateral
% Distance Measurement tool from the Planform Statistics toolbox.
First,
% you will be prompted to select the 'to' centerline to which distances
% will be measured to determine how far the channel has moved - this is
the
% earlier (in time) centerline. Next select the 'from' or reference
% centerline (the latter dated image) that is used to store the
migration
% distance data. You will then be asked whether you want to consider
apex
% lines that connect bends that move by downstream translation; you
usually
% will not need this tool (but consult the PowerPoint for more
information)
% and you can just click OK. After the tool runs you will be asked to
% specify an output file name and a lateral distance from the centerline
for
% drawing polygons created by this tool. A value about 1.5 times the
mean
% channel width when the images were acquired should be sufficient. The
% tool will run some more and a number of lines will appear on your
map,
% representing the inferred migration trajectory of the channel
centerline

```

```

% between your two image dates.

% The lines indicating inferred migration trajectories are actually
just
% graphics that are not included in a shapefile. The migration distance
% algorithm described in the PowerPoint file also creates a set of
three
% intermediate centerlines, which you can delete by selecting them with
the
% black arrow tool and pressing delete; be careful to select the
% intermediate centerlines and not the perpendicular lines, which
represent
% inferred migration trajectories. Once you have isolated the
trajectory
% lines, convert them into a separate shapefile by right clicking on
the
% name of the data frame (i.e., Layers) in the table of contents, and
the
% choosing Convert Graphics to Features. In the resulting dialog, make
sure
% Line graphics is selected, specify an output shapefile name, and
click
% OK. You can then add the new migration trajectory line shapefile
directly
% to your ArcMap document. To add the migration distance information to
% these lines, open the attribute table, select Add Field from the drop
% down list in the upper left, and provide a field name (e.g.,
MigrDist),
% change the Data Type to Float, and set Precision to 10 and Scale to
4.
% Next, right click on the name of the new field and select Calculate
% Geometry, click Yes to continue if prompted, and then OK to calculate
the
% length of each of these lines.

%% Calculate statistical significance of migration vectors
% Create a new variable in MATLAB called MigVecChng, which will be an n
x 5
% matrix, where n is the number of migration vector endpoint vertices
% (the number of migration vectors multiplied by two). The five columns
% will be copied in from the migration vectors shapefile attribute
table
% in ArcMap and will contain the following values:
% column 1 = ID
% column 2 = Pair ID
% column 3 = Migration Dist calculated with Planform Statistics
% column 4 = X coordinate (real-world coordinate; e.g., UTM)
% column 5 = Y coordinate (real-world coordinate; e.g., UTM)
% An example of how your data should look when copied into MATLAB (you
% might want to paste from ArcMap to Excel, clean up the variables in
% Excel, then copy from Excel to MATLAB) is provided in TestData.xlsx.

% Assess the significance of lateral migration vectors against
spatially

```



```

% variable error.
% First, create a series of interpolants that can evaluate the value of
E_y
% and E_x at any query point (i.e., this will be the endpoints of the
% migration vectors) based on the E_y and E_x values supplied at the
% location of each GCP in the base image. The current selected
% interpolation is linear, but see MATLAB's documentation for
% scatteredInterpolant for other possible interpolation methods.
% Fx2 and Fy2 stand for the function being calculated for the second
image
% in the time series (assuming the first image is the base image). If
more
% than one warped image will be used, a sequential numbering can be
% continued, as in the example below.
Xresid = Xresid';
Yresid = Yresid';
Fx2 = scatteredInterpolant(b_GCPs(:,1),b_GCPs(:,2),Xresid,'linear');
Fy2 = scatteredInterpolant(b_GCPs(:,1),b_GCPs(:,2),Yresid,'linear');
%Fx3 =
scatteredInterpolant(btiepnts_2011(:,1),btiepnts_2011(:,2),resid_X,'lin
ear');
%Fy3 =
scatteredInterpolant(btiepnts_2011(:,1),btiepnts_2011(:,2),resid_Y,'lin
ear');

% Create an empty list to populate with 0's (not significant change)
and
% 1's (significant change) for each migration vector.
sigList_SVE = [];
% Start loop for length of the matrix
for ii = 1:length(MigVecChng)
    % If the row number is odd, create a 2 x 2 matrix that contains the
x
    % and y coordinates for the two vertexes defining the end points of
a
    % single migration vector
    if mod(ii,2) ~= 0
        chng = [MigVecChng(ii,4) MigVecChng(ii,5); MigVecChng(ii+1,4)
MigVecChng(ii+1,5)];
        % Use the endpoint of the migration vector that was on the
channel
        % centerline in time 1 to calculate error for E_y and E_x at
that
        % location in space using scatteredinterpolant
        Ey_time2 = Fy2(chng(1,1),chng(1,2));
        Ex_time2 = Fx2(chng(1,1),chng(1,2));
        %Ey_time3 = Fy3(chng(1,1)-300310,4562610-chng(1,2));
        %Ex_time3 = Fx3(chng(1,1)-300310,4562610-chng(1,2));
        % Calculate \epsilon
        Exy_time2 = sqrt(((Ey_time2)^2)+((Ex_time2)^2));
        %Exy_time3 = sqrt(((Ey_time3)^2)+((Ex_time3)^2));
        % Define the error ellipse
        % Assume ellipse center coordinates are at (0,0)
        x0 = 0;

```

```

y0 = 0;
% Define points in a vector used to create the ellipse
t = -pi:0.01:pi;
% If the channel centerline from the base image was used to
infer
% migration vector distances being assessed for statistical
% significance, use the first set of x and y equations provided
% Example: You have 3 images in a time series. The three images
% were acquired in 2009, 2011, and 2012, and 2012 was the base
% image to which 2009 and 2011 were registered. Use the
following
% equations if you are assessing the statistical significance
of
% the migration vector distances between 2011 and 2012 channel
% centerlines, because we are assuming the base image (2012)
has
% E_x and E_y values of 0 meters. Digitizing error should be
% provided in the manual inputs section.
x=(x0+(sqrt(((Ex_time2)^2)+((digError)^2))))*cos(t);
y=(y0+(sqrt(((Ey_time2)^2)+((digError)^2))))*sin(t);
% If the channel centerline from the base image was not used to
% infer migration vector distances being assessed for
statistical
% significance, use the second set of x and y equations
provided.
% Said another way, use the second set if both images used to
infer
% migration vector distances were warped to a separate base
image
% Example: You have 3 images in a time series. The three images
% were acquired in 2009, 2011, and 2012, and 2012 was the base
% image to which 2009 and 2011 were registered. Use the
following
% equations if you are assessing the statistical significance
of
% the migration vector distances between 2009 and 2011 channel
% centerlines, because neither image was the base image during
% image registration. Digitizing error should be provided in
the
% manual inputs section.

%x=(x0+(sqrt(((Ex_time2)^2)+((Ex_time3)^2)+((digError)^2))))*cos(t);

%y=(y0+(sqrt(((Ey_time2)^2)+((Ey_time3)^2)+((digError)^2))))*sin(t);
% Calculate angle \theta and use to rotate all points (x, y) in
% in vector t to new locations (xr, yr)
% NOTE: x' and y' from eqns. 7 and 8 in the Lea and Legleiter
% manuscript are equivalent to xr and yr
thet = atand((abs(Ey_time2)/(abs(Ex_time2))));
xr = x*cos(thet)-y*sin(thet);
yr = x*sin(thet)+y*cos(thet);
% Translate the rotated ellipse to its actual location in space
% along the time 1 channel centerline, defined as xt, yt.
xt = xr + chng(1,1);

```

```

        yt = yr + chng(1,2);
        % Determine if the endpoint of the migration vector located on
the
        % time 2 channel centerline is inside or outside the rotated
error
        % ellipse positioned with its center at the endpoint vertex for
the
        % selected migration vector along the time 1 channel
centerline.
        in = inpolygon(chng(2,1),chng(2,2),xt,yt);
        % If the vertex along the time 2 channel centerline is not
inside
        % the error ellipse (i.e., migration vector distance > error
% ellipse), the change is statistically significant. Elseif the
% vertex along the time 2 channel centerline is inside the
error
        % ellipse (i.e., migration vector distance < error ellipse),
the
        % change is not statistically significant
        if in == 0
            sig = 1;
        elseif in == 1
            sig = 0;
        end
        % Add either a 1 (significant change) or 0 (not significant
change)
        % to a list, denoting the chosen migration vector either
% significant or not significant.
        sigList_SVE = [sigList_SVE sig];
    end
end
% Transpose sigList
sigList_SVE = sigList_SVE';

% If desired, assess the significance of lateral migration vectors
against
% RMSE
% Create an empty list to populate with 0's (not significant change)
and
% 1's (significant change) for each migration vector.
sigList_RMSE = [];
% Manually set RMSE
RMSE_time2 = .82;
RMSE_time3 = .82;
% Start loop for length of the matrix
for ii = 1:length(MigVecChng)
    % If the row number is odd, create a 2 x 2 matrix that contains the
x
    % and y coordinates for the two vertexes defining the end points of
a
    % single migration vector
    if mod(ii,2) ~= 0
        chng = [MigVecChng(ii,4) MigVecChng(ii,5); MigVecChng(ii+1,4)
MigVecChng(ii+1,5)];
    end
end

```

```

    % Calculate migration vector length
    Mag_xy = pdist(chng);
    % Use this eqn if base image is one of the images being used
    % e.g. 2011 and 2012, where 2012 is base
    %RMSE_total = sqrt((((RMSE_time2)^2)+((digError)^2)));
    % Use this eqn if both images were warped to a separate base
year
    % e.g. 2009 and 2011, where 2012 is base
    RMSE_total =
sqrt((((RMSE_time2)^2)+((RMSE_time3)^2)+((digError)^2)));
    % Assess if migration vector length exceeds RMSE value
    if Mag_xy > RMSE_total
        sig = 1;
    elseif Mag_xy <= RMSE_total
        sig = 0;
    end
    sigList_RMSE = [sigList_RMSE sig];
end
end
%Transpose sigList
sigList_RMSE = sigList_RMSE';

% If desired, assess the significance of lateral migration vectors
against
% 90th percentile error
% Calculate 90th percentile for 2nd order polynomial error vectors
Perc90_time2 = prctile(XYresid,90);
%Perc90_time3 = prctile(resid_XY,90);
% Create an empty list to populate with 0's (not significant change)
and
% 1's (significant change) for each migration vector.
sigList_90 = [];
% Start loop for length of the matrix
for ii = 1:length(MigVecChng)
    % If the row number is odd, create a 2 x 2 matrix that contains the
x
    % and y coordinates for the two vertexes defining the end points of
a
    % single migration vector
    if mod(ii,2) ~= 0
        chng = [MigVecChng(ii,4) MigVecChng(ii,5); MigVecChng(ii+1,4)
MigVecChng(ii+1,5)];
        % Calculate migration vector length
        Mag_xy = pdist(chng);
        % Use this eqn if base image is one of the images being used
        % e.g. 2011 and 2012, where 2012 is base
        Perc90E_total = sqrt((((Perc90_time2)^2)+((digError)^2)));
        % Use this eqn if both images were warped to a separate base
year
        % e.g. 2009 and 2011, where 2012 is base
        %Perc90E_total =
sqrt((((Perc90_time2)^2)+((Perc90_time3)^2)+((digError)^2)));
        % Assess if migration vector length exceeds 90 percentile error
        if Mag_xy > Perc90E_total

```

```

        sig = 1;
    elseif Mag_xy <= Perc90E_total
        sig = 0;
    end
    sigList_90 = [sigList_90 sig];
end
end
sigList_90 = sigList_90';

% Devon Libby's additions to simplify and automate the process of
creating a
% csv file containing the information of significant and nonsignificant
% migration.

% Creating the header names in an array
ColumnNames = {'FID', 'Sig_SVE', 'Sig_RMSE', 'Sig90'};
% Creating the ID field which will serve as the foreign key in
% to join the significant/insignificant table with the migration
% measurement table in ArcMap. This is accomplished by selecting every
% other entry from column two in the MigVecChng variable and moving it
% into a standalone matrix
ID = MigVecChng(1:2:end, 2:2);
% This concatenates the ID field, SVE, RMSE, and 90th percentile
% significant/insignificant tables into one.
sigList_All = [ID sigList_SVE sigList_RMSE sigList_90];
% This function was downloaded from
% https://www.mathworks.com/matlabcentral/fileexchange/29933-csv-with-
column-headers
% (credit: Keith Brady) and allows a csv file to be written from the
newly
% concatenated list and given the header from "ColumnNames".
csvwrite_with_headers('MATLABoutput.csv', sigList_All, ColumnNames)

% Devon Note: This next paragraph is no longer necessary to do since
the previous block of script was written to accomplish this
automatically.
%% Displaying statistical significance in ArcMAP

% After creating SigList for SVE, RMSE, and 90th percentile, you can
copy
% and paste the results into a Microsoft Excel file, save as a .csv
file,
% and join the data to your lateral migration vectors in ArcGIS to
visually
% inspect where channel change was and was not statistically
significant.
% First, open a new Microsoft Excel sheet and copy the sigList_SVE n x
1
% vector into column B and starting with the first value in row 2.
% Similarly, copy the sigList_RMSE and SigList_90 n x 1 vectors into
% columns C and D, respectively, and also starting in row 2. For each
of
% these three columns, provide an appropriate name label in row 1. For

```

```
% column A, give the name 'FID' to match to the attribute table of the
% channel migration vectors in ArcGIS. Starting in row 2, enter the
value
% 0, in row 3 enter a value of 1, and then extend the values to match
the
% number of migration vector endpoint verticies. When ready, save the
file
% as a .csv file. Keep saving through any warnings - note you can only
have
% a single sheet as part of the .csv file format (no multiple tabs at
the
% bottom).

% Devon Note: Again most of this is unnecessary to manually do if the
"Post MATLAB Processing" script is run which again automates the
process. The symbology will still need to be changed to fit the users
graphical display purposes.

% Now in ArcMap with your migration vector shapefile (the ones you
% saved from the line graphics), open the attribute table and add three
new
% fields for spatially variable error, RMSE, and 90th percentile error.
% Suggested names are 'Sig_SVE', 'Sig_RMSE' and 'Sig90'. Then right
click
% on the layer in the Table of Contents and go to Joins and Relates ->
Join.
% In the Join Data menu that appears, choose the field the join will be
% based on as 'FID'. Then load the .csv file from disk, and choose the
% field in the table to base the join on as 'FID'. Now if you open the
% attribute table you can see the joined columns to the attribute
table. To
% save the joined columns to their respective columns you added to the
% attribute table, right click one of the column headings and select
Field
% Calculator. Ignore any warnings, and in the Field Calculator window
set
% the variable equal to the equivalent variable from the joined .csv
file.
% The list should change then from a list of all 0's to a list of mixed
0's
% and 1's, assuming any change occurred. Repeat this for all three
error
% metrics, then remove the join to the .csv file. You can display the
1's
% and 0's as different colors under Properties -> Symbology.
```

Appendix E

“Pre MATLAB Processing” script created by Devon Libby.

```
# -----
# Pre MATLAB Processing Script.py
# Created 11/9/16
# Author Devon Libby
# Description: The purpose of this script is to take the existing trajectory polyline
# shapefile and give it correct measurements that identify migration rates to the
# left with positive values and migration to the right with negative values. This script
# also retrieves a point shapefile that identifies the two ends of each migration
# line and assigns them x and y coordinates so it can be ran in the MATLAB script
# "ChannelChangeSignif" produced by Lea and Legleiter (2016). This code can be
# retrieved
# from http://www.fluvialremotesensing.org/tools.html
# -----

# Set the necessary product code
# import arcinfo

# Import modules
import arcpy
import shutil

#Set Workspace
arcpy.env.workspace = arcpy.GetParameterAsText (0)
arcpy.env.overwriteOutput = True

# Local variables:
#Mandatory Changes
#This is the trajectory polyline file
TRJLF = arcpy.GetParameterAsText (1)
TRJLF_LYR = "TRJLF_lyr" #This is the temporary layer file needed to be able to
"Select Layer by Location" and make calculations
#This needs to be the centerline of the earlier of the two years (T1)
T1_CL = arcpy.GetParameterAsText (2)

#Other Variables
TFPath = arcpy.env.workspace #Path to store intermediate files produced during
geoprocessing
```

```

TF = "Temp_Folder" #Folder the intermediate files are stored in
Buffer = r"\Temp_Folder\Buffer.shp" #Buffer needed to select migration downstream
right
XY = "XYpoints.shp" #The point file that will contain the the columns needed for
"ChannelChangeSignif" Matlab Code
ExTable = "MigVecChng.xls"

#Create a place to house temporary/intermediate files to avoid cluttering primary folder
arcpy.CreateFolder_management(TFPath, TF)

# Add Field - This adds the field where migration measures will be stored
arcpy.AddField_management(TRJLF, "Mig_Dist", "DOUBLE", "7", "2", "", "",
"NULLABLE", "NON_REQUIRED", "")

# Calculate Field- Calculates and populates "Mig_Dist" field in meters
arcpy.CalculateField_management(TRJLF, "Mig_Dist", "\"!shape.length@meters!\\"",
"PYTHON_9.3", "")

# Buffer- Buffer created on the downstream right side of the river to differentiate left and
right migration
arcpy.Buffer_analysis(T1_CL, Buffer, "1000 Meters", "RIGHT", "ROUND", "NONE",
"", "PLANAR")

# TRJLF first needs to have a layer file associated with it so it can then be used to "Select
Layer by Location"
arcpy.MakeFeatureLayer_management(TRJLF, TRJLF_LYR)

#Select Layer By Location - uses the layer file and buffer to select only the migration
trajectories that are downstream right
arcpy.SelectLayerByLocation_management(TRJLF_LYR,
"HAVE_THEIR_CENTER_IN", Buffer, "", "NEW_SELECTION", "NOT_INVERT")

# Calculate Field - Assigns a negative value to all downstream right migration
arcpy.CalculateField_management(TRJLF_LYR, "Mig_Dist", "!Mig_Dist! *-1",
"PYTHON_9.3", "")

# Select Layer By Attribute - Clears selected features so all attributes are able to be
geoprocessed
arcpy.SelectLayerByAttribute_management(TRJLF_LYR, "CLEAR_SELECTION", "")

# Feature Vertices To Points - Every trajectory line has a point created for each end

```



```
arcpy.FeatureVerticesToPoints_management(TRJLF, XY, "BOTH_ENDS")

# Add XY Coordinates - The point file created from the trajectory file is assigned XY
coordinates
arcpy.AddXY_management(XY)

#Table to Excel - Allows easy access to variables that need to be entered into the
"ChannelChangeSignif" code in Matlab
arcpy.TableToExcel_conversion(XY, ExTable, "NAME", "CODE")

#Deletes the Temporary Folder that was used to store intermediate data. Comment the
following line out to preserve intermediate file.
shutil.rmtree(arcpy.env.workspace + r"\Temp_Folder")

print "Alright Alright Alright"
```

Appendix F

The script for the function “`csvwrite_with_headers`” written by Keith Brady and retrieved from <http://www.mathworks.com/matlabcentral/fileexchange/29933-csv-with-column-headers?focused=5176300&tab=function> on 4/19/2017

```
% This function functions like the build in MATLAB function csvwrite
but
% allows a row of headers to be easily inserted
%
% known limitations
% The same limitation that apply to the data structure that exist
with
% csvwrite apply in this function, notably:
%     m must not be a cell array
%
% Inputs
%
% filename    - Output filename
% m           - array of data
% headers     - a cell array of strings containing the column
headers.
%             The length must be the same as the number of columns
in m.
% r           - row offset of the data (optional parameter)
% c           - column offset of the data (optional parameter)
%
%
% Outputs
% None
function csvwrite_with_headers(filename,m,headers,r,c)

%% initial checks on the inputs
if ~ischar(filename)
    error('FILENAME must be a string');
end

% the r and c inputs are optional and need to be filled in if they are
% missing
if nargin < 4
    r = 0;
end
if nargin < 5
    c = 0;
end

if ~iscellstr(headers)
    error('Header must be cell array of strings')
end

if length(headers) ~= size(m,2)
```

```

        error('number of header entries must match the number of columns in
the data')
end

%% write the header string to the file

%turn the headers into a single comma seperated string if it is a cell
%array,
header_string = headers(Aadland);
for i = 2:length(headers)
    header_string = [header_string, ',', headers(Aadland)];
end
%if the data has an offset shifting it right then blank commas must
%be inserted to match
if r>0
    for i=1:r
        header_string = [',', header_string];
    end
end

%write the string to a file
fid = fopen(filename, 'w');
fprintf(fid, '%s\r\n', header_string);
fclose(fid);

%% write the append the data to the file

%
% Call dlmwrite with a comma as the delimiter
%
dlmwrite(filename, m, '-append', 'delimiter', ',', 'roffset',
r, 'coffset', c);

```

Appendix G

“Post MATLAB Processing” script created by Devon Libby.

```
# -----
# Post MATLAB Processing Script.py
# Created 11/7/16 Modified 4/24/17
# Author Devon Libby
# Description: The purpose of this script is to take the existing trajectory polyline
# shapefile and populate fields that show if the lateral
# migration is statistically significant or insignificant according to Spatial Variable Error
# (SVE), Root-Mean-Square-Error (RMSE), and 90th
# percentile. In addition, each trajectory line is assigned a downstream distance giving it a
# spatial location. A field is also populated on
# every file with annual migration rates. Final outputs include a shapefile and excel table
# with all measures of error, as well as, standalone
# shapefiles and excel files that replace statistically insignificant migration distances with
# a value of zero. Finally, a point shapefile named
# "Color_Mig" is created that can be used in combination with a desired symbology (e.g.
# hot and cold color scheme) and data
# classification to create maps that visually represent channel mobility.
# -----

# Import modules
import arcpy
import shutil

#Set Workspace: This workspace must contain both 1)the polyline file that stores the
#trajectories and 2) the output CSV from Matlab
#with column 1 being "FID" column 2 being "SVE" column 3 being "RMSE", and
#column 4 being "Nintey" Note: These must be exact spellings
#and capitalizations
arcpy.env.workspace = arcpy.GetParameterAsText (0)
arcpy.env.overwriteOutput = True

# Local variables:
#User Changes
#This is the trajectory polyline file
TrjLF = arcpy.GetParameterAsText (1)
```

```

#This is output CSV storing "FID", "SVE", "RMSE", and "Nintey" columns that were
copied from Matlab output variables
SigCSV = arcpy.GetParameterAsText (2)
#The number of years between the two centerlines
NumYears = arcpy.GetParameterAsText (3)
#Depending on the River direction flow, the Coordinate Priority along which the river
(route.shp) accumulates measure may need to be changed
CoordPriority = arcpy.GetParameterAsText (4)
#Centerline for T1/Earlier year in the interval
T1 = arcpy.GetParameterAsText (5)

#Other Variables
TFPath = arcpy.env.workspace #Path to store intermediate files produced during
geoprocessing
TF = "Temp_Folder" #Folder the intermediate files are stored in
TempTable = "\\Temp_Folder\\Temp.dbf" #csv converted to dbf for quicker indexing
PKey = "FID" #Join Primary Key
FKey = "OID" #Join Foreign Key
##F2Point = "\\Temp_Folder\\F2Point_temp.shp" #Feature to Point output generated
from the centroid of the trajectory polyline files
##P2Line = "\\Temp_Folder\\P2L_temp.shp" #Point to Line output using F2Point as the
input
IntPoint = "\\Color_Mig.shp"
Route = "\\Temp_Folder\\Route_Temp.shp" #Turning P2Line into a route in order to get
downstream distances
LFAR = "\\Temp_Folder\\LFAR" #Event table created during the Locate Feature Along
Route (LFAR) tool in order to get attributes with correct distances
OETP = "RID POINT MEAS" #Out Event Table Properties which consists of route
location fields and the events that will be written to the output table
SVE = "SVE.shp" #StandAlone .shp file for statistically significant measurements
according to SVE
SVEFields = ["SVE", "Mig_Dist", "An_Mig"] #fields used with update cursor
RMSE = "RMSE.shp" #StandAlone .shp file for statistically significant measurements
according to RMSE
RMSEFields = ["RMSE", "Mig_Dist", "An_Mig"] #fields used with update cursor
Nintey = "Nintey.shp" #StandAlone .shp file for statistically significant measurements
according to 90th percentile error
NinteyFields = ["Nintey", "Mig_Dist", "An_Mig"] #fields used with update cursor
ExTableAll = "Excel_Table_All.xls" #Final table is with all information exported to an
excel document in the working directory

```

```

ExTableSVE = "Excel_Table_SVE.xls" #Final table is with SVE information exported to
an excel document in the working directory
ExTableRMSE = "Excel_Table_RMSE.xls"#Final table is with RMSE information
exported to an excel document in the working directory
ExTableNinety = "Excel_Table_Ninety.xls"#Final table is with 90th percentile error
information exported to an excel document in the working directory

#Create a place to house temporary/intermediate files to avoid cluttering primary folder
arcpy.CreateFolder_management(TFPath, TF)

# Delete Field - Drop unnecessary field "Name"
arcpy.DeleteField_management(TrjLF, "Name")

# Table to Table- Takes the csv file and converts it into a dbf for quicker indexing
arcpy.TableToTable_conversion(SigCSV, TF, "Temp.dbf", "", "", "")

# Join Field - This takes the statistically significant (1) and insignificant(0) measurement
information generated in Matlab
# and permanetly joins it to the appropriate trajectory measurements in the polyline
shapefile. Note: Spelling and Capitalization must
# exact to the last parameter below
arcpy.JoinField_management(TrjLF, PKey, TempTable, FKey, "SVE;RMSE;Ninety")

#The following 4 lines have been commented out since they only work when TRJ lines
are unedited without additional lines being added for corrections
## Feature To Point - This take the center of ever line in the trajectory file and creates a
point
##arcpy.FeatureToPoint_management(TrjLF, F2Point, "CENTROID")
## Points To Line - This takes the points generated in the last tool and creates a line from
them
##arcpy.PointsToLine_management(F2Point, P2Line, "", "", "NO_CLOSE")

# Intersect Analysis - This creates points at the intersection of the TRJ polyline file and
the T1 centerline
arcpy.Intersect_analysis([T1, TrjLF], IntPoint, "ALL", "0.1 Meters", "POINT")

# Create Routes - This takes the line created in the last tool and converts it to a route in
order to give it measure
arcpy.CreateRoutes_lr(T1, "Id", Route, "LENGTH", "", "", CoordPriority, "1", "0",
"NO_IGNORE", "INDEX")

```

```

# Locate Features Along Routes - This takes the points that were created and assigns
them downstream measure which will inturn give the
# trajectory lines measure in the next step
arcpy.LocateFeaturesAlongRoutes_lr(IntPoint, Route, "Id", "1 Meters", LFAR, OETP,
"FIRST", "NO_DISTANCE", "ZERO", "FIELDS", "M_DIRECTON")

# Wildcard is needed in order to automate selection of the foreign key since it inserts the
shapefiles name and could vary among users
fid_year = arcpy.ListFields(LFAR, "FID_*_*")[0].name
# Join Field - This steps permanently joins the downstream measurements from the point
file to the corresponding trajectory line
arcpy.JoinField_management(TrjLF, PKey, LFAR, fid_year, "MEAS")

#Add Field for annual migration rates
arcpy.AddField_management(TrjLF, "An_Mig", "DOUBLE", "7", "2", "", "",
"NULLABLE", "REQUIRED", "")
arcpy.AddField_management(IntPoint, "An_Mig", "DOUBLE", "7", "2", "", "",
"NULLABLE", "REQUIRED", "")

#Calculate Field to populate annual migration rates
arcpy.CalculateField_management(TrjLF, "An_Mig", "!Mig_Dist!/(Aadland 2015)"
.format(NumYears), "PYTHON_9.3", "")
arcpy.CalculateField_management(IntPoint, "An_Mig", "!Mig_Dist!/(Aadland 2015)"
.format(NumYears), "PYTHON_9.3", "")

# Copy Feature: Allows for new files that look at specific methods of source error
arcpy.CopyFeatures_management (TrjLF, SVE)
arcpy.CopyFeatures_management (TrjLF, RMSE)
arcpy.CopyFeatures_management (TrjLF, Ninety)

#This uses the Update Cursor to update the Migration Distances (Mig_Dist) for each of
the newly created files so if the distance is not
#statistically significant based on its individual error method then the the Migration
Distance will equal zero. Delete field is also used
#in order to cleanup the final output tables

#Update SVE
with arcpy.da.UpdateCursor(SVE, SVEFields) as cursor:
    for row in cursor:
        if row[0]==0:
            row[1]="0"

```

```

        row[2]="0"
        cursor.updateRow(row)
del row
del cursor

#delete excess fields
arcpy.DeleteField_management(SVE, ["RMSE", "Ninety"])

#Update RMSE
with arcpy.da.UpdateCursor(RMSE, RMSEFields) as cursor:
    for row in cursor:
        if row[0]==0:
            row[1]="0"
            row[2]="0"
            cursor.updateRow(row)
del row
del cursor

#delete excess fields
arcpy.DeleteField_management(RMSE, ["SVE", "Ninety"])

#Update Ninety
with arcpy.da.UpdateCursor(Ninety, NinetyFields) as cursor:
    for row in cursor:
        if row[0]==0:
            row[1]="0"
            row[2]="0"
            cursor.updateRow(row)
del row
del cursor

#delete excess fields
arcpy.DeleteField_management(Ninety, ["SVE", "RMSE"])

#Conversion of the final trajectory files to an excel table
arcpy.TableToExcel_conversion(TrjLF, ExTableAll)
arcpy.TableToExcel_conversion(SVE, ExTableSVE)
arcpy.TableToExcel_conversion(RMSE, ExTableRMSE)
arcpy.TableToExcel_conversion(Ninety, ExTableNinety)

```


#Deletes the Temporary Folder that was used to store intermediate data. Comment the following line out to preserve intermediate file.

```
#shutil.rmtree(arcpy.env.workspace + "\\Temp_Folder")
```

```
print "Alright Alright Alright"
```

Appendix H

Reach Break Down

Reach 1

- Anthropogenically controlled stretch (city of Mankato)
- Little evidence of sandbar presence
- Beginning of the overall study reach (Minnesota/Blue Earth Confluence)
- Is almost immediately met by rip-rap/earthen levee which transitions into a cement flood control structure
- 3 Bridges (HWY 169, Veterans Memorial/Belgrade, and HWY 14 – Respectively Downstream)
- After HWY 14, 3 wing-dams followed by a slight bend in the river
 - This bend is at a bedrock outcrop
 - Historic Meander Bend (prior to 1937)
 - Noticeable decrease in channel width at this point
 - End of Reach 1

Reach 2

- Outside the city of Mankato
- Large amount and size of bars/depositional areas
- 5 Cutoffs from 1937-2013
 - 1 from 1951-1964
 - 1 from 1964-1980
 - 1 from 1980-1991
 - 2 from 1991-2013
 - reducing stream length significantly
- End of Reach 2 and the HWY 22 Bridge (City of St. Peter)
 - Width appears to bottle-neck at this bridge

Reach 3

- Beginning at HYW 22 Bridge
- Passes under the 99 bridge
- Valley width gets significantly bigger
- Significant appearance of bars again
- Contains 3 Cutoffs from 1937-2013
 - 1 from 1937-1951
 - 1 from 1964-1980
 - 1 from 1991-2013
- Fairly sinuous stretch

- Ends at Geomorphic break (see Reach 4)

Reach 4

- Almost completely straight
- Very few bars – small in size
- Reach is pressed up against east side of the valley (DS right)
- Evidence of historic meanders in this section, but little migration in the past 76 years
- Ends at Geomorphic Break (See Reach 5)

Reach 5

- Very sinuous
- Dominated with large point bars
- Small reach but contains two cutoffs from 1937-2013
 - 1 from 1937-1951
 - 1 from 1964-1980
- Ends at 336th Street Bridge/Bridge Street (Le Sueur)

Reach 6

- Begins at 336th Street Bridge/Bridge Street (Le Sueur)
- Only a few small depositional features
- Short reach yet it contain a 1 meander with a wavelength extending from the east river valley wall (City of Le Sueur) to the west valley wall (HWY 169).
- Amplitude of the meander very large compared to Reach 6.
- End at HWY 169 Bridge

Reach 7

- Begins at the HWY 169 Bridge
- Significantly more depositional features than the prior reach
- Low sinuosity
- Majority pressed up against the east valley wall
- Contains 3 Cutoffs from 1937-2013
 - 1 from 1951-1964
 - 2 from 1991-2013
- Rush River flows in near the beginning and appears to have a high amount of sediment
- End at a Geomorphic Break
 - Reduced width
 - Press up against east valley wall
 - Beginning of few depositional features

Reach 8

- Increase in sinuosity
- Contains 3 Cutoffs from 1937-2013
 - 1 from 1964-1980
 - 2 from 1991-2013cc
- Ends at geomorphic break

Reach 9

- Small section characterized by lack of depositional features and completely straight

Reach 10

- High sinuosity
- Meanders through out the entire river valley
- Significant increase in depositional features

Reach 11

- Low sinuosity – Multiple long straight sections of river
- Very little evidence of in channel depositional features outside one point bar
- Ends just upstream of Beaven's Creek

Reach 12

- Beginning at Beaven's Creek
- Increased sinuosity, in channel depositional features, and width
 - Including mid-channel point
- Meander Translation dominates this stretch

Reach 13

- This has a distinct pattern change from the previous reach with much larger meanders
- The river swings back and forth between the valley walls multiple times
- This stretch is also on the edge of the Metro with agricultural land use still being dominate especially on the east side.
- Ends at the HWY 41 Bridge (Chaska)

Reach 14

- This stretch is starts the HWY 41 Bridge
- This stretch also is the beginning of dominate urban land use
- The sinuosity is lower than the prior reach

- This reach also occupied the entire river valley but doesn't bounce around as much as the prior reach
- Ends at the beginning of where the channel is actively dredged

Reach 15

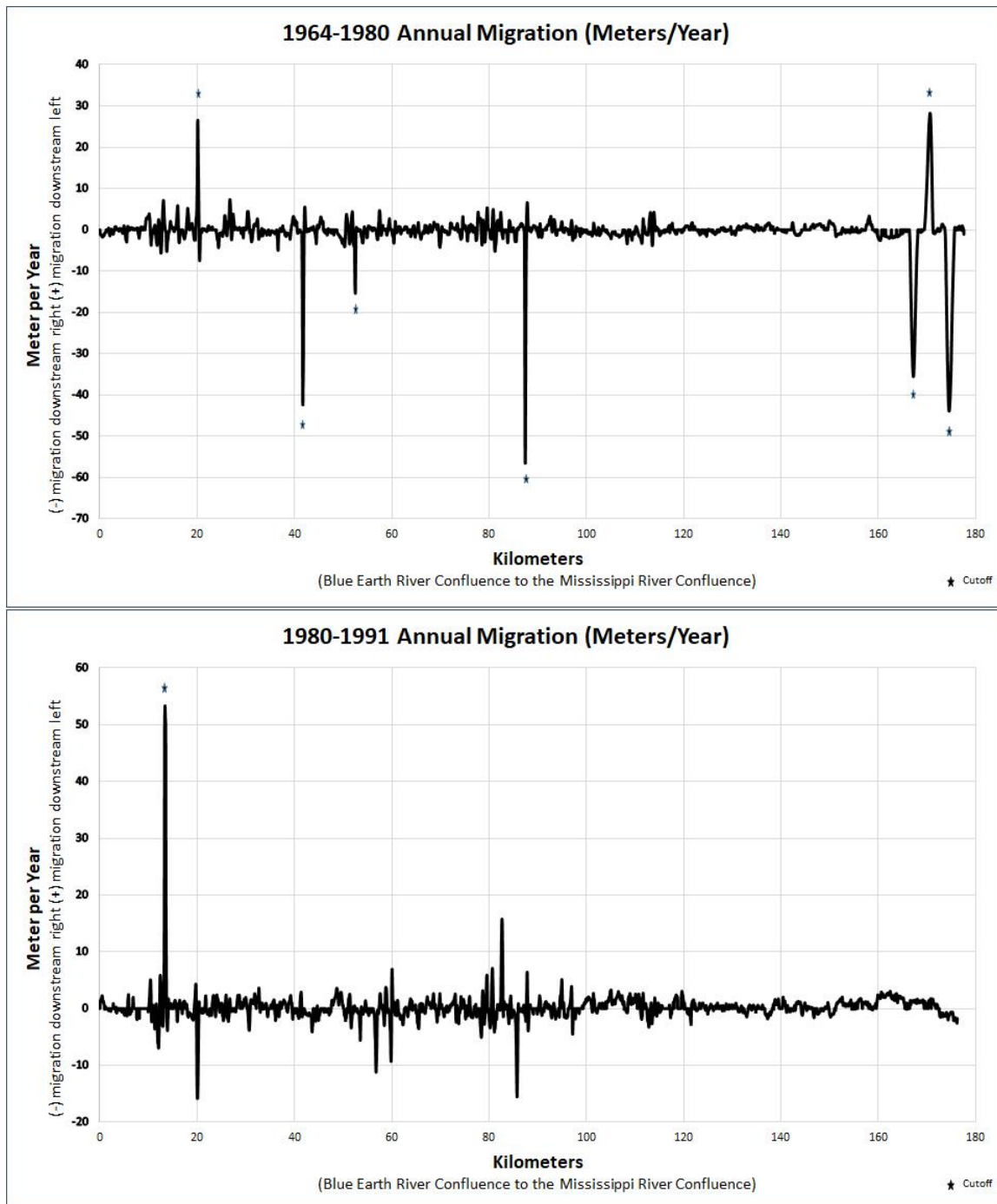
- Begins at the beginning of the channel that is actively managed for barge traffic
- Has meanders that start to straighten towards the end of the reach
- Contains the beginning of barge traffic and dredged channel
 - Two of the Four dredging locations are contained in this reach
 - Heavy industrial encroachment on the river within the river valley
- Ends at 35W bridge

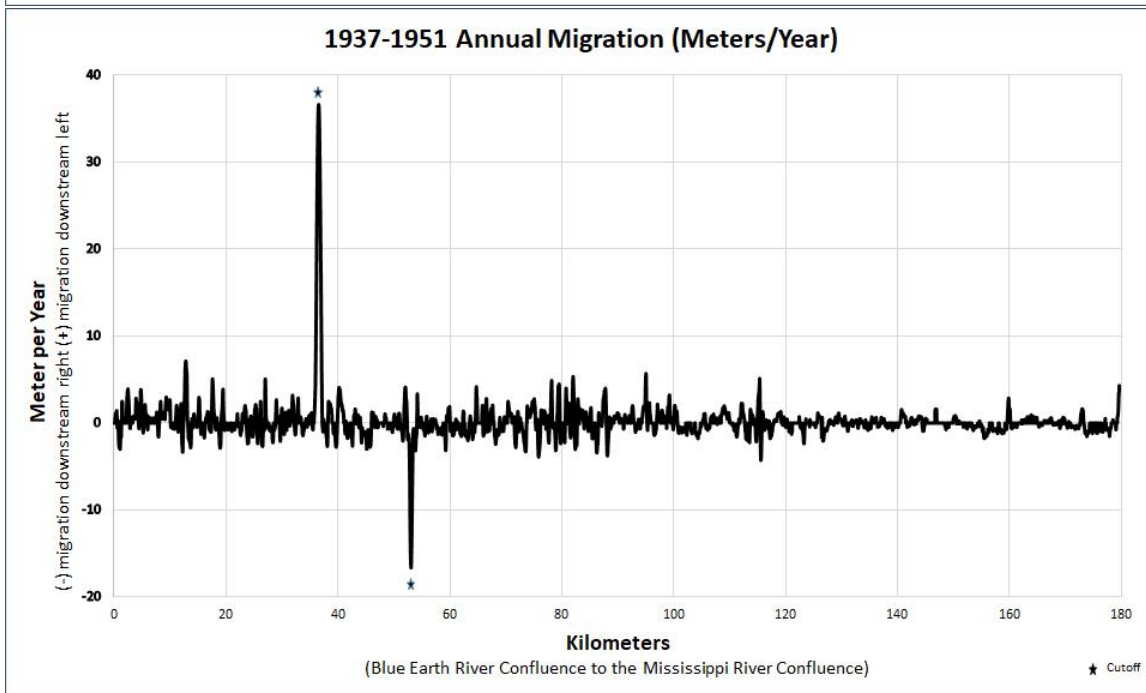
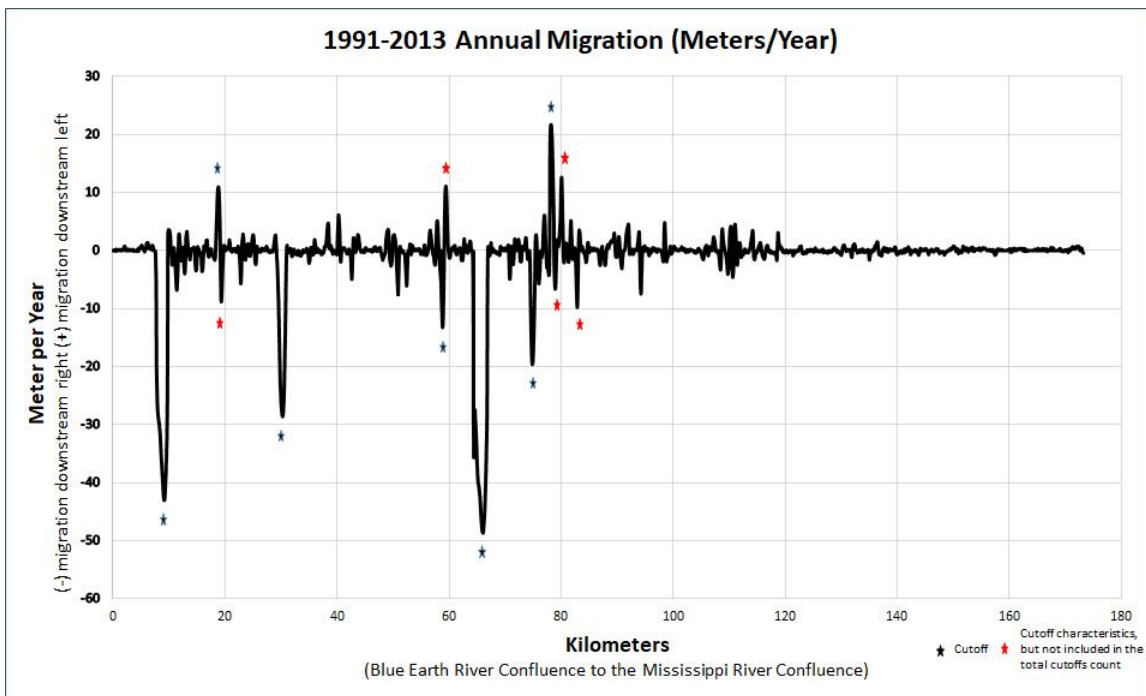
Reach 16

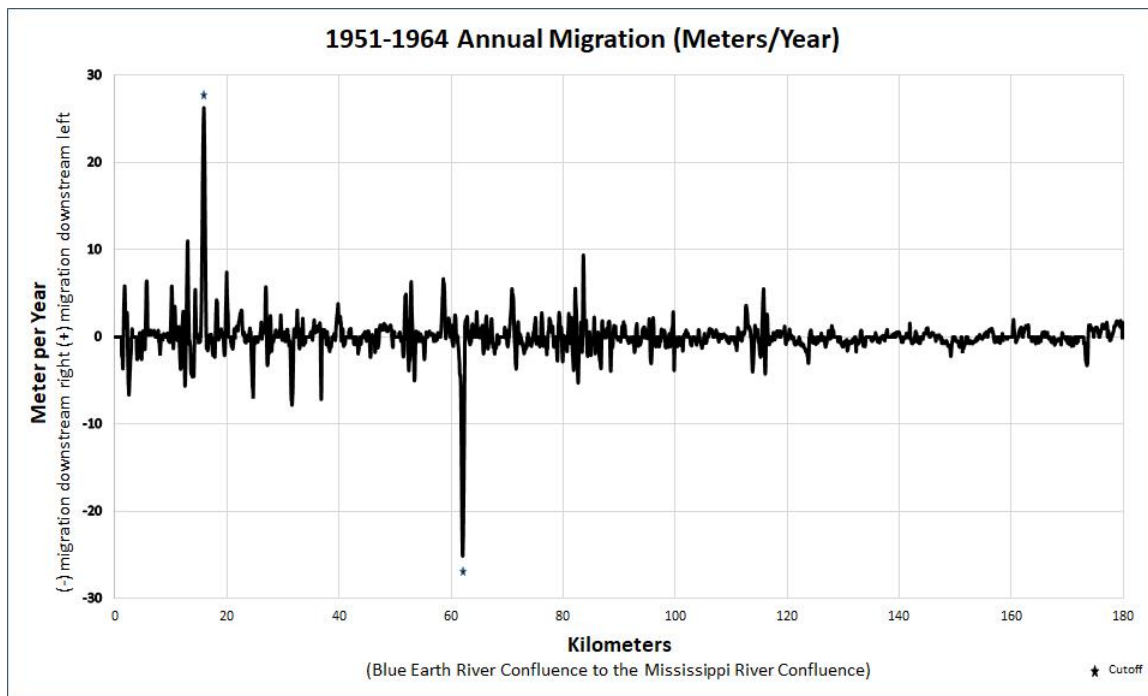
- Begins at the 35W Bridge
- This stretch is very straight with many wetlands and lakes present of both sides of the river within the valley
- The stretch has been modified for barge traffic
 - The other two of four dredging locations are in this stretch
 - 3 Cutoffs are present from 1964-1980 and are most likely engineered
- Ends at the confluence of the Mississippi River

Appendix I

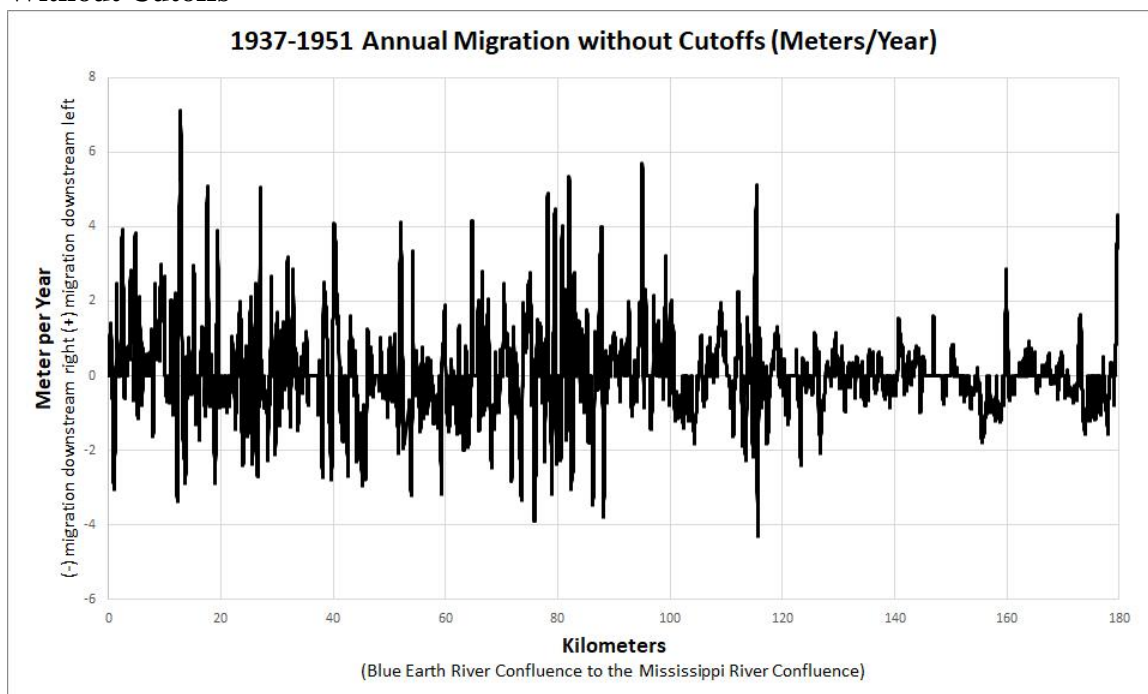
With Cutoffs

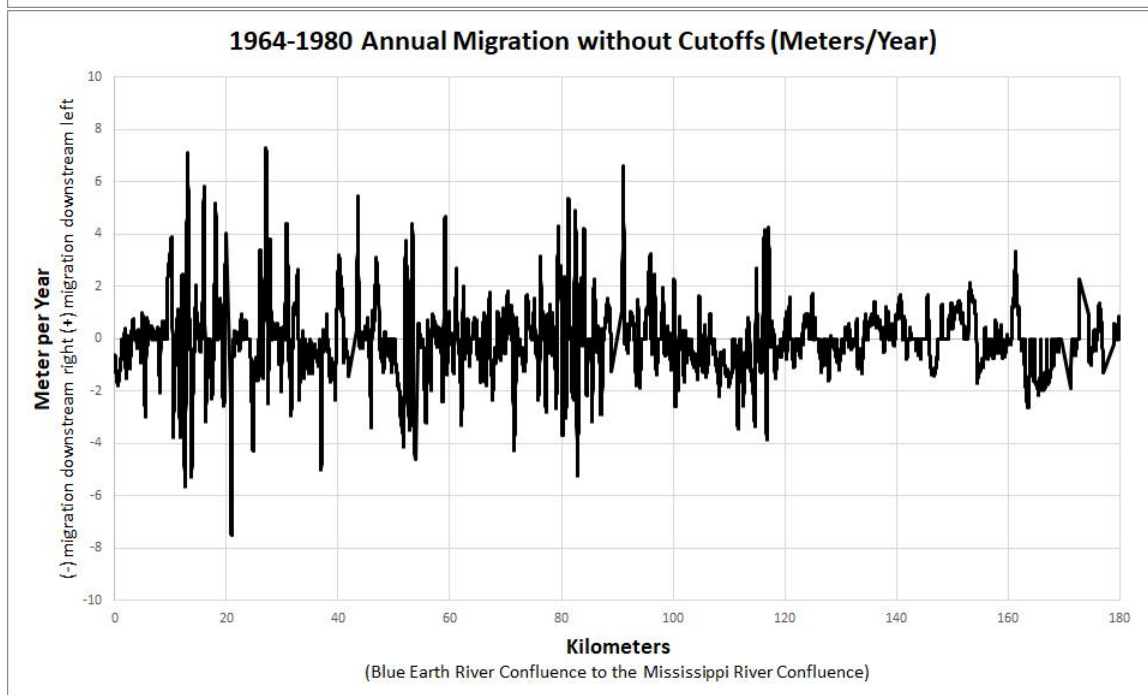
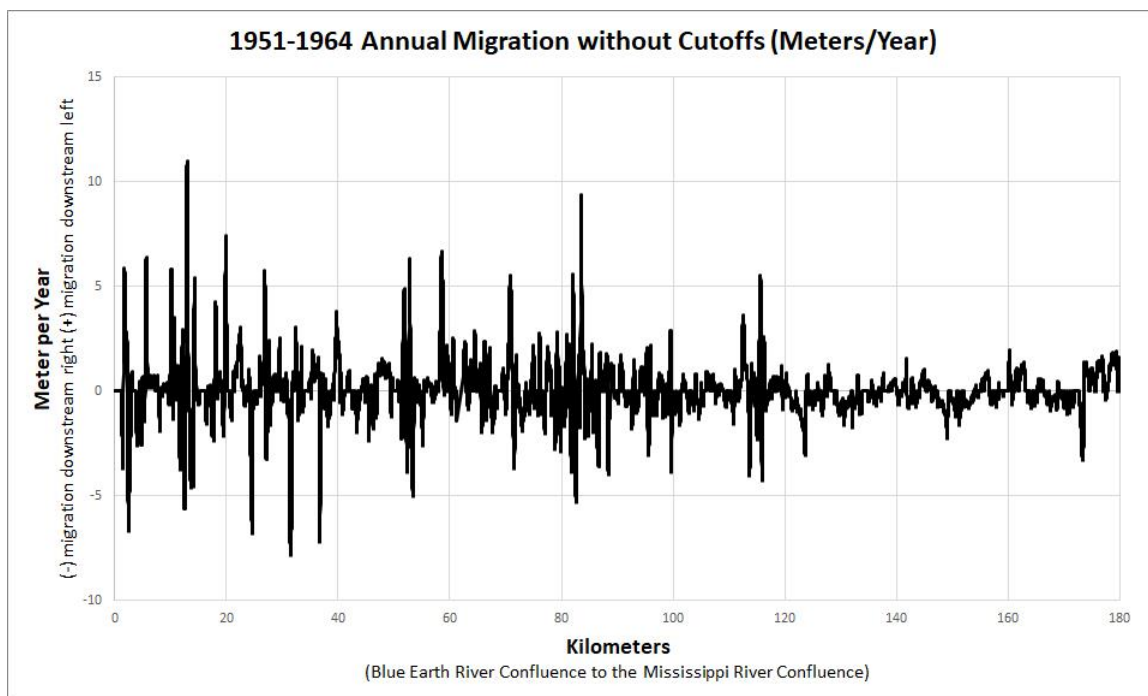


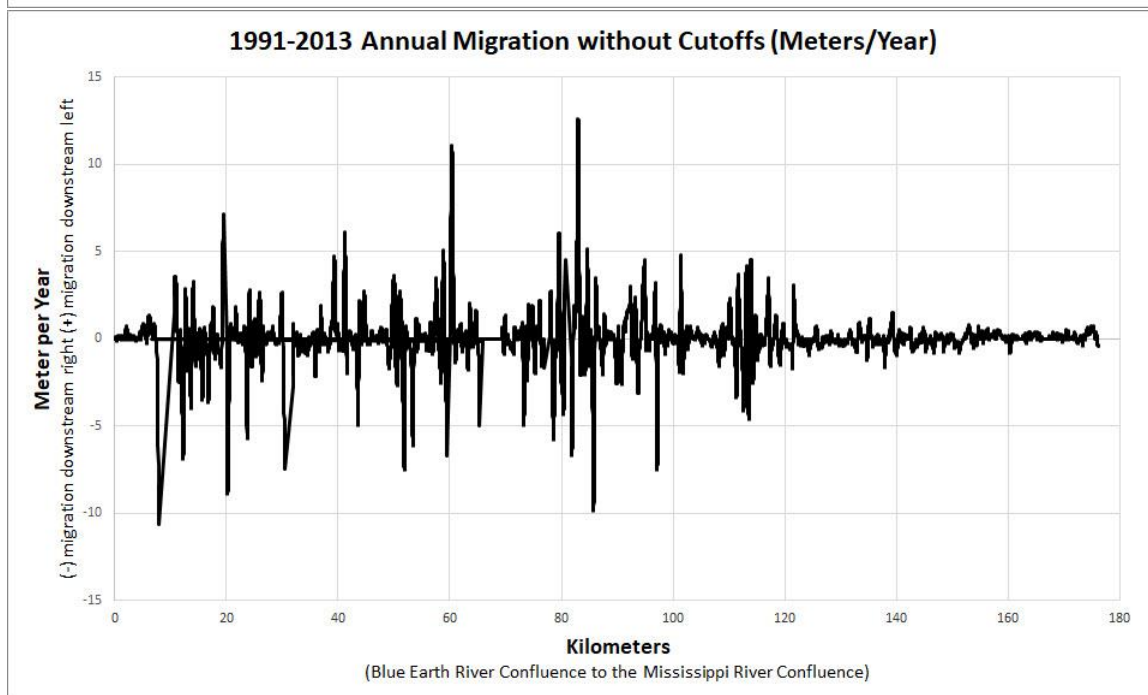
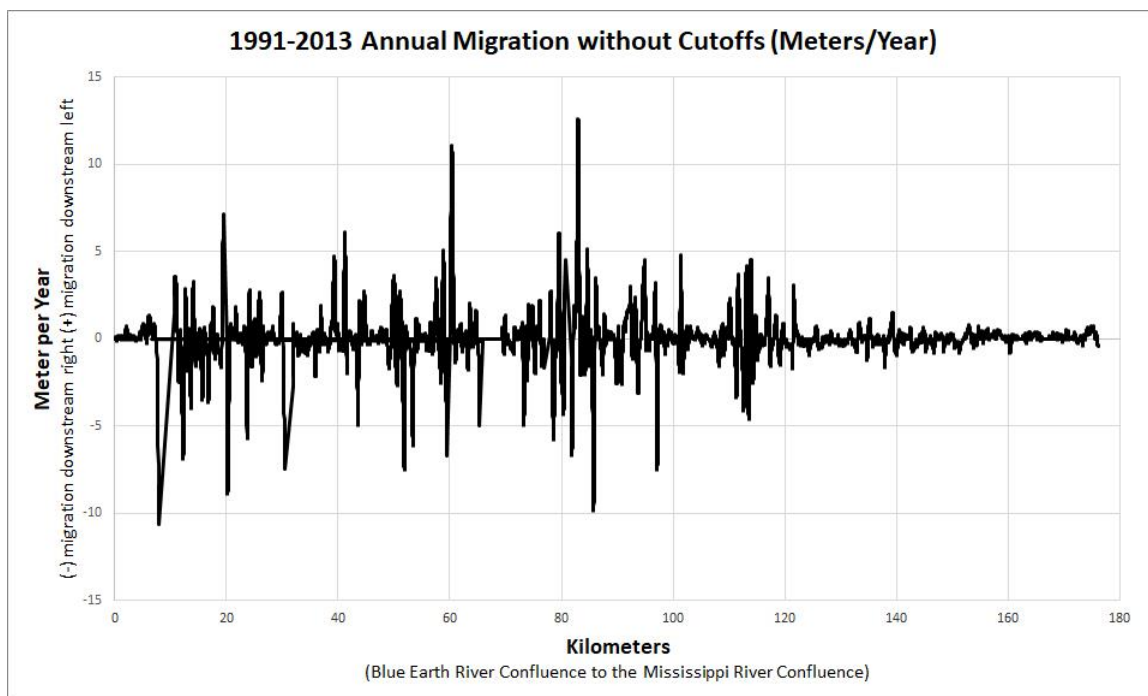




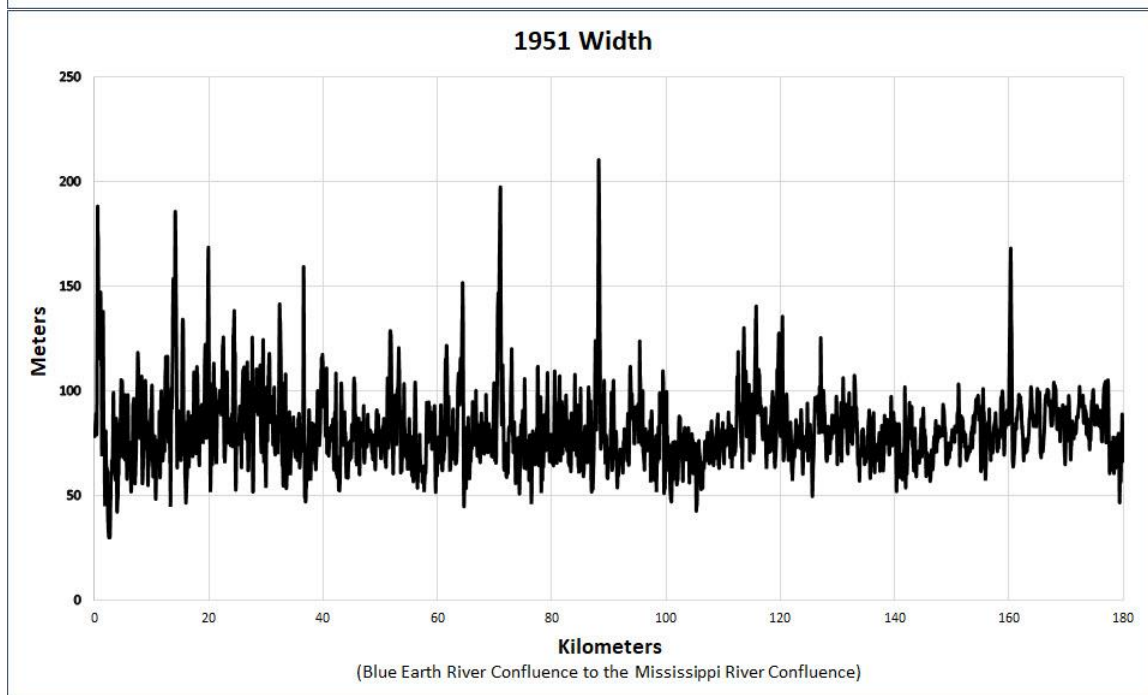
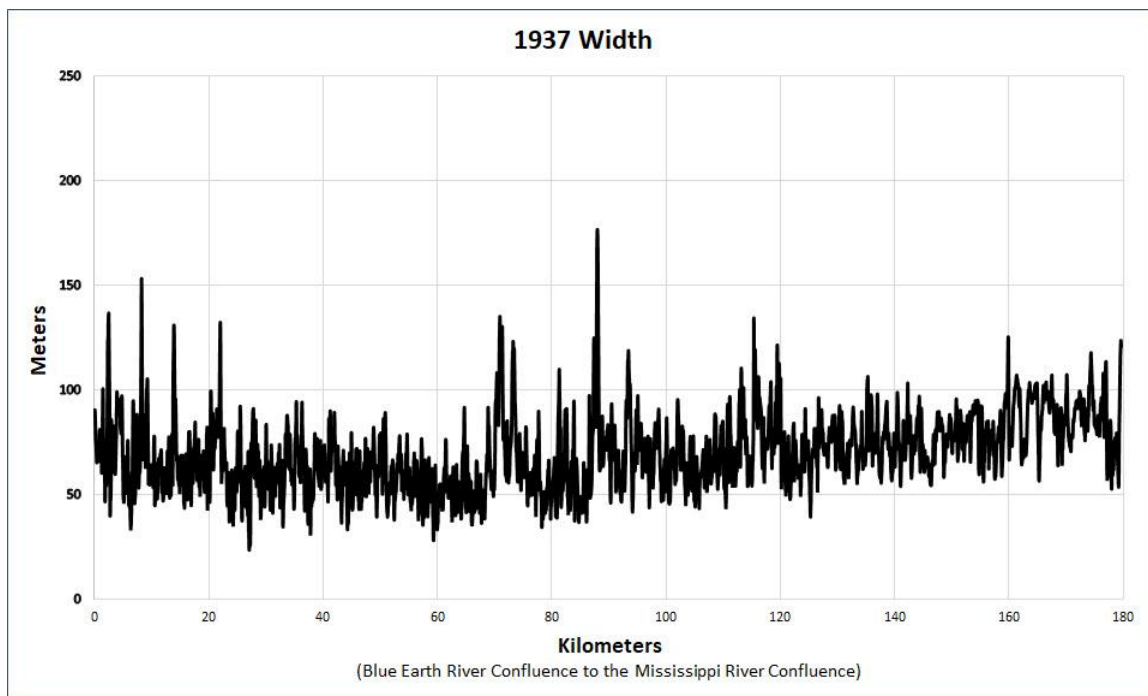
Without Cutoffs

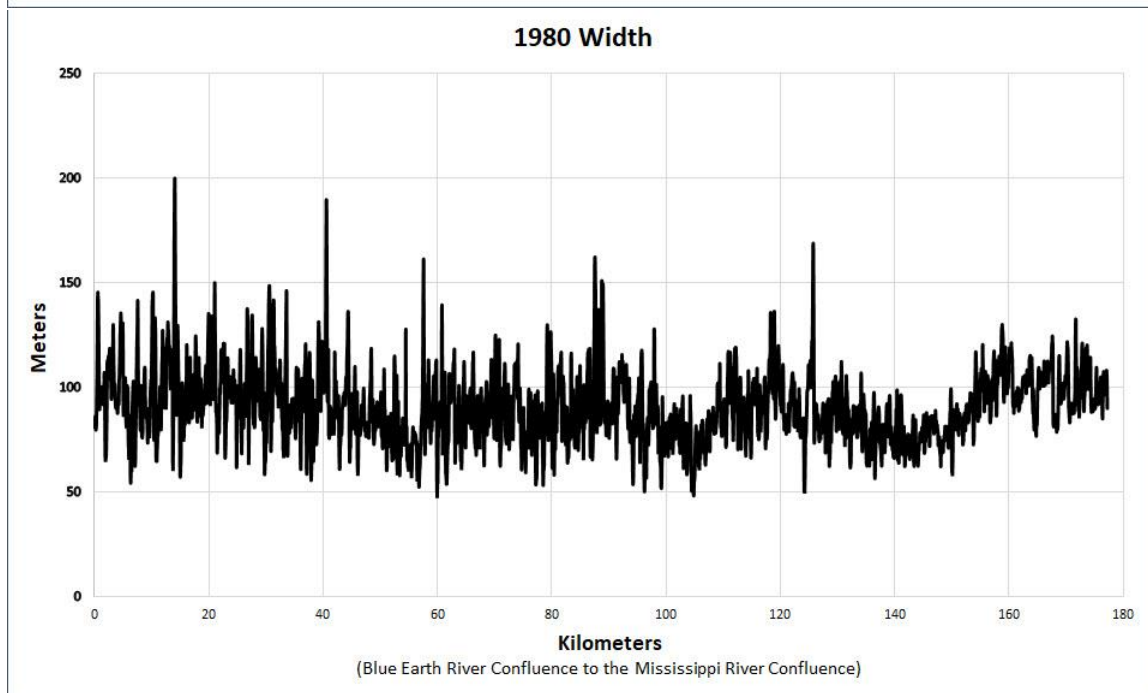
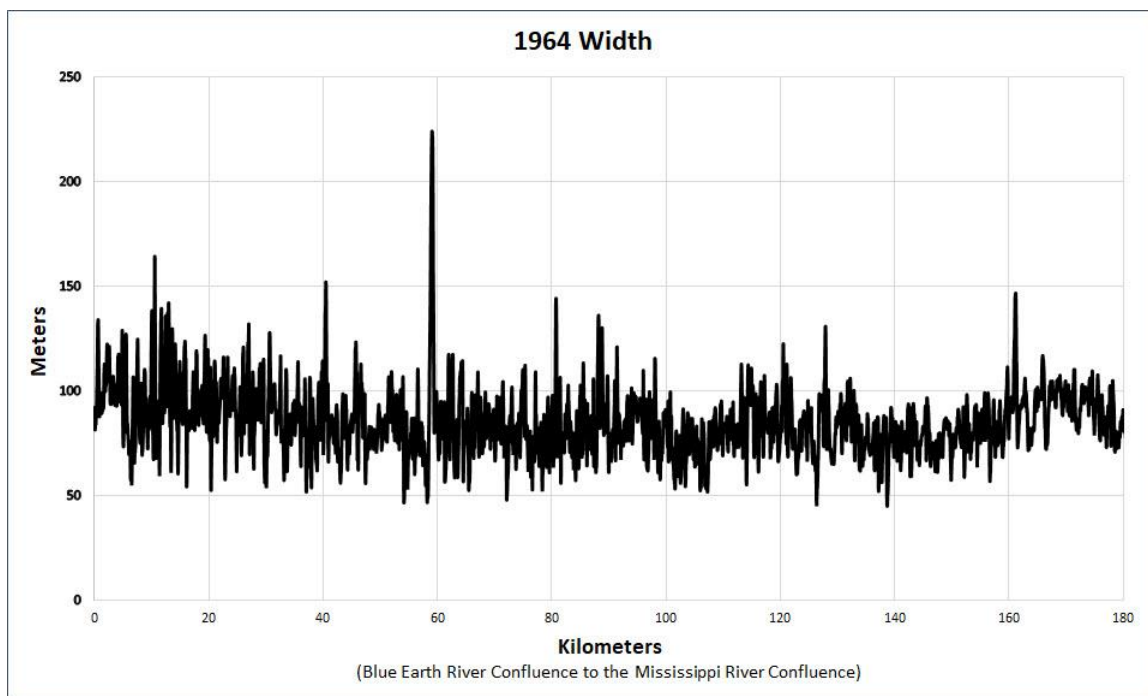


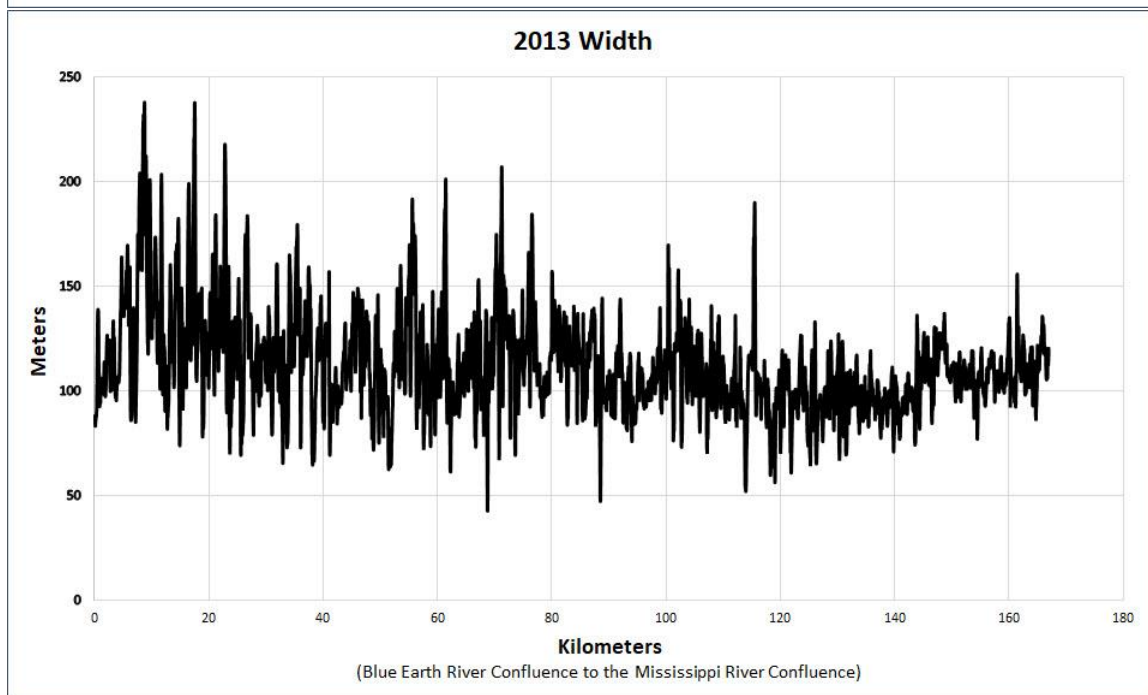
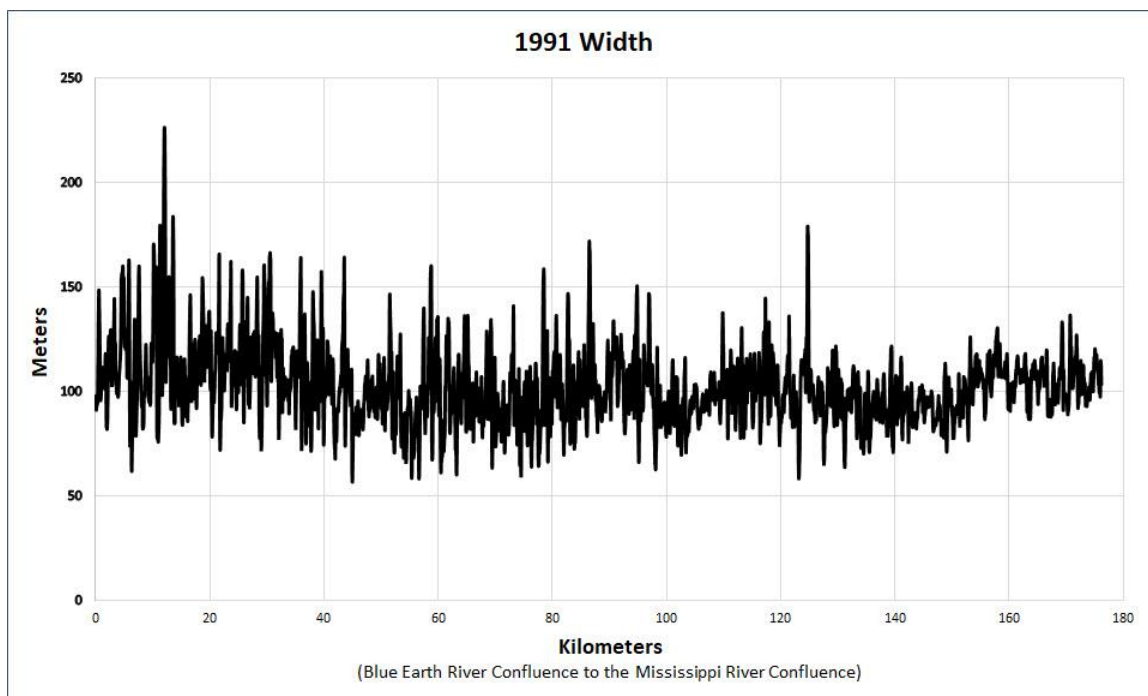




Appendix J



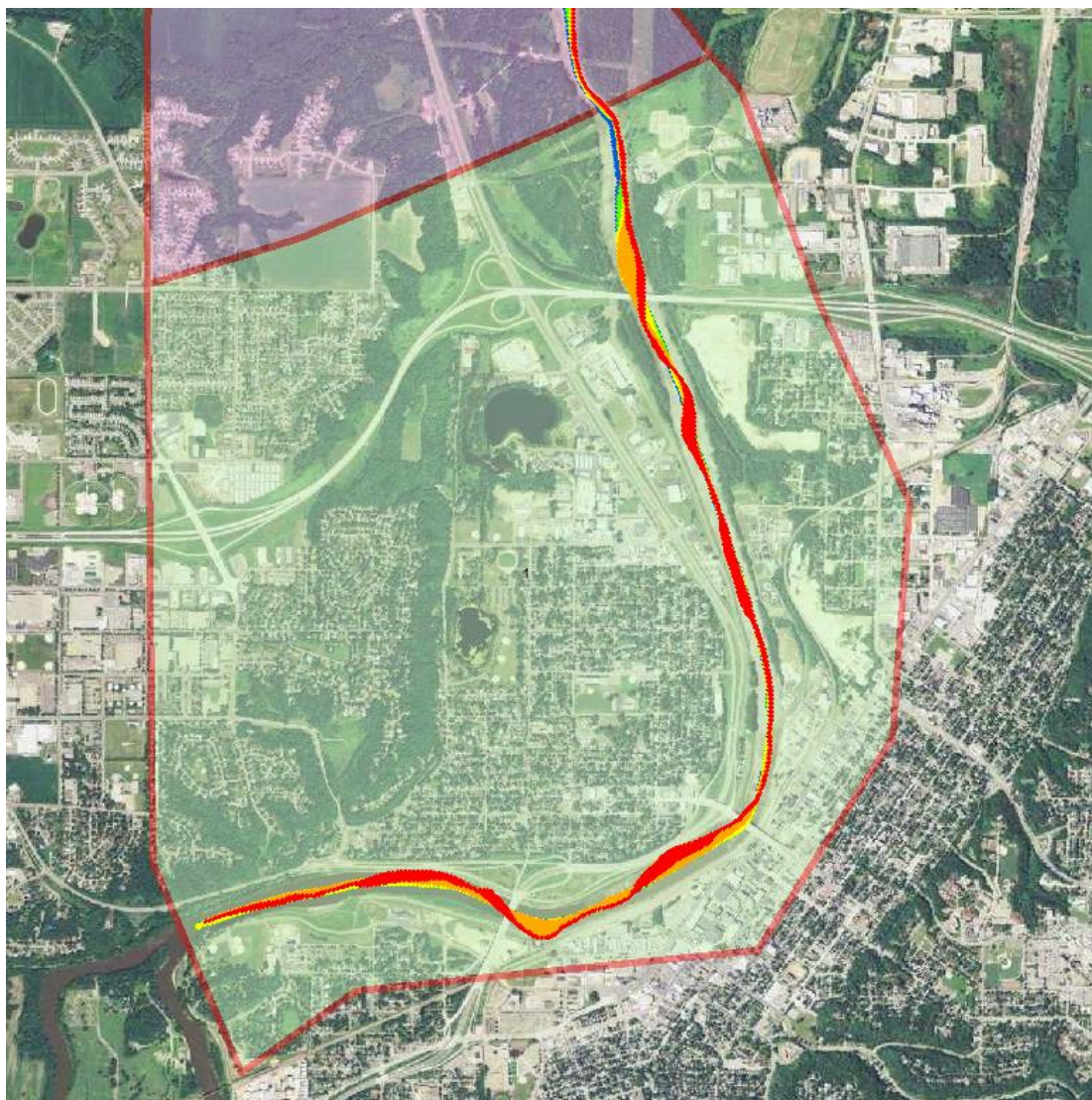




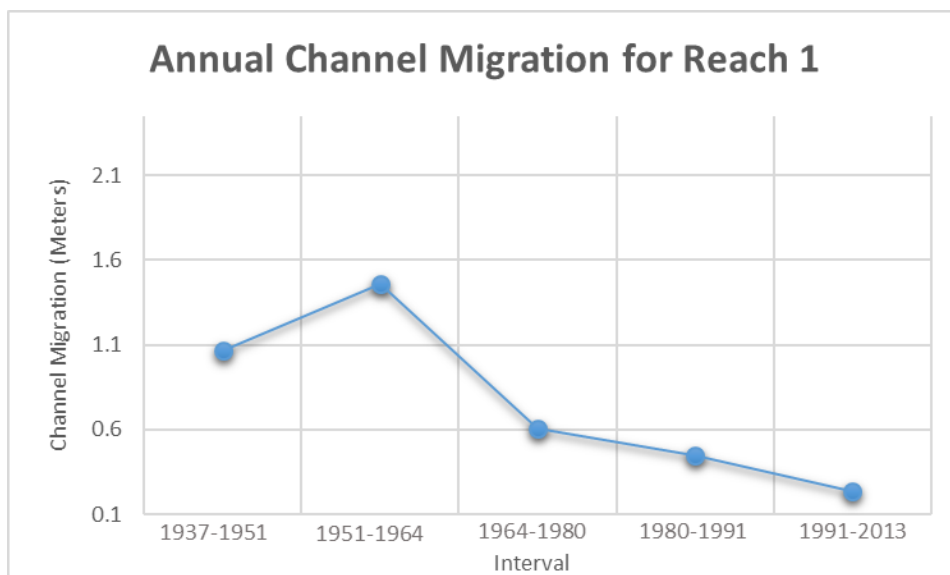
Appendix K

Reach 1

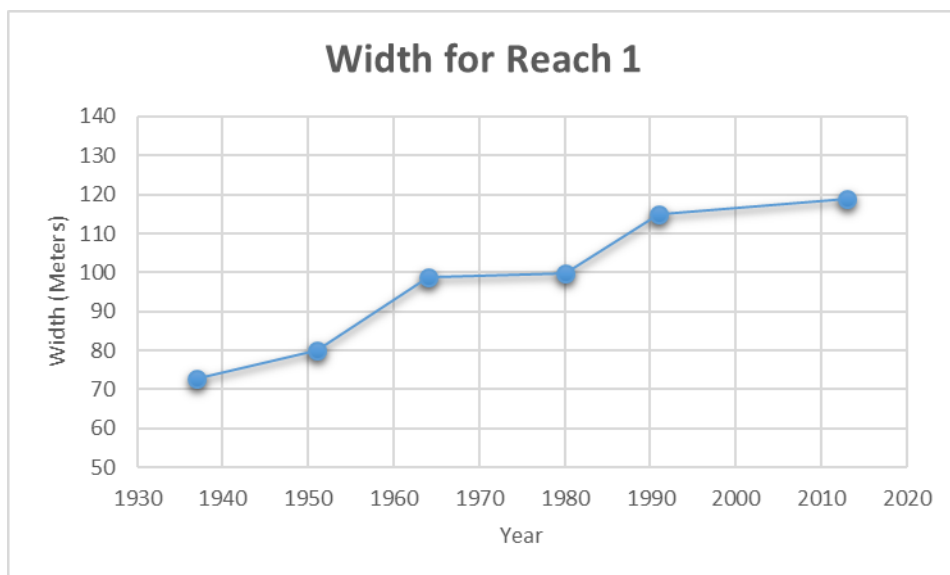
River Reach 1 closely mirrors the analysis from section 3.4.2.1 which focused on the city of Mankato's heavily engineered river stretch containing riprap, earthen levees, and cement flood walls. This characteristic is what was used to define this first river reach. The biggest anomaly seen in this stretch is the decrease in channel migration starting in the 1964-1980 interval and extending to the present. The timing of this decrease correlates to the flood control structure being built in the city in the mid-1960's. Despite the river migration decreasing, width in this reach still increased while sinuosity saw very little variability of the time of record.



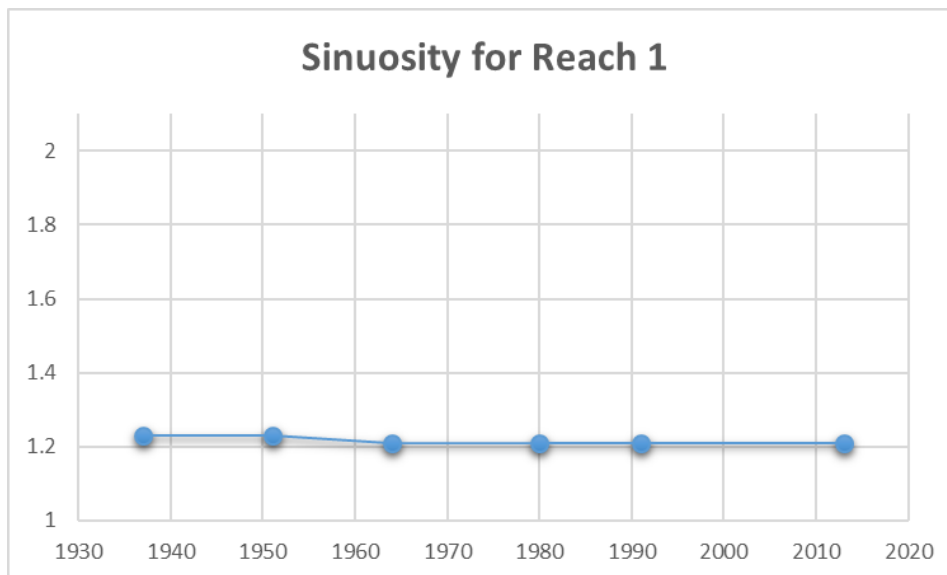
Reach 1 with migration displayed (Red = 1937-1951, Orange = 1951-1964, Yellow = 1964-1980, Green = 1980-1991, Blue = 1991-2013)



Reach 1 annual channel migration from 1937-2013



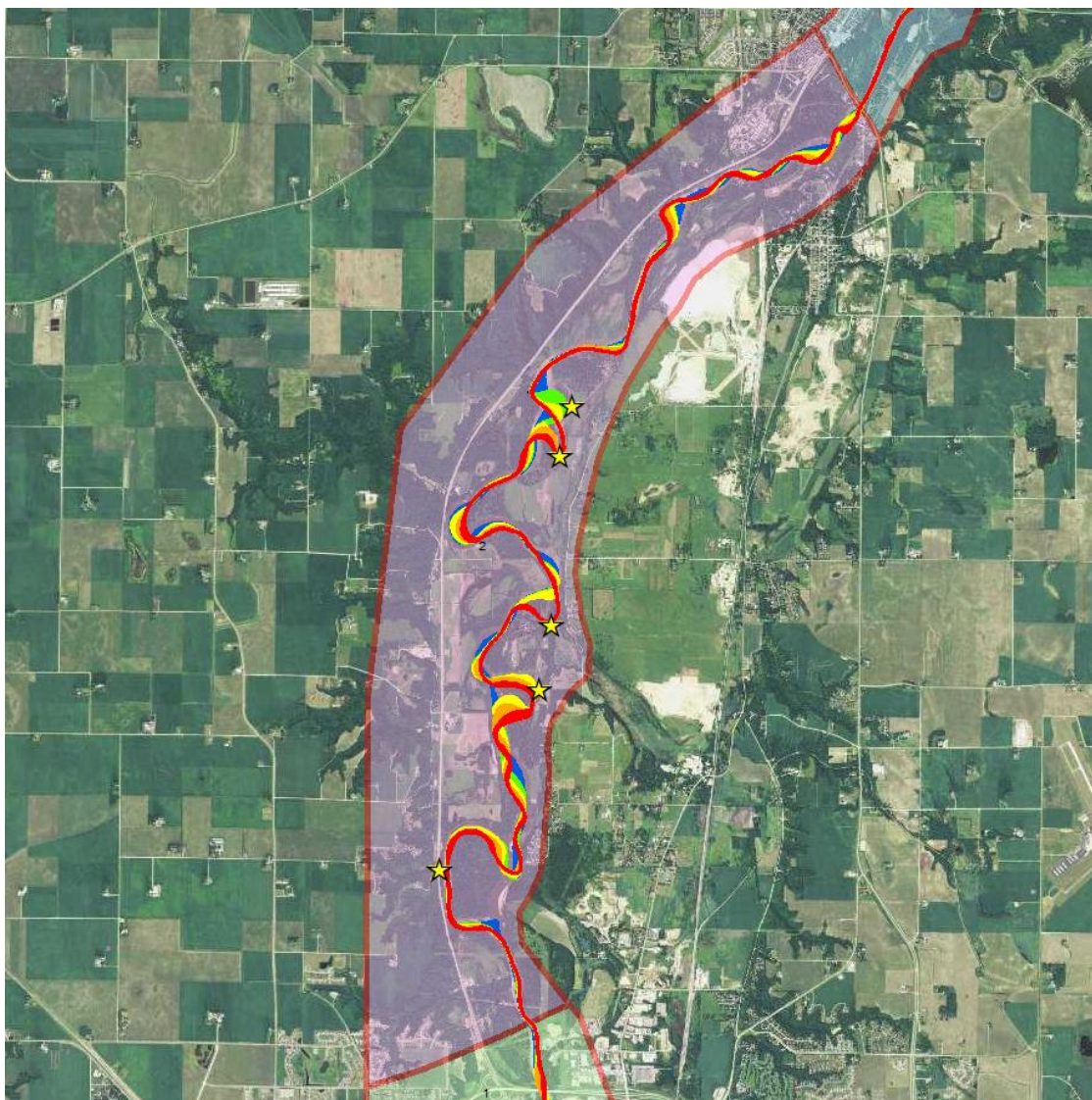
Reach 1 width change from 1937-2013



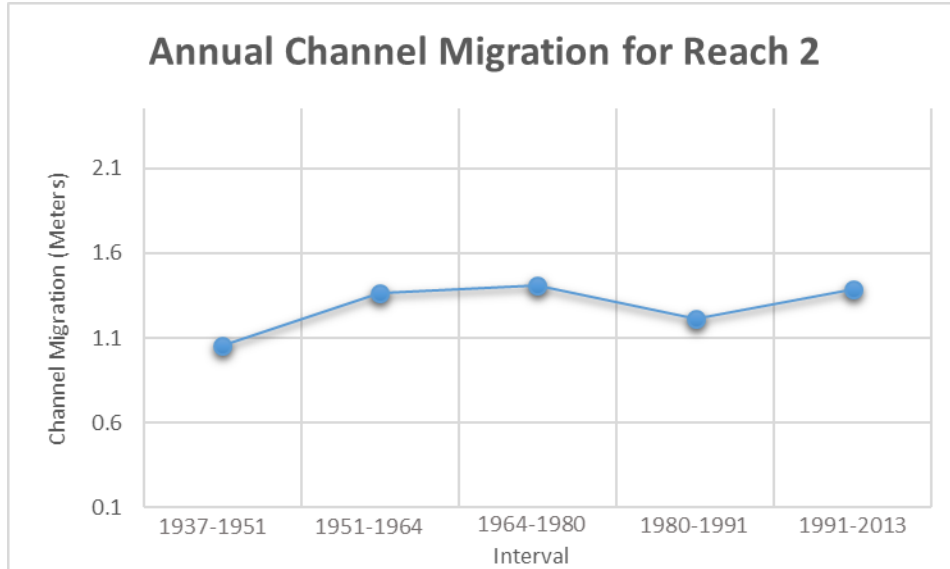
Reach 1 sinuosity from 1937-2013

Reach 2

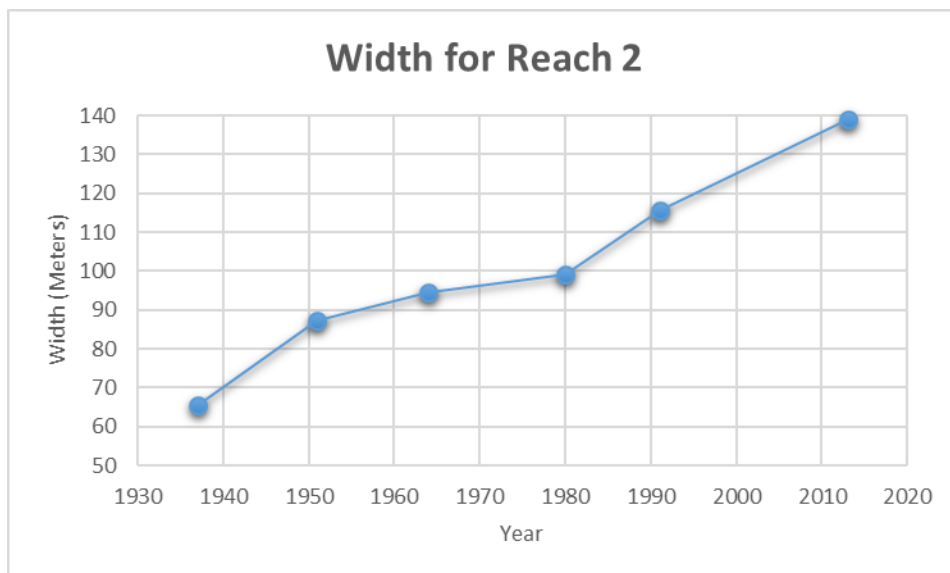
Reach 2 extends from the city of Mankato to St. Peter. This stretch contains a much higher annual migration than the prior reach that is temporally increasing. The width in this stretch has more than doubled in size from 1937-2013. This reach has also seen a significant decrease in sinuosity due to the five cutoffs of record. This reach has experienced the most cutoffs of any of the reaches in this study. This stretch has been highly dynamic in all planform metrics. This is likely due to being the first unconfined stretch downstream from the Blue Earth River confluence which doubles the flow on the Minnesota River and contributes a large amount of sediment to the system. Since Mankato is largely confined it can pass the flow and sediment comparatively effectively making Reach 2 the first unconfined stretch able to adjust to the change in hydrology and sediment load.



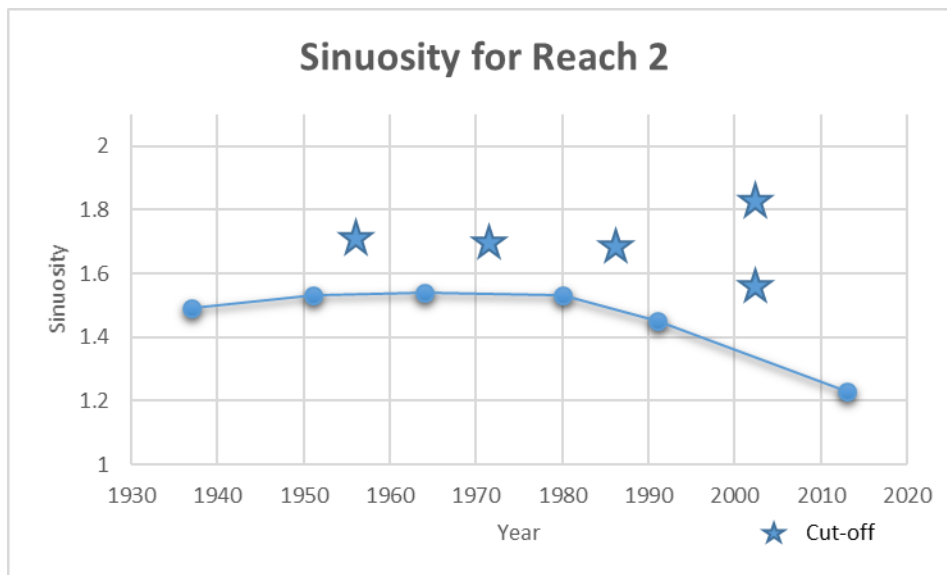
Reach 2 with migration displayed (Red = 1937-1951, Orange = 1951-1964, Yellow = 1964-1980, Green = 1980-1991, Blue = 1991-2013)



Reach 2 annual channel migration from 1937-2013



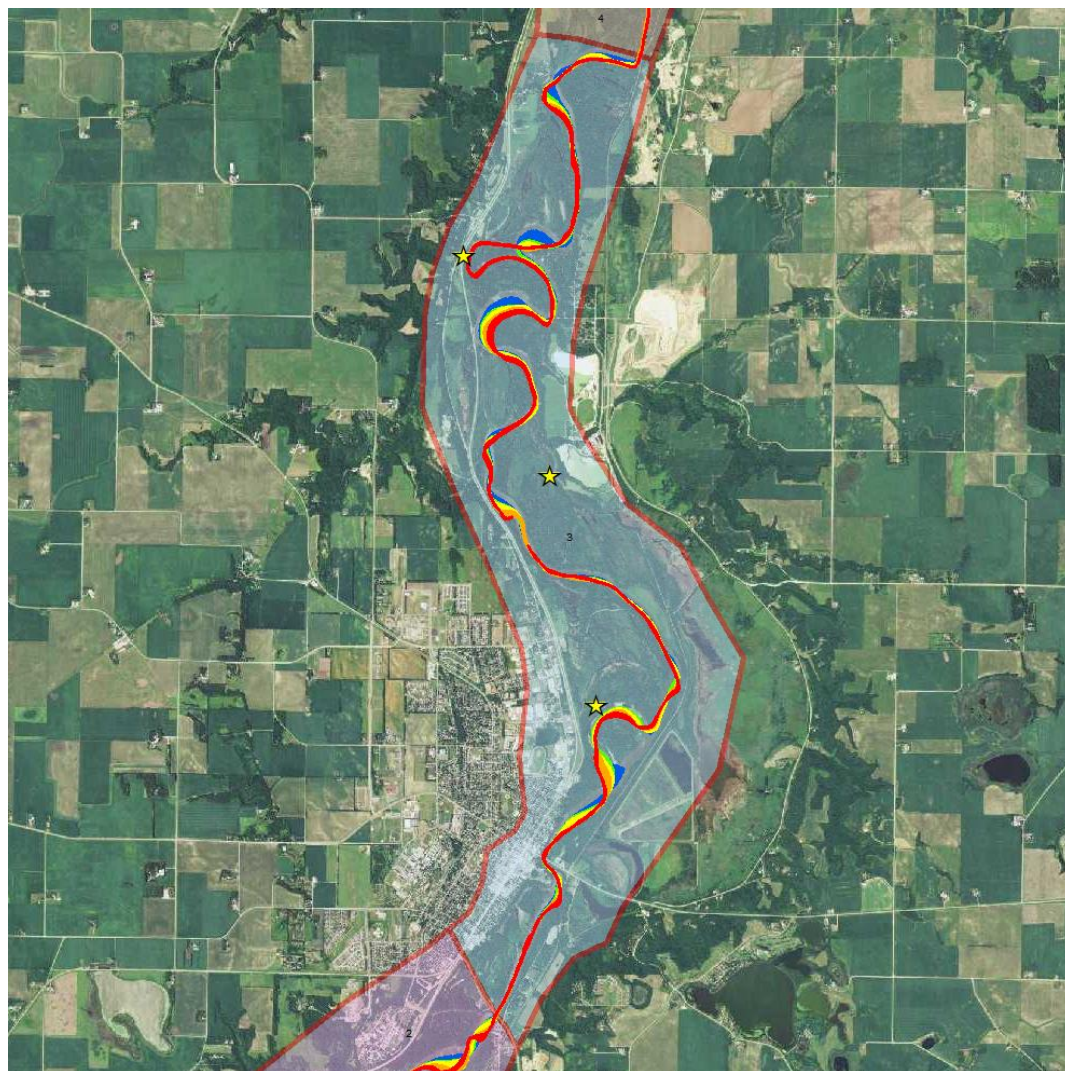
Reach 2 width change from 1937-2013



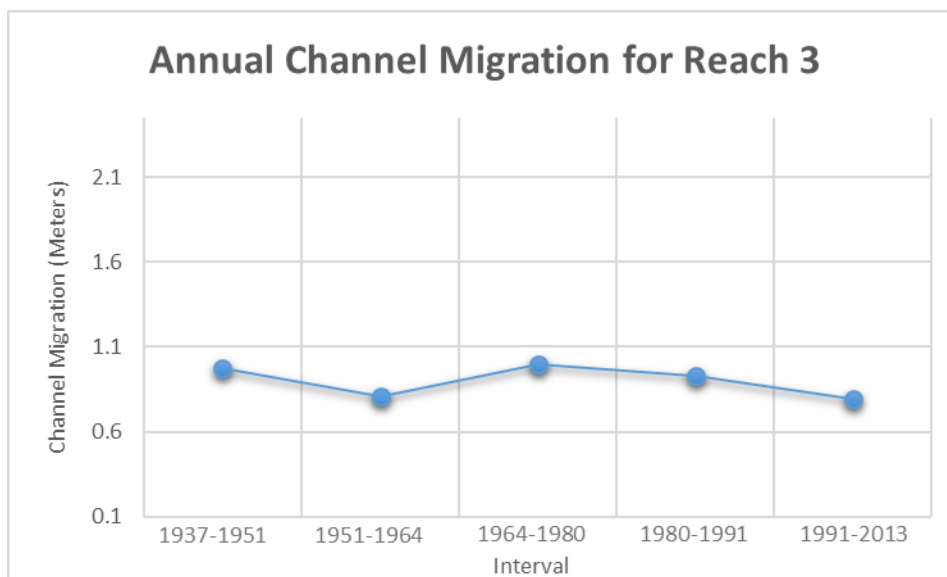
Reach 2 sinuosity from 1937-2013

Reach 3

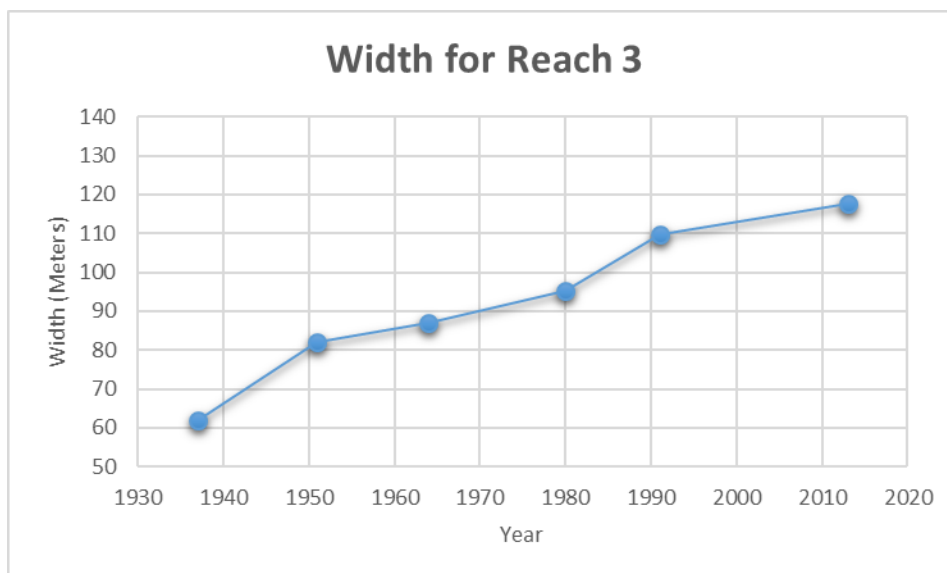
Reach 3 begins at Highway 22 Bridge on the south end of St. Peter and extends into a rural landscape with Highway 169 bordering the west side. The migration in this reach is less dynamic and overall temporally stable. Width has shown a normal increase, but not as dynamic as Reach 2, and sinuosity has seen a decrease due to three cutoffs of record, but remains relatively sinuous overall.



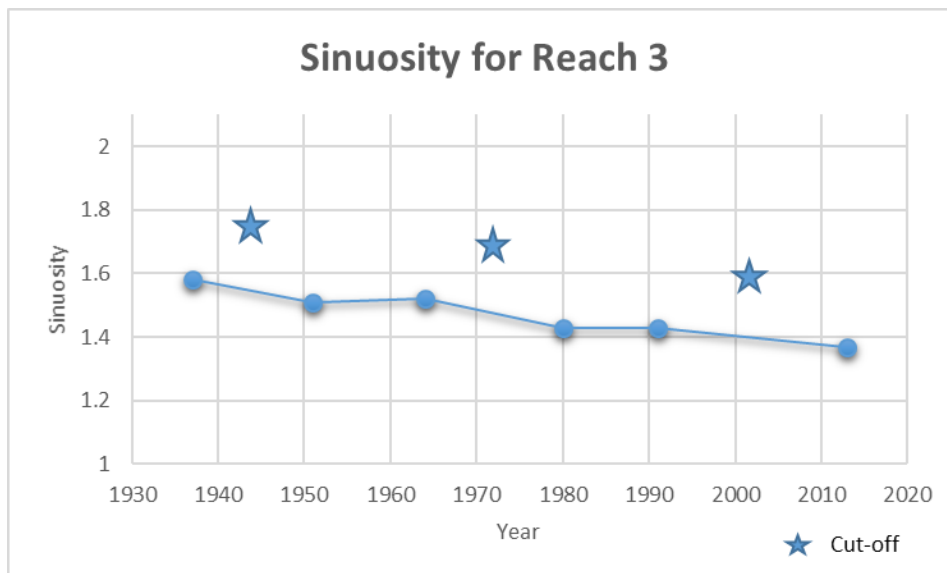
Reach 3 with migration displayed (Red = 1937-1951, Orange = 1951-1964, Yellow = 1964-1980, Green = 1980-1991, Blue = 1991-2013)



Reach 3 annual channel migration from 1937-2013



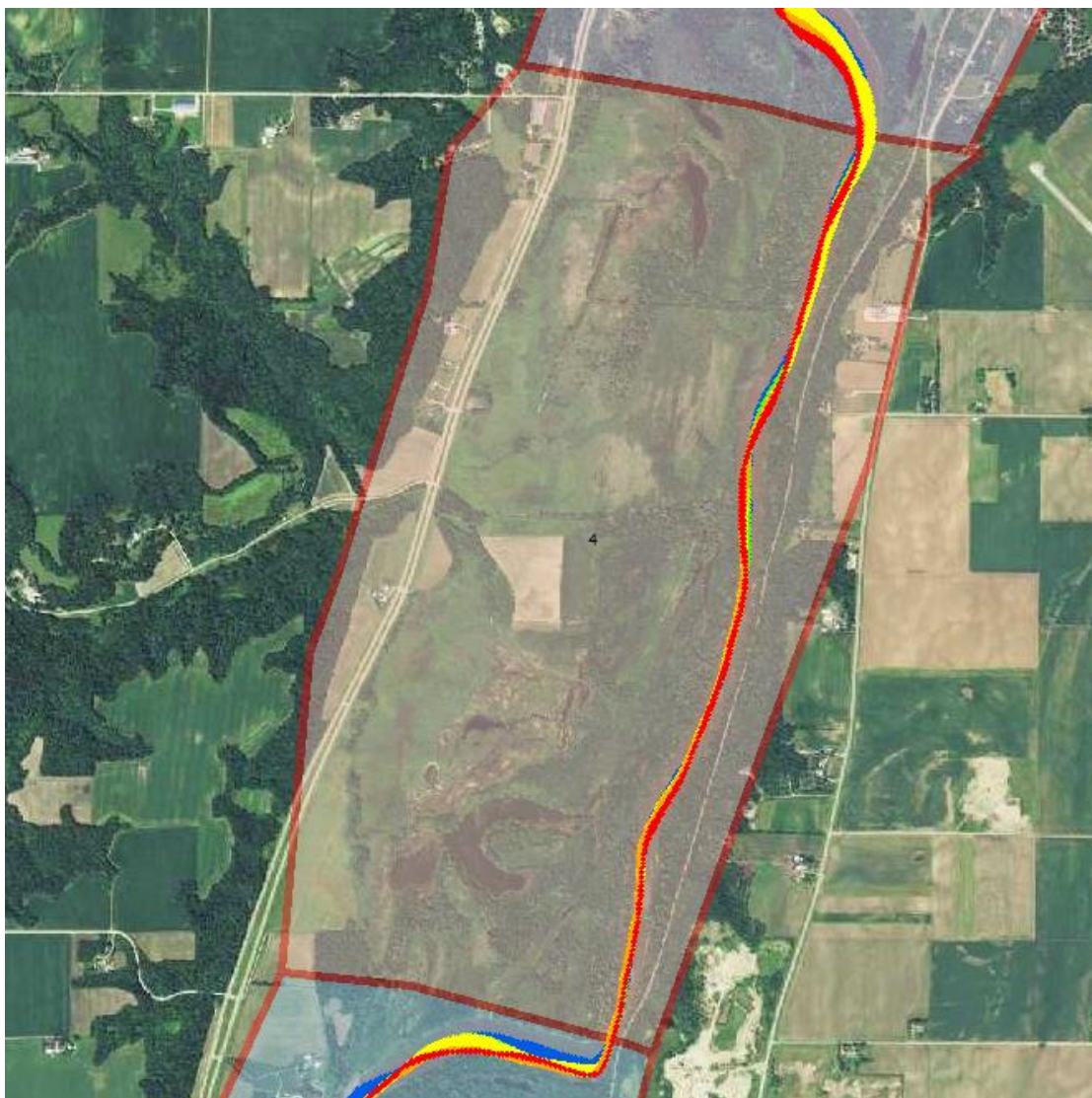
Reach 3 width change from 1937-2013



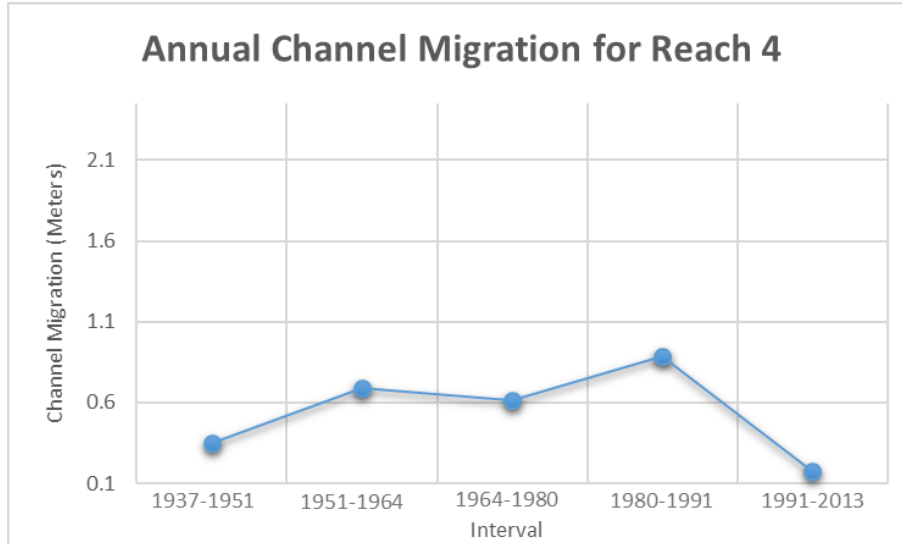
Reach 3 sinuosity from 1937-2013

Reach 4

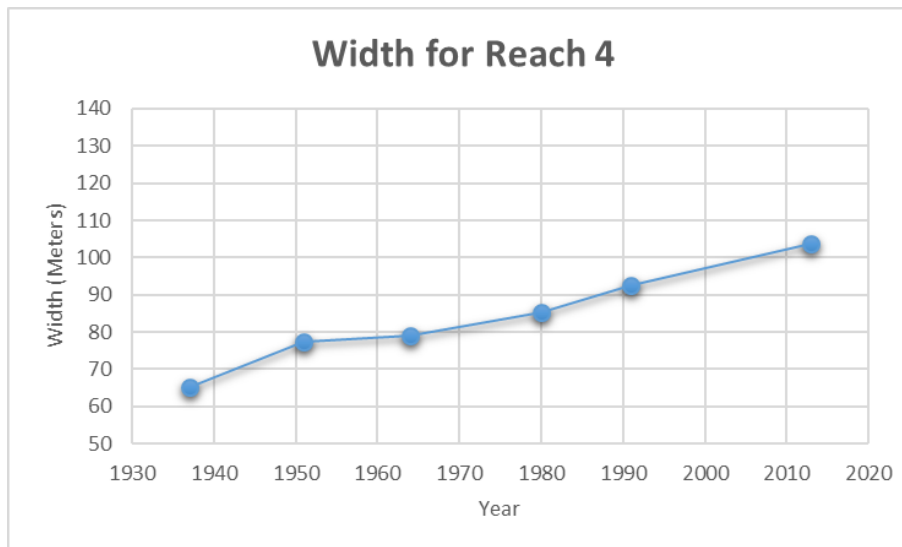
Reach 4 is ~3.6 km rural stretch of river that is abnormally straight in terms of the reach upstream and downstream of it, the study area overall, and naturally meandering rivers in general. There has been some migration observed in this reach but has been contained to the east side of the valley. Width has increased in this reach but not as dramatically as other reaches. Since the channel is so straight in this reach, a sinuosity just above one has been observed over the record of time. Despite the river being so straight over a 76 year period of time, the oxbow lake observed in the south-west portion of the reach shows this straight channel has not always been characteristic. Based on the LiDAR an initial hypothesis that this stretch of river is being pressed up against the east valley wall by a large alluvial fan from a large sediment laden tributary (Barney Fry Creek) entering from the west side of the valley.



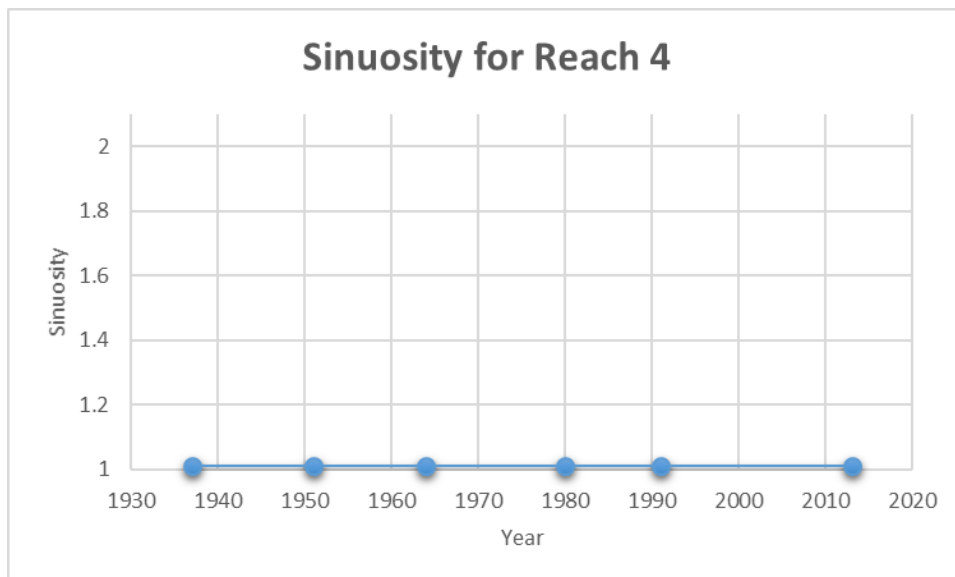
Reach 4 with migration displayed (Red = 1937-1951, Orange = 1951-1964, Yellow = 1964-1980, Green = 1980-1991, Blue = 1991-2013)



Reach 4 annual channel migration from 1937-2013



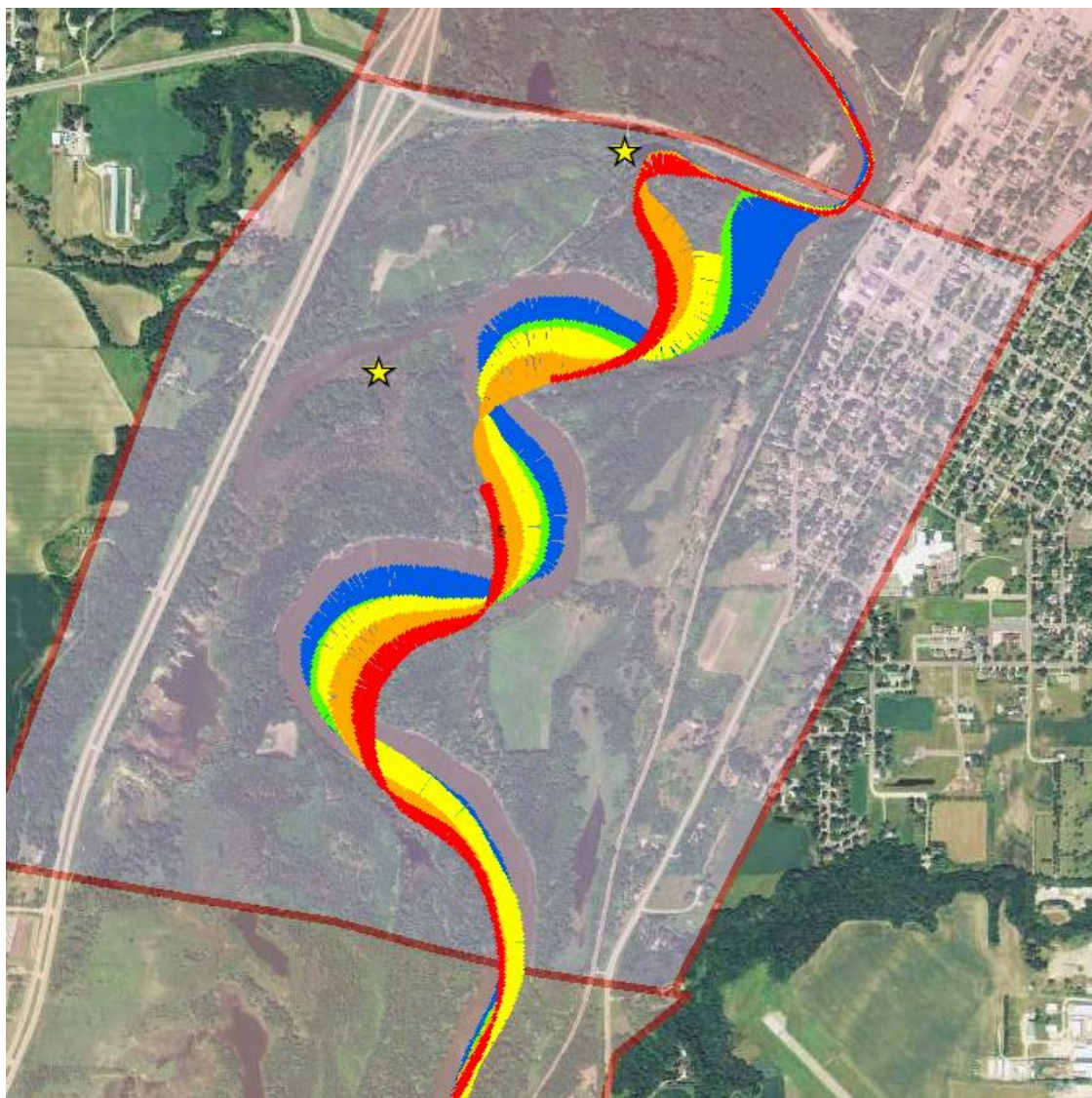
Reach 4 width change from 1937-2013



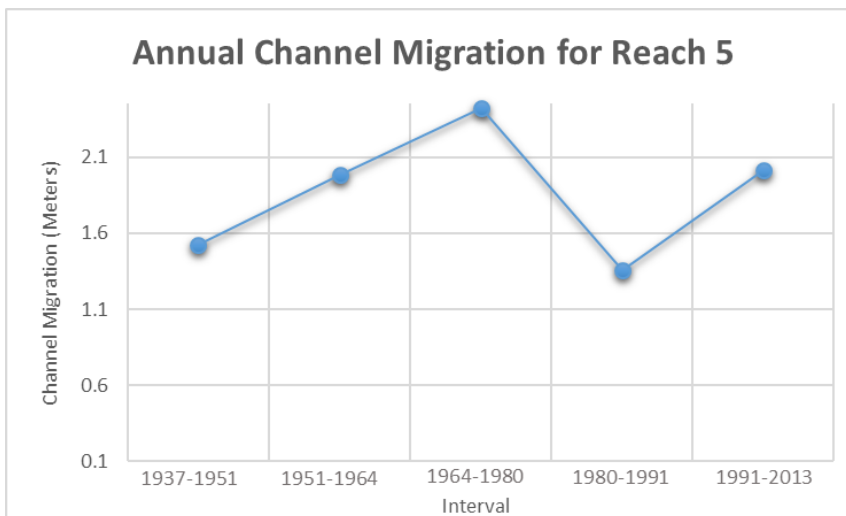
Reach 4 sinuosity from 1937-2013

Reach 5

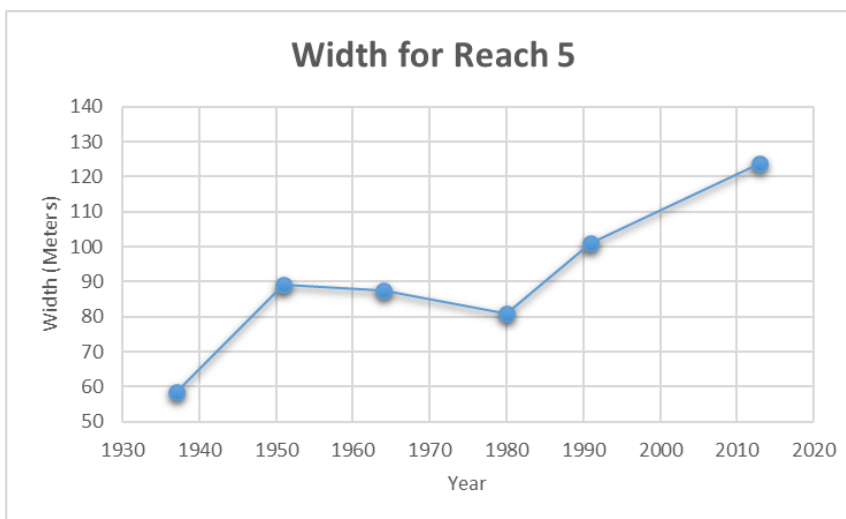
Reach 5 is approximately the same stream length as Reach 4 but juxtaposes the former reach in planform characteristics. This reach is highly active in terms of channel migration, with significant width increase, and a sinuosity between 1.5-1.7 and two cutoffs over the record of time. If the prior zone in being controlled by an alluvial fan this area could mark the transition away from that control allowing the river to react in a highly dynamic way much like Reach 2 from Reach 1.



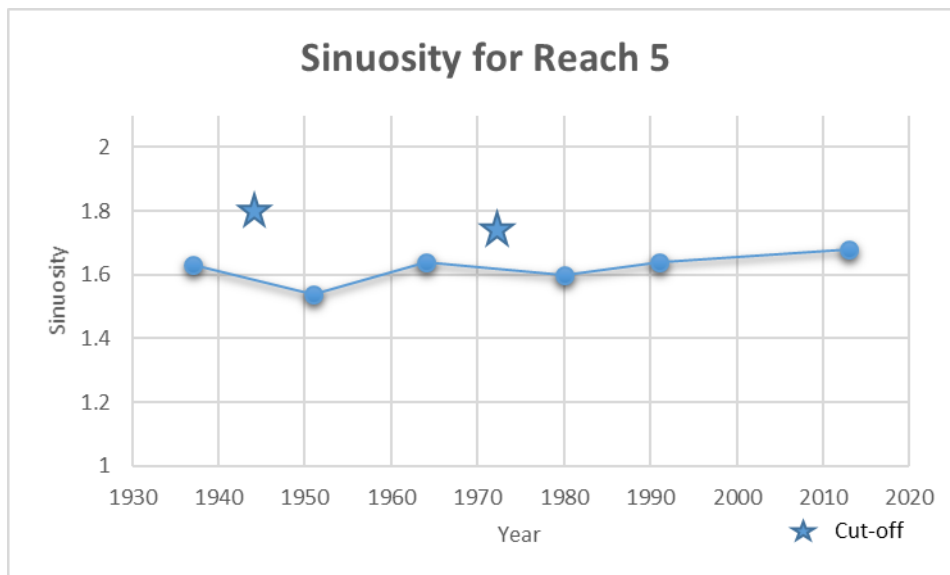
Reach 5 with migration displayed (Red = 1937-1951, Orange = 1951-1964, Yellow = 1964-1980, Green = 1980-1991, Blue = 1991-2013)



Reach 5 annual channel migration from 1937-2013



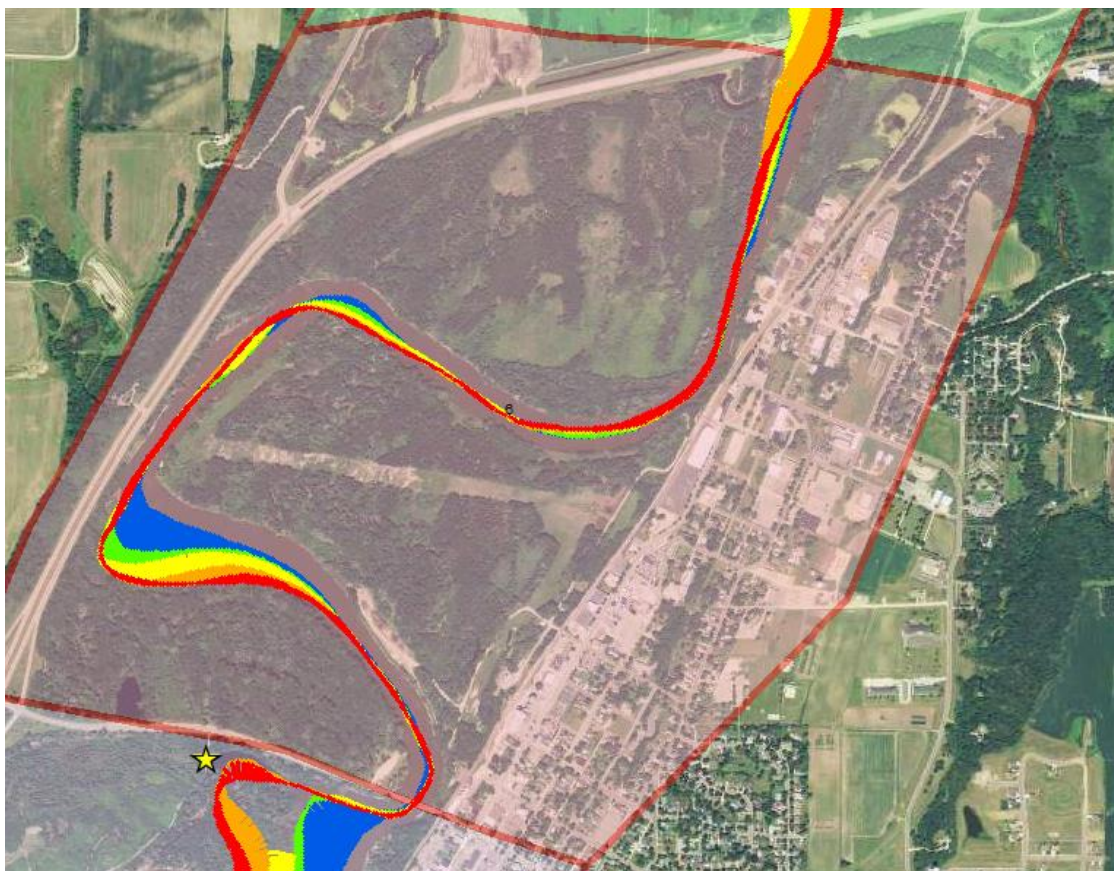
Reach 5 width change from 1937-2013



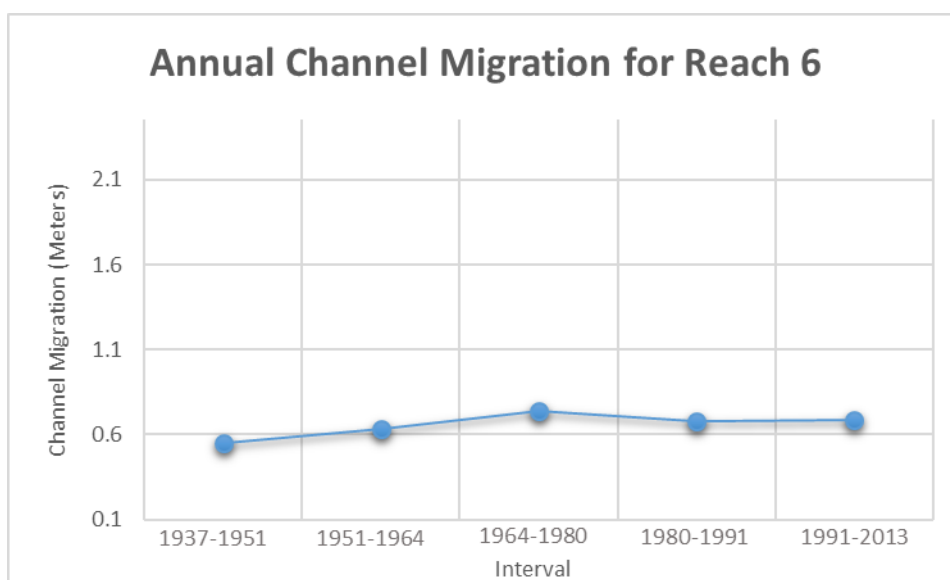
Reach 5 sinuosity from 1937-2013

Reach 6

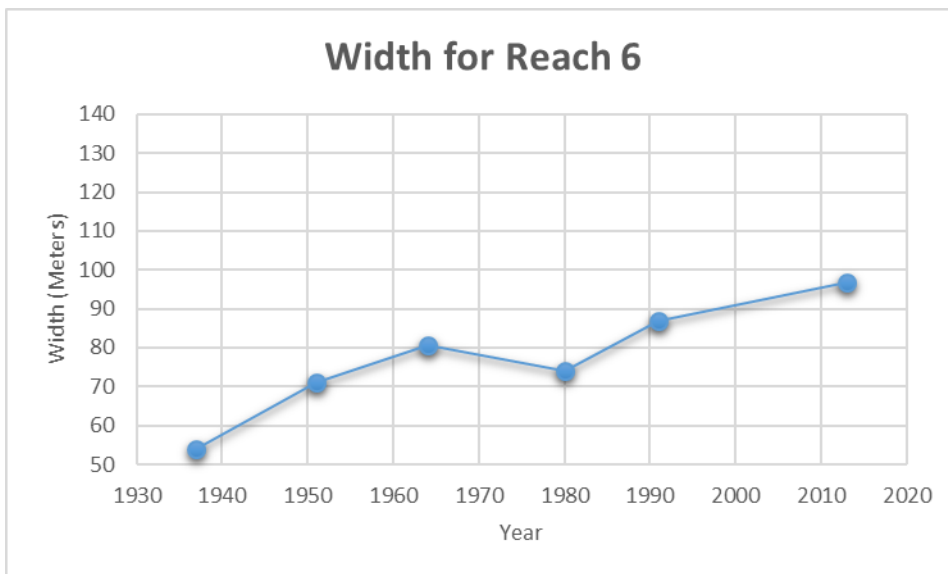
Reach 6 is approximately the length of prior two reaches, but again displays a differing planform. This reach is between the at 336th Street Bridge and Highway 169 Bridge with the city of Le Sueur on the east side and Highway 169 running along the west and north west side. The annual migration is rather steady temporally hovering right around 0.6 meter/year. The width in this reach saw an increase over time, but not as great as most other reaches. The sinuosity has remained very high in this stretch with the channel traveling between the valley walls twice in a short span. The geometry of this stretch of channel is likely influenced greatly by the encroachment and confinement of anthropogenic structures.



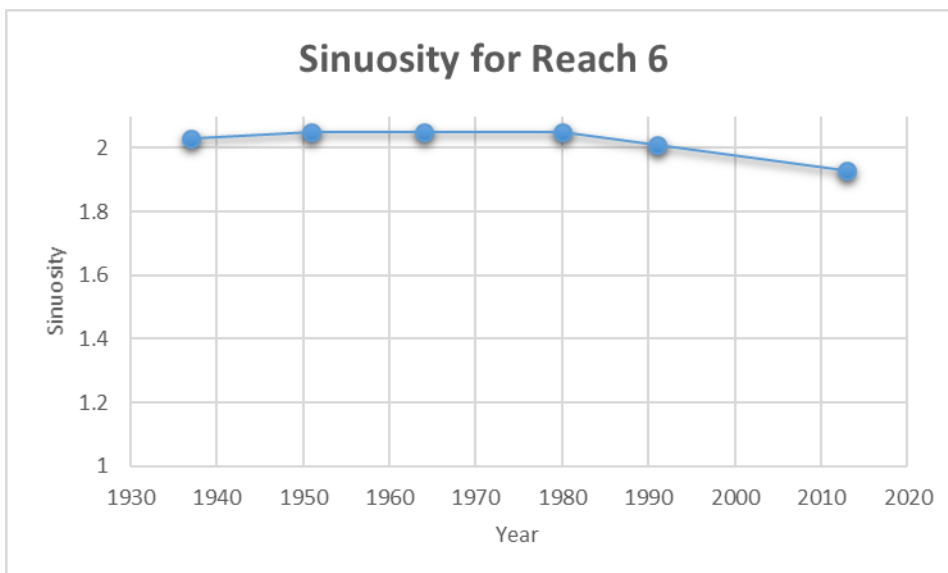
Reach 6 with migration displayed (Red = 1937-1951, Orange = 1951-1964, Yellow = 1964-1980, Green = 1980-1991, Blue = 1991-2013)



Reach 6 annual channel migration from 1937-2013



Reach 6 width change from 1937-2013

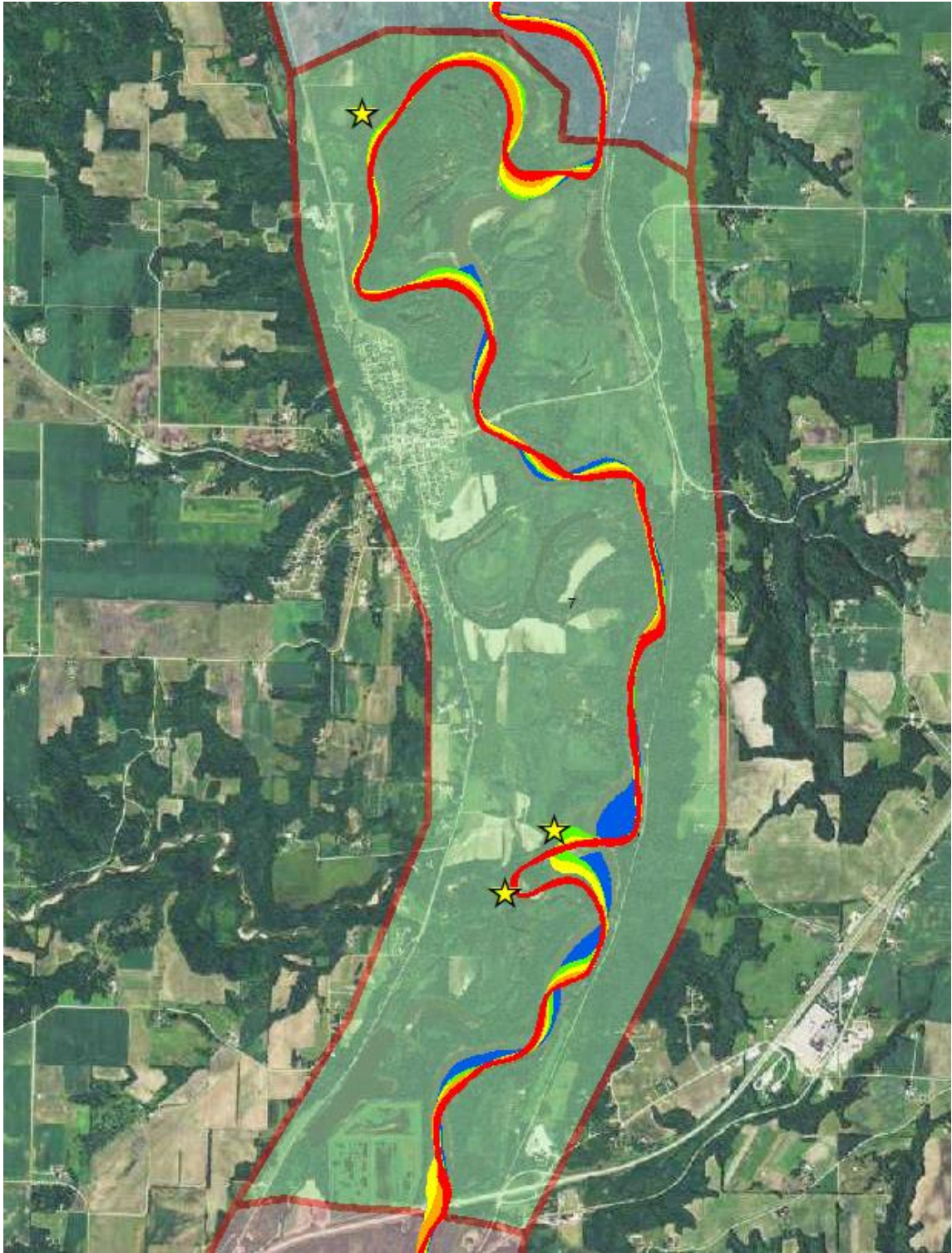


Reach 6 sinuosity from 1937-2013

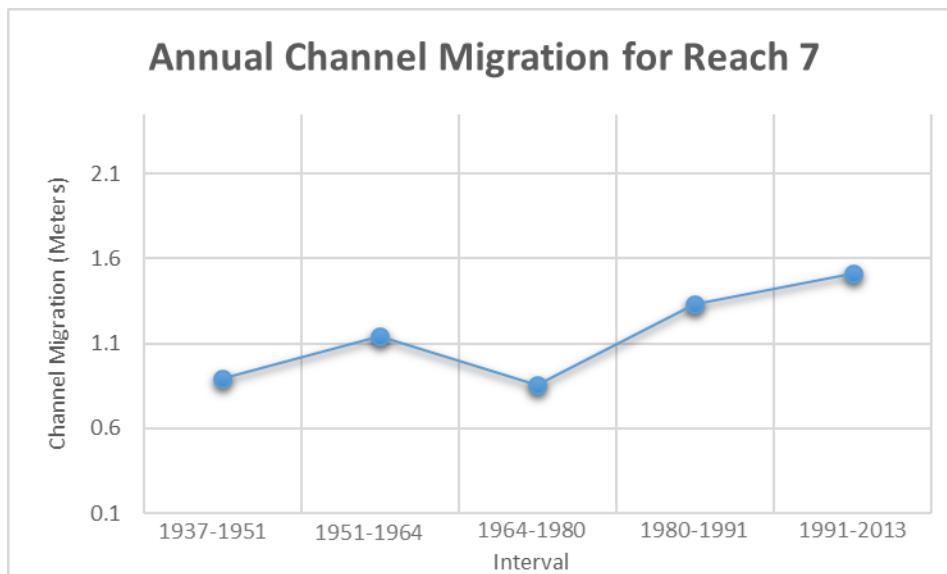
Reach 7

Reach 7 extends from the Highway 169 Bridge in Le Sueur into a rural area past the town of Henderson. This reach has seen a fairly significant increase in migration and

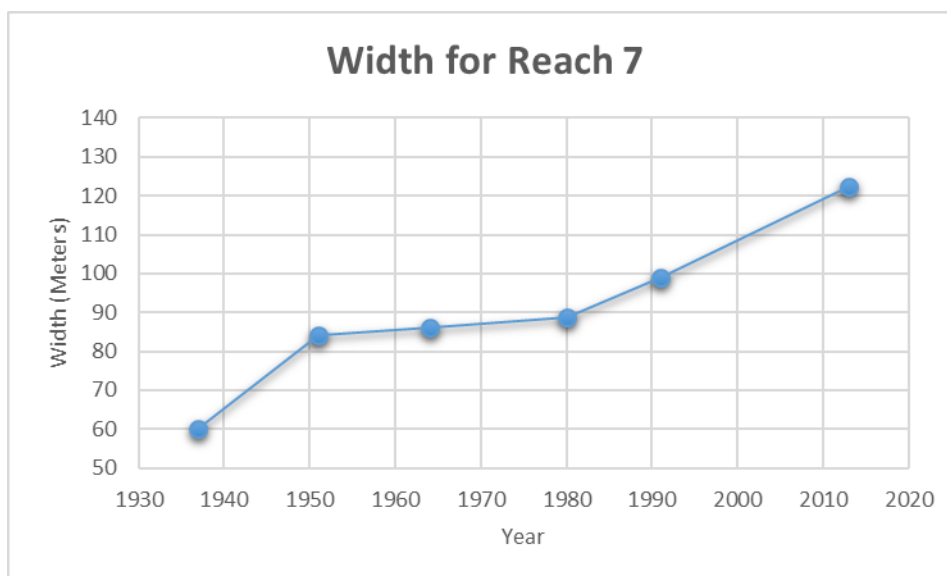
width temporally. This stretch was very sinuous compared to other reaches but has experienced three cutoffs of record with one in the 1991-2013 interval which reduced the stream length by 4 km decreasing sinuosity by 0.5. The reach also has another very sediment laden tributary (Rush River) entering from the west. Two of the three cutoff occurred right at the confluence of the Rush River. It is also interesting to note that a section of this reach is rather straight and in close proximity to the east wall much in the same way Reach 4 is. This furthers the hypothesis of high sediment tributaries ability to constrain and straighten the channel against a valley wall. Also like Reach 4, there are old oxbow lakes present indicating this has not always been characteristic. This leads to furthering the hypothesis to increases in hydrology and bank erosion altering the characteristics of the modern channel.



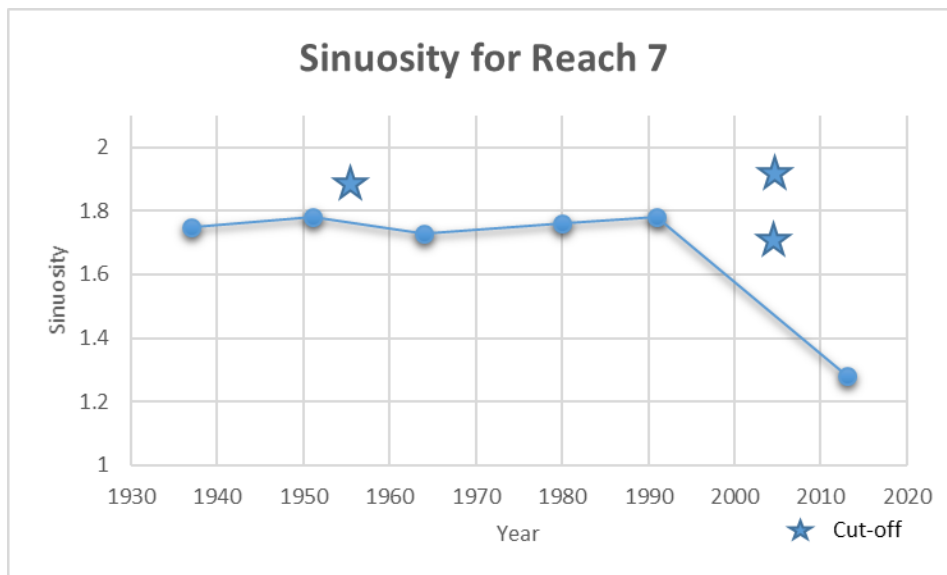
Reach 7 with migration displayed (Red = 1937-1951, Orange = 1951-1964, Yellow = 1964-1980, Green = 1980-1991, Blue = 1991-2013)



Reach 7 annual channel migration from 1937-2013



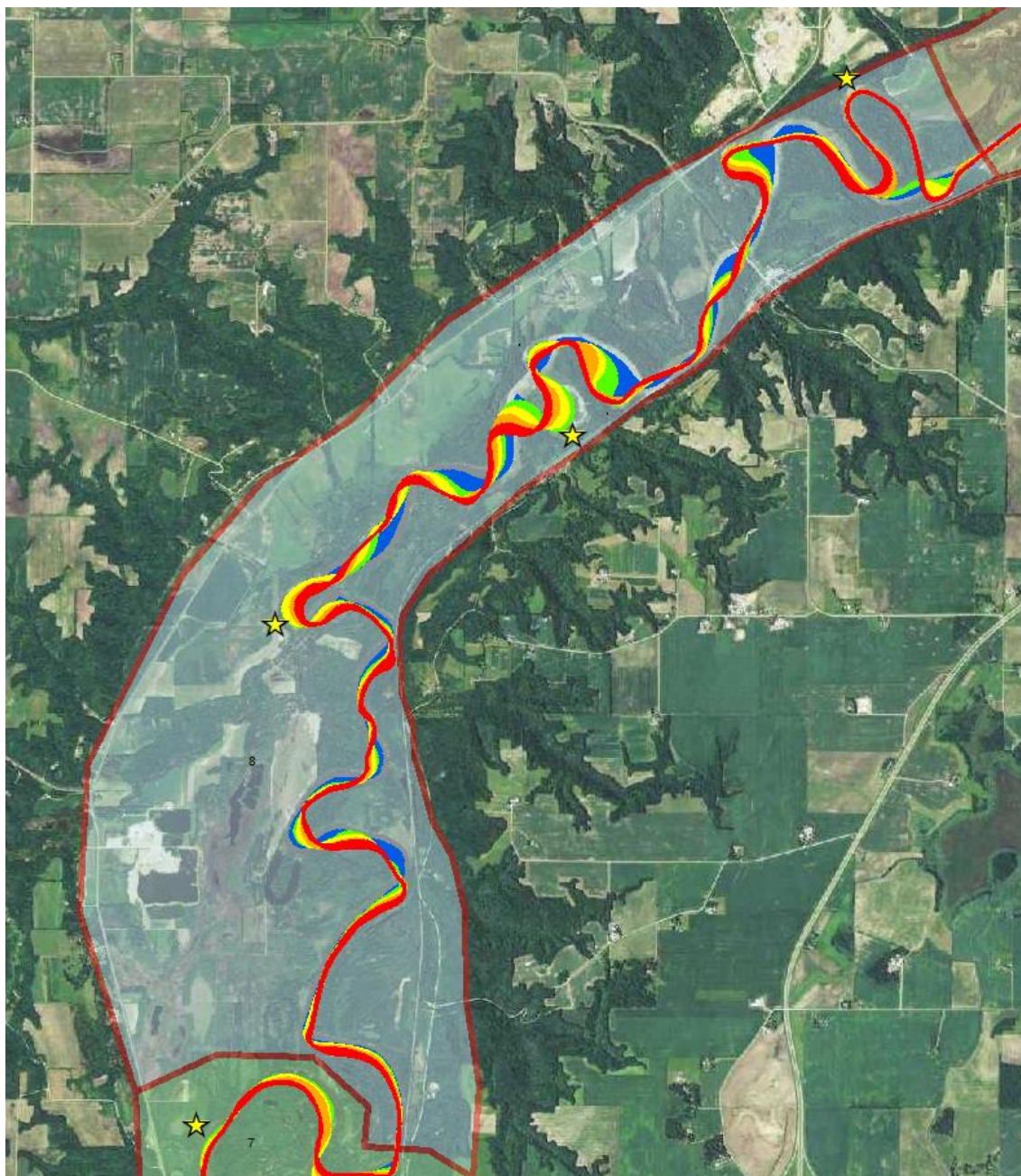
Reach 7 width change from 1937-2013



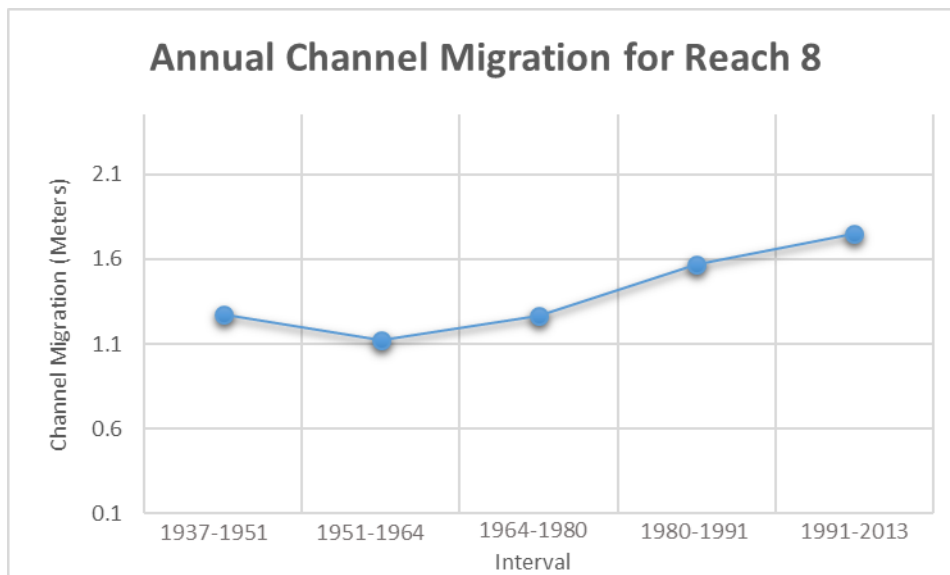
Reach 7 sinuosity from 1937-2013

Reach 8

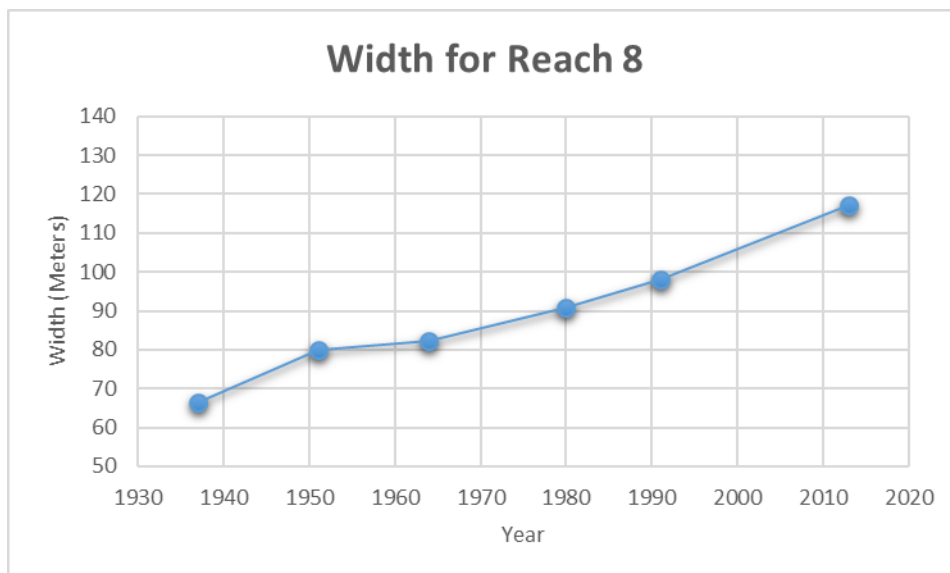
Reach 8 is another stretch of river that is highly active in terms of channel migration and increasing temporally along with width increasing steadily temporally as well. This reach has seen a decline in sinuosity due to the present of three cutoffs, two of which occurred between 1991-2013. These are the last cutoffs seen in the lower portion of the study area.



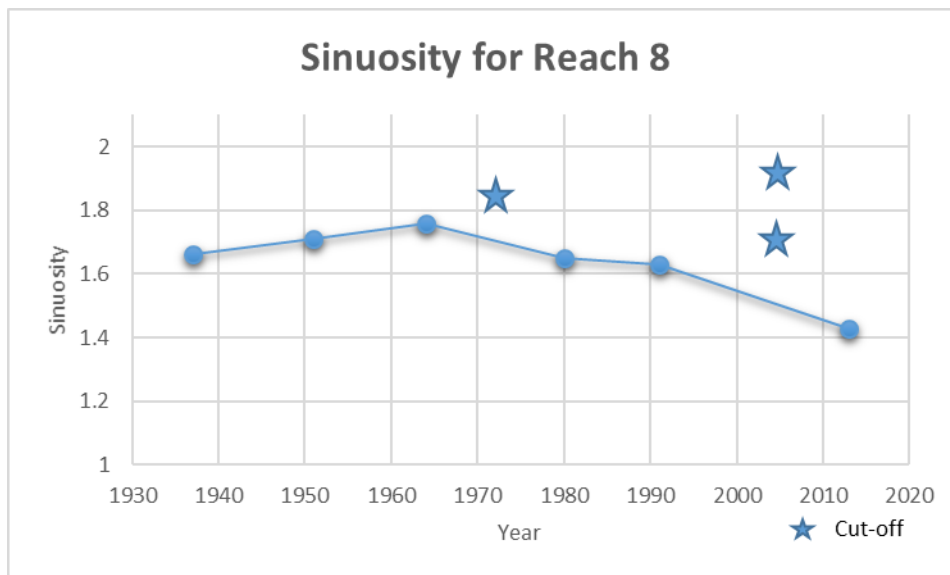
Reach 8 with migration displayed (Red = 1937-1951, Orange = 1951-1964, Yellow = 1964-1980, Green = 1980-1991, Blue = 1991-2013)



Reach 8 annual channel migration from 1937-2013



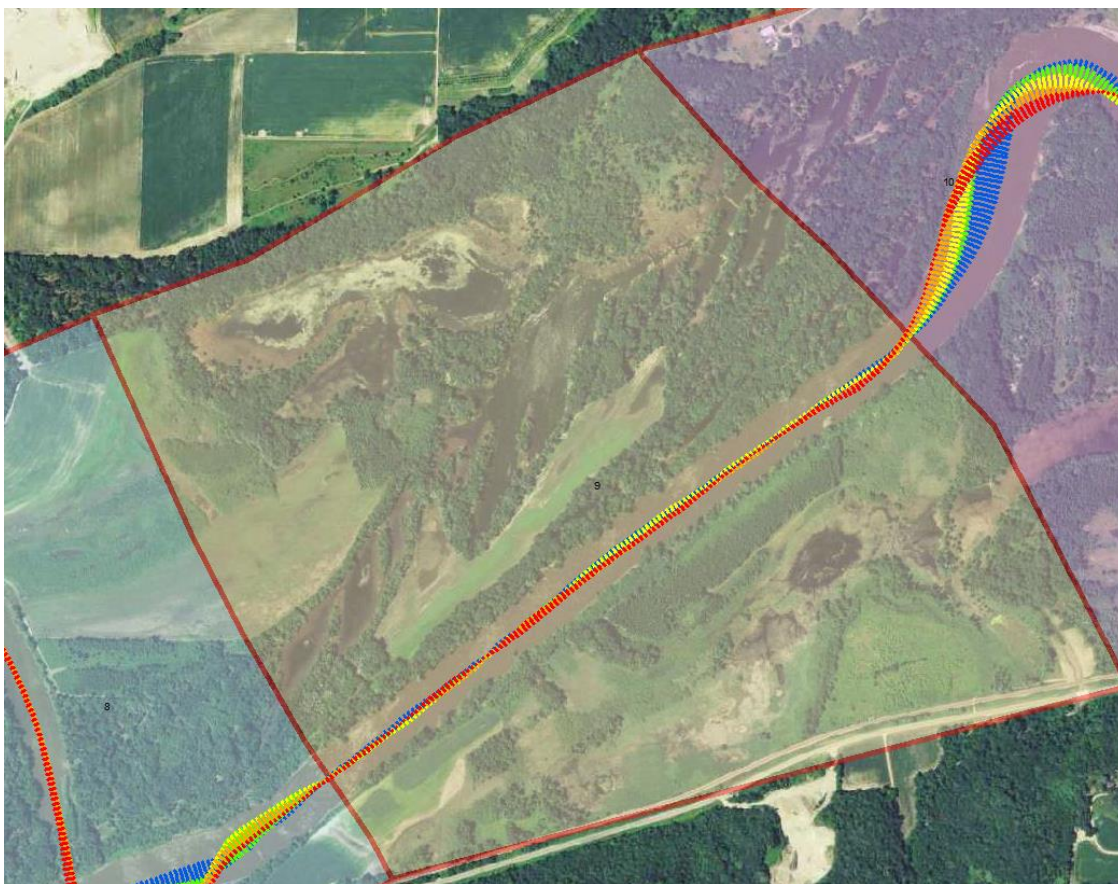
Reach 8 width change from 1937-2013



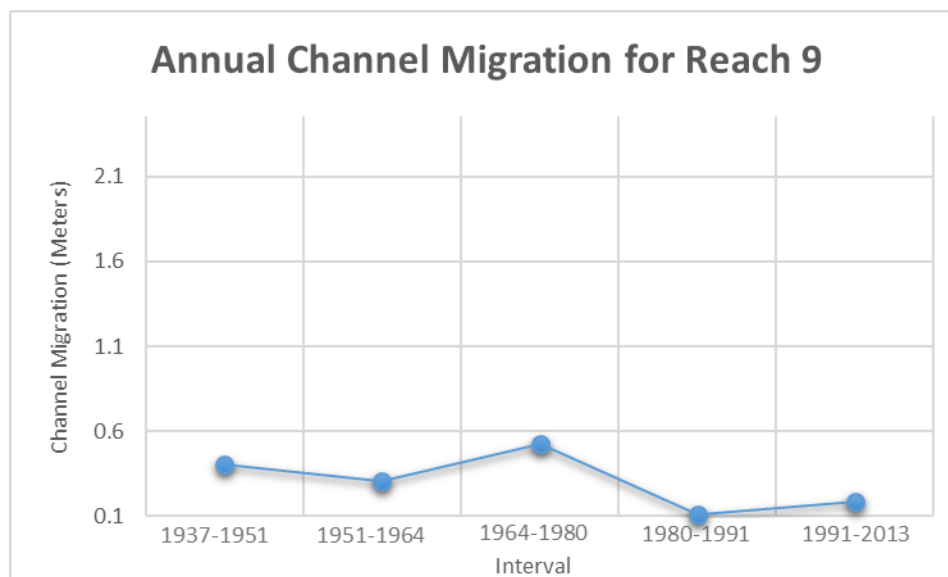
Reach 8 sinuosity from 1937-2013

Reach 9

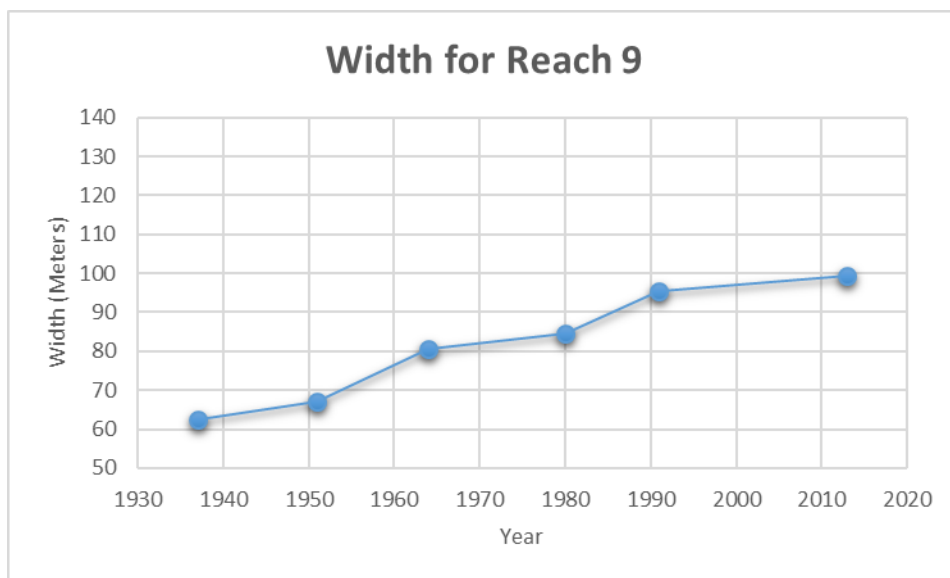
Reach 9 is another very straight stretch of river. Little channel migration has occurred in this area and has experienced channel widening but less than that of other reaches. Sinuosity has steadily stayed just above over the past 76 years. Although it was hypothesized that other straight stretches were being constrained by high amounts of sediment contributed from tributaries pressing the channel up against the valley wall, this is not the case in this stretch. This reach is not against the valley wall and no major tributaries are present. However this stretch does contain various wetland areas surrounding it which could have a stabilizing effect.



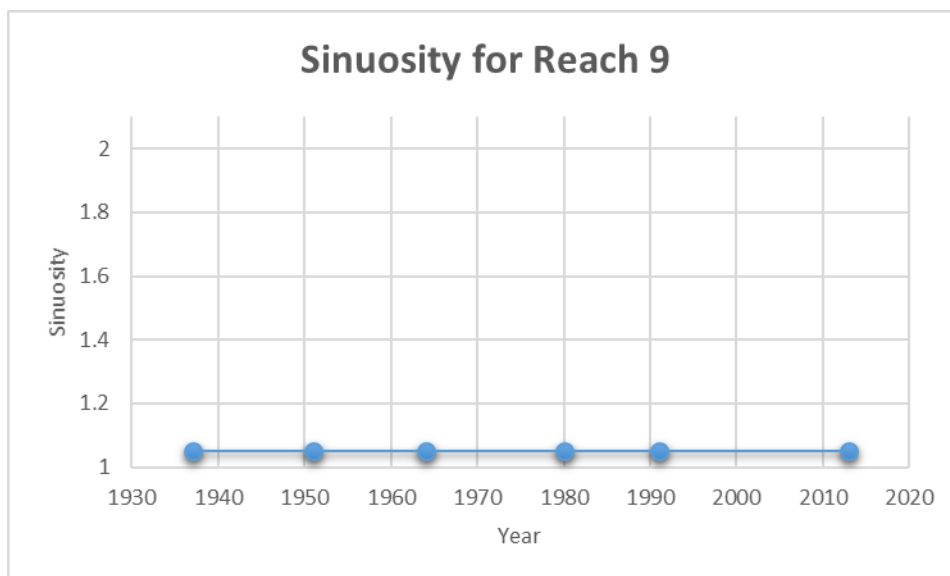
Reach 9 with migration displayed (Red = 1937-1951, Orange = 1951-1964, Yellow = 1964-1980, Green = 1980-1991, Blue = 1991-2013)



Reach 9 annual channel migration from 1937-2013



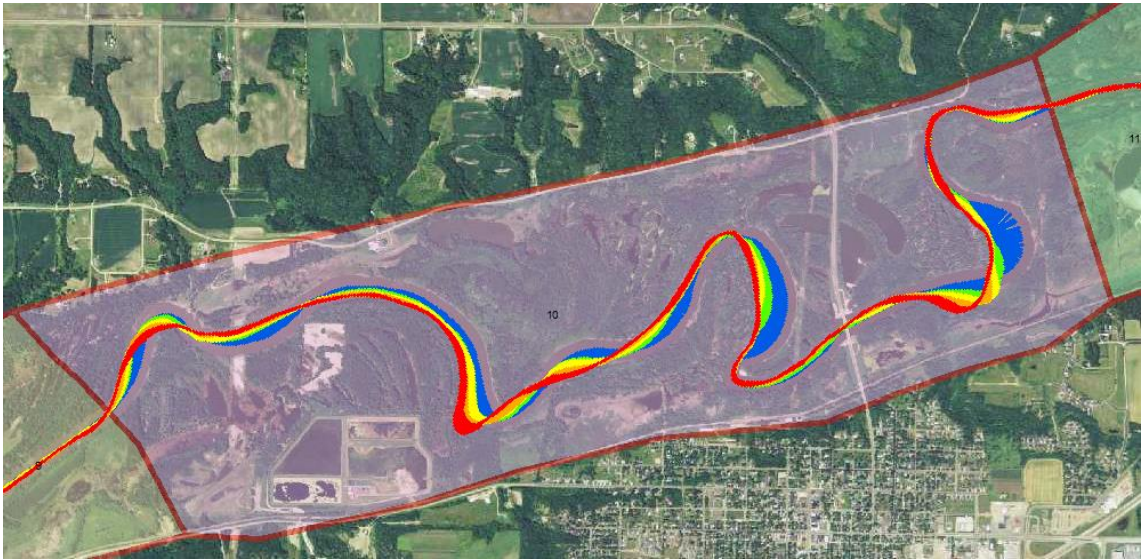
Reach 9 width change from 1937-2013



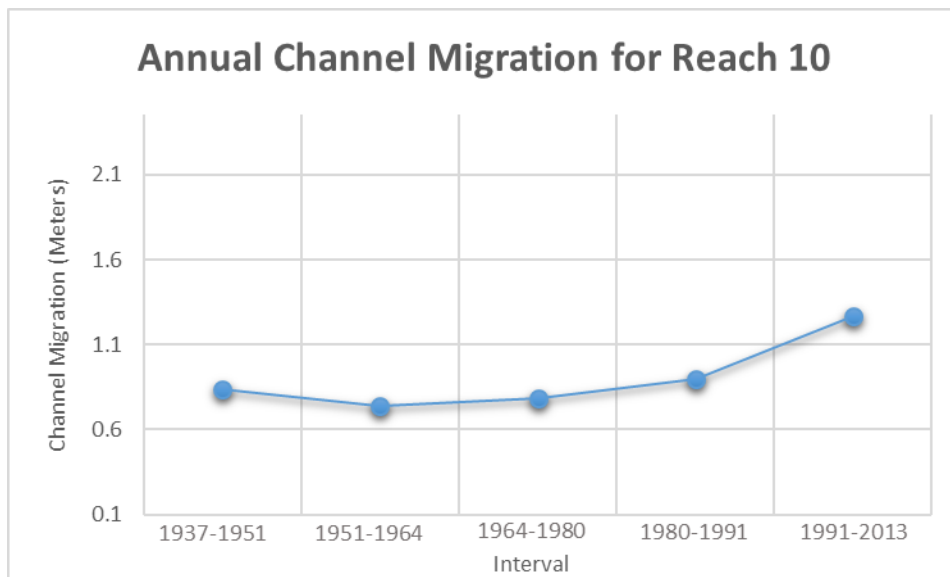
Reach 9 sinuosity from 1937-2013

Reach 10

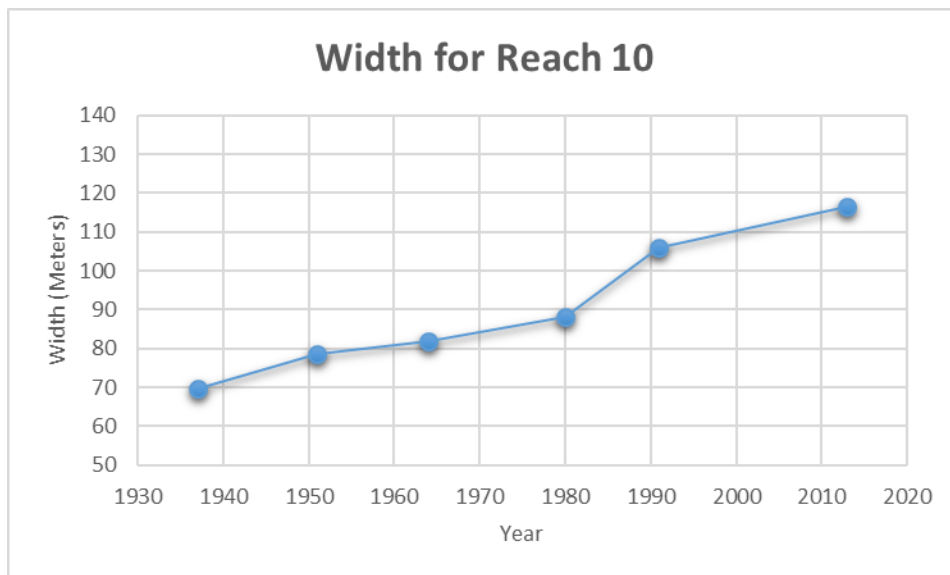
Reach 10 is has a moderate but increasing channel migration and a common increasing channel width. This reach however differs from its upstream and downstream reaches in having a significantly greater sinuosity. It also occupying the entire river valley and has historic fluvial features (oxbows, scroll bars) throughout the valley.



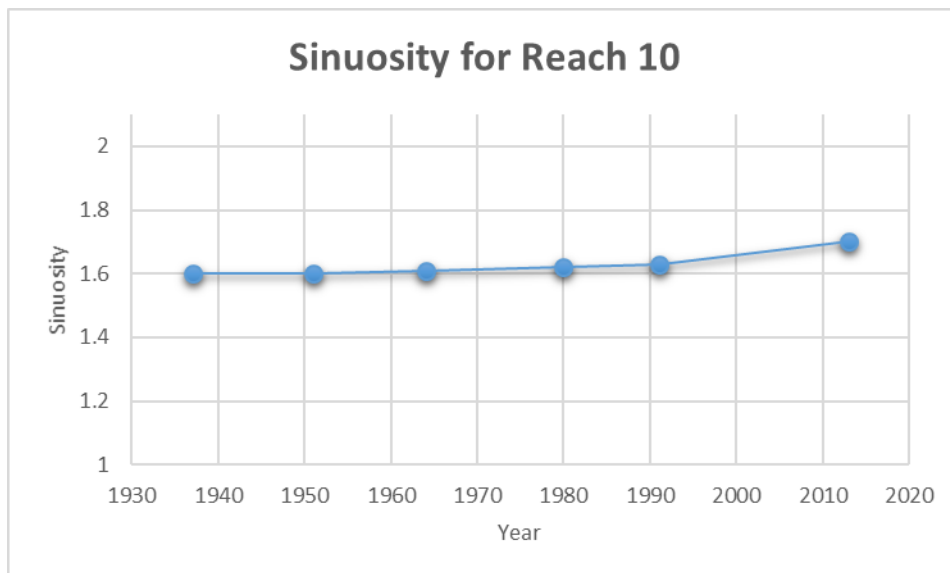
Reach 10 with migration displayed (Red = 1937-1951, Orange = 1951-1964, Yellow = 1964-1980, Green = 1980-1991, Blue = 1991-2013)



Reach 10 annual channel migration from 1937-2013



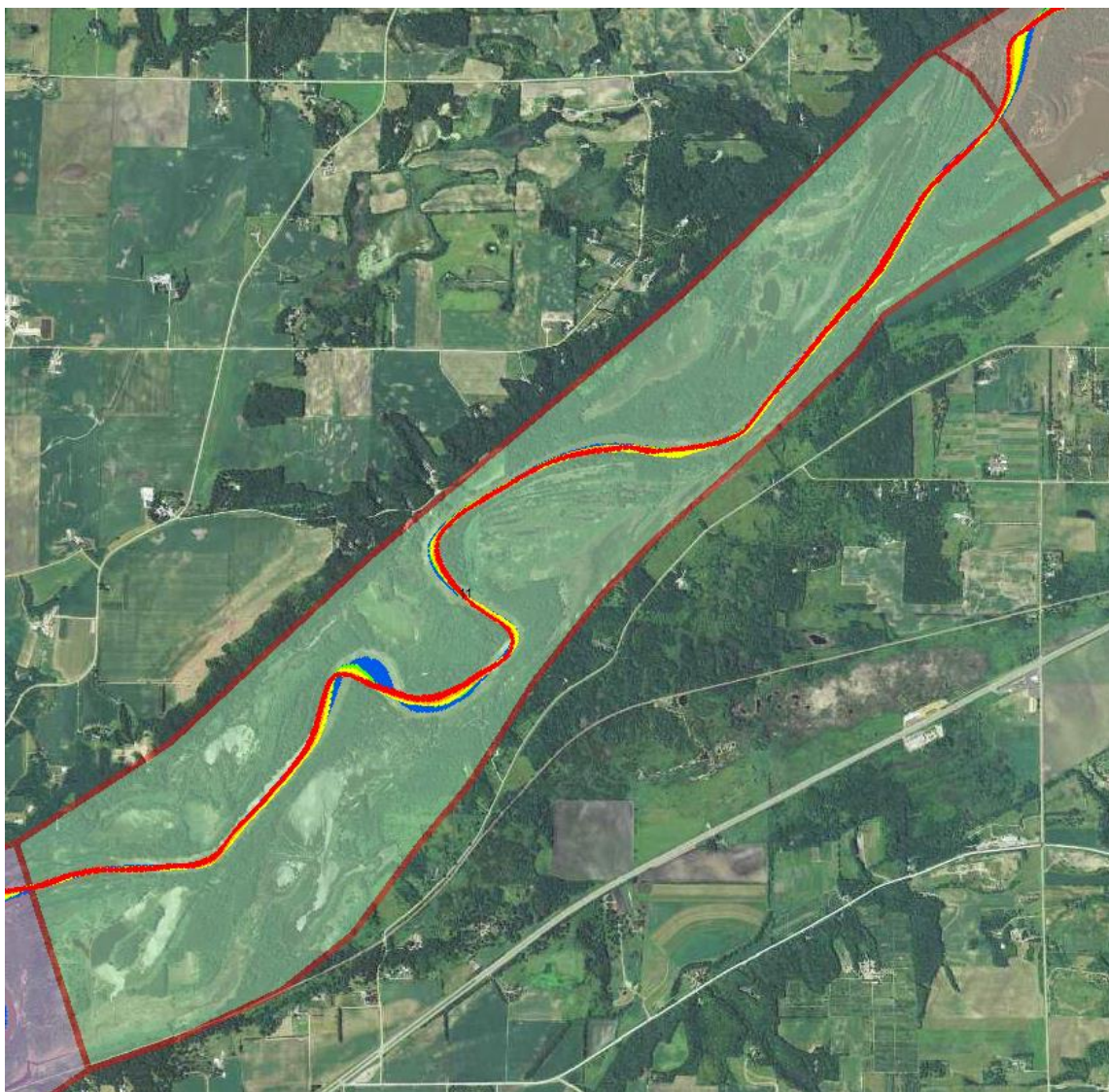
Reach 10 width change from 1937-2013



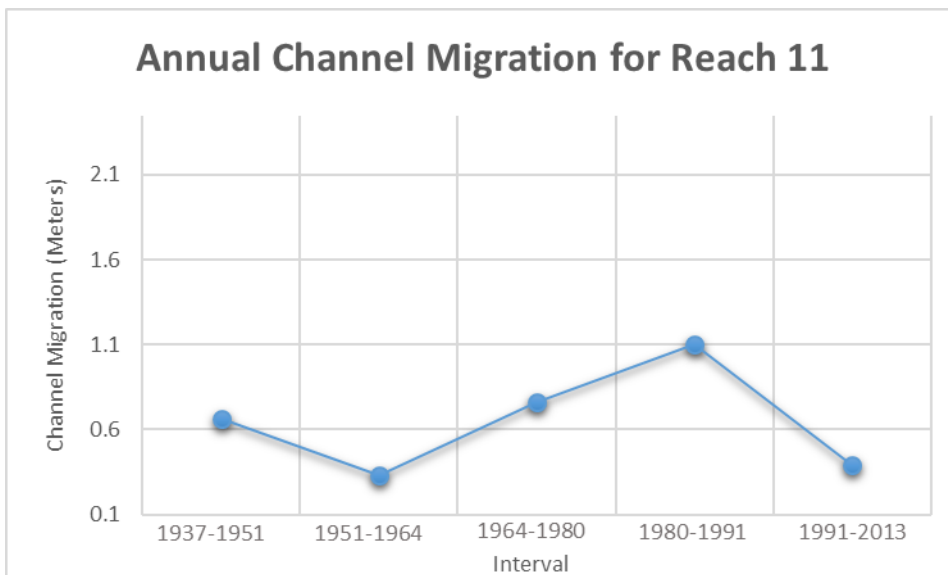
Reach 10 sinuosity from 1937-2013

Reach 11

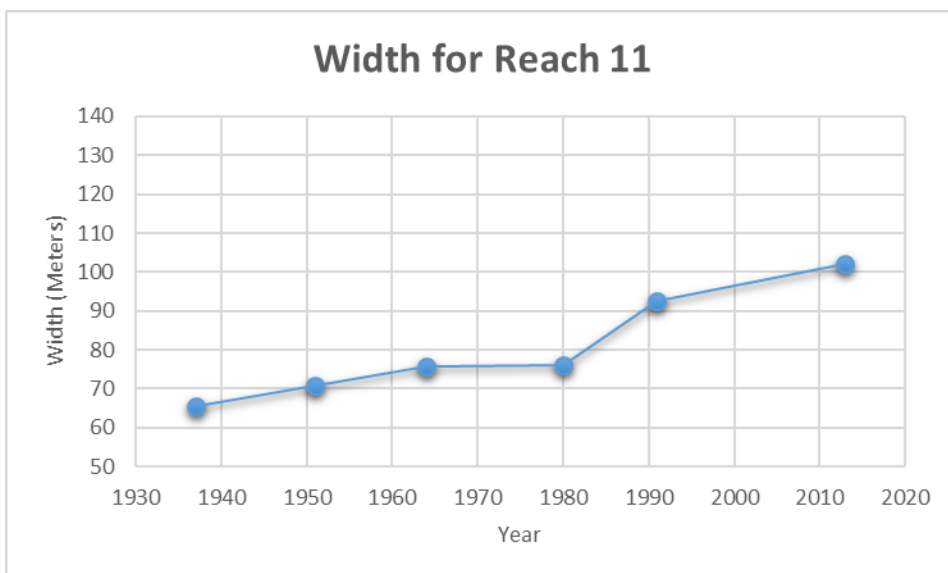
Reach 11 is a relatively static compared to its upstream and downstream reaches. Except for two meanders very little migration has been seen in this reach with a significant decline in the 1991-2013 interval. Channel width has also seen a relatively gradual increase compared to other reaches which is typical of other reaches that experience less migration. Sinuosity has also remained static and low through the record of time.



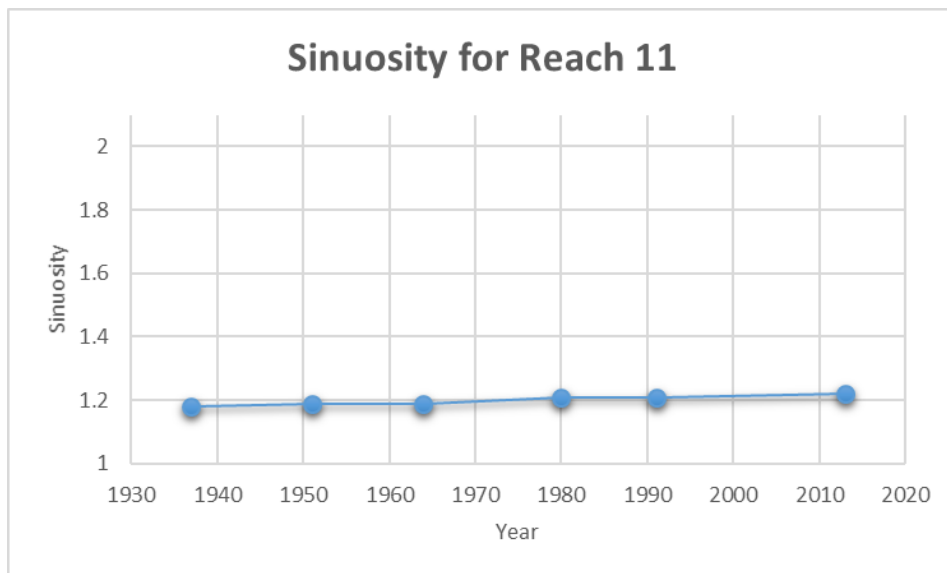
Reach 11 with migration displayed (Red = 1937-1951, Orange = 1951-1964, Yellow = 1964-1980, Green = 1980-1991, Blue = 1991-2013)



Reach 11 annual channel migration from 1937-2013



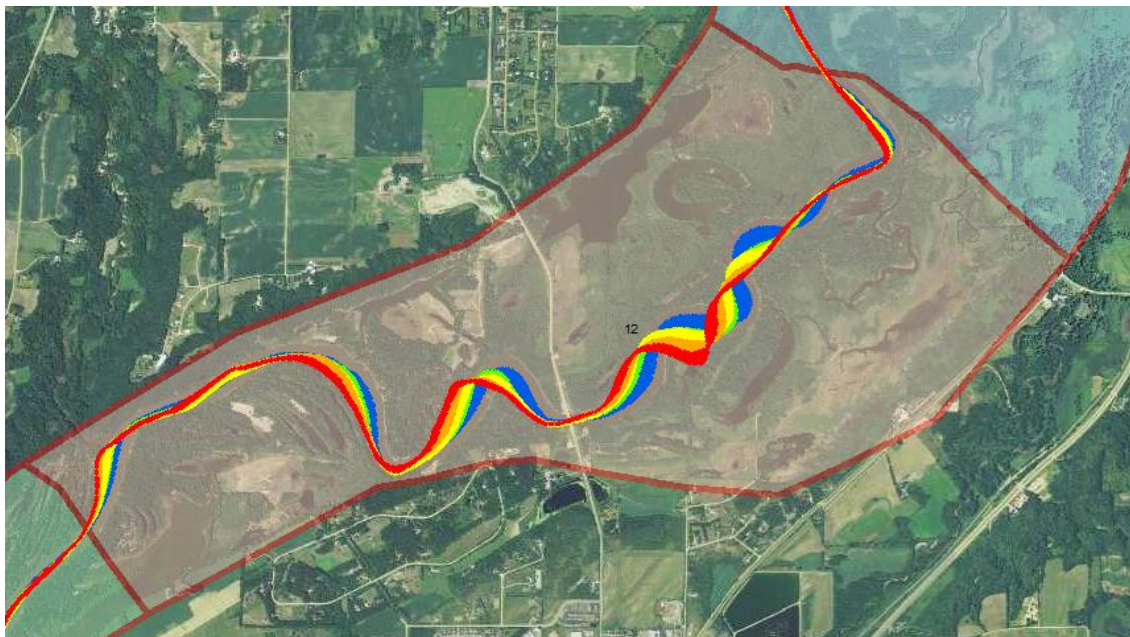
Reach 11 width change from 1937-2013



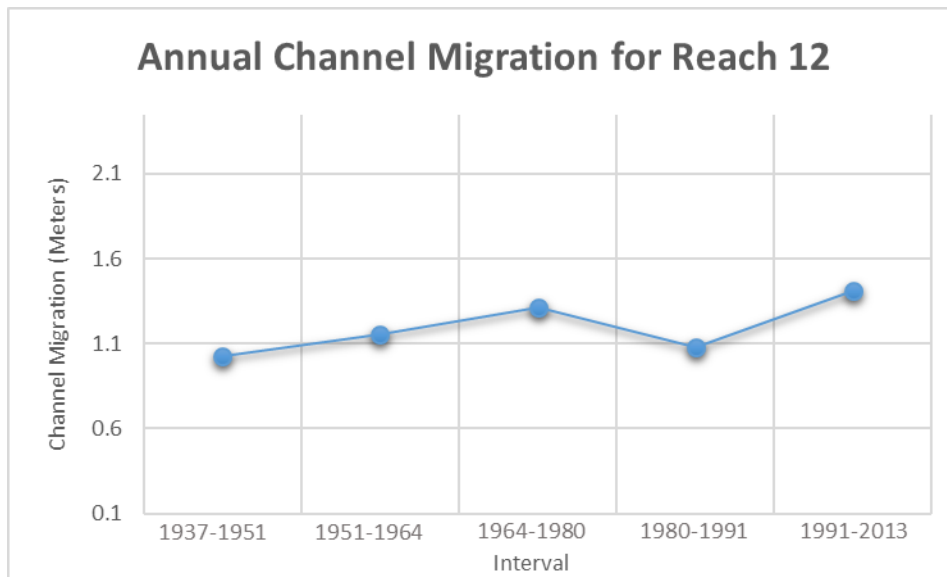
Reach 11 sinuosity from 1937-2013

Reach 12

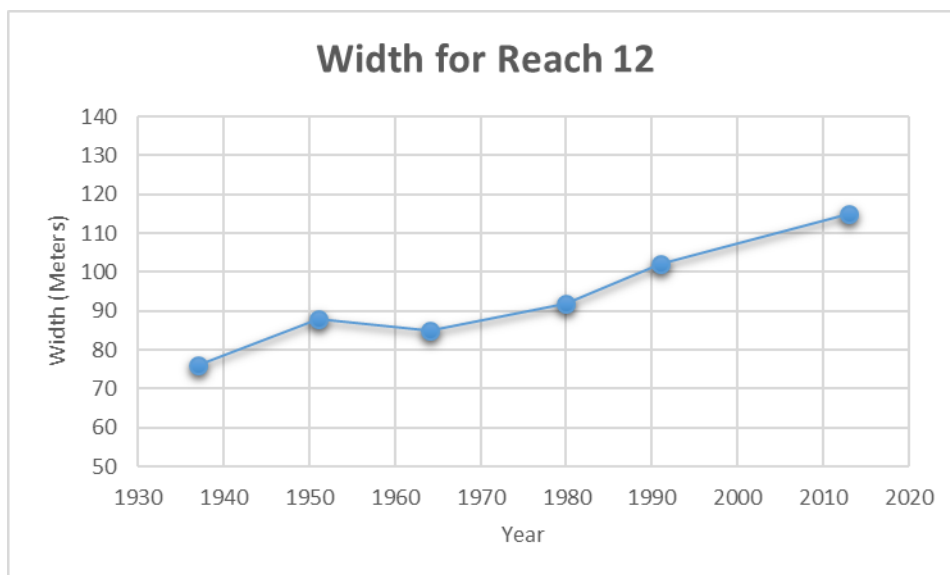
Reach 12 marks a significant reach for several interrelated reasons. The middle of this reach is the city of Jordan which is where Groten, Ellison, and Hendrickson 2016 noted the sediment yield is two and half times greater than at Mankato with a sharp decline following this area indicating this reach is a significant sediment sink. Due to this, this is the last highly dynamic region in planform channel change, especially channel migration. Channel width is increasing and relatively high in this reach and in sinuosity has remained stable and high. This reach is also downstream another high sediment contributing tributary, Beavens Creek. This area is dominated by translation.



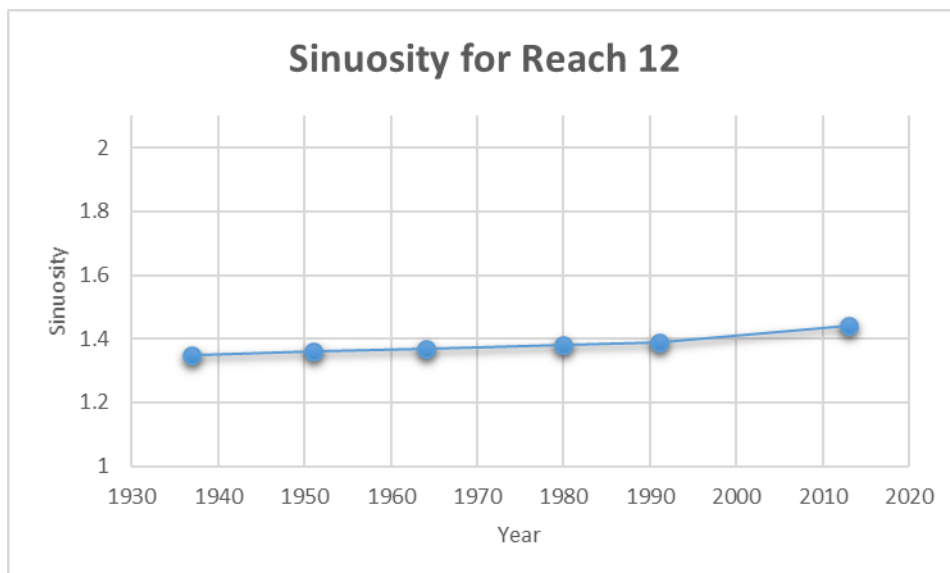
Reach 12 with migration displayed (Red = 1937-1951, Orange = 1951-1964, Yellow = 1964-1980, Green = 1980-1991, Blue = 1991-2013)



Reach 12 annual channel migration from 1937-2013



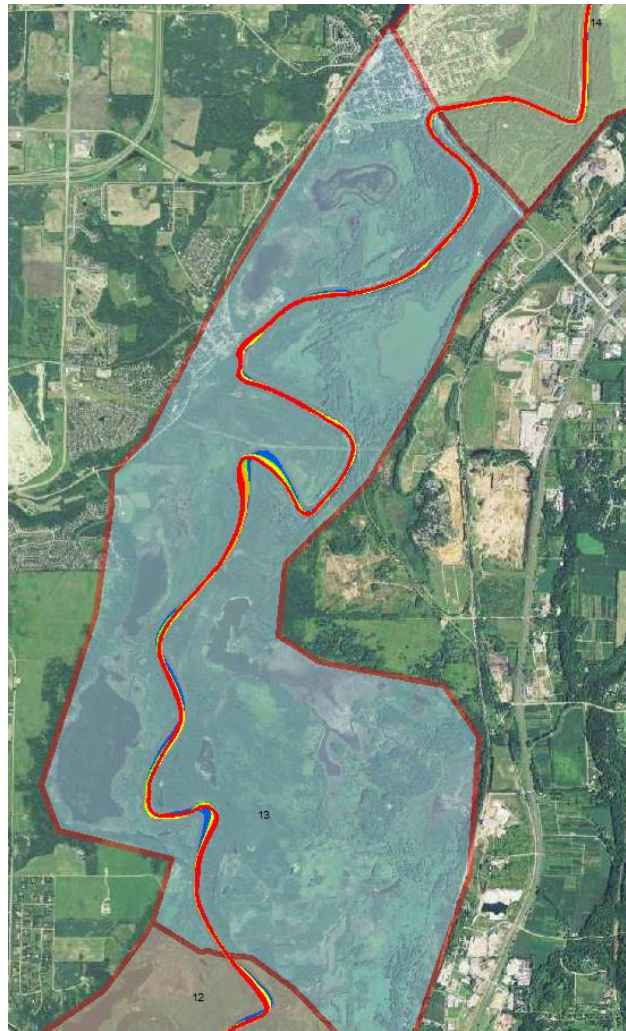
Reach 12 width change from 1937-2013



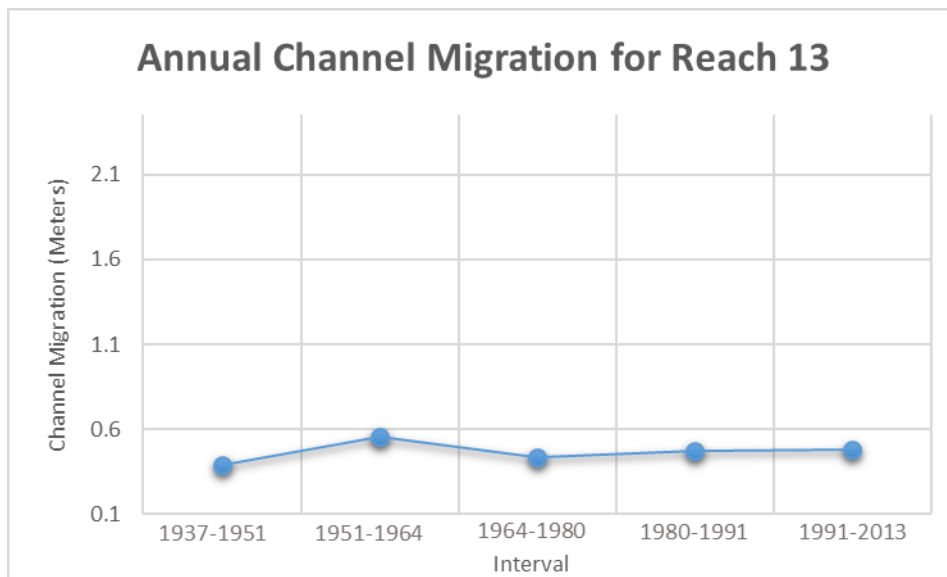
Reach 12 sinuosity from 1937-2013

Reach 13

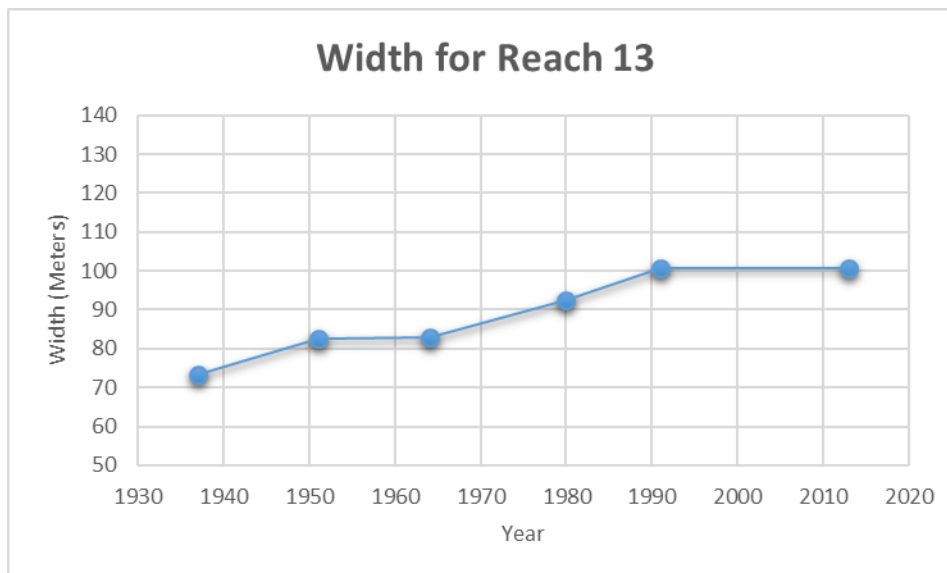
Reach 13 marks the beginning of the reaches with relatively little channel migration. It is also right on the edge of entering the metro area with agricultural land use still dominating outside of the river valley. This reach has had an increase in channel width but has remained the same since 1980. Despite the stability it is a highly sinuous stretch. This channel has a distinct pattern of large meanders that swing across the valley multiple times.



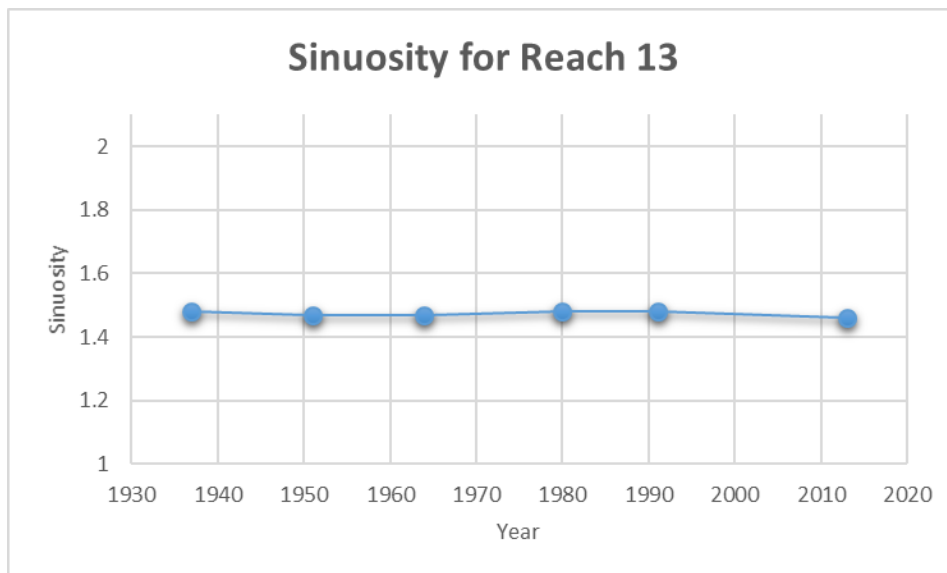
Reach 13 with migration displayed (Red = 1937-1951, Orange = 1951-1964, Yellow = 1964-1980, Green = 1980-1991, Blue = 1991-2013)



Reach 13 annual channel migration from 1937-2013



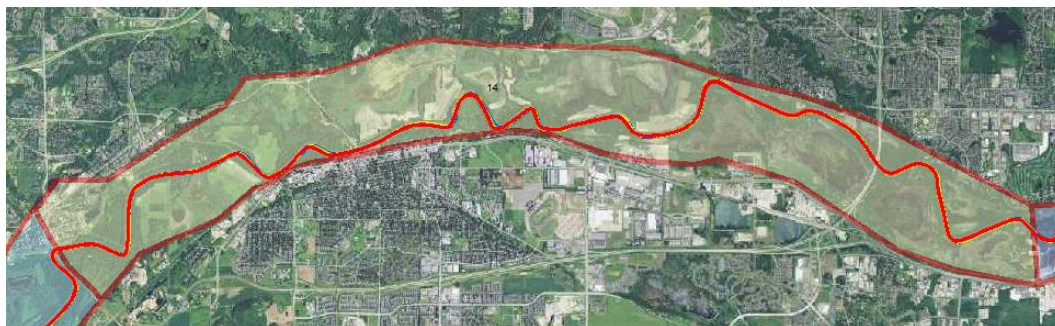
Reach 13 width change from 1937-2013



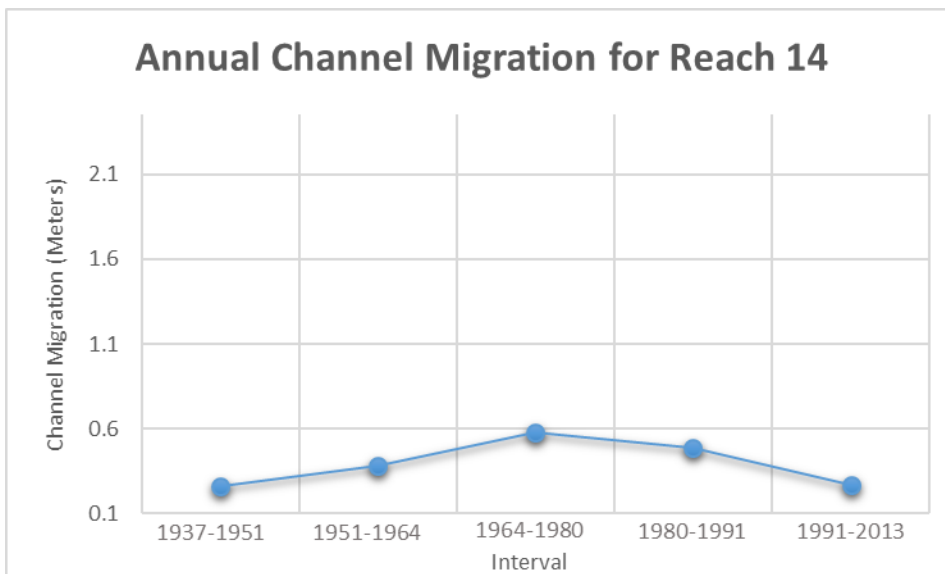
Reach 13 sinuosity from 1937-2013

Reach 14

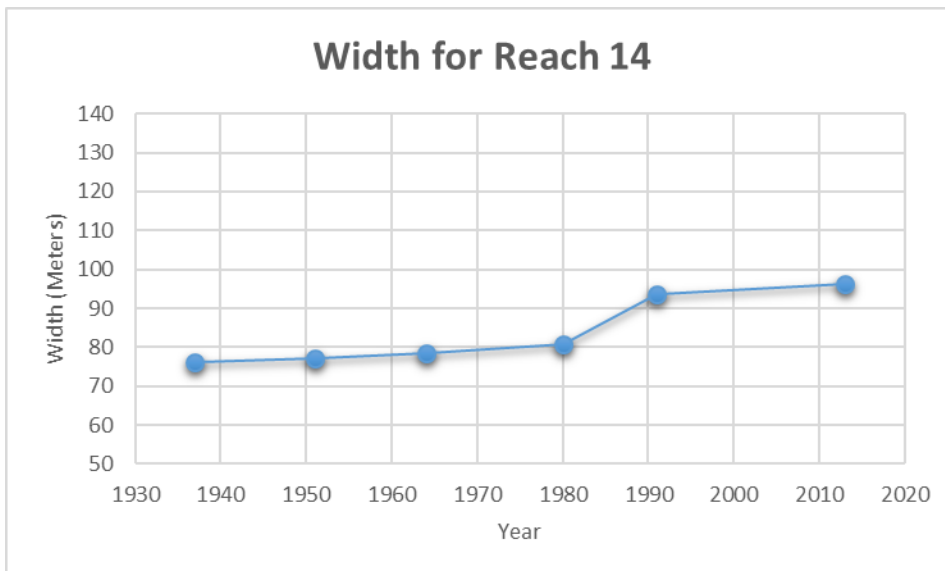
Reach 14 marks the first stretch that is in dominate urban land use, yet ends before where the channel is actively dredged for barge traffic. Very little channel migration has historically been seen in this reach with highest rate being ~0.6 meters per year in the 1964-1980 interval. Channel width in this stretch has only increase from an average of ~75 meters to ~95 meters, and sinuosity has remained static at ~1.2 which is lower than the prior reach.



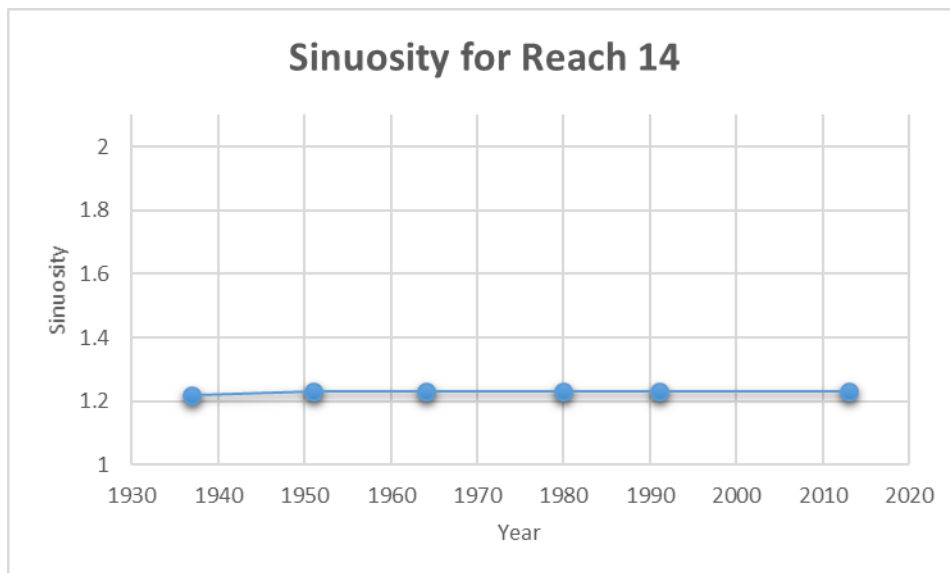
Reach 14 with migration displayed (Red = 1937-1951, Orange = 1951-1964, Yellow = 1964-1980, Green = 1980-1991, Blue = 1991-2013)



Reach 14 annual channel migration from 1937-2013



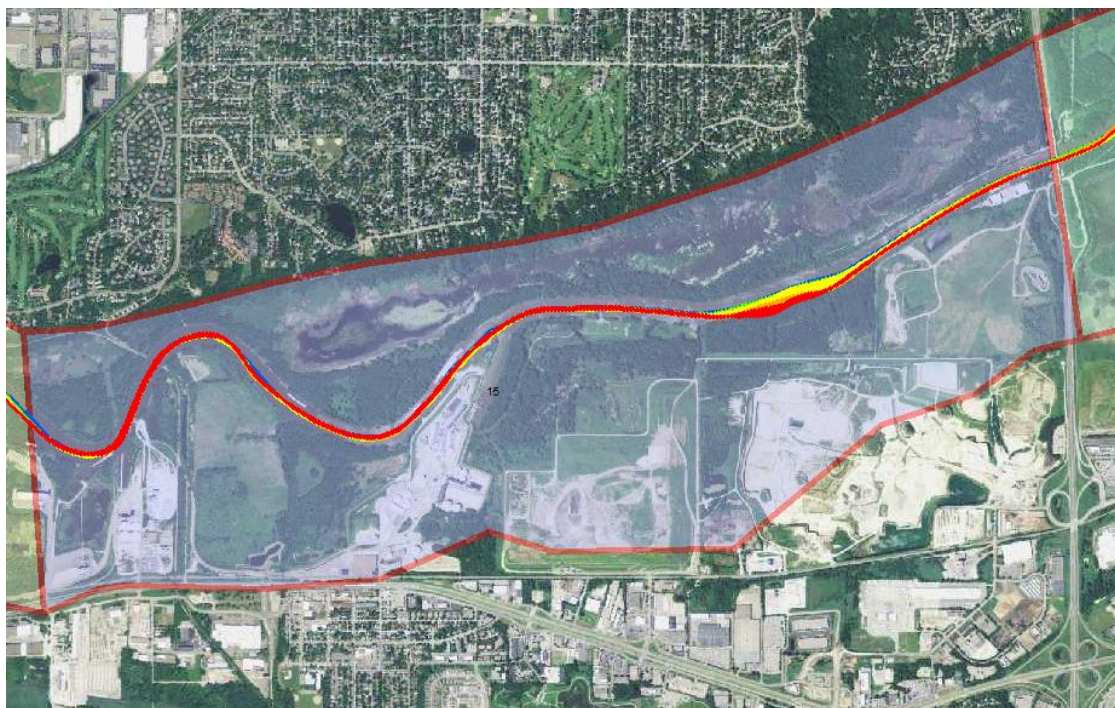
Reach 14 width change from 1937-2013



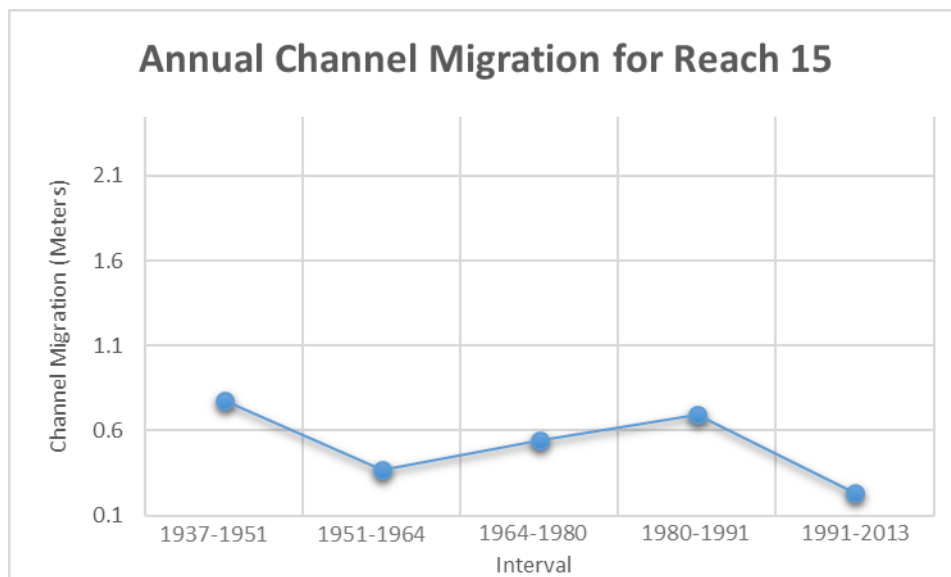
Reach 14 sinuosity from 1937-2013

Reach 15

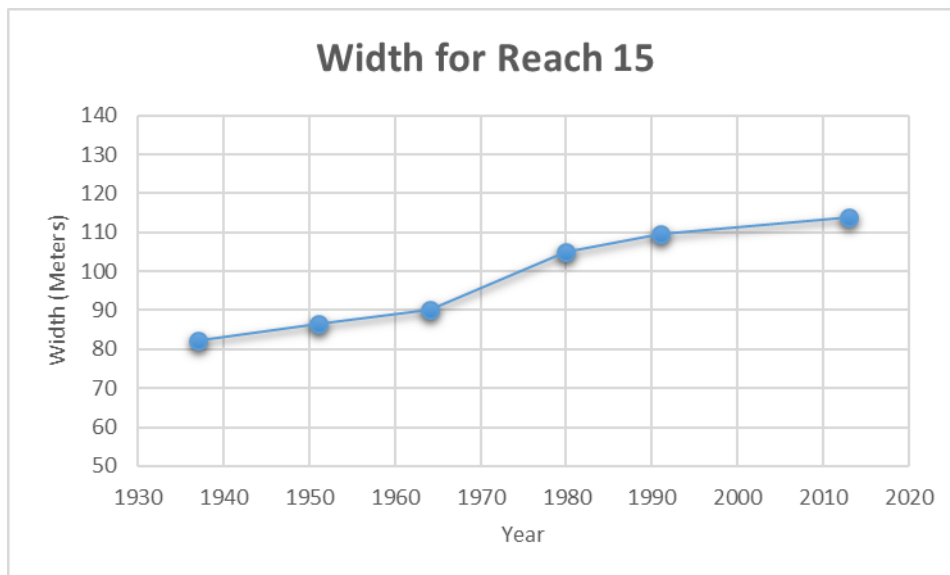
Reach 15 begins the channel that is actively dredging for barge traffic with two of the four dredging locations contained in it. This stretch also has heavy industrial encroachment in the river valley from barge loading areas. Migration has been low in this area with very little in the past 22 years, and width has increased more so than the prior reach. However, sinuosity decreased even more than the prior reach.



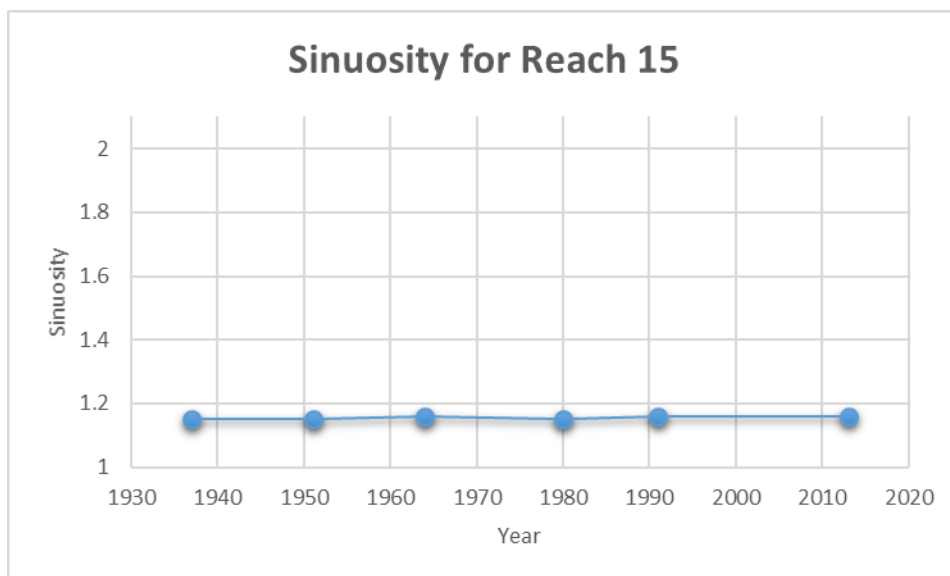
Reach 15 with migration displayed (Red = 1937-1951, Orange = 1951-1964, Yellow = 1964-1980, Green = 1980-1991, Blue = 1991-2013)



Reach 15 annual channel migration from 1937-2013



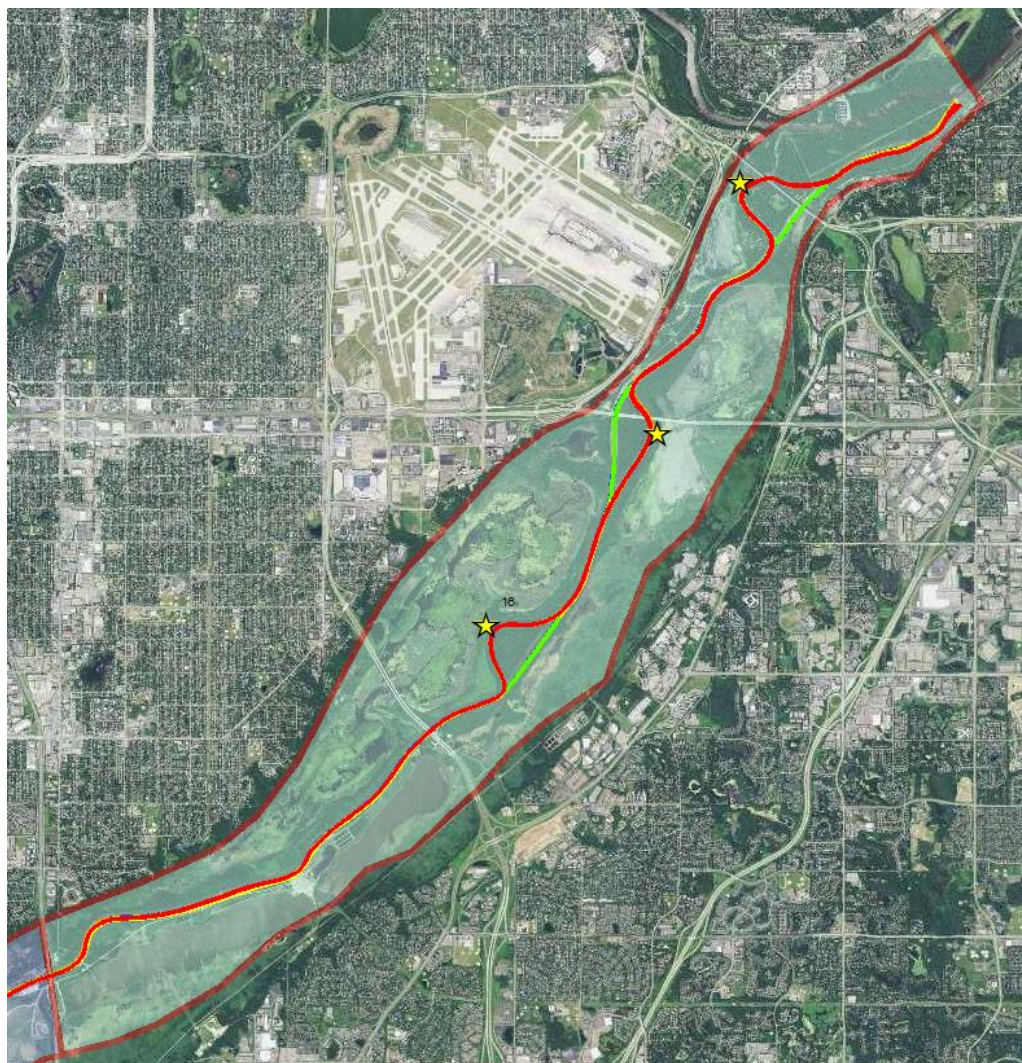
Reach 15 width change from 1937-2013



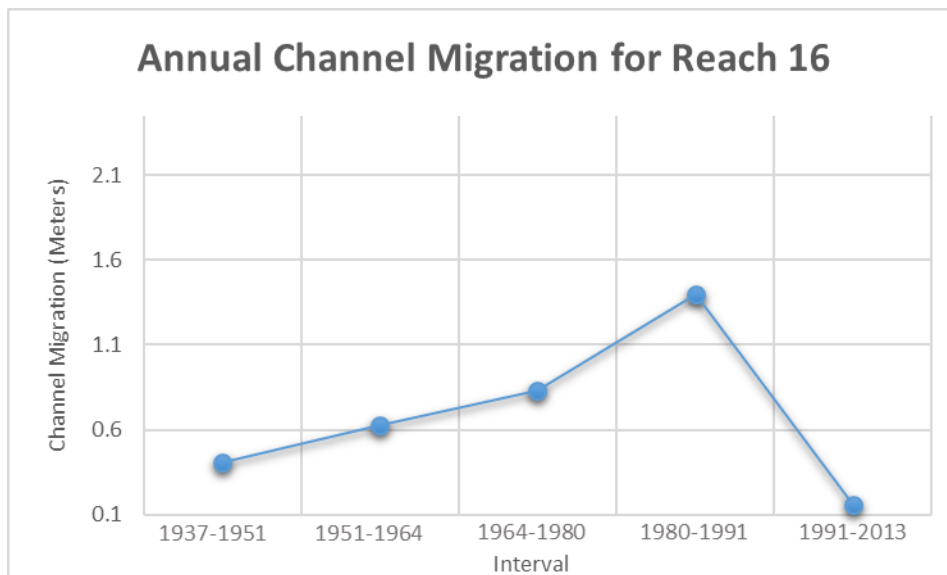
Reach 15 sinuosity from 1937-2013

Reach 16

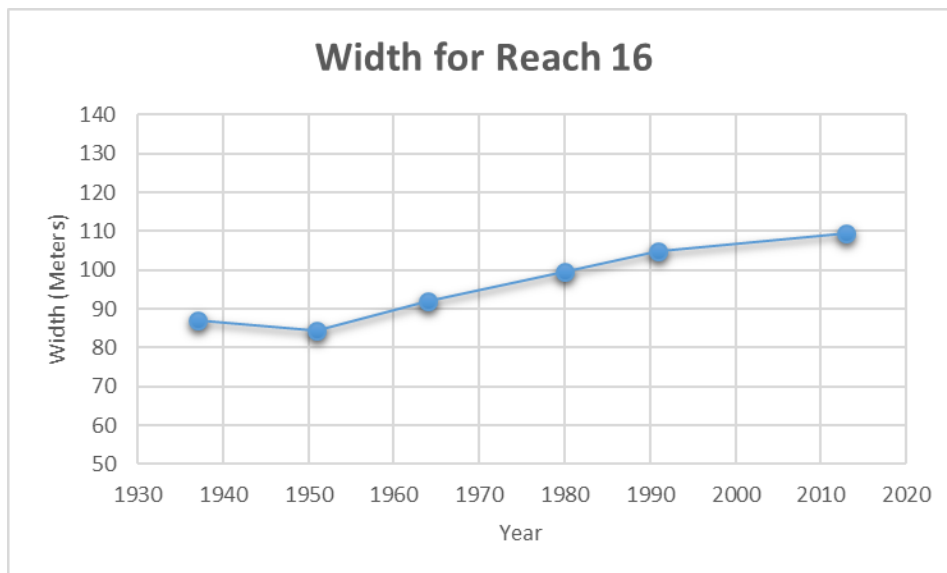
Reach 16 marks the last stretch ending at the confluence with the Mississippi. This reach has multiple characteristics that make it unique. The channel migration was significantly increasing over time until almost becoming completely stable in 1991-2013 interval. This could likely be do to the channel being managed for barge traffic. Width change has steadily increased. This reach also had very low sinuosity, yet still experienced three cutoffs in the 1964-1980 reducing it even further. These cutoffs are of interest since they are spatially out of place compared to the other cutoffs in the study area. No evidence could be found that these were created to increase the ease of barge traffic, yet further investigation would be required to make the formation of these fully intelligible.



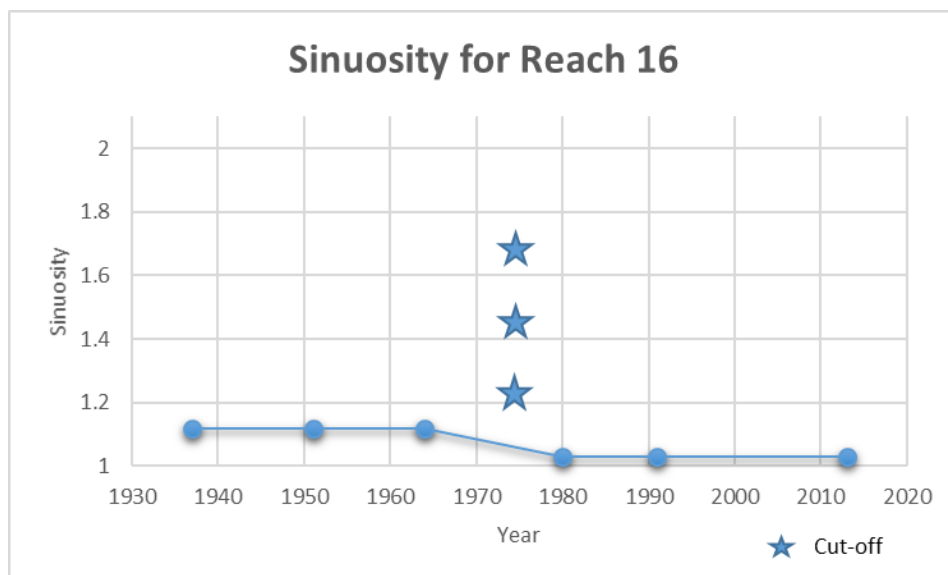
Reach 16 with migration displayed (Red = 1937-1951, Orange = 1951-1964, Yellow = 1964-1980, Green = 1980-1991, Blue = 1991-2013)



Reach 16 annual channel migration from 1937-2013



Reach 16 width change from 1937-2013



Reach 16 sinuosity from 1937-2013